Title
Estimating Seismic Demands for Performance-Based Engineering of Buildings

Author
Reyes, Juan Carlos

Publication Date
2009

Peer reviewed|Thesis/dissertation

Estimating Seismic Demands for Performance-Based Engineering of Buildings

by

Juan Carlos Reyes

B.S. (Universidad Industrial de Santander, Colombia) 1998
M.S. (Universidad de los Andes, Colombia) 2002

A dissertation submitted in partial satisfaction of the

requirements for the degree of

Doctor of Philosophy

in

Engineering-Civil and Environmental Engineering

in the

GRADUATE DIVISION

of the

UNIVERSITY of CALIFORNIA, BERKELEY

Committee in charge:

Professor Anil K. Chopra, Chair
Professor Stephen A. Mahin
Professor Douglas Dreger

Fall 2009

Abstract

Estimating Seismic Demands for Performance-Based

Engineering of Buildings

by

Juan Carlos Reyes

Doctor of Philosophy in Engineering-Civil and Environmental Engineering

University of California, Berkeley

Professor Anil K. Chopra, Chair

Earthquake engineering practice is increasingly using performance-based procedures for evaluating existing buildings and proposed designs of new buildings. Both nonlinear static and nonlinear response history analyses (RHA) are used for estimating engineering demand parameters (EDPs)—floor displacements, story drifts, internal forces, hinge rotation, etc—in performance-based engineering of buildings. Topics related to both analysis procedures are investigated in this dissertation.

In the first part, the original modal pushover analysis (MPA) to estimate seismic demands due to one component of ground motion is extended to consider two horizontal components simultaneously in three-dimensional analysis of buildings, and to estimate internal forces and plastic hinge rotations directly from pushover analyses. Subsequently, the accuracy of MPA in estimating EDPs for tall buildings and unsymmetric-plan buildings is evaluated. Seismic demands for recently designed and built 48- and 62-story buildings with ductile concrete core walls—designed according to the alternative provisions of the 2001 San Francisco Building Code (SFBC)—due to an ensemble of 30

ground motions are computed by MPA and nonlinear RHA, and compared. We demonstrate that MPA procedure shows degree of accuracy that is sufficient for practical application in estimating median values of EDPs for tall buildings subjected to two horizontal components of ground motion. The accuracy of the extended MPA procedure is also evaluated for low- and medium-rise unsymmetric-plan buildings with ductile frames designed in accordance with the 1985 Uniform Building Code (UBC85) and the 2006 International Building Code (IBC06). Seismic demands are computed for six unsymmetric-plan buildings due to 39 ground motions acting simultaneously in two orthogonal horizontal directions. Comparing these results with those from nonlinear RHA, we demonstrate that MPA provides good estimates of EDPs whereas the procedures specified in the ASCE/SEI 41-06 standard and the Eurocode 8 are not satisfactory for estimating seismic demands for unsymmetric-plan buildings.

The second part of the dissertation concerns nonlinear response history analysis of buildings. With the goal of developing effective procedures for selection and scaling of multi-component ground motions to be used in nonlinear RHA, a modal-pushover-based-scaling (MPS) procedure is developed in this investigation. The developed MPS procedure is an extension of the original MPS procedure for one component of ground motion to two horizontal components. In this investigation, each horizontal component of ground motion is scaled by a factor selected to match the deformation of its first-"mode" inelastic SDF system to a target inelastic deformation that may be estimated using a design (or response) spectrum. The properties of the first-"mode" inelastic SDF system are determined by pushover analysis of the building using the first-mode distribution. Based on the results for medium-rise symmetric-plan and unsymmetric-plan buildings

with ductile frames, we demonstrate that the MPS procedure provides much superior results than the scaling procedure specified in the ASCE/SEI 7-05 standard.

Chair _____ Date _____

Dedicated to God, the sense and light of my life

Contents

1 Introduction 1

1.1 Motivation 1

1.2 Objectives 8

1.3 Outline 8

2 Three-dimensional Nonlinear Response History Analysis 10

2.1 Equations of Motion 10

2.2 Numerical Solution 12

2.2.1 Time-Stepping Methods 12

2.2.2 Numerical Procedure Selected 13

2.3 Response Statistics 15

3 Three-dimensional Modal Pushover Analysis (MPA) 17

3.1 Modal expansion of forces 17

3.2 Uncoupled Modal Response History Analysis (UMRHA) 18

3.2.1 Linear systems 18

3.2.2 Nonlinear systems 20

3.3 Modal Pushover Analysis (MPA) 26

3.3.1 Linear systems 26

3.3.2 Nonlinear systems 28

3.4 Step-by-step Summary 32

3.5 Simplified MPA for Practical Applications 38

4 Evaluation of MPA for Tall Buildings 43

4.1 Structural Systems and Modeling Assumptions 43

4.1.1 Structural systems 43
4.1.2 Modeling of Shear Walls 46
4.1.3 Modeling of Beams and Slabs 47
4.1.4 Geometric Nonlinear Effects 49
4.1.5 Vibration Periods and Modes 49
4.1.6 Rayleigh Damping 54
4.1.7 Three-dimensional Modeling 54
4.2 Ground Motions 55
4.2.1 Selected Earthquake Records 55
4.2.2 Ground-Motion Scaling Procedure 57
4.3 Evaluation of MPA procedure 59
4.3.1 Modal Pushover Curves and Reference Displacements 59
4.3.2 Higher Mode Contribution in Seismic Demands 62
4.3.3 Evaluation of Modal Pushover Analysis 64
4.4 Evaluation of Modified MPA (MMPA) 64
4.5 Evaluation of Practical MPA (PMPA) 65
4.5.1 Floor Displacements and Story Drifts at the C.M 65
4.5.2 Other Response Quantities 70
5 Evaluation of MPA for Unsymmetric-Plan Buildings 74
5.1 Selected Structural Systems and Modeling Assumptions 74
5.1.1 Structural Systems 74
5.1.2 Modeling 76
5.1.3 Natural Vibration Periods and Modes 77

5.2 Ground Motions 88
5.2.1 Selected Earthquake Records 88
5.2.2 Ground-Motion Scaling Procedure 89
5.3 Evaluation of MPA 92
5.3.1 Modal Pushover Curves and Reference Displacements 92
5.3.2 Higher Mode Contributions in Seismic Demands 99
5.3.3 Evaluation of Modal Pushover Analysis 102
5.4 Evaluation of ASCE41-06 and Eurocode8 procedures 103
5.4.1 ASCE41-06 Nonlinear Static Procedure 103
5.4.2 Eurocode8 Nonlinear Static Analysis 107
5.4.3 Comparative Evaluation of ASCE41-06, Eurocode8 and MPA 108
5.5 Evaluation of Modified MPA (MMPA) 115
5.6 Evaluation of Practical MPA (PMPA) 118
5.6.1 Floor Displacements and Story Drifts at the C.M. 118
5.6.2 Other Response Quantities 125
6 Modal-Pushover-Based-Scaling of Ground Motions 130
6.1 MPS Procedure 130
6.1.1 MPS Procedure: Different Scaling Factors for Two Components 131
6.1.2 MPS Procedure: Same Scaling Factor for Two Components 135
6.2 ASCE/SEI 7-05 Procedure 138
6.2.1 One Component of Ground Motion 138
6.2.2 Two Components of Ground Motion 141
6.3 Ground motions 143

6.4 Modeling of the Symmetric-Plan Building 146
6.4.1 Structural System 146
6.4.2 Modeling 150
6.4.3 System Identification and Response Prediction 150
6.5 Evaluating Scaling Procedures: One Component of Ground Motion 155
6.5.1 Benchmark Responses 155
6.5.2 Evaluation of One-mode MPS Procedure 156
6.5.3 Comparative Evaluation of MPS and ASCE7 Scaling Procedures 159
6.5.4 Higher Mode Considerations 161
6.6 Evaluating Scaling Procedures: Symmetric-Plan Building Subjected to Two Components of Ground Motion 163
6.6.1 Benchmark Responses 163
6.6.2 One-Mode MPS Procedure: Same Scaling Factors 164
6.6.3 One-Mode MPS Procedure: Different Scaling Factors 169
6.6.4 Comparative Evaluation of MPS and ASCE7 Scaling Procedures 173
6.6.5 Higher Mode Considerations 175
6.7 Evaluating Scaling Procedures: Unsymmetric-Plan Buildings Subjected to Two Components of Ground Motion 177
6.7.1 Benchmark Responses 178
6.7.2 Evaluation of One-Mode MPS Procedure 178
6.7.3 Comparative Evaluation of MPS and ASCE7 Scaling Procedures 187
6.7.4 Higher Mode Considerations 192
7 Conclusions 195

8 Bibliography 203

Appendix A: Implementation of Step 11 of MPA 211

Appendix B: Unsymmetric-Plan Buildings (Member Sizes) 213

Appendix C: Notation 216

Acknowledgments

It has been a great honor to work under the supervision of Professor Anil K. Chopra; I thank him for his valuable technical advice, and his constant support, encouragement and guidance during my years as a graduate student at Berkeley. I would like to express my appreciation to Professor Stephen A. Mahin for his advice throughout my dissertation, and to Professor Douglas Dreger for reviewing the manuscript. I would like to thank my mother, Basilia, as well as my brother Fernando, and my girlfriend Lina for all their love and support.

Thanks to the Fulbright commission, Colciencias, Universidad de los Andes and University of California, Berkeley for making my dreams come true by providing the funding of my doctoral studies.

1 Introduction

1.1 Motivation

The earthquake engineering profession has been moving away from traditional code procedures to performance-based procedures for evaluating existing buildings and proposed designs of new buildings. Both nonlinear static and nonlinear response history analyses (RHA) are now used for estimating engineering demand parameters (EDPs)[†]—floor displacements, story drifts, internal forces, hinge rotations, etc—in performance-based engineering of buildings.

According to the nonlinear static procedure (NSP) described in ASCE/SEI 41-06 [ASCE, 2007] and Eurocode 8 [British Standards, 2004], EDPs may be computed by nonlinear static analysis of the structure subjected to monotonically increasing lateral forces with an invariant height-wise distribution until a pre-determined target displacement is reached. Also known as pushover analysis, these procedures are now standard in structural engineering practice, because they provide a better assessment of the actual capacity and expected performance of the structure compared to traditional code-based linear static analysis, but require much less computational effort compared to rigorous nonlinear RHA. The pushover procedures are attractive for the additional reason that their implementation requires only the design spectrum; there is no need for ground motion records.

[†] The terminology "engineering demand parameters (EDPs)" and "seismic demands" are used interchangeably.

The ASCE/SEI 41-06 and Eurocode 8 approaches are akin to previous NSP procedures, whose limitations have been widely demonstrated [Krawinkler and Seneviratna, 1998; Naeim and Lobo, 1998; Gupta and Krawinkler, 1999; Kim and D'Amore, 1999; Elnashai, 2001; Fajfar, 2002]. In general, these procedures underestimate seismic demands in intermediate and upper stories of medium- and high-rise buildings where higher-"mode" contributions to response can be significant and do not consider torsional contributions to the response for unsymmetric-plan buildings.

To overcome some of these limitations for symmetric-plan buildings, researchers have proposed adaptive force distributions that attempt to follow more closely the time-variant distributions of inertia forces [Bracci et al, 1997; Gupta and Kunnath, 2000], developed incremental response spectrum analysis [Aydinoglu, 2003], and considered modes higher than the fundamental vibration mode [Sasaki et al, 1998; Gupta and Kunnath, 2000; Kalkan and Kunnath, 2004; Poursha et al, 2009]. Rooted in structural dynamics theory, the modal pushover analysis (MPA) has been developed to include the contributions of all "modes" of vibration that contribute significantly to seismic demands [Chopra and Goel, 2002]. MPA has been shown to achieve superior estimates of EDPs for steel and concrete moment-resisting-frame (MRF) buildings, while retaining the conceptual simplicity and computational attractiveness of standard nonlinear static procedures. By analyzing several such buildings covering a range of heights and a range of ground-motion intensities, these studies have demonstrated that the MPA procedure estimates seismic demands for steel and concrete MRF buildings responding into the inelastic range to a degree of accuracy that is comparable to that of the standard response spectrum analysis (RSA) procedure for estimating the response of linearly elastic systems

[Goel and Chopra, 2004; Bobadilla and Chopra, 2008]. The preceding studies are all limited to symmetric-plan MRF buildings up to 20 stories high.

Starting in 1997, various researchers have extended pushover analysis to unsymmetric-plan buildings. By applying a height-wise distribution of lateral forces typical of standard planar pushover analysis at the floor centers of mass, an approximate non-linear static analysis procedure was developed [Kilar and Fajfar, 1997]. Another procedure consists of two steps: (i) three-dimensional elastic response spectrum analysis to determine roof displacement and height-wise distribution of lateral forces for each resisting element (frames, walls, etc.), and (ii) planar pushover analysis of each resisting element [Moghadam and Tso, 1998]. Some studies have focused on special considerations necessary to consider interaction between walls and frames in pushover analysis of wall-frame structures [De Stefano and Rutenberg, 1998]. Another paper investigated the accuracy of applying lateral forces at different locations in the plan of unsymmetric buildings [Faella and Kilar, 1998]. The few comparisons of pushover analysis results with non-linear RHA give the impression of limited success.

Because the MPA procedure is rooted in structural dynamics theory, this procedure could be generalized to unsymmetric-plan buildings, which respond in coupled lateral-torsional motions during earthquakes [Chopra and Goel, 2004]. It was demonstrated that the MPA estimate of seismic demand due to an intense ground motion is accurate for unsymmetric systems to a similar degree as it was for a symmetric building. However, this conclusion was based on a limited investigation, comparing the MPA estimate of demand and its exact value determined by non-linear RHA for three structural systems

with different degrees of coupling between lateral and torsional motions subjected to a single ground motion.

The preceding studies are all limited to one component of ground motion, although at least the two horizontal components of ground motion should be considered in computing seismic demands by three-dimensional analysis of multistory buildings. Pushover analysis including higher modes effects for buildings subjected to two components of ground motion has received relatively little attention. The need for developing improved approximate procedures rooted in structural dynamics theory for estimating seismic demands for symmetric-plan and unsymmetric-plan buildings, ranging from low-rise to very high-rise buildings subjected to at least two horizontal components of ground motion is critical. Current engineering practice is based on judgmental extensions of methods initially developed for planar analysis of buildings.

Several tall buildings have been designed recently and are under construction in the west coast of the USA, a region known for its high seismicity. Because many of these buildings use high-performance materials or exceed the height limits specified in building codes, they are designed by an alternative performance-based procedure, allowed in the alternative provision clause of codes [Moehle, 2007]. For such projects, nonlinear response history analysis (RHA) is now being increasingly employed to determine the EDPs for an ensemble of multi-component ground motions. Selection and scaling of ground motions necessary for nonlinear RHA is a subject of much research in recent years.

Among the many procedures proposed to modify ground motion records, the most widely used approaches are amplitude scaling and spectrum matching. In the first

approach only the amplitude of the record is modified; therefore, the original focal mechanism, wave propagation effects and non-stationary characteristics of the ground motion are preserved. In contrast, spectral matching methods modify the frequency content and/or phasing of the record to match its response spectrum to a target spectrum. Although these modifications can lead to unrealistic ground motions [Bommer and Acevedo, 2004], spectral matching methods using wavelets in the time domain can result in realistic motions that preserve the non-stationary characteristics of the original ground motions [Lilhanand and Tseng, 1987, 1988; Abrahamson, 1992; Hancock et al, 2006].

The objective of amplitude scaling procedures is to determine scale factors for a small number of records such that the scaled records provide an accurate estimate of median structural responses, and, at the same time, are efficient, i.e. reduce the record-to-record variability of response. In earlier approaches, ground motion records were scaled to match a target intensity measure such as peak ground acceleration (PGA), effective peak acceleration, Arias intensity, or effective peak velocity [Nau and Hall, 1984; Kurama and Farrow, 2003]. These approaches are generally inaccurate and inefficient for structures responding in the inelastic range [Shome and Cornell, 1998; Kurama and Farrow, 2003]. Scaling of records to match the target spectrum at the fundamental vibration period of the structure T_1 provides improved results for elastic structures whose response is dominated by its first mode of vibration [Shome et al, 1998]. However, if the contributions of higher modes are important or the structure deforms significantly into the inelastic range, this scaling method becomes less accurate and less efficient [Mehanny, 1999; Alavi and Krawinkler, 2000; Kurama and Farrow, 2003]. Modifications of this method that considers the target spectrum ordinates at the first and second vibration

periods have been proposed [Bazzurro, 1998; Shome and Cornell, 1999]; however, efficiency of these modified methods is compromised for near-fault records with a dominant velocity pulse [Baker and Cornell 2006].

To account for higher-mode contributions to response and the lengthening of the apparent vibration period after the structure deforms into the inelastic range, the scaling factor for a ground motion record can be chosen to minimize the difference between its elastic response spectrum and the target spectrum over a period range [Kennedy et al, 1984; Malhotra, 2003; Alavi and Krawinkler, 2004; Naeim et al, 2004; Youngs et al, 2007; PEER GMSM Group, 2009]. The period ranges recommended include $0.2T_1$ to $1.5T_1$ [ASCE, 2005], and T_{min} to $\sqrt{\mu}\,T_1$, where T_{min} is the period of the highest vibration mode that contributes significantly to the response and μ is the displacement ductility demand imposed on the structure [Beyer and Bommer, 2007].

Because the preceding methods do not consider explicitly the inelastic behavior of the structure, they may not be appropriate for near-fault sites where the inelastic deformation can be significantly larger than the deformation of the corresponding linear system [Bozorgnia and Mahin, 1998; Alavi and Krawinkler, 2000; Baez and Miranda, 2000; Chopra and Chintanapakdee, 2004]. For such sites, scaling methods that are based on the inelastic deformation spectrum or consider the response of the first-"mode" inelastic SDF system are more appropriate [Luco and Cornell, 2007 and Tothong and Cornell, 2008; PEER GMSM Group, 2009].

These ideas were utilized by Kalkan and Chopra [2009a] to develop a modal-pushover-based-scaling (MPS) procedure for selecting and scaling earthquake ground motion records in a form convenient for evaluating existing structures and proposed

designs of new structures. This procedure explicitly considers structural strength, determined from the first-"mode" pushover curve, and determines a scaling factor for each record to match a target value of the deformation of the first-"mode" inelastic SDF system. The MPS procedure has proven to be accurate and efficient for low-, medium-, and high-rise buildings with symmetric plan subjected to one component of ground motion [Kalkan and Chopra, 2009 and 2010].

Scaling two horizontal components for use in three-dimensional analysis of buildings has received little attention. Researchers have proposed that both components of a record be scaled by the same factor, selected to match their *geometric mean* spectrum to the target spectrum over a period range [Malhotra, 2003; Beyer and Bommer, 2007]. The ASCE/SEI 7-05 standard [ASCE, 2005], requires that the ground motion records be scaled such that the average value of the SRSS spectra for all horizontal-component pairs does not fall below 1.3 times the target spectrum by more than 10 percent. Beyer and Bommer [2007] present a comprehensive summary of various aspects that should be included in the process of selecting and scaling two components of ground motions. They conclude that selecting and scaling records according to their "goodness-of-fit" with the target spectrum leads to efficient estimates of median responses. However, inelastic behavior of the structure is not considered in existing methods for scaling two components of ground motion.

Clearly, there is a need to develop procedures for selection and scaling of ground motions to be used in nonlinear RHA of symmetric-plan and unsymmetric-plan buildings, ranging from low-rise to high-rise buildings subjected to multi-component ground motions.

1.2 Objectives

The main objectives of this dissertation are to: (1) Extend the modal pushover analysis (MPA) procedure developed by Chopra and Goel [2004] to three dimensional analyses of buildings subjected to two horizontal components of ground motion, simultaneously. (2) Evaluate the accuracy of the extended MPA procedure for estimating seismic demands for tall buildings with ductile concrete shear walls. (3) Evaluate the accuracy of the extended MPA procedure for estimating seismic demands for low- and medium-rise unsymmetric-plan buildings with ductile frames. (4) Comparatively evaluate the accuracy of the MPA procedure and the ASCE/SEI 41-06 [ASCE, 2007] and Eurocode 8 [British Standards, 2004] procedures in evaluating seismic demands for low- and medium-rise unsymmetric-plan buildings with ductile frames. (5) Extend the original modal-pushover-based-scaling (MPS) procedure originally developed by Kalkan and Chopra [2009a] for one component of ground motion to two horizontal components of ground motion for use in three-dimensional nonlinear RHA of symmetric-plan and unsymmetric-plan buildings. (6) Comparatively evaluate the accuracy and efficiency of the proposed MPS procedure and the ASCE/SEI 7-05 scaling method [ASCE, 2005].

1.3 Outline

This dissertation is organized in seven chapters. Chapter 2 presents the equations of motion governing the nonlinear response of buildings subjected to two horizontal components of ground motion, and outlines numerical methods.

Chapter 3 extends the original MPA procedure for one component of ground motion to estimate seismic demands for three-dimensional models of buildings subjected to two

horizontal components of ground motion applied, simultaneously. The theoretical background, underlying assumptions, and a step-by-step summary of the MPA procedure are included; also presented are two additional versions of MPA that are especially convenient for practical application.

Chapter 4 evaluates the accuracy of the MPA procedures of Chapter 3 in estimating seismic demands for tall buildings with ductile concrete shear walls. Seismic demands are computed for two buildings due to 30 ground motions acting simultaneously in the longitudinal and transverse directions.

Chapter 5 evaluates the accuracy of the MPA procedures of Chapter 3 in estimating seismic demands for low- and medium-rise unsymmetric-plan buildings with ductile frames. This is followed by a comparative evaluation of the accuracy of MPA and code—ASCE/SEI 41-06 [ASCE, 2007] and Eurocode 8 [British Standards, 2004]—procedures. Seismic demands are computed for six buildings due to 39 ground motions acting simultaneously in two orthogonal horizontal directions.

Chapter 6 extends the original MPS procedure for one component of ground motion to two horizontal components, and investigates the accuracy and efficiency of the extended MPS procedure for nonlinear RHA of three-dimensional models of medium-rise symmetric-plan and unsymmetric-plan buildings with steel frames. Subsequently, the scaling procedures recommended in the ASCE/SEI 7-05 standard [ASCE, 2005] are evaluated.

The conclusions of this dissertation are presented in Chapter 7.

2 Three-dimensional Nonlinear Response History Analysis

2.1 Equations of Motion

Consider an assemblage of moment-resisting frames that make up an *N*-story building (Fig. 2.1). Its plan (shown in Fig. 2.1b) may not be symmetric about *x* or/and *y* axes. This implies that the floor mass distribution and/or framing plan may be unsymmetric; or the framing plan is symmetric but the stiffness properties of symmetrically-located frames differ. Each floor diaphragm is rigid in its own plane and has three degrees of freedom (DOFs) defined at the center of mass (C.M.). The DOFs of the *j*th floor are: translation u_{jx} along *x*-axis, u_{jy} along *y*-axis, and torsional rotation $u_{j\theta}$ about the vertical axis; u_{jx} and u_{jy} are defined relative to the ground (Fig. 2.1b).

The displacement vector $\mathbf{u}$ of size $3N\times1$ for the system includes three $N\times1$ subvectors $\mathbf{u}_x$, $\mathbf{u}_y$, and $\mathbf{u}_\theta$ where $\mathbf{u}_x$ is the vector of *x*-lateral floor displacements u_{jx}; $\mathbf{u}_y$ is the vector of *y*-lateral floor displacements u_{jy}; and $\mathbf{u}_\theta$ is the vector of *N*-torsional rotations:

$$\mathbf{u}_x = \langle u_{1x} \quad u_{2x} \quad \ldots \quad u_{Nx} \rangle^T \qquad \mathbf{u}_y = \langle u_{1x} \quad u_{2x} \quad \ldots \quad u_{Ny} \rangle^T \qquad \mathbf{u}_\theta = \langle u_{1\theta} \quad u_{2\theta} \quad \ldots \quad u_{N\theta} \rangle^T$$

The system of differential equations of motion governing the response of the building subjected to bidirectional earthquake excitation, i.e., ground motion along two horizontal components applied simultaneously is:

$$\mathbf{M}\ddot{\mathbf{u}} + \mathbf{c}\dot{\mathbf{u}} + \mathbf{f}_s(\mathbf{u}) = -\mathbf{M}\boldsymbol{\iota}_a \ddot{u}_{ga}(t) - \mathbf{M}\boldsymbol{\iota}_b \ddot{u}_{gb}(t) \tag{2.1}$$

where **M** is a diagonal mass matrix, **c** is the damping matrix, and $\mathbf{f}_s$ is the vector of resisting forces; $\boldsymbol{\iota}_a$ and $\boldsymbol{\iota}_b$ are the influence vectors associated with components $\ddot{u}_{ga}(t)$ and $\ddot{u}_{gb}(t)$ of the ground motion (Fig. 2.1a).

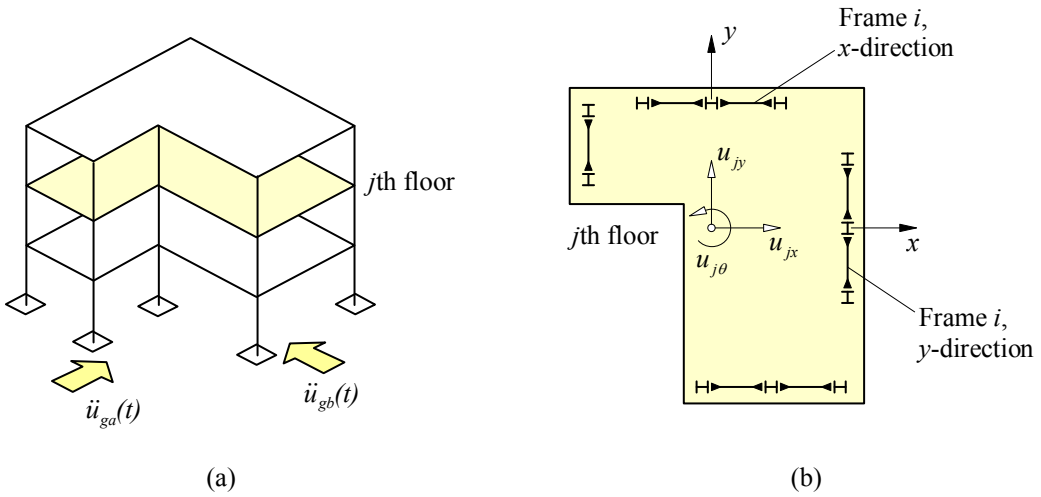

(a) (b)

Figure 2.1 (a) Multiple story building with the ground motion directions noted; (b) *j*th floor plan with DOFs noted.

The matrices (or vectors) **M**, $\mathbf{f}_s, \boldsymbol{\iota}_a$ and $\boldsymbol{\iota}_b$ may be expressed in terms of submatrices (or subvectors):

$$\mathbf{M} = \begin{bmatrix} \mathbf{m} & \mathbf{0} & \mathbf{0} \\ \mathbf{0} & \mathbf{m} & \mathbf{0} \\ \mathbf{0} & \mathbf{0} & \mathbf{I}_O \end{bmatrix} \quad \mathbf{f}_s = \begin{bmatrix} \mathbf{f}_{sx} \\ \mathbf{f}_{sy} \\ \mathbf{f}_{s\theta} \end{bmatrix} \quad \boldsymbol{\iota}_a = \begin{bmatrix} \mathbf{1} \\ \mathbf{0} \\ \mathbf{0} \end{bmatrix} \quad \boldsymbol{\iota}_b = \begin{bmatrix} \mathbf{0} \\ \mathbf{1} \\ \mathbf{0} \end{bmatrix} \tag{2.2}$$

where **m** is a diagonal matrix of order *N* with $m_{jj} = m_j$, the mass lumped at the *j*th floor level; $\mathbf{I}_O$ is a diagonal matrix of order *N* with $I_{O\,jj} = I_{O\,j}$, the moment of inertia of the *j*th floor diaphragm about a vertical axis trough the C.M.; and **1** and **0** are vectors of dimension *N* with all elements equal to one and zero, respectively. The force-deformation

relations between the displacements $\mathbf{u}_x$, $\mathbf{u}_y$ and $\mathbf{u}_\theta$ and the x-lateral forces $\mathbf{f}_{sx}$, y-lateral forces $\mathbf{f}_{sx}$, and torques $\mathbf{f}_{s\theta}$ are nonlinear and hysteretic.

2.2 Numerical Solution

2.2.1 Time-Stepping Methods

Because Eq. (2.1) can not be solved analytically, numerical time-stepping methods are employed. The time scale is divided into a series of time steps, usually of constant duration Δt. The ground motion is given at discrete time instants $t_i = i\Delta t$, denoted as time i, and the excitation vector is $\mathbf{p}_i \equiv -\mathbf{M}\boldsymbol{\iota}_a \ddot{u}_{ga}(t_i) - \mathbf{M}\boldsymbol{\iota}_b \ddot{u}_{gb}(t_i)$. Numerical solution provides the response at the same time instants and is denoted by $\mathbf{u}_i \equiv \mathbf{u}(t_i)$, $\dot{\mathbf{u}}_i \equiv \dot{\mathbf{u}}(t_i)$, and $\ddot{\mathbf{u}}_i \equiv \ddot{\mathbf{u}}(t_i)$.

Starting with the known response of the system at time i that satisfies Eq. (2.1) at time i,

$$\mathbf{M}\ddot{\mathbf{u}}_i + \mathbf{c}\dot{\mathbf{u}}_i + (\mathbf{f}_s)_i = \mathbf{p}_i \tag{2.3}$$

time-stepping methods enable us to step ahead to determine the response $\mathbf{u}_{i+1}$, $\dot{\mathbf{u}}_{i+1}$, and $\ddot{\mathbf{u}}_{i+1}$ of the system at time $i+1$ that satisfies Eq. (2.1) at time $i+1$:

$$\mathbf{M}\ddot{\mathbf{u}}_{i+1} + \mathbf{c}\dot{\mathbf{u}}_{i+1} + (\mathbf{f}_s)_{i+1} = \mathbf{p}_{i+1} \tag{2.4}$$

When applied successively with $i = 0, 1, 2, 3, \ldots$ the time-stepping procedure gives the desired response at all time instants $i = 0, 1, 2, 3, \ldots$ The known initial conditions $\mathbf{u}(0)$ and $\dot{\mathbf{u}}(0)$ at time $i = 0$, provide the information necessary to start the procedure.

2.2.2 Numerical Procedure Selected

In this study, the structural systems were modeled in the PERFORM-3D computer program [CSI, 2006], which implements Newmark's method with parameters $\gamma = \frac{1}{2}$ and $\beta = \frac{1}{4}$ (also known as constant average acceleration method, or trapezoidal rule) as the time stepping method with an event-to-event solution strategy.

Newmark's Method

Newmark's equations specialized for $\gamma = \frac{1}{2}$ and $\beta = \frac{1}{4}$, are:

$$\dot{\mathbf{u}}_{i+1} = \dot{\mathbf{u}}_i + \frac{\Delta t}{2}\left(\ddot{\mathbf{u}}_i + \ddot{\mathbf{u}}_{i+1}\right) \tag{2.5a}$$

$$\mathbf{u}_{i+1} = \mathbf{u}_i + (\Delta t)\,\dot{\mathbf{u}}_i + \frac{(\Delta t)^2}{4}\left(\ddot{\mathbf{u}}_i + \ddot{\mathbf{u}}_{i+1}\right) \tag{2.5b}$$

From Eq. (2.5b), $\ddot{\mathbf{u}}_{i+1}$ can be expressed in terms of $\mathbf{u}_{i+1}$:

$$\ddot{\mathbf{u}}_{i+1} = \frac{4}{(\Delta t)^2}\left(\mathbf{u}_{i+1} - \mathbf{u}_i\right) - \frac{4}{\Delta t}\,\dot{\mathbf{u}}_i - \ddot{\mathbf{u}}_i \tag{2.6}$$

Substituting Eq. (2.6) into Eq. (2.5a) gives:

$$\dot{\mathbf{u}}_{i+1} = \frac{2}{\Delta t}\left(\mathbf{u}_{i+1} - \mathbf{u}_i\right) - \dot{\mathbf{u}}_i \tag{2.7}$$

Next, Eqs. (2.6) and (2.7) are substituted into the governing equation (2.4) at time $i+1$ leading to:

$$-\mathbf{M}\,\ddot{\mathbf{u}}_i - \mathbf{a}\,\dot{\mathbf{u}}_i - \mathbf{b}\,\mathbf{u}_i + \mathbf{b}\,\mathbf{u}_{i+1} + \left(\mathbf{f}_s\right)_{i+1} = \mathbf{p}_{i+1} \tag{2.8}$$

where:

$$\mathbf{a} = \frac{4}{\Delta t}\mathbf{M} + \mathbf{c} \qquad \mathbf{b} = \frac{4}{(\Delta t)^2}\mathbf{M} + \frac{2}{\Delta t}\mathbf{c} \tag{2.9}$$

Equation (2.8) can also be written as:

$$\hat{\mathbf{p}}_{i+1} - \mathbf{b}\,\mathbf{u}_{i+1} - \left(\mathbf{f}_s\right)_{i+1} = \mathbf{0} \tag{2.10}$$

where $\hat{\mathbf{p}}_{i+1} = \mathbf{p}_{i+1} + \mathbf{M}\,\ddot{\mathbf{u}}_i + \mathbf{a}\,\dot{\mathbf{u}}_i + \mathbf{b}\,\mathbf{u}_i$ is known from the system properties and the response at time i, the beginning of the time step.

The system of nonlinear algebraic equations (2.10) can be solved for $\mathbf{u}_{i+1}$ by Newton or Quasi-Newton methods [Nocedal and Wright, 2006: Chapters 6 and 11]; alternatively, an event-to-event solution strategy can be employed.

Event-to-event solution strategy

In the event-to-event solution strategy, the time step i is subdivided into smaller sub-steps and the structure properties are re-formed if a nonlinear event occurs. Nonlinear events are defined as stiffness changes in the force-deformation relationship of the structural elements. PERFORM-3D uses this strategy to avoid possible convergence problems in an iterative procedure; however, because the solution is assumed to be linear between events, the P-Delta geometric stiffness is only evaluated at each event.

Substitution of $\mathbf{u}_i = \mathbf{u}^{(j)}$, $\mathbf{u}_{i+1} = \mathbf{u}^{(j)} + \Delta\mathbf{u}^{(j)}$, $\left(\mathbf{f}_s\right)_{i+1} = \left(\mathbf{f}_s\right)^{(j)} + \left(\Delta\mathbf{f}_s\right)^{(j)}$ and $\left(\mathbf{f}_s\right)^{(j)} = \mathbf{p}^{(j)} - \mathbf{M}\,\ddot{\mathbf{u}}^{(j)} - \mathbf{c}\,\dot{\mathbf{u}}^{(j)}$ into Eq. (2.8) leads to an incremental equation for the j th sub-step:

$$\Delta\hat{\mathbf{p}}^{(j)} - \mathbf{b}\,\Delta\mathbf{u}^{(j)} - \left(\Delta\mathbf{f}_s\right)^{(j)} = \mathbf{0} \tag{2.11}$$

where $\Delta\mathbf{u}^{(j)} = \mathbf{u}_{i+1} - \mathbf{u}^{(j)}$; $\Delta\hat{\mathbf{p}}^{(j)} = \mathbf{p}_{i+1} - \mathbf{p}^{(j)} + 2\mathbf{M}\,\ddot{\mathbf{u}}^{(j)} + (\mathbf{a}+\mathbf{c})\,\dot{\mathbf{u}}^{(j)}$; $\mathbf{u}^{(0)} = \mathbf{u}_i$; $\dot{\mathbf{u}}^{(0)} = \dot{\mathbf{u}}_i$; $\ddot{\mathbf{u}}^{(0)} = \ddot{\mathbf{u}}_i$; and $\mathbf{p}^{(0)} = \mathbf{p}_i$.

Eq. (2.11) can be solved for $\mathbf{u}_{i+1}$ by implementing the following procedure [adapted from Simons and Powell, 1982]:

1. Linearize about the current state. Assume the structure to be linear with stiffness $(\mathbf{k}_T)^{(j)}$, the tangent stiffness matrix at $\mathbf{u}^{(j)}$. Note that $(\mathbf{k}_T)^{(0)} = (\mathbf{k}_T)_i$.

2. Solve Eq. (2.11) for $\Delta\mathbf{u}^{(j)}$ assuming $(\Delta\mathbf{f}_s)^{(j)} = (\mathbf{k}_T)^{(j)}\Delta\mathbf{u}^{(j)}$:

   $$\Delta\mathbf{u}^{(j)} = \left[\mathbf{b} + (\mathbf{k}_T)^{(j)}\right]^{-1}\Delta\hat{\mathbf{p}}^{(j)}$$

3. Calculate the *event factor* λ_j as the fraction of the displacement increment $\Delta\mathbf{u}^{(j)}$ that can be applied before an event occurs [Chung and Campbell, 2006].

4. If no event takes place in the current j sub-step (i.e. $\lambda_j = 1.0$), the solution of Eq. (2.10) is $\mathbf{u}_{i+1} = \mathbf{u}^{(j)} + \Delta\mathbf{u}^{(j)}$. If λ_j is less than 1.0, determine the state of the structure at $\mathbf{u}^{(j+1)} = \mathbf{u}^{(j)} + \lambda_j\Delta\mathbf{u}^{(j)}$ and repeat steps 1 to 3.

2.3 Response Statistics

Nonlinear RHA of a building will be conducted to determine its response to each of n_{EQ} pairs of ground motions applied simultaneously in two horizontal directions (Fig. 2.1a). From the resulting data set of n_{EQ} values (x_i, $i = 1, 2, ...n_{EQ}$) for a response quantity, its median value $\hat{x}$ will be determined as the geometric mean of x_i [Benjamin and Cornell, 1970]:

$$\hat{x} = exp\left[\frac{1}{n_{EQ}}\sum_{i=1}^{n_{EQ}}\ln x_i\right] \tag{2.12}$$

In case one or more excitations cause collapse of the building or numerical instability in the response computation, the median is determined by the counting method. The x_i values are sorted in ascending order and the median is calculated as follows:

- If n_{EQ} is odd, $\hat{x}$ is the $[\frac{1}{2}(n_{EQ}+1)]$th value starting from the lowest value.
- If n_{EQ} is even, $\hat{x}$ is the average of the $[\frac{1}{2}n_{EQ}]$th and the $[\frac{1}{2}n_{EQ}+1]$th values.

3 Three-dimensional Modal Pushover Analysis (MPA)

This chapter presents the MPA procedure to estimate seismic demands for three-dimensional models of buildings subjected to two horizontal components of ground motion applied simultaneously, and its practical implementation. We introduce two approximate procedures to solve the equations of motion presented in Section 2.1: uncoupled modal response history analysis (UMRHA) and modal pushover analysis (MPA). Not intended for practical applications, UMRHA is included only to provide a rationale for the MPA procedure. Next, a step-by-step implementation of MPA is presented, followed by two additional versions of the MPA procedure: Modified MPA (MMPA) and Practical MPA (PMPA), the latter being especially convenient for practical application.

3.1 Modal expansion of forces

The right hand side of Eq. (2.1) may be interpreted as the effective earthquake forces:

$$\mathbf{p}_{eff}(t) = -\mathbf{s}_a\, \ddot{u}_{ga}(t) - \mathbf{s}_b\, \ddot{u}_{gb}(t) = -\mathbf{M}\boldsymbol{\iota}_a\, \ddot{u}_{ga}(t) - \mathbf{M}\boldsymbol{\iota}_b\, \ddot{u}_{gb}(t) \tag{3.1}$$

The spatial distribution of these forces over the building is defined by the vectors $\mathbf{s}_a = \mathbf{M}\boldsymbol{\iota}_a$ or $\mathbf{s}_b = \mathbf{M}\boldsymbol{\iota}_b$, and the time variation by $\ddot{u}_g(t) = \ddot{u}_{ga}(t)$ or $\ddot{u}_{gb}(t)$. This force distribution can be expanded as a summation of modal inertia force distributions $\mathbf{s}_n$ [Chopra, 2007]:

$$\mathbf{s}_a = \sum_{n=1}^{3N} \mathbf{s}_{na} = \sum_{n=1}^{3N} \Gamma_{na} \mathbf{M}\boldsymbol{\phi}_n \qquad \mathbf{s}_b = \sum_{n=1}^{3N} \mathbf{s}_{nb} = \sum_{n=1}^{3N} \Gamma_{nb} \mathbf{M}\boldsymbol{\phi}_n \tag{3.2}$$

where ϕ_n is the nth natural vibration mode of the system vibrating at small amplitudes (within its linearly elastic range) and

$$\Gamma_{na} = \frac{L_{na}}{M_n} = \frac{\phi_n^T \mathbf{M} \boldsymbol{\iota}_a}{\phi_n^T \mathbf{M} \phi_n} \qquad \Gamma_{nb} = \frac{L_{nb}}{M_n} = \frac{\phi_n^T \mathbf{M} \boldsymbol{\iota}_b}{\phi_n^T \mathbf{M} \phi_n} \tag{3.3}$$

Therefore, the effective earthquake forces can be expressed as the sum of the contributions of the 3N modes:

$$\mathbf{p}_{eff} = \sum_{n=1}^{3N} \mathbf{p}_{eff,n}(t) = \sum_{n=1}^{3N} \left[\mathbf{p}_{eff,na}(t) + \mathbf{p}_{eff,nb}(t) \right] = -\sum_{n=1}^{3N} \left[\mathbf{s}_{na} \ddot{u}_{ga}(t) + \mathbf{s}_{nb} \ddot{u}_{gb}(t) \right] \tag{3.4}$$

The $\mathbf{s}_n$ vectors associated with a and b components of ground motions may be expressed as:

$$\mathbf{s}_{na} = \begin{bmatrix} \mathbf{s}_{xn,a} \\ \mathbf{s}_{yn,a} \\ \mathbf{s}_{\theta n,a} \end{bmatrix} = \Gamma_{na} \begin{bmatrix} \mathbf{m}\phi_{xn} \\ \mathbf{m}\phi_{yn} \\ \mathbf{I}_O \phi_{\theta n} \end{bmatrix} \qquad \mathbf{s}_{nb} = \begin{bmatrix} \mathbf{s}_{xn,b} \\ \mathbf{s}_{yn,b} \\ \mathbf{s}_{\theta n,b} \end{bmatrix} = \Gamma_{nb} \begin{bmatrix} \mathbf{m}\phi_{xn} \\ \mathbf{m}\phi_{yn} \\ \mathbf{I}_O \phi_{\theta n} \end{bmatrix} \tag{3.5}$$

3.2 Uncoupled Modal Response History Analysis (UMRHA)

3.2.1 Linear systems

The classical modal analysis procedure may be interpreted as finding the response of the structure to $\mathbf{p}_{eff,n}(t)$ for each n and superposing the response for all n. The response of the system to $\mathbf{p}_{eff,n}(t)$ is entirely in the nth-mode, with no contribution from other modes, which implies that the modes are uncoupled. Then, the floor displacements are given by:

$$\mathbf{u}_n(t) = \phi_n q_n(t) \tag{3.6}$$

where the modal coordinate is governed by:

$$\ddot{q}_n(t) + 2\zeta_n \omega_n \dot{q}_n(t) + \omega_n^2 q_n(t) = -\Gamma_{na} \ddot{u}_{ga}(t) - \Gamma_{nb} \ddot{u}_{gb}(t) \tag{3.7}$$

in which ω_n is the natural frequency and ζ_n is the damping ratio of the *n*th mode. The solution $q_n(t)$ of Eq. (3.7) is given by:

$$q_n(t) = \Gamma_{na} D_{na}(t) + \Gamma_{nb} D_{nb}(t) \tag{3.8}$$

where $D_{na}(t)$ and $D_{nb}(t)$ are the deformation responses of the *n*th-mode SDF system, an SDF system with vibration properties—natural frequency ω_n (natural period $T_n = 2\pi / \omega_n$) and damping ratio ζ_n—of the *n*th-mode of the MDF system, subjected to $\ddot{u}_{ga}(t)$ and $\ddot{u}_{gb}(t)$, respectively. They are governed by:

$$\ddot{D}_n(t) + 2\zeta_n \omega_n \dot{D}_n(t) + \omega_n^2 D_n(t) = -\ddot{u}_g(t)$$

$$D_n(t) = D_{na}(t) \text{ or } D_{nb}(t) \qquad \ddot{u}_g(t) = \ddot{u}_{ga}(t) \text{ or } \ddot{u}_{gb}(t) \tag{3.9}$$

Substituting Eq. (3.8) into (3.6) gives the lateral displacements in the *x* and *y* directions and torsional rotations of the floors:

$$\mathbf{u}_n(t) = \Gamma_{na} \boldsymbol{\phi}_n D_{na}(t) + \Gamma_{nb} \boldsymbol{\phi}_n D_{nb}(t) \tag{3.10}$$

Superposing the response of the system to $\mathbf{p}_{eff,n}(t)$ [Eq. (3.10)] gives the response of the system due to total excitation $\mathbf{p}_{eff}(t)$:

$$r(t) = \sum_{n=1}^{3N} r_n(t) \tag{3.11}$$

where $r_n(t)$ may represent any response quantity (floor displacements, floor accelerations, floor velocities, story drifts, or element forces).

This is the UMRHA procedure for exact analysis of elastic systems, which is equivalent to the classical modal RHA. Equation (3.7) is the standard equation governing the modal coordinate $q_n(t)$; Eq. (3.10) defines the contribution of the *n*th-mode to the

response, and Eq. (3.11) combines the response contribution of all modes. However, these standard equations have been derived in an unconventional way. In contrast to the classical derivation found in textbooks [e.g., Chopra, 2007: Chapter 13], we have used the modal expansion of spatial distribution of the effective forces. This concept will provide a rational basis for the modal pushover analysis procedure to be developed later.

3.2.2 Nonlinear systems

Although modal analysis is not valid for a nonlinear system, its response can be usefully discussed in terms of the modal coordinates of the corresponding linear system. Each structural element of this linear system is defined to have the same stiffness as the initial stiffness of the same structural element of the nonlinear system. Both systems have the same mass and damping. Therefore, the natural vibration periods and modes of the corresponding linear system are the same as the vibration properties—referred to as natural "periods" and "modes"—of the nonlinear system undergoing small oscillation.

The response of a nonlinear system to excitation $\mathbf{p}_{eff,n}(t)$ will no longer be described by Eq. (3.6) because "modes" other than the nth "mode" will also contribute to the response, implying that the vibration modes of the corresponding linear system are now coupled; thus the floor displacements are given by the first part of Eq. (3.12)

$$\mathbf{u}_n(t) = \sum_{i=1}^{3N} \phi_i q_i(t) \approx \phi_n q_n(t) \tag{3.12}$$

However, because for linear systems $q_r(t) = 0$ for all modes other than the nth-mode, it is reasonable to expect that $q_r(t)$ may be small for nonlinear systems, implying that the "modes" are, at most, weakly coupled.

The above-mentioned expectation is investigated numerically in Figs. 3.1 to 3.3 for buildings with coupled shear walls (Fig. 3.1), unsymmetric-plan (Fig. 3.2), and metallic dampers (Fig. 3.3). Their response to $\mathbf{p}_{eff,n}(t)$ associated with one component of ground motion was determined by nonlinear RHA and the resulting roof displacement histories in the x-direction at the C.M. were decomposed into its modal components. Figures 3.1 to 3.3 include only the four modes that have the largest contribution to roof displacement in the x-direction. The roof-displacement response for the 48-story building with coupled shear walls (Fig. 3.1) and for the nine-story unsymmetric-plan building (Fig. 3.2) is dominated by the nth-"mode" component, but the other modes start responding after the structure yields. For both buildings, responses in modes other than the nth mode are small. For the nine-story building with metallic dampers, the degree of modal coupling is significant for $\mathbf{p}_{eff,n}(t)$ with n=4 and 7. For n=4, the contribution of the first mode is about 74% of that from the fourth mode (Fig. 3.3b). For n=7, the contribution of the fourth mode is about 43% of that from the seventh mode (Fig. 3.3c). For n=1 and 9, however, the degree of modal coupling is insignificant.

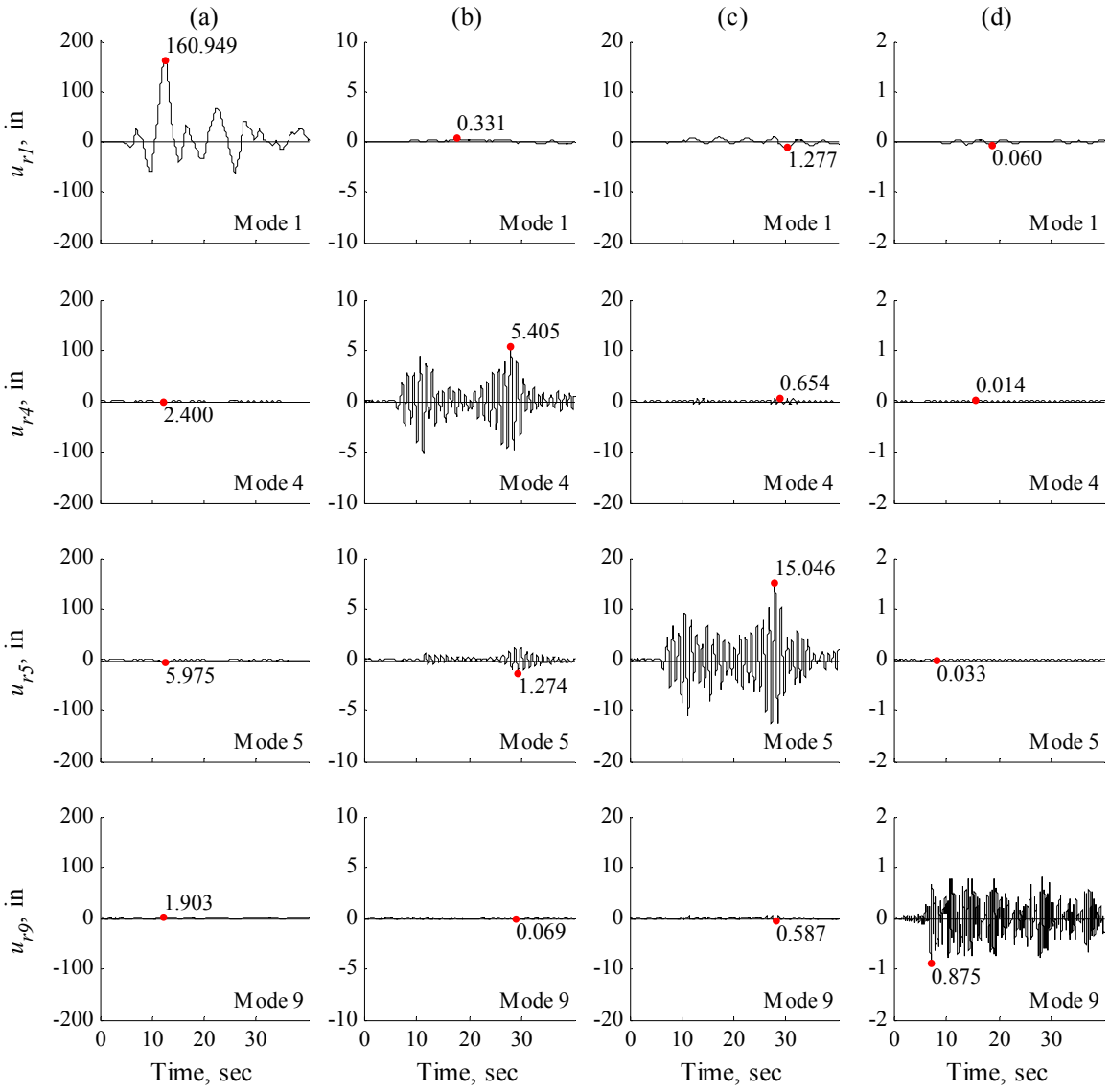

Figure 3.1 Modal decomposition of roof displacements in the *x*-direction for a 48-story building with coupled shear walls due to $\mathbf{p}_{eff,n}(t)=-\mathbf{s}_n\,\ddot{u}_g(t)$, n=1, 4, 5, and 9, where $\ddot{u}_g(t)$=component 1 of the 1999 Chi-chi earthquake at TCU065 station scaled by a factor of 1.55: (a) $\mathbf{p}_{eff,1}(t)=-\mathbf{s}_1\,\ddot{u}_g(t)$; (b) $\mathbf{p}_{eff,4}(t)=-\mathbf{s}_4\,\ddot{u}_g(t)$; (c) $\mathbf{p}_{eff,5}(t)=-\mathbf{s}_5\,\ddot{u}_g(t)$; and (d) $\mathbf{p}_{eff,9}(t)=-\mathbf{s}_9\,\ddot{u}_g(t)$. Modes 1, 4, 5 and 9 have the highest contribution to roof displacement in the *x*-direction.

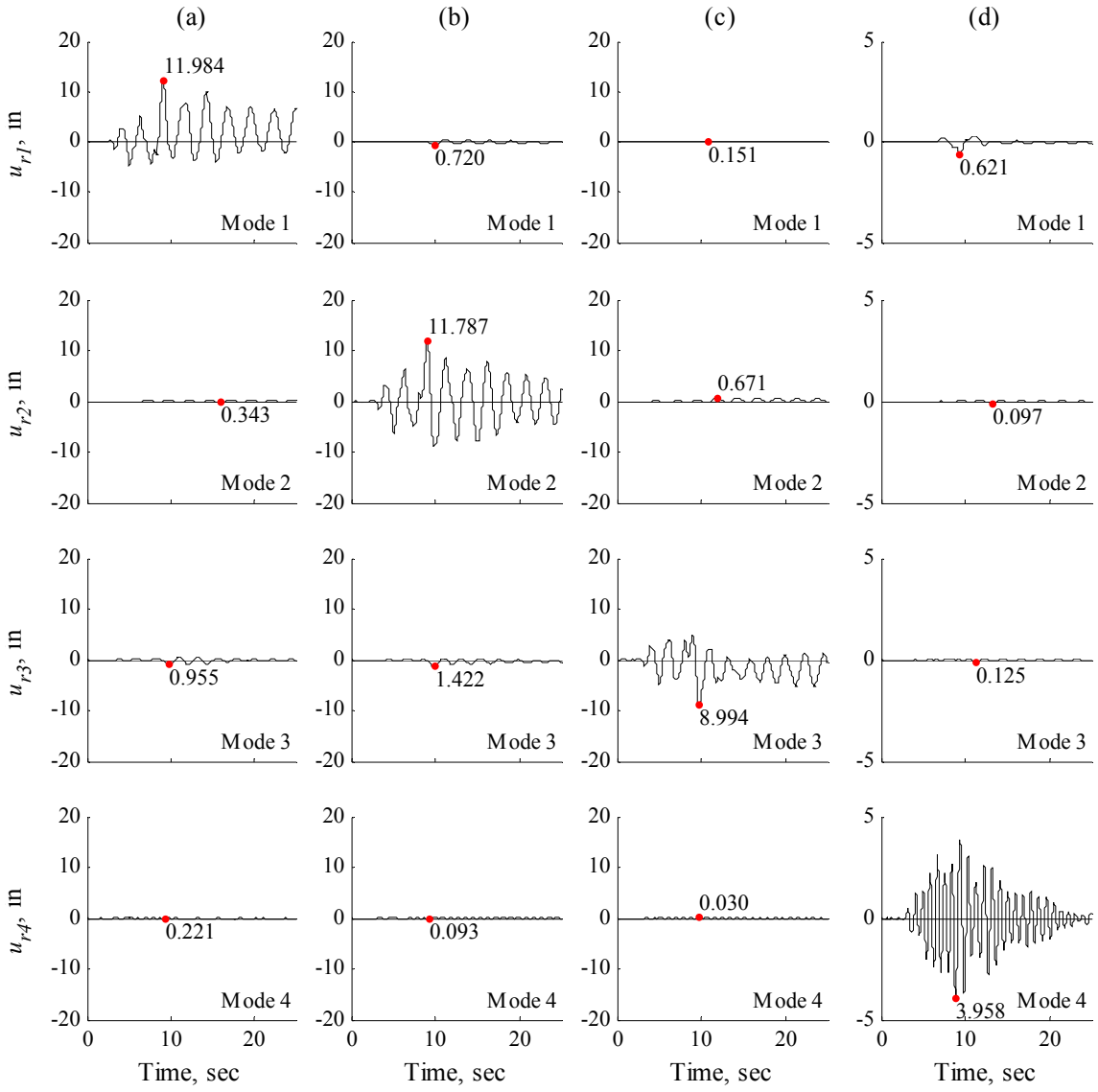

Figure 3.2 Modal decomposition of roof displacements in the *x*-direction for a nine-story unsymmetric-plan building designed according to 1985 Uniform Building Code due to $\mathbf{p}_{eff,n}(t)=-\mathbf{s}_n\,\ddot{u}_g(t)$, n=1, 2, 3, and 4, where $\ddot{u}_g(t)$=component 1 of the 1994 Northridge earthquake at Beverly Hills 14145 Mulhol station scaled by a factor of 2.07: (a) $\mathbf{p}_{eff,1}(t)=-\mathbf{s}_1\,\ddot{u}_g(t)$; (b) $\mathbf{p}_{eff,2}(t)=-\mathbf{s}_2\,\ddot{u}_g(t)$; (c) $\mathbf{p}_{eff,3}(t)=-\mathbf{s}_3\,\ddot{u}_g(t)$; and (d) $\mathbf{p}_{eff,4}(t)=-\mathbf{s}_4\,\ddot{u}_g(t)$.

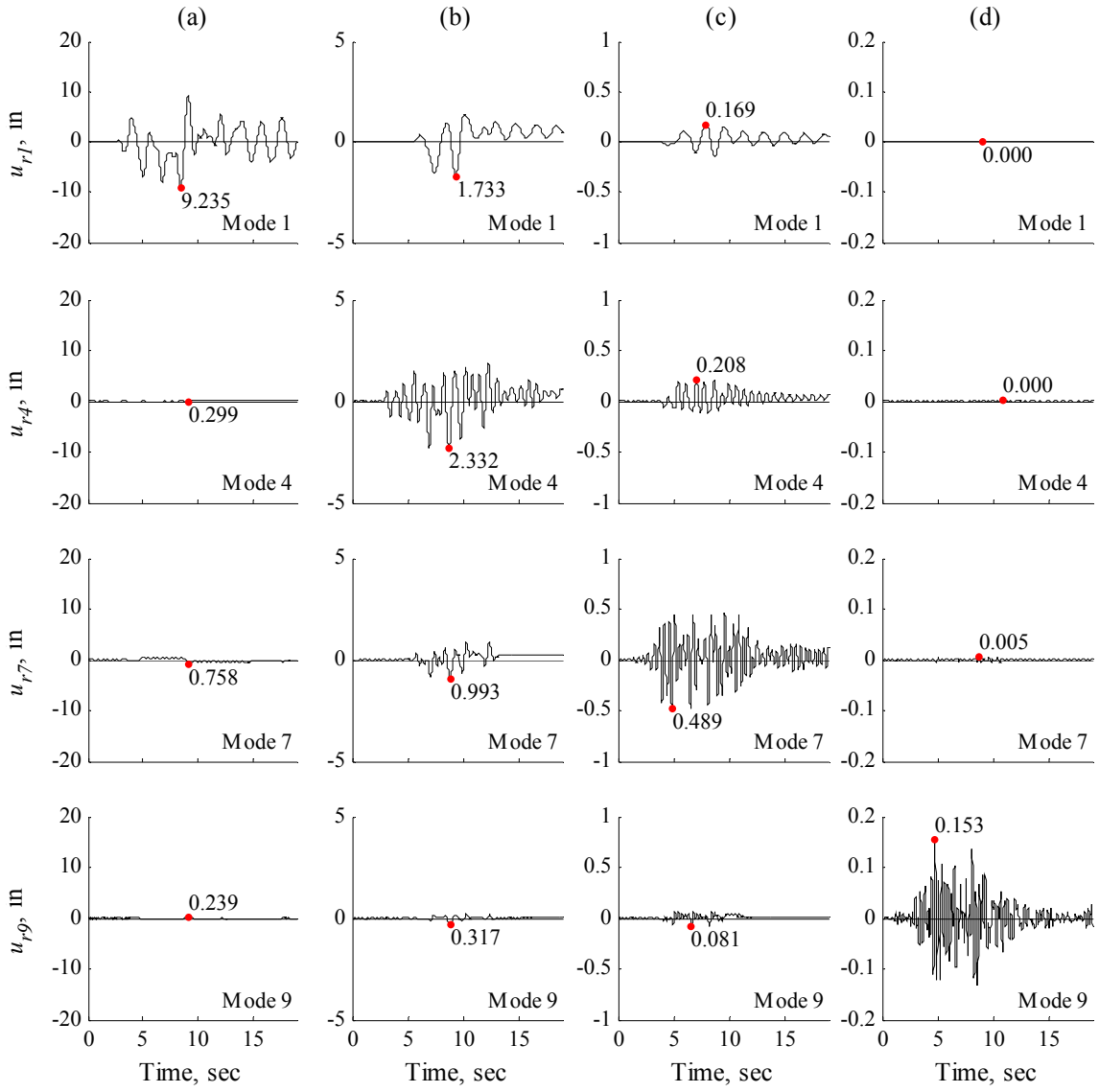

Figure 3.3 Modal decomposition of roof displacements in the *x*-direction for a symmetric nine-story building with metallic dampers due to $\mathbf{p}_{eff,n}(t)=-\mathbf{s}_n \ddot{u}_g(t)$, n=1, 4, 7, and 9, where $\ddot{u}_g(t)$=component 1 of the 1994 Northridge earthquake at Beverly Hills 14145 Mulhol station scaled by a factor of 0.99: (a) $\mathbf{p}_{eff,1}(t)=-\mathbf{s}_1 \ddot{u}_g(t)$; (b) $\mathbf{p}_{eff,4}(t)=-\mathbf{s}_4 \ddot{u}_g(t)$; (c) $\mathbf{p}_{eff,7}(t)=-\mathbf{s}_7 \ddot{u}_g(t)$; and (d) $\mathbf{p}_{eff,9}(t)=-\mathbf{s}_9 \ddot{u}_g(t)$. Modes 1, 4, 7 and 9 have the highest contribution to roof displacement in the *x*-direction.

These observations suggest that approximate analysis procedures based on modal uncoupling approximation are expected to be accurate for the 48-story building with coupled shear walls and the nine-story building with unsymmetric-plan. For such cases, it is possible to approximate the structural response due to excitation $\mathbf{p}_{eff,n}(t)$ by the second half of Eq. (3.12) where $q_n(t)$ due to one component of ground motion is governed by:

$$\ddot{q}_n(t) + 2\zeta_n \omega_n \dot{q}_n(t) + \frac{F_{sn}}{M_n} = -\Gamma_n \ddot{u}_g(t) \tag{3.13}$$

where F_{sn} is a nonlinear hysteretic relationship that depends on q_n:

$$F_{sn} = F_{sn}(q_n) = \phi^T \mathbf{f}_s(q_n) \tag{3.14}$$

If the contributions of other modes had not been neglected, F_{sn} would depend on all modal coordinates, implying coupling of modal coordinates because of yielding of the structure.

With the above-stated approximation, the solution of Eq. (3.13) can be expressed by Eq. (3.8), specialized for one component of ground motion, where $D_n(t)$ is governed by:

$$\ddot{D}_n(t) + 2\zeta_n \omega_n \dot{D}_n(t) + \frac{F_{sn}}{L_n} = -\ddot{u}_g(t) \tag{3.15}$$

$D_n(t)$ may be interpreted as the deformation response of the *n*th-"mode" inelastic SDF system, an SDF with (1) small-oscillation vibration properties—natural frequency ω_n and damping ratio ζ_n—of the *n*th-mode of the corresponding linear system; and (2) $F_{sn}/L_n - D_n$ relation between resisting force and deformation, where

$$F_{sn} = F_{sn}(D_n) = \phi_n^T \mathbf{f}_s(D_n) \tag{3.16}$$

which will be determined by nonlinear static analysis of the system using modal force distributions based on $\mathbf{s}_n$ [Eq. (3.5)]. Introducing the *n*th-"mode" inelastic SDF system permitted extension of the well-established concepts for linear systems to nonlinear systems; compare Eq. (3.7) to (3.13), Eq. (3.9) to (3.15), and note that Eq. (3.8) applies for both systems.

Solution of the nonlinear Eq. (3.15) provides $D_n(t)$, which when substituted into Eq. (3.10) gives floor displacements. Equation (3.10) approximates the response of the nonlinear MDF system to $\mathbf{p}_{eff,n}(t)$, the *n*th-mode contribution to $\mathbf{p}_{eff}(t)$. The superposition of responses to $\mathbf{p}_{eff,n}(t)$, according to Eq. (3.11) to find the total response to $\mathbf{p}_{eff}(t)$, is exact for linear systems but only approximate for nonlinear systems. This is the UMRHA procedure for approximate analysis of nonlinear systems. When specialized for linearly elastic systems, it becomes identical to the rigorous classical modal RHA.

3.3 Modal Pushover Analysis (MPA)

3.3.1 Linear systems

Consider the lateral forces $\mathbf{f}_{xn}$ and $\mathbf{f}_{yn}$ in the *x* and *y* directions and torques $\mathbf{f}_{\theta n}$ defined by Eq. (3.17) for one component of ground motion.

$$\mathbf{f}_{xn} = \mathbf{s}_{xn} A_n \qquad \mathbf{f}_{yn} = \mathbf{s}_{yn} A_n \qquad \mathbf{f}_{\theta n} = \mathbf{s}_{\theta n} A_n \tag{3.17}$$

where $\mathbf{s}_{xn}$, $\mathbf{s}_{yn}$, and $\mathbf{s}_{\theta n}$ are given by Eq. (3.5), A_n is equal to $\omega_n^2 D_n$, and D_n is the peak deformation of the *n*th-mode linear SDF system, determined by solving Eq. (3.9) for $D_n(t)$. Note that A_n is also the ordinate $A(T_n, \zeta_n)$ of the earthquake pseudo-acceleration response spectrum for the *n*th-mode SDF system. Static analysis of the structure

subjected to forces defined by Eq. (3.17) will provide the peak value r_n of the nth-mode contribution $r_n(t)$ to $r(t)$ [Chopra, 2007; Section 13.9]; recall that the $r_n(t)$ for floor displacements due to one ground motion component is given by one term of Eq. (3.10).

Alternatively, this peak modal response can be obtained by static analysis of the structure subjected to lateral forces and torques defined by the modal force distribution $\mathbf{s}_n^* = \mathbf{s}_{na}^*$ or $\mathbf{s}_{nb}^*$:

$$\mathbf{s}_n^* = sign(\Gamma_n) \begin{bmatrix} \mathbf{m}\phi_{xn} \\ \mathbf{m}\phi_{yn} \\ \mathbf{I}_O\phi_{\theta n} \end{bmatrix} \tag{3.18}$$

and increasing forces to push the structure to the reference displacements:

$$u_{rxn} = \Gamma_n \phi_{rxn} D_n \qquad u_{ryn} = \Gamma_n \phi_{ryn} D_n \qquad u_{r\theta n} = \Gamma_n \phi_{r\theta n} D_n$$

$$\Gamma_n = \Gamma_{na} \text{ or } \Gamma_{nb} \qquad D_n = D_{na} \text{ or } D_{nb} \tag{3.19}$$

The reference point can be located at any floor of the structure; usually, it is chosen as the roof. For linear structures, $\mathbf{s}_n^*$ is the only force distribution that produces displacements proportional to the nth vibration mode. Therefore, the three components of roof displacement of a linear system will simultaneously reach the values given by Eq. (3.19).

The peak modal response $r_n = r_{na}$ or r_{nb}, each determined by one modal pushover analysis, can be combined by the Complete Quadratic Combination (CQC) rule [Chopra, 2007; Section 13.7], a rule suitable for unsymmetric-plan buildings, which may have closely-spaced frequencies of vibration. This MPA procedure for linear elastic systems is identical to the standard response spectrum analysis (RSA) procedure.

The RSA procedure determines the peak response of the structure to one component of ground motion, thus, such analyses are implemented for each component of the ground

motion (*a* and *b*), independently, and the final results (r_a and r_b) are combined using one of the available multi-component combination rules [Newmark, 1976; Rosenblueth and Contreras, 1977; Menun and Der Kiureghian, 1998]. For this research, we use the SRSS rule:

$$r = \sqrt{r_a^2 + r_b^2} \tag{3.20}$$

The basic assumption of this rule is that the response quantities r_a and r_b are statistically independent. This rule is accurate if the assumed horizontal ground motion components are along the principal axes of the earthquake, or if input components are of equal intensity [Smeby and Der Kiureghian, 1985]. The first condition is usually not satisfied because the directions of the recorded ground motion components are chosen to coincide with the longitudinal and transverse axis of the structure. Because the median response spectra for the two horizontal components of the ensemble of ground motions considered in this investigation are of comparable intensity, the SRSS rule is selected.

3.3.2 Nonlinear systems

In the MPA procedure, the peak response r_n of the building to the *n*th mode component of the effective earthquake forces $\mathbf{p}_{eff,n}(t)$ associated with one component of ground motion is estimated by a non-linear static analysis of the structure subjected to lateral forces and torques distributed over the building height according to $\mathbf{s}_n^*$ [Eq. (3.18)] with the forces increased to push the structure up to reference displacements u_{rxn}, u_{ryn} and $u_{r\theta n}$. These values of the reference displacement components are determined from Eq. (3.19), as for linear systems, but D_n is now the peak deformation of the *n*th-"mode" inelastic SDF system [Eq. (3.15)]. The results of nonlinear static analysis at this reference

displacement provides an estimate of the peak value r_n of response quantity $r_n(t)$: floor displacements, story drifts, and other deformation quantities.

For a nonlinear system, no invariant distribution of forces will produce displacements proportional to the *n*th elastic mode. Therefore, the three components of reference displacements of a nonlinear system will not simultaneously reach the values given by Eq. (3.19). One of the two lateral components will be selected as the controlling displacement; the choice of the component would be in the direction of the dominant motion in the mode being considered. For this controlling component, the reference displacement can be calculated as:

$$u_{rn} = u_{rg} + \Gamma_n \phi_{rn} D_n$$

$$\Gamma_n = \Gamma_{na} \text{ or } \Gamma_{nb} \qquad D_n = D_{na} \text{ or } D_{nb} \tag{3.21}$$

where u_{rg} is the displacement at the reference point due to gravity loads.

Nonlinear static analysis using force distribution $\mathbf{s}_n^* = \mathbf{s}_{na}^*$ or $\mathbf{s}_{nb}^*$ leads to the *n*th-mode pushover curve, a plot of base shear V_{bn} versus the displacement at the reference point u_{rn} in the appropriate (*x* or *y*) direction. From the *n*th "mode" pushover curve is obtained the force-deformation $(F_{sn} / L_n - D_n)$ relation for the *n*th "mode" inelastic SDF system, which is required in Eq. (3.15). The forces and deformations in the two sets of curves are related as follows:

$$\frac{F_{sn}}{L_n} = \frac{V_{bn}}{M_n^*} \qquad D_n = \frac{u_{rn} - u_{rg}}{\Gamma_n \phi_{rn}} \tag{3.22}$$

in which $M_n^* = L_n \Gamma_n$ is the effective modal mass of the *n*th-mode.

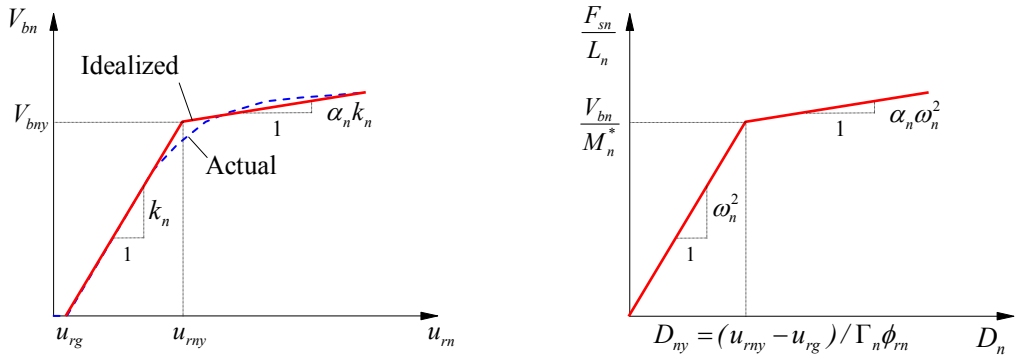

Figure 3.4 Properties of the *n*th "mode" inelastic SDF system from the pushover curve: (a) idealized pushover curve; (b) F_{sn} / L_n—D_n relationship.

Figure 3.4 shows schematically the *n*th "mode" pushover curve and its bilinear idealization; at the yield point the force F_{sny} and deformation D_{ny} are related through:

$$\frac{F_{sny}}{L_n} = \omega_n^2 D_{ny} \tag{3.23}$$

Knowing F_{sny} / L_n and D_{ny} from Eq. (3.23), the elastic vibration period T_n of the *n*th "mode" inelastic SDF system is given by:

$$T_n = 2\pi \left(\frac{L_n D_{ny}}{F_{sny}} \right)^{1/2} \tag{3.24}$$

In an unsymmetric-plan building the nonlinear static procedure leads to two pushover curves corresponding to the two lateral directions, *x* and *y*. It would be natural to use the *x* (or *y*) pushover curve for a mode in which the *x* (or *y*) component of displacements is dominant compared to their *y* (or *x*) component.

The response value r_n determined by pushover analysis is an estimate of the peak value of the response $r_n(t)$ of the nonlinear structure to $\mathbf{p}_{eff,n}(t)$; but it is not identical to another estimate determined by UMRHA. As mentioned earlier, r_n determined by

pushover analysis of a linearly elastic system is the exact peak value $r_n(t)$, the nth-mode contribution to response $r(t)$. Thus we will refer to r_n as the peak "modal" response even in the case of nonlinear systems. However, for nonlinear systems the two—UMRHA and MPA—estimates of the peak "modal" response are both approximate and different from each other; the only exception is the controlling component of the reference displacement. They differ because the underlying analyses involve different assumptions. The UMRHA is based on the approximation contained in the second half of Eq. (3.12), which is avoided in MPA because the displacements and drifts are determined by non-linear static analysis using force distribution $\mathbf{s}_n^*$. As a result, the floor displacements are no longer proportional to the mode shape, as implied by Eq. (3.12). In this sense, the MPA procedure represents the nonlinear behavior of the structure better than UMRHA.

However, the MPA procedure contains a different source of approximation, which does not exist in UMRHA. The peak "modal" responses r_n, each determined by one pushover analysis, are combined by the CQC rule, just as for linear systems. This application of modal combination rules to nonlinear systems obviously lacks a rigorous theoretical basis, but seems reasonable if the modes are only weakly coupled.

The MPA procedure determines the peak response of the structure to one component of ground motion; such analyses are implemented for each component of the ground motion (*a* and *b*), independently, and the responses due to individual components are combined using one of the available multi-component combination rules (Section 3.3.1). The use of multi-component combination rules which are intended for linear systems, introduces an additional source of approximation in the MPA procedure.

For nonlinear systems subjected to two horizontal components of ground motion applied simultaneously, the MPA procedure is based on three approximations: (1) neglecting the weak coupling of modes in computing the peak "modal" responses $r_{n,a}$ (and $r_{n,b}$) of the nonlinear system; (2) the use of combination rules to obtain the total response r_a (and r_b); and (3) the use of multi-component combination rules to determine the response to both components of ground motion, simultaneously.

3.4 Step-by-step Summary

The seismic demands—floors displacements and story drifts at the C.M.—for a symmetric or unsymmetric plan building subjected to two horizontal components of ground motion can be estimated by the MPA procedure, which is summarized in step-by-step form (adapted from Chopra [2007]):

1. Compute the natural frequencies, ω_n, and modes, ϕ_n, for linearly elastic vibration of the building.
2. For the *n*th mode, develop the base shear-reference displacement, $V_{bn,a} - u_{rn,a}$, pushover curve by non-linear static analysis of the building applying the force distribution $\mathbf{s}_{na}^{*}$ [Eq. (3.18)]. The reference point is located at the C.M. of the roof, but other floors may be chosen; and the component chosen is in the direction of the dominant motion in the mode being considered. Gravity loads are applied before the lateral forces causing roof displacement u_{rg}.
3. Idealize the $V_{bn,a} - u_{rn,a}$ pushover curve pushover curve as a bilinear or trilinear curve, as appropriate, and convert it into the force-deformation, $F_{sn} / L_n - D_n$, relation for the *n*th-mode inelastic SDF system by utilizing Eq. (3.22). Starting with

this initial loading curve, define the unloading and reloading branches appropriate for the structural system and material being considered.

4. Calculate the reference displacement $u_{rn,a} = u_{rg} + \Gamma_{na}\,\phi_{rn}\,D_{na}$ (Eq. 3.21) for the *a*-component of the ground motion. The peak deformation D_{na} of the *n*th mode inelastic SDF system, defined by the force-deformation relation developed in Step 3 and estimated damping ratio ζ_n, is determined by solving Eq. (3.15) using nonlinear RHA. Figure 3.5 presents a summary of steps 1 through 4.
5. From the pushover database (step 2), extract the response values $r_{n+g,a}$ due to the combined effects of gravity and lateral forces at reference displacements $u_{rn,a}$ determined in Step 4.
6. Compute the dynamic response due to the *n*th "mode": $r_{na} = r_{n+g,a} - r_g$; where $r_{n+g,a}$ are the response quantities obtained in step 5, and r_g are the contributions of gravity loads alone.
7. Repeat steps 2 through 6 for as many modes as required for sufficient accuracy.
8. Determine the total dynamic responses for the *a*-component of the ground motion by combining the peak modal responses using the CQC rule, i.e. $r_a = \left(\sum_i \sum_n \rho_{in} r_{ia} r_{na} \right)^{1/2}$.
9. Repeat steps 2 through 8 to determine the total dynamic response r_b due to the *b*-component of ground motion. Figure 3.6 presents a summary of steps 5 through 9.

10. Combine the responses r_a and r_b by a multi-component combination rule (e.g. Eq. 3.20) to determine the dynamic response r, and, then, compute the total responses $r_T = r_g \pm r$ (Fig. 3.7); where r_g are the responses due to gravity loads.

Steps 1 through 10 can be used to estimate floor displacements and story drifts at the C.M., but not directly for member forces or end rotations.

The MPA procedure for estimating seismic deformation for buildings subjected to one component of ground motion has been extended to estimate member forces [Goel and Chopra, 2005]. In this approach, the member forces are first computed by implementing the above-described MPA procedure and compared with the member capacity. If the computed member force exceeds the member capacity, it is recomputed from the MPA estimate of member end rotations using the nonlinear force-deformation (or moment-rotation) relationship for the member. In its present form, this procedure does not lead itself to automation in a large computer code. To overcome this disadvantage, this procedure is implemented by first applying gravity loads, and then imposing at the C.M. of the building model a set of displacements that are compatible with the MPA estimates of story drifts. This nonlinear static analysis provides internal forces if both ends of an element develop plastic hinges. Otherwise, internal forces are determined by implementing Steps 1-10 described above. This alternative procedure has the advantage of determining internal forces directly from the computer model.

The preceding procedure, extended to two components of ground motion, is implemented as follows:

11. Estimate other deformation quantities such as story drifts at locations other than the C.M., and plastic hinge rotations from the total displacements. First apply gravity loads and then impose at the C.M. a set of displacements $\mathbf{u}'_x$ and $\mathbf{u}'_y$ that are compatible with the drifts calculated in Step 10, i.e. $u'_{jx} = \sum_{i=1}^{j} \Delta_{jx}^T$ and $u'_{jy} = \sum_{i=1}^{j} \Delta_{jy}^T$. Four combinations of these displacements should be imposed: $\mathbf{u}'_x + \mathbf{u}'_y$, $\mathbf{u}'_x - \mathbf{u}'_y$, $-\mathbf{u}'_x + \mathbf{u}'_y$, $-\mathbf{u}'_x - \mathbf{u}'_y$. The largest of the resulting four values of a response quantity is taken as the PMPA estimate. Required for this purpose is a computer program—such as SAP2000—that allows displacements to be imposed instead of loads on the structure. In computer programs that do not allow imposing displacements—such as PERFORM-3D—a model combining lateral forces with bidirectional "gap" elements at each floor could be implemented (see Appendix A).
12. Using the plastic hinge rotations obtained in Step 11, internal forces are determined as follows. If both ends of an element deform into the inelastic range, internal forces are those obtained in Step 11. Otherwise, determine internal forces by implementing Steps 2 to 10. These results are valid if the calculated bending moments, M, do not exceed the yield capacities, M_y, of the structural members. If $M > M_y$, scale the internal forces by a factor equal to M_y / M.

The preceding computational steps were implemented for each of the n_{EQ} ground motions and the median of the resulting data set values for a response quantity was calculated as explained in Section 2.3.

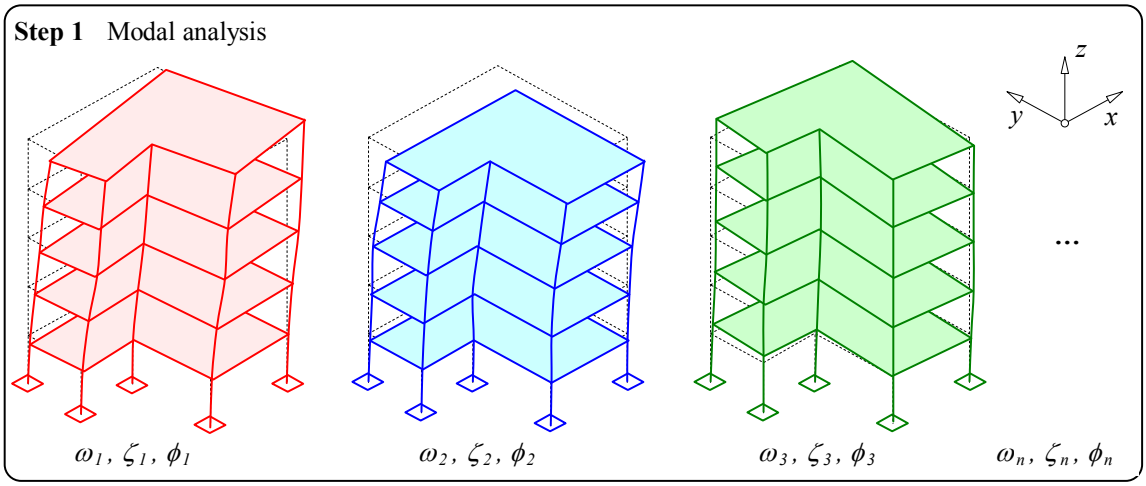

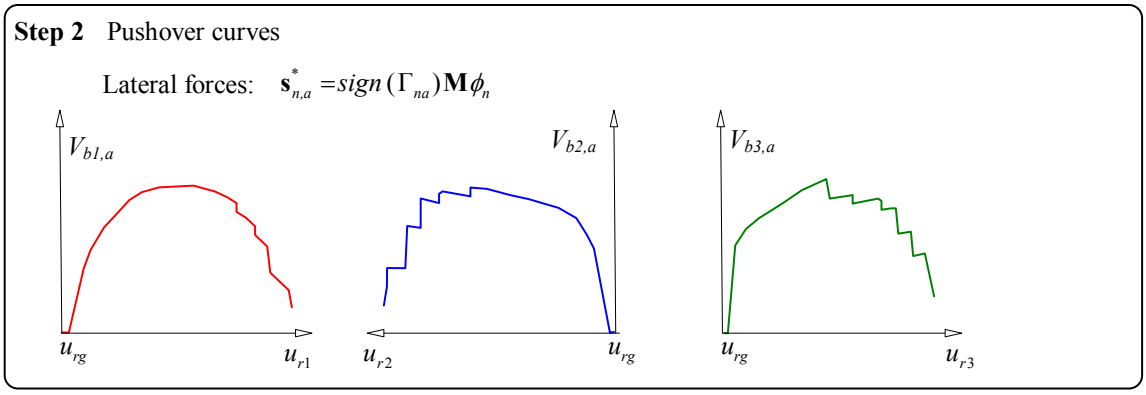

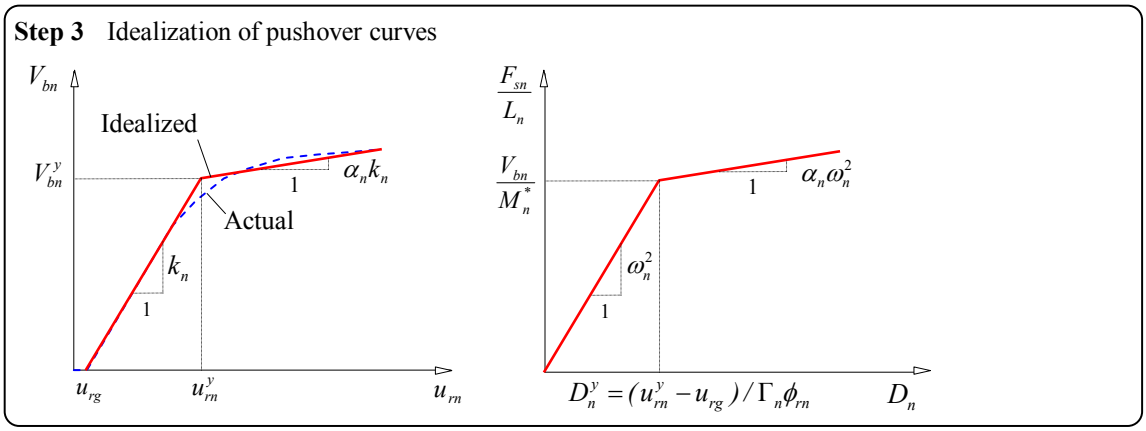

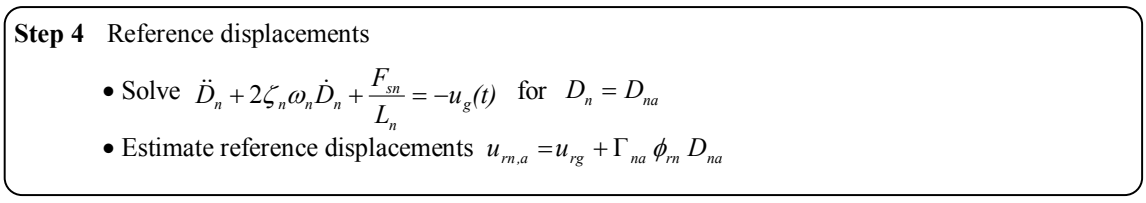

Figure 3.5 Step-by-step summary of the MPA procedure (steps 1 through 4).

Step 5 Extraction of response values from the pushover database

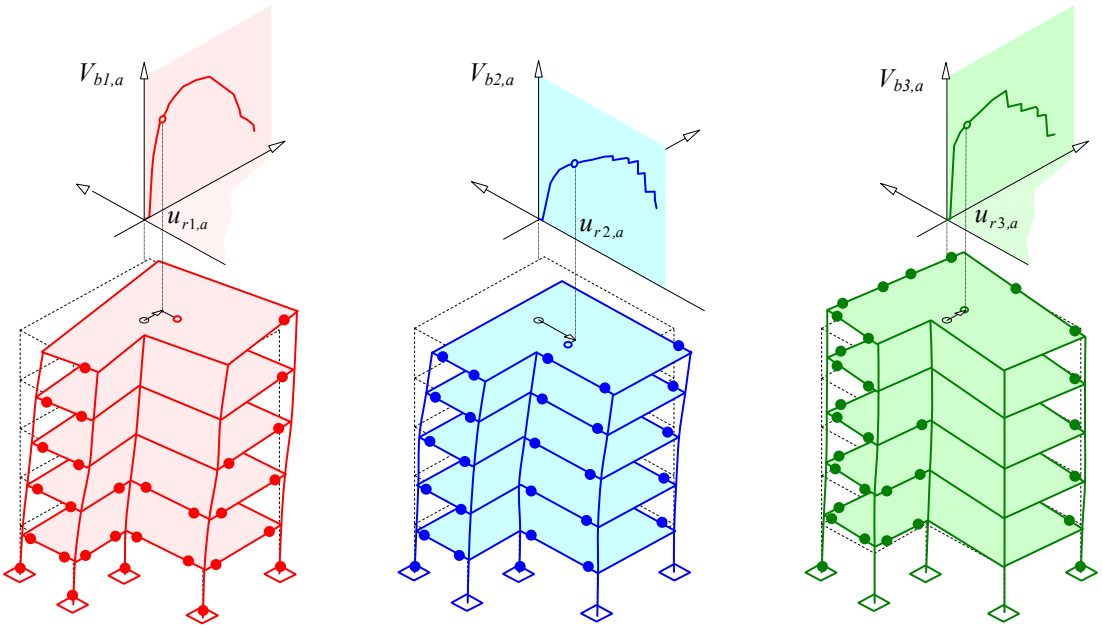

Step 6 Nonlinear modal dynamic responses

$$r_{na} = r_{n+g,a} - r_g \quad \begin{cases} \mathbf{u}_{na} = \mathbf{u}_{n+g,a} - \mathbf{u}_g \\ \boldsymbol{\Delta}_{na} = \boldsymbol{\Delta}_{n+g,a} - \boldsymbol{\Delta}_g \end{cases}$$

Step 7 Repeat steps 2 to 5 for as many modes as required for sufficient accuracy

Step 8 Seismic responses at the center of mass for a single component of the ground motion

$$r_a = \left(\sum_i \sum_n \rho_{in} r_{ia} r_{na} \right)^{1/2}$$

Step 9 Repeats steps 2 to 8 to determine the total dynamic response r_b due to the *b*-component of ground motion.

Figure 3.6 Step-by-step summary of the MPA procedure (Steps 5 through 9).

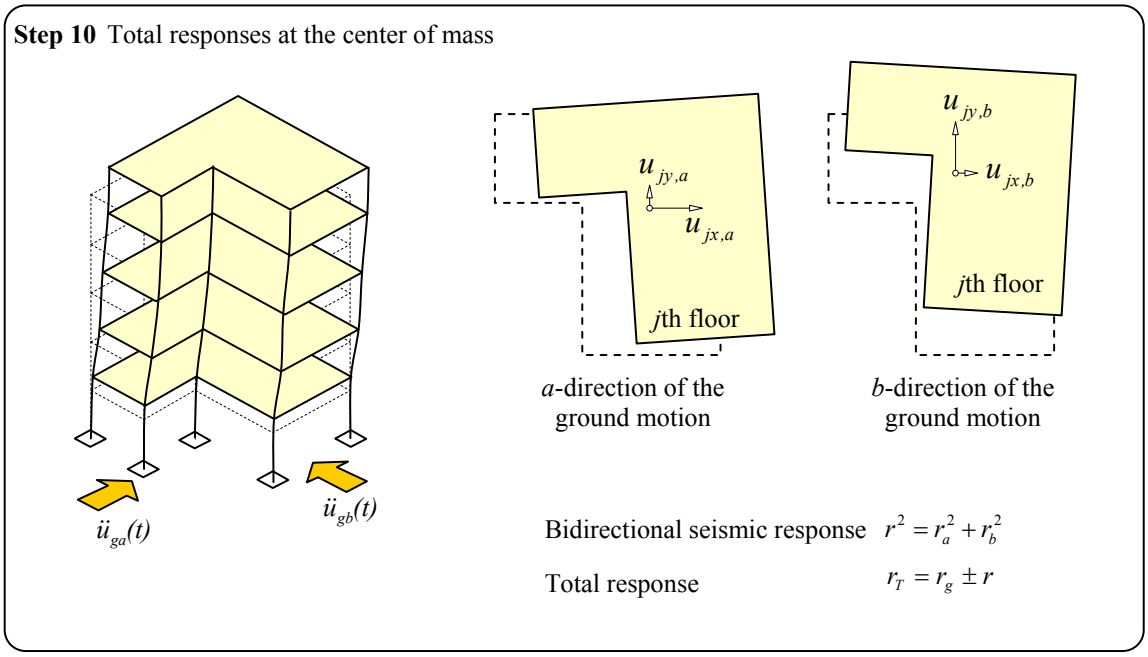

Figure 3.7 Step-by-step summary of the MPA procedure (Step 10).

3.5 Simplified MPA for Practical Applications

The MPA procedure summarized in Section 3.3 can be simplified in two ways. The first simplification comes in computing the response contributions of modes higher than the first three modes. As it will be shown later in Chapters 4, 5 and 6, consideration of nonlinear behavior of the structure is essential in estimate the seismic demands due to the first triplet of "modes", but may not be as important for the higher-mode (higher than the third) analyses; consequently, structures could be treated as linearly elastic in estimating higher-mode contributions to seismic demand. Introducing this approximation in MPA leads to the Modified MPA (MMPA) procedure [Chopra et al, 2004]. Additionally, the contribution of torsional modes is negligible in the response of symmetric-plan buildings to lateral ground motions; therefore, those modes can be ignored. MMPA can be implemented using the MPA procedure of Section 3.4, but changing Step 7 by:

7. Repeat steps 2 through 6 for the first triplet of modes. Compute seismic demands due to higher modes that contribute significantly by assuming the structure to remain elastic. Thus, classical modal analysis can be used to compute higher mode demands without any pushover analysis.

All other computational steps and the calculation of the median demand remain as before.

The second simplification comes in determining the median value of peak deformation D_n of the *n*th-mode inelastic SDF system that is needed to estimate the reference displacement u_{rn} (Eq. 3.21). Instead of using nonlinear RHA (Eq. 3.15) for each excitation, D_n can be estimated by multiplying the median peak deformation $\hat{D}_{no}$ of the corresponding linear system (Fig. 3.8), known from the design spectrum, by the inelastic deformation ratio C_{Rn}:

$$\hat{D}_n = C_{Rn}\hat{D}_{no} \tag{3.25}$$

One of the equations proposed for C_{Rn} is [Chopra and Chintanapakdee, 2004]:

$$C_{Rn} = 1 + \left[\left(L_{Rn} - 1\right)^{-1} + \left(\frac{61}{R_{yn}^{2.4}} + 1.5 \right) \left(\frac{T_n}{T_c} \right)^{2.4} \right]^{-1} \tag{3.26}$$

where R_y is the yield strength reduction factor defined as $R_{yn} = D_{no} / D_n^y$ (Fig. 3.5); T_c is the period that separates the acceleration-sensitive and the velocity-sensitive regions of the median response spectrum (Fig. 3.9); L_{Rn} is the limiting value of C_{Rn} as T_n tends to zero for systems with constant R_{yn}:

$$L_{Rn} = \frac{1}{R_{yn}}\left(1 + \frac{R_{yn} - 1}{\alpha_n}\right) \tag{3.27}$$

where α_n is the post yield stiffness ratio (Fig. 3.8). Figure 3.10 shows plots of C_{Rn} versus T_n / T_c for $\alpha = 0.10$ and R_{yn}=1.5, 2, 4 and 6. Other equations to estimate C_{Rn} are available in Ruiz-Garcia and Miranda [2003], FEMA-356 [FEMA, 2000], FEMA-440 [FEMA, 2005], and ASCE/SEI 41-06 [ASCE, 2007]. Using this approach to estimate the median D_n in MMPA leads to the Practical MPA (PMPA) procedure. PMPA can be implemented using the MPA procedure of Section 3.4, with Steps 4 and 7 modified as follows:

4. Calculate the reference displacement $u_{rn,a}$ given by $u_{rn,a} = u_{rg} + \Gamma_n \phi_{rn} D_{na}$ (Eq. 3.21) for the *a*-component of the ground motion. The median peak deformation $\hat{D}_{na}$ of the modal SDF system is determined by Eq. (3.25) through (3.27).
7. †Repeat steps 2 through 6 for the first triplet of modes. Compute seismic demands due to higher modes that contribute significantly by assuming the structure to remain elastic. Thus, classical modal analysis can be used to compute higher mode demands without any pushover analysis.

All other computational steps remain the same, and at the end of Step 10, PMPA results in values of the median peak demands over all excitations.

† This step is identical to that in MMPA; it is repeated for convenience.

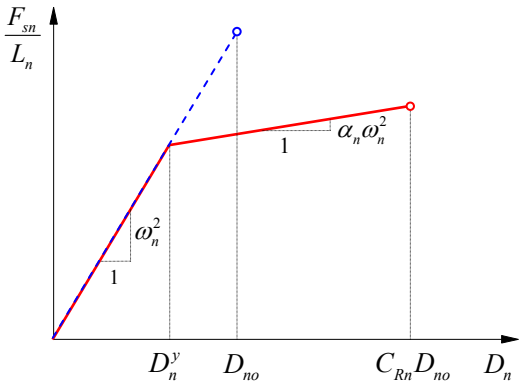

Figure 3.8 Bilinear F_{sn}/L_n—D_n relationship of inelastic SDF system and the corresponding elastic system.

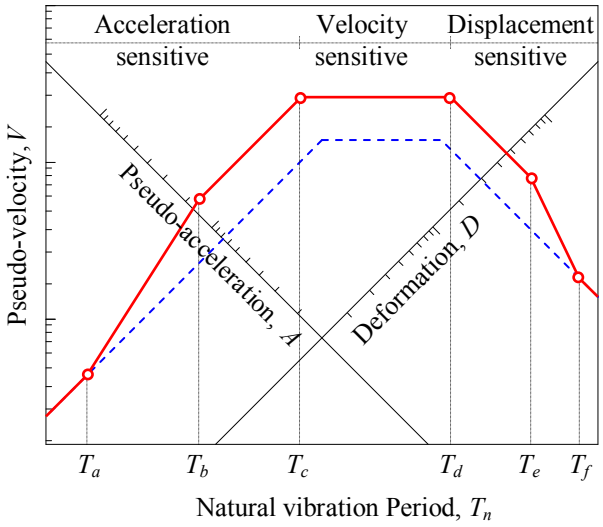

Figure 3.9 Idealized elastic response spectrum with acceleration, velocity and displacement sensitive regions noted.

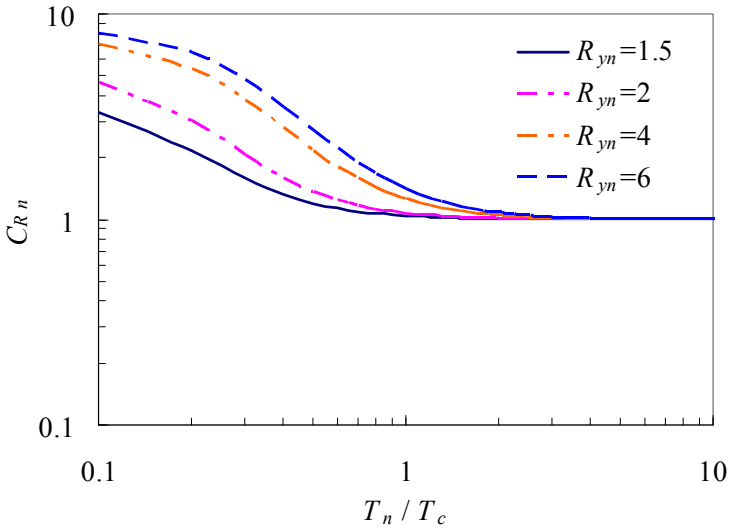

Figure 3.10 Inelastic deformation ratio C_{Rn} versus T_n/T_c for α=0.1 and R_{yn}=1.2, 2, 4, and 6.

4 Evaluation of MPA for Tall Buildings

This chapter evaluates the accuracy of the MPA, MMPA, and PMPA procedures (Chapter 3) for estimating seismic demands for tall buildings with ductile concrete shear walls. Seismic demands are computed for a 48-story and 62-story buildings subjected to 30 ground motions acting simultaneously in the longitudinal and transverse directions. The lateral force resisting system of the buildings is a ductile concrete core wall consisting of channel-shaped, L-shaped and rectangular walls connected by coupling beams.

4.1 Structural Systems and Modeling Assumptions

4.1.1 Structural systems

The structural systems considered are 48- and 62-story buildings taken from the Tall Building Initiative project at the Pacific Earthquake Engineering Research Center (PEER) [http://peer.berkeley.edu/~yang/]. The buildings are identified by the letters CW (concrete wall) followed by the number of stories. The lateral resisting system of the buildings is a ductile concrete core wall consisting of two channel-shaped walls connected to rectangular walls by coupling beams, as shown in Figs. 4.1 and 4.2. The channel-shaped walls of the CW48 building have openings creating L-shaped walls at some stories (Figs. 4.1a and 4.2a). The typical floors are 8-inch-thick post-tensioned slabs spanning between the core and perimeter concrete columns. The total height of the CW48 and CW62 buildings is 471 and 630 feet, respectively. The height-to-width aspect ratio of the core of the 62-story building is 12:1 in the long direction (x-direction) and 18:1 in the short direction (y-direction), as shown in Fig. 4.2. To increase the aspect ratio and

stiffness of the system in the short direction, concrete outrigger columns are included. The outrigger columns are connected to the core with buckling restrained braces (BRBs) at the 28th and 51st floors. Additionally, this building has a tuned liquid mass damper at the roof to help reduce sway during strong wind to acceptable comfort levels [Post, 2008].

These buildings are designed according to the 2001 San Francisco Building Code (SFBC) for soil class S_d. Because these buildings exceed the height limit of 160 feet imposed in the SFBC for concrete bearing wall systems, the buildings were designed by an alternative performance-based procedure, allowed in section 1629.10.1, to meet the equivalent criteria of section 104.2.8 of SFBC.

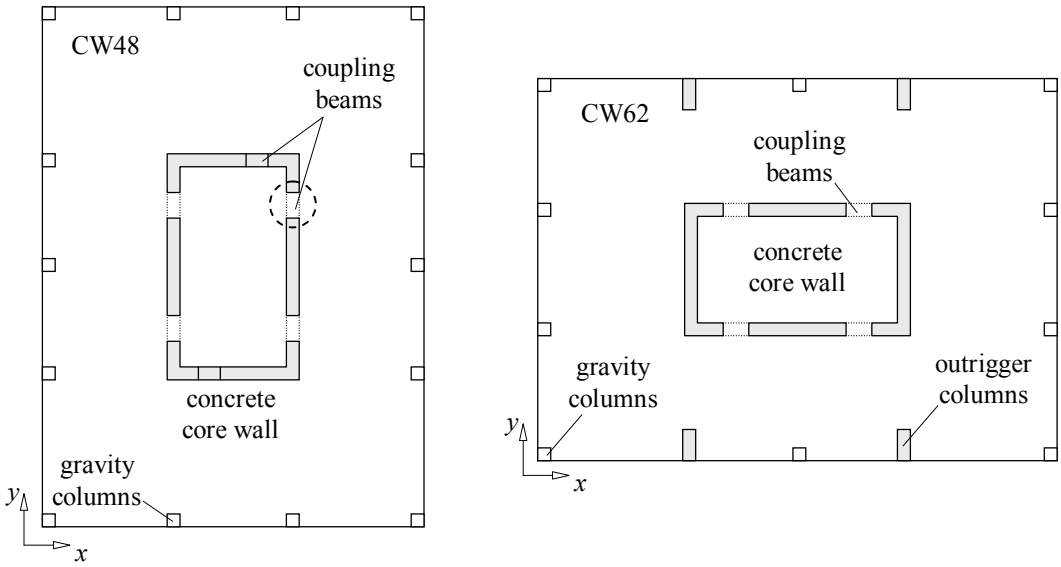

(a) (b)

Figure 4.1 Schematic plans: (a) CW48 building; (b) CW62 building.

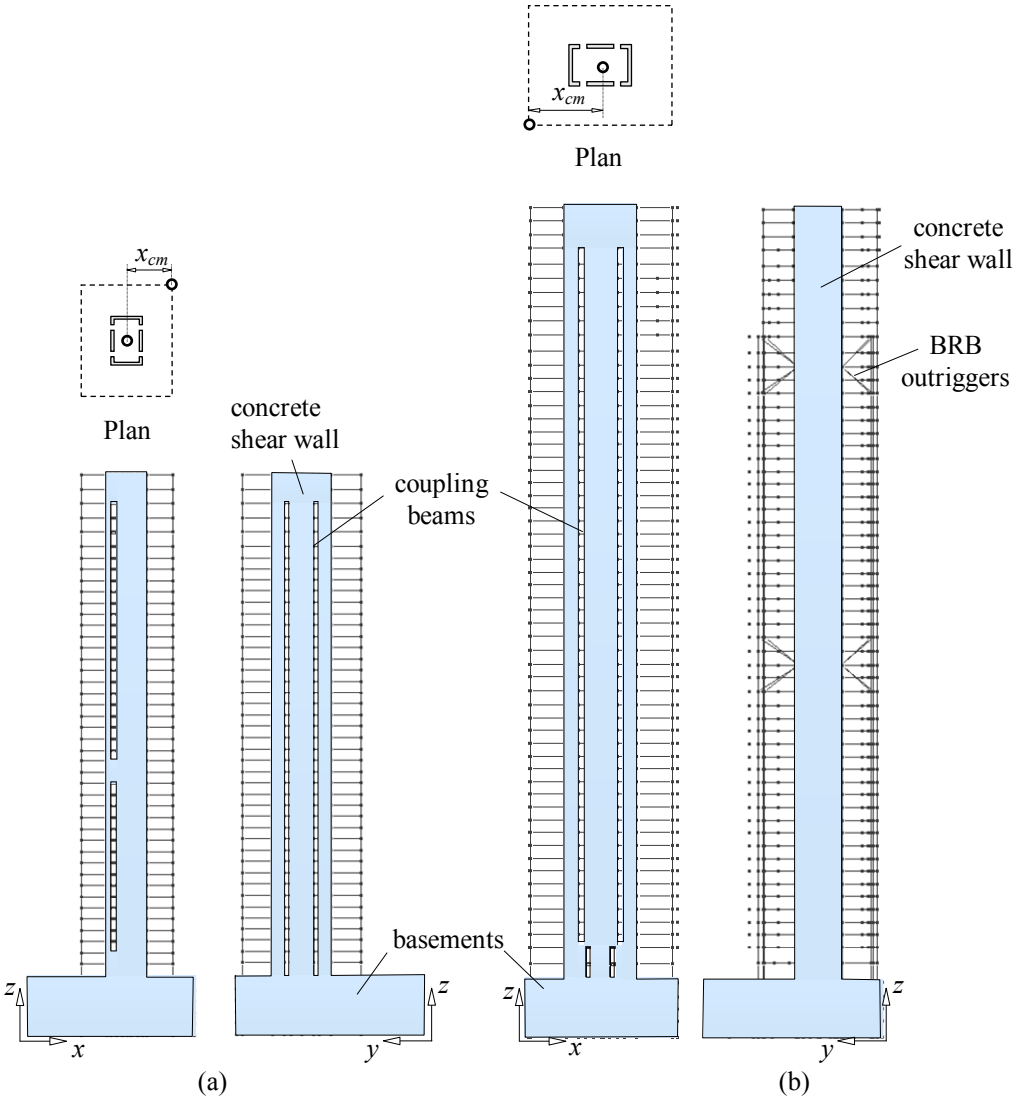

Figure 4.2 Elevations: (a) CW48 building; (b) CW62 building.

The seismic forces were determined for site-specific design spectrum corresponding to a design basis earthquake (DBE) and for a maximum considered earthquake (MCE). The earthquake forces for preliminary design were determined by linear response spectrum analysis (RSA) of the building with the spectrum reduced by a response modification factor of 4.5. Subsequently, the preliminary design was refined based on results of nonlinear response history analysis of the buildings for seven ground motions.

The core walls were detailed according to Chapter 21 of the ACI 318-99 code. To ensure a ductile response of the system, the following features were included:

- Capacity design of the core walls to avoid shear failure and guarantee a predominantly flexural behavior at plastic hinge zones.
- Increased moment strength was assigned above the base of the CW48 building to ensure that the plastic hinge forms at the base of the wall.
- Capacity design of joint shear strength, in order to avoid brittle shear failure at the slab-column and slab-core joints.

These buildings were modeled in the PERFORM-3D computer program [CSI, 2006] using the following nonlinear models for the various structural components.

4.1.2 Modeling of Shear Walls

The shear wall element in PERFORM-3D is an area finite element with nonlinear fibers including P-delta effects for both in-plane and out-plane deformations. With four nodes and 24 degrees of freedom, this element has multiple layers that act independently, but are connected at the element nodes, as shown in Fig. 4.3. The behavior of the element is defined by the combined behavior of the layers, which are [CSI, 2006]:

- Axial-bending layer for the vertical axis, as shown in Fig. 4.3(a). The cross section of this layer is comprised of concrete and steel fibers, with linear or nonlinear stress-strain relations.
- Axial-bending layer for the horizontal axis, as shown in Fig. 4.3(b). Because this is a secondary effect in a slender wall, the cross section of this layer is assumed to be linearly elastic.

- Conventional shear layer, as shown in Fig. 4.3(c). This layer assumes constant shear stress and a uniform wall thickness. The shear material of this layer may be elastic or inelastic.
- Out-of-plane bending, as shown in Fig. 4.3(d). Because this effect is secondary in concrete walls, it is modeled as elastic.

These layers have the following characteristics. First, in-plane deformations such as axial strain, shear strain and curvature are assumed constant along the element length. Second, the hysteretic behavior of the fibers in the axial-bending layer and the material of the shear layer can be represented by a tri-linear model with in-cycle strength deterioration (strength loss) and cyclic stiffness degradation, as shown in Fig. 4.4. Finally, the model for the steel fibers can incorporate buckling effects on its cyclic force-deformation relationship.

The core walls of the buildings were modeled using this shear wall element considering inelastic fibers with in-cycle strength deterioration, but without cyclic stiffness degradation or buckling of the steel bars. Figure 4.5 shows the finite element mesh for the top stories of the CW48 building.

4.1.3 Modeling of Beams and Slabs

The nonlinear behavior of the coupling beams, slabs and girders was modeled by a linear 1D element with tri-linear plastic hinges at the ends. The ductility capacities of those elements were specified according to the FEMA 356 pre-standard [FEMA, 2000]. The plastic hinges of the coupling beams include in-cycle strength deterioration (Fig. 4.4a) and cyclic stiffness degradation associated with the unloading and reloading stiffness (Fig. 4.4b) adjusted to reduce the area of the hysteresis loops by 40%.

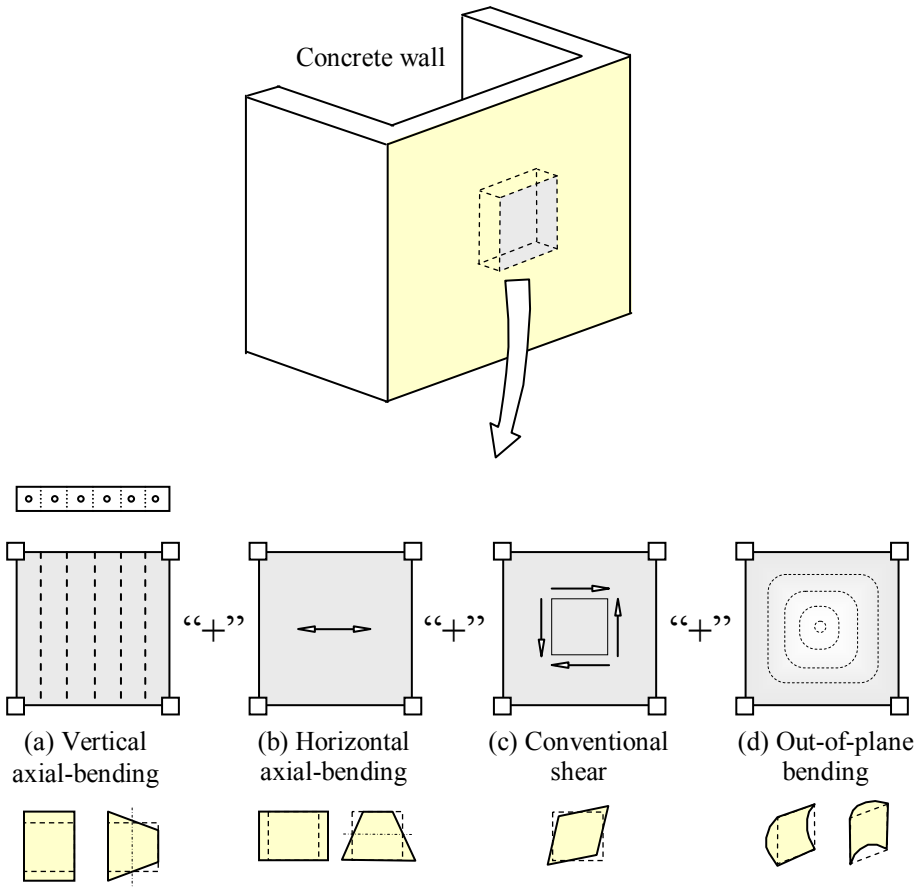

Figure 4.3 Parallel layers of the shear wall element in Perform-3D; adapted from CSI [2006].

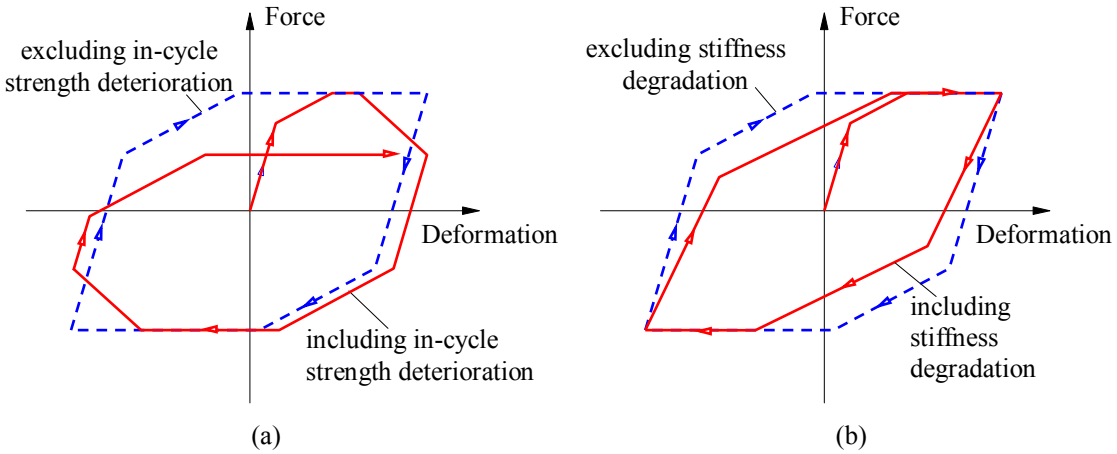

Figure 4.4: Tri-linear force-deformation relationships considering: (a) in-cycle strength deterioration (strength loss); (b) cyclic stiffness degradation.

4.1.4 Geometric Nonlinear Effects

The geometric nonlinear effects are considered by a standard P-Delta formulation for the overall building using an equivalent leaning column to represent the gravity frames, and also locally at the finite element level in the core wall.

4.1.5 Vibration Periods and Modes

Figures 4.6 through 4.8 show natural periods and modes of vibration of the CW48 and CW62 buildings; where x_{cm} is the distance from the C.M. to a corner of the building (Fig. 4.2). Figure 4.6 shows the height-wise variation of lateral displacements and torsional rotations, whereas Figs. 4.7 and 4.8 show the motion of the roof in plan. Figure 4.9 presents the height-wise variation of story drifts ($\phi_j - \phi_{j-1}$) in the first and second mode of vibration, which correspond to the first mode of lateral vibration in the x- and y-direction, respectively. The effective modal masses for the first nine modes of vibration are presented in Fig. 4.10.

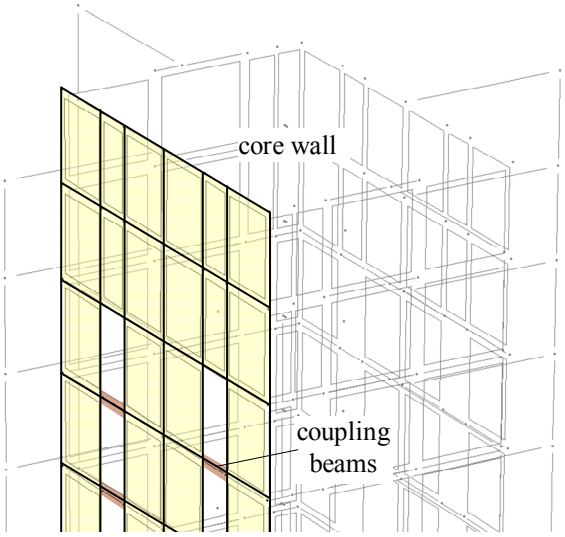

Figure 4.5 Finite element mesh of the top stories for the CW48 building.

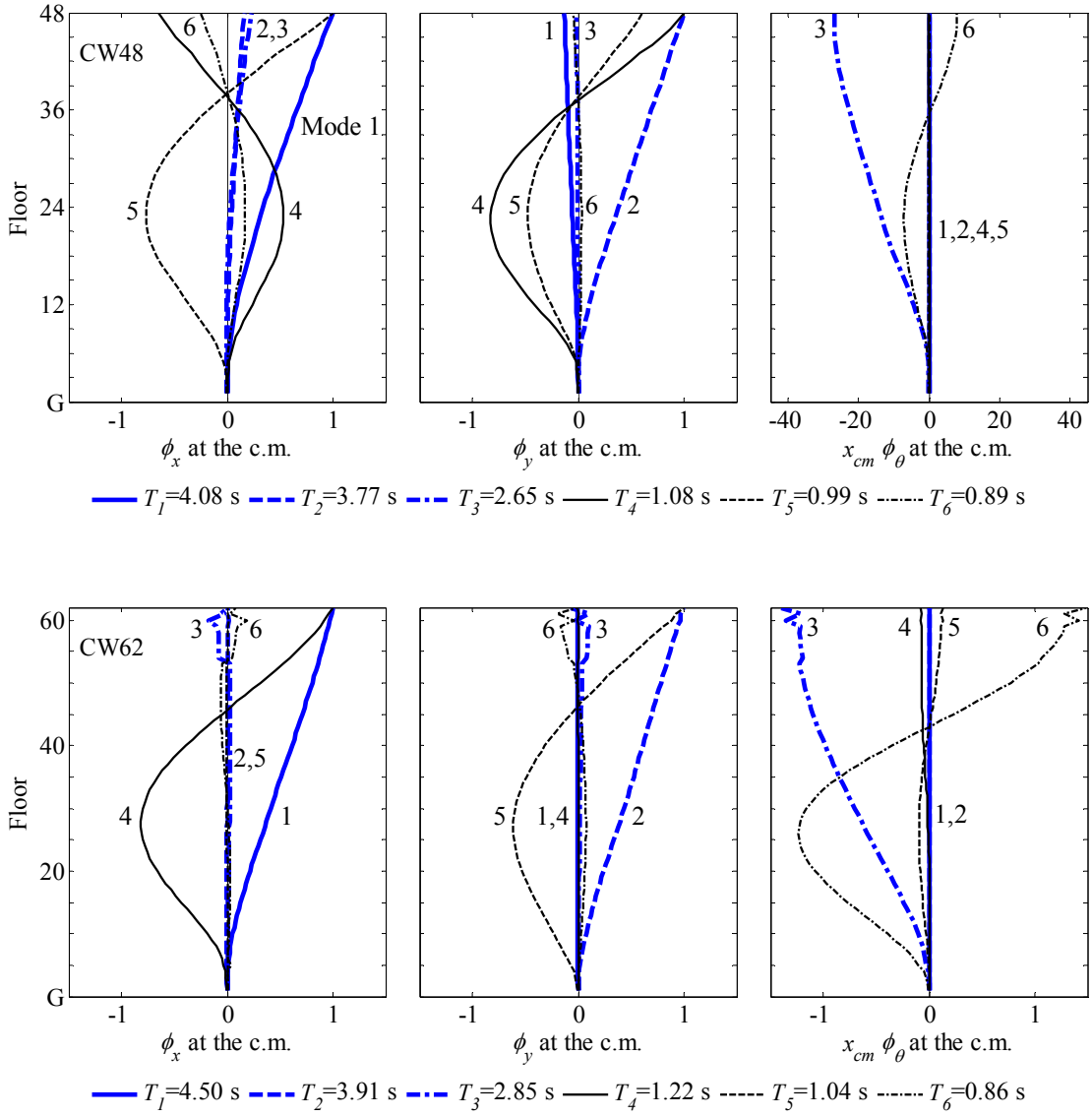

Figure 4.6 Natural periods and modes of vibration of CW48 (top row) and CW62 (bottom row) buildings; shown in the three boxes are *x*-traslational, *y*-traslational, and torsional components of displacements.

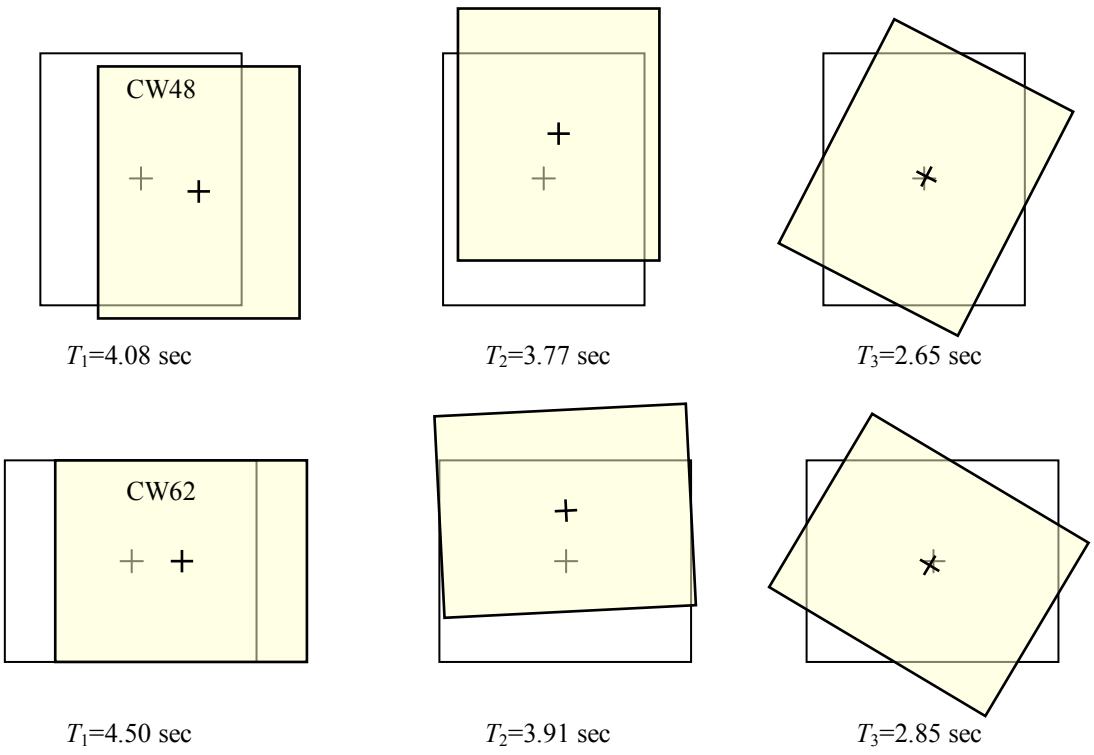

T_1=4.08 sec T_2=3.77 sec T_3=2.65 sec

T_1=4.50 sec T_2=3.91 sec T_3=2.85 sec

Figure 4.7 First triplet of periods and modes of vibration of CW48 and CW62 buildings (only the motion at the roof is shown).

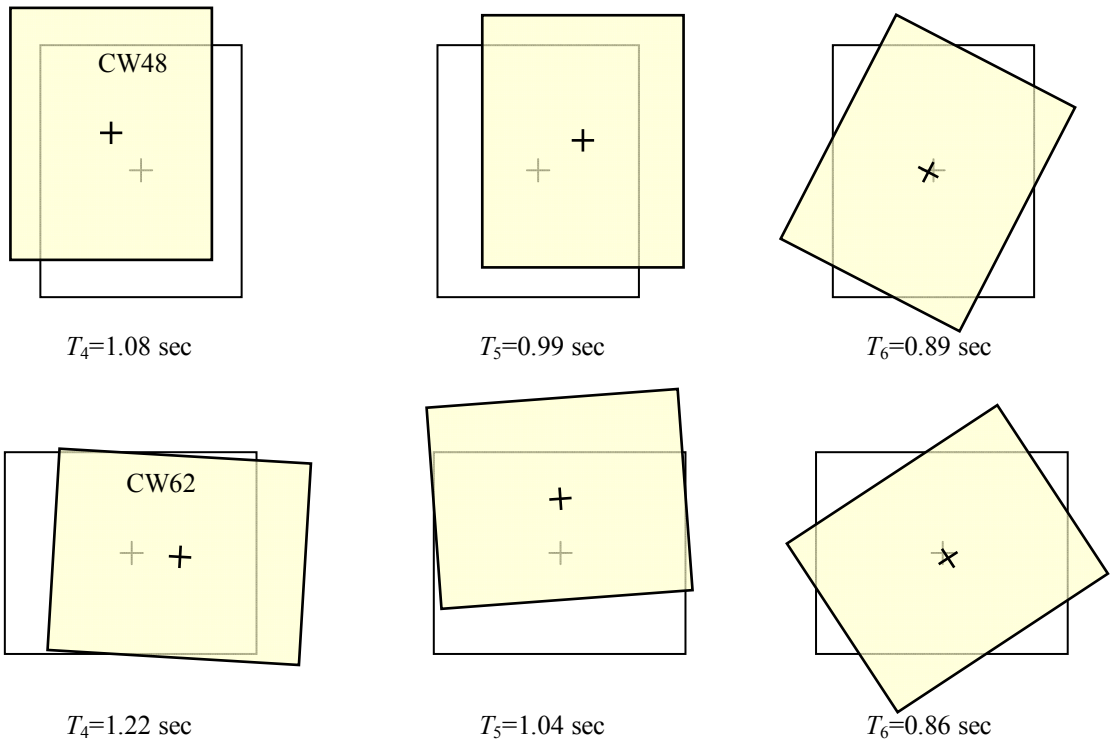

T_4=1.08 sec T_5=0.99 sec T_6=0.89 sec

T_4=1.22 sec T_5=1.04 sec T_6=0.86 sec

Figure 4.8 Second triplet of periods and modes of vibration of CW48 and CW62 buildings (only the motion at the roof is shown).

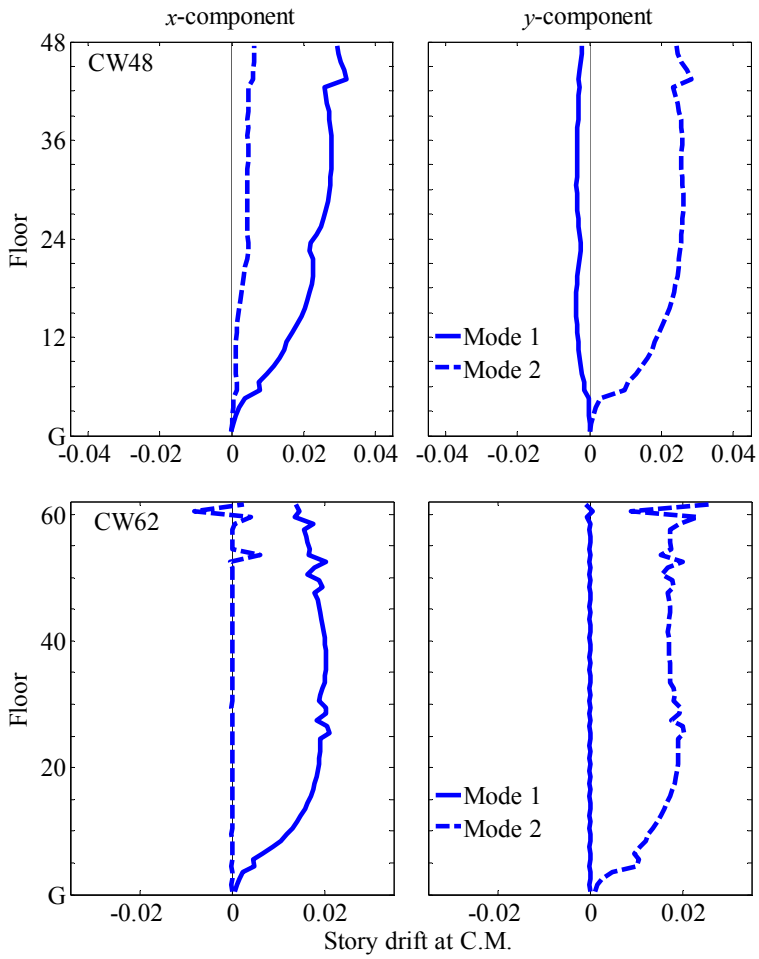

Figure 4.9 Story drifts in the first two modes of vibration of CW48 and CW62 buildings; *x* and *y* components are shown.

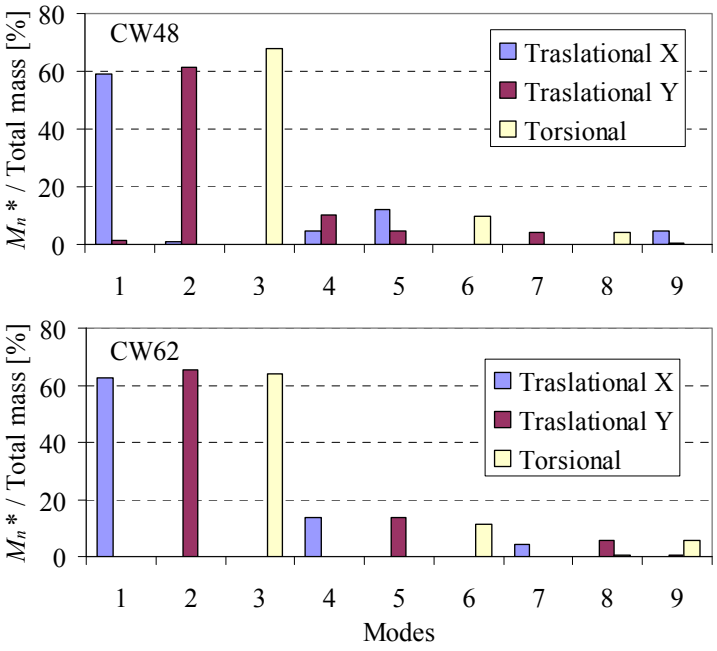

Figure 4.10 Effective modal masses: CW48 and CW62 buildings

Figures 4.6 through 4.10 permit the following observations. (1) Lateral displacements dominate motion of the first mode of lateral vibration in the *x*- and *y*-direction of both buildings, whereas torsional rotations dominate motion in the third mode. (2) The fundamental vibration periods of the CW48 and CW62 buildings are 4.08 sec and 4.50 sec, respectively. The period of the dominantly-torsional mode is much shorter than that of the dominantly-lateral modes. (3) In modes 1, 2, 4 and 5, the CW48 building moves simultaneously in the two lateral directions without torsion (Figs. 4.7 and 4.8). (4) The higher-mode contributions to forces are expected to be significant because the effective mass of the first mode is only 60% of the total mass (Fig. 4.10). (5) The unusual fluctuations in drifts in the upper part of the CW62 building (Fig. 4.9) is due to reduction of the core wall stiffness and presence of a tuned liquid mass damper, electromechanical equipment and architectural setbacks at those floors.

4.1.6 Rayleigh Damping

The damping of these buildings was modeled by *Rayleigh damping*—a linear combination of the mass and initial stiffness matrix—with its two constants selected to give 5% damping ratio at the fundamental period of vibration T_1 and a period of $0.1T_1$. Figure 4.11 shows the damping ratio values for the first twelve vibration modes of both buildings, which range from 2.9% to 7.6%.

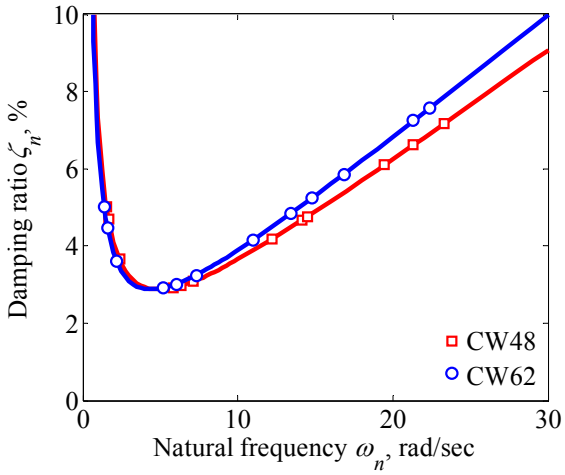

Figure 4.11 Modal damping ratios identified in the damping ratio versus frequency curves for CW48 and CW62 buildings

4.1.7 Three-dimensional Modeling

A symmetric-plan building, such as the CW62 building, could be analyzed using planar models for each of the principal directions of the building; however, it is more convenient to analyze three-dimensional models when using general purpose computer software, such as PERFORM-3D.

4.2 Ground Motions

4.2.1 Selected Earthquake Records

A total of 30 ground acceleration records from nine different earthquakes with magnitudes ranging from 7.3 to 7.9 were selected according to the following criteria [http://peer.berkeley.edu/~yang/]:

- Closest distance to the fault < 40 km.
- Longest usable period > 6.4 sec. This is the period below which the response spectrum for the high-pass filtered ground motion is unaffected by filtering of the data. This requirement is imposed to ensure that selected ground motions are appropriate for analysis of these buildings with fundamental periods of 4.0 and 4.5 sec.
- Average shear-wave velocity in upper 30 meters of soil, V_{s30} > 200 m/s.

Table 4.1 lists the selected records and their relevant data. Each of the 30 records includes two orthogonal components of horizontal ground motion. Figure 4.12 shows the magnitude-distance distribution for the selected ensemble of records, wherein R_{JB} is the distance of the site to the surface projection of fault rupture, as defined by Joyner and Boore [1981].

Table 4.1 List of 30 ground motion records

Record	Year	Earthquake Name	M_w	Mechanism	Station Name	V_{s30} (m/s)	NEHRP based on V_{s30}	R_{JB} (km)	Longest Usable Period - Ave. Component (sec)	Geometric mean of the two components		
										PGA (g)	PGV (cm/sec)	PGD (cm)
1	1952	Kern County	7.36	Reverse	Taft Lincoln School	385.4	C	38.42	16.0	0.17	15.72	9.34
2	1978	Tabas, Iran	7.35	Reverse	Boshrooyeh	338.6	D	24.07	6.4	0.11	19.66	14.83
3	1978	Tabas, Iran	7.35	Reverse	Dayhook	659.6	C	0.00	8.0	0.35	28.31	9.03
4	1978	Tabas, Iran	7.35	Reverse	Tabas	766.8	B	1.79	16.0	0.85	110.30	61.07
5	1992	Landers	7.28	Strike-slip	Coolwater	271.4	D	19.74	8.0	0.37	34.64	12.81
6	1992	Landers	7.28	Strike-slip	Mission Creek Fault	345.4	D	26.96	8.9	0.13	15.27	15.02
7	1992	Landers	7.28	Strike-slip	Lucerne	684.9	C	2.19	10.0	0.73	108.80	190.35
8	1992	Landers	7.28	Strike-slip	Barstow	370.8	C	34.86	14.3	0.12	21.58	16.95
9	1992	Landers	7.28	Strike-slip	Desert Hot Springs	345.4	D	21.78	14.3	0.14	18.54	9.62
10	1992	Landers	7.28	Strike-slip	Joshua Tree	379.3	C	11.03	14.3	0.25	34.24	11.89
11	1992	Landers	7.28	Strike-slip	Palm Springs Airport	207.5	D	36.15	14.3	0.09	11.79	6.44
12	1992	Landers	7.28	Strike-slip	Yermo Fire Station	353.6	D	23.62	14.3	0.23	38.08	31.18
13	1999	Kocaeli, Turkey	7.51	Strike-slip	Izmit	811.0	B	3.62	8.0	0.20	27.02	14.61
14	1999	Kocaeli, Turkey	7.51	Strike-slip	Iznik	274.5	D	30.74	8.0	0.11	23.06	12.55
15	1999	Kocaeli, Turkey	7.51	Strike-slip	Gebze	792.0	B	7.57	10.0	0.18	38.06	32.31
16	1999	Kocaeli, Turkey	7.51	Strike-slip	Arcelik	523.0	C	10.56	11.4	0.18	28.90	24.45
17	1999	Kocaeli, Turkey	7.51	Strike-slip	Yarimca	297.0	D	1.38	11.4	0.31	60.51	54.70
18	1999	Chi-Chi, Taiwan	7.62	Reverse-Oblique	TCU088	553.4	C	4.67	10.0	0.53	19.31	13.99
19	1999	Chi-Chi, Taiwan	7.62	Reverse-Oblique	CHY010	473.9	C	19.93	26.7	0.21	20.29	8.77
20	1999	Chi-Chi, Taiwan	7.62	Reverse-Oblique	CHY041	492.3	C	19.37	20.0	0.46	27.73	9.84
21	1999	Chi-Chi, Taiwan	7.62	Reverse-Oblique	TCU101	272.6	D	2.13	20.0	0.23	61.21	58.89
22	1999	Chi-Chi, Taiwan	7.62	Reverse-Oblique	TCU061	272.6	D	17.19	20.0	0.14	43.28	36.41
23	1999	Chi-Chi, Taiwan	7.62	Reverse-Oblique	TCU067	433.6	C	0.64	26.7	0.43	75.58	70.87
24	1999	Chi-Chi, Taiwan	7.62	Reverse-Oblique	CHY101	258.9	D	9.96	20.0	0.39	91.25	59.72
25	1999	Chi-Chi, Taiwan	7.62	Reverse-Oblique	TCU065	305.9	D	0.59	13.3	0.68	99.53	81.76
26	1999	Chi-Chi, Taiwan	7.62	Reverse-Oblique	TCU068	487.3	C	0.00	26.7	0.54	206.05	336.33
27	1972	Sitka, Alaska	7.68	Strike-slip	Sitka Observatory	659.6	C	34.61	12.5	0.09	10.58	10.41
28	1979	St Elias, Alaska	7.54	Reverse	Icy Bay	274.5	D	26.46	25.0	0.13	26.39	10.73
29	1990	Manjil, Iran	7.37	Strike-slip	Abbar	724.0	C	12.56	7.7	0.50	43.13	17.61
30	2002	Denali, Alaska	7.9	Strike-slip	TAPS Pump Station #10	329.4	D	0.18	40.0	0.32	101.36	102.46

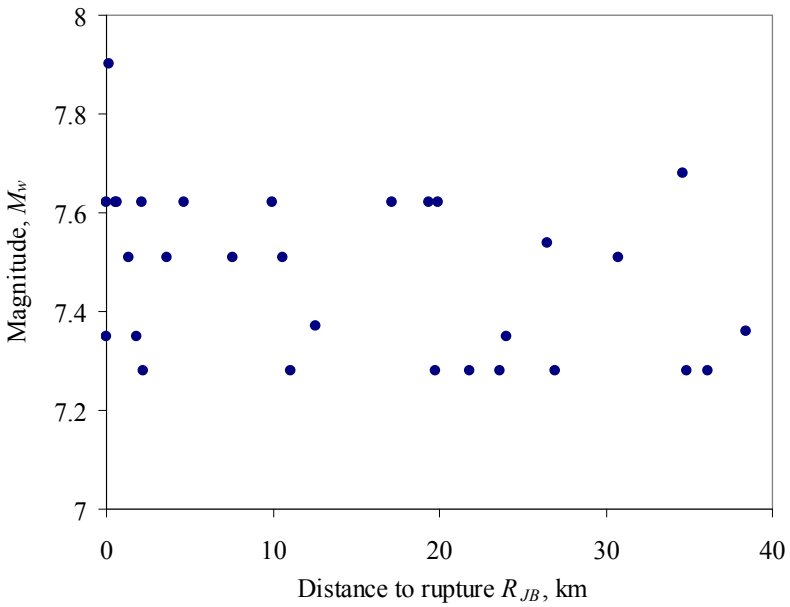

Figure 4.12 Distribution of magnitude, M_w, and distance of site to surface projection of fault rupture, R_{JB}.

4.2.2 Ground-Motion Scaling Procedure

All the 30 records were scaled to represent the same seismic hazard defined by $A(T_1)$, the pseudo-acceleration at the fundamental vibration period T_1 of the structure. Both components of a record were scaled by the same factor selected to match their *geometric mean* to the selected seismic hazard. The *geometric mean* is defined as:

$$A(T_1) = \sqrt{A_a(T_1) \times A_b(T_1)} \tag{4.1}$$

where $A_a(T_1)$ and $A_b(T_1)$ are the $A(T_1)$ values for the two horizontal components of the record.

The selected seismic hazard spectrum was determined as the average of three uniform hazard spectra for 2% probability of exceedance in 50 years (return period of 2475 years) obtained using attenuation relationships developed by Campbell and Bozorgnia [2008], Boore and Atkinson [2008], and Abrahamson and Silva [2008] as part of the "Next Generation of Ground-Motion Attenuation Models" (NGA) project. These

2008 NGA relationships consider natural periods ranging from 0.01 to 10 sec, magnitudes from 4.0 to 8.0, and distances from 0 to 200 km, which cover the periods of vibration of the two buildings and ground motions.

Table 4.2 lists the values of $A(T_1)_{2\%/50}$ selected to define ground motion ensembles. Figures 4.13 shows the 5%-damped median response spectra for the ensemble of 30 ground motions along the *a* and *b* directions scaled to match $A(T_1)_{2\%/50}$, and the 5%-damped seismic hazard spectrum defined earlier, corresponding to 2% probability of exceedance in 50 years. As imposed by the scaling criterion, the median pseudo-acceleration of the ensemble at the fundamental period is matched to the seismic hazard spectrum; because T_1 differs for each structure, the scaling factors for ground motions and hence their median spectra vary with the building.

Table 4.2 Selected values of $A(T_1)$ corresponding to two ground-motion intensities.

Building	$A\,(T_1)_{\,2\%/50}$ (g)
CW48	0.148
CW62	0.137

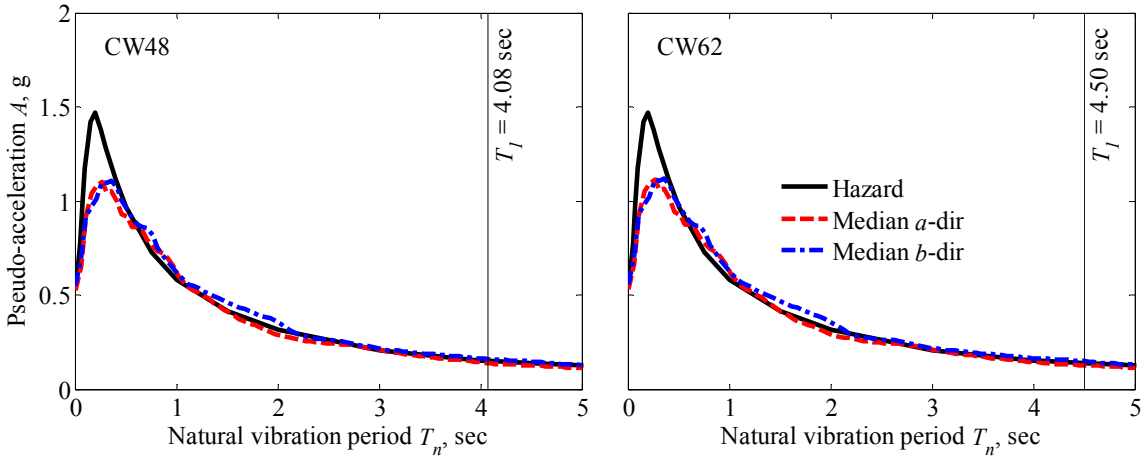

Figure 4.13 Seismic hazard spectrum for building site corresponding to 2% probability of exceedance in 50 years (solid line), and the median response spectra of 30 scaled ground motions in the *a* and *b* directions (dashed lines): CW48 and CW62 buildings.

4.3 Evaluation of MPA procedure

4.3.1 Modal Pushover Curves and Reference Displacements

As a first step in evaluating the MPA procedure, this section presents the modal pushover curves and the reference displacement response of each building due to the scaled ground motions.

Figures 4.14 and 4.15 show pushover curves and their tri-linear idealization for each building associated with their first and second "modes" in both lateral directions, respectively. These are modes 1, 2, 4 and 5 of the three-dimensional model of the building; modes 3 and 6 are not shown because the building motion is dominantly torsional and the lateral displacements are negligible. Pushover analyses for the first "mode" of the CW62 building and the first two "modes" of the CW48 building, lead to the following observations, with reference to the tri-linear idealization of the pushover curves, shown schematically in Fig. 4.16. At displacements up to u_1, the building remains essentially elastic, but cracking is initiated in some sections of the wall; at the first yield displacement u_1, the reinforcement in the post-tensioned slabs starts to yield whereas the stresses at the extreme fiber of the core wall have just reached the tensile strength of concrete. As displacement increases, the tensile force in the concrete of the core wall and coupling beams is transferred to the steel until the reinforcement yields at displacements around the second yield point u_2; yielding in the core wall is concentrated in the first six stories above grade; The building reaches its maximum strength and develops a collapse mechanism at a displacement between u_2 and u_3; nonlinear geometric effects induce negative stiffness in the pushover curve before u_3. After u_3, coupling beams begin to loose strength degrading the strength of the building and leading to its eventual collapse.

The second "mode" of vibration of the CW62 building, which is the first mode of lateral vibration in the *y*-direction, is less ductile than its first "mode", the first mode of lateral vibration in the *x*-direction (compare Figs. 4.14c and d). At the first yield displacement u_1, yielding starts in the BRBs, and in some sections of the slabs, the coupling beams and the wall near the base. At displacements between u_1 and u_2 , sections of the wall around the 28th and 33rd stories yield. From u_2 to u_3, the building strength degrades progressively until it abruptly looses its strength at u_3 due to damage in some coupling beams (Fig. 4.14d). These coupling beams continue to deteriorate at displacements larger than u_3 until they reach their maximum deformation capacity.

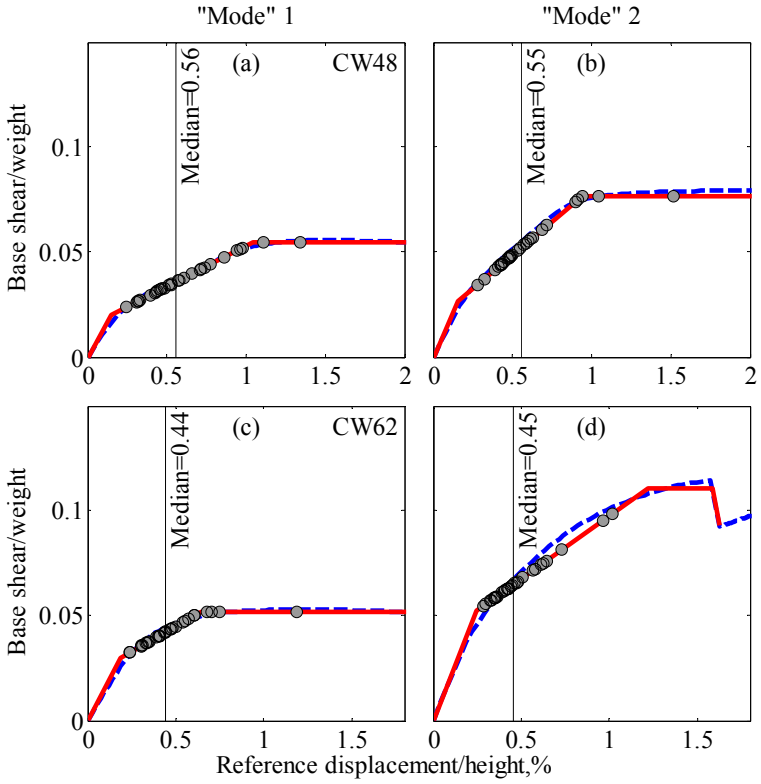

Figure 4.14 Modal pushover curves for first two "modes" of CW48 and CW62 buildings. The reference displacement due to 30 scaled ground motions is identified and the median value is also noted.

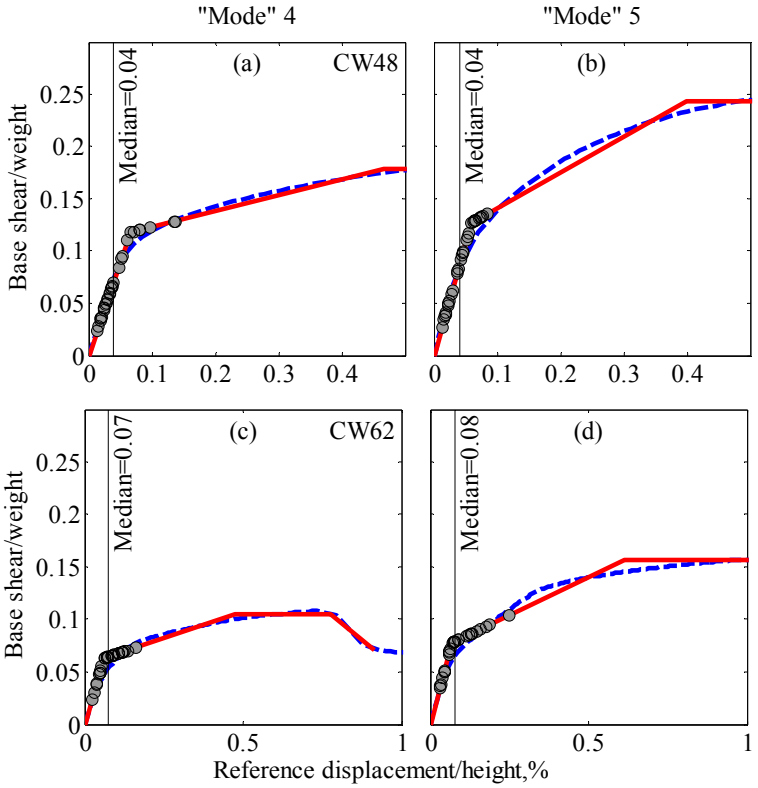

Figure 4.15 Modal pushover curves for the fourth and fifth "modes" of CW48 and CW62 buildings. The reference displacement due to 30 scaled ground motions is identified and the median value is also noted.

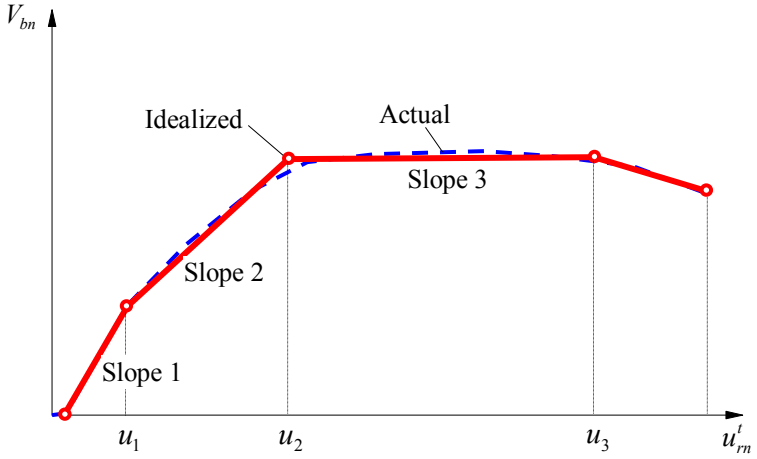

Figure 4.16 Idealized tri-linear pushover curve.

Figures 4.14 and 4.15 also identify reference displacements due to each of the 30 scaled ground motions, and their median value; these reference displacements were determined in Step 4 of the MPA procedure (Section 3.4). All ground motions drive both buildings beyond the first yield displacement u_1 in the first and second "modes;" the median displacement of the CW48 building exceeds its yield displacement u_1 by factors of 3.8 and 3.5 in the *x* and *y* directions, respectively, and by factors of 2.4 and 1.9 in case of the CW62 building. More than half of the excitations drive the CW62 building beyond its first yield displacement u_1 in the second mode of lateral vibration in the *x* and *y* directions, but the median displacement is only slightly larger than the yield displacement u_1. Only a few ground motions drive the CW48 building beyond its first yield displacement u_1, and the median displacement is smaller than u_1. These results show that the median displacement in "modes" higher than the first pair of "modes" is either close to or exceeds the first yield displacement u_1 only by a modest amount. This is consistent with results of past research on steel MRF buildings [Goel and Chopra, 2004].

4.3.2 Higher Mode Contribution in Seismic Demands

Figure 4.17 shows the median values of floor displacements and story drifts in the *x* and *y* directions at the C.M. including a variable number of "modes" in MPA superimposed with the "exact" result from nonlinear RHA for each building subjected to both components of ground motion, simultaneously. The variation of story drifts over building height is typical of tall buildings except for the rapid fluctuations near the top of the CW62 building; such fluctuations first noted in the mode shapes (Section 4.1.5) are due to reduction of core wall stiffness and presence of a tuned liquid mass damper, electromechanical equipment and architectural setbacks at those floors. The observations

presented in this section and in sections 4.4 and 4.5 will exclude the upper three stories of the CW62 building and basements of both buildings.

The first pair of "modes" alone is adequate in estimating floor displacements; including higher "modes" does not significantly improve this estimate (Fig. 4.17a). Although the first pair of "modes" alone is inadequate in estimating story drifts, with the second pair of "modes" (fourth- and fifth-"mode") included, story drifts estimated by MPA are much better, and resemble nonlinear RHA results (Fig. 4.17b). However, notable discrepancies between MPA and nonlinear RHA results remain for both buildings; these discrepancies are discussed in the following section.

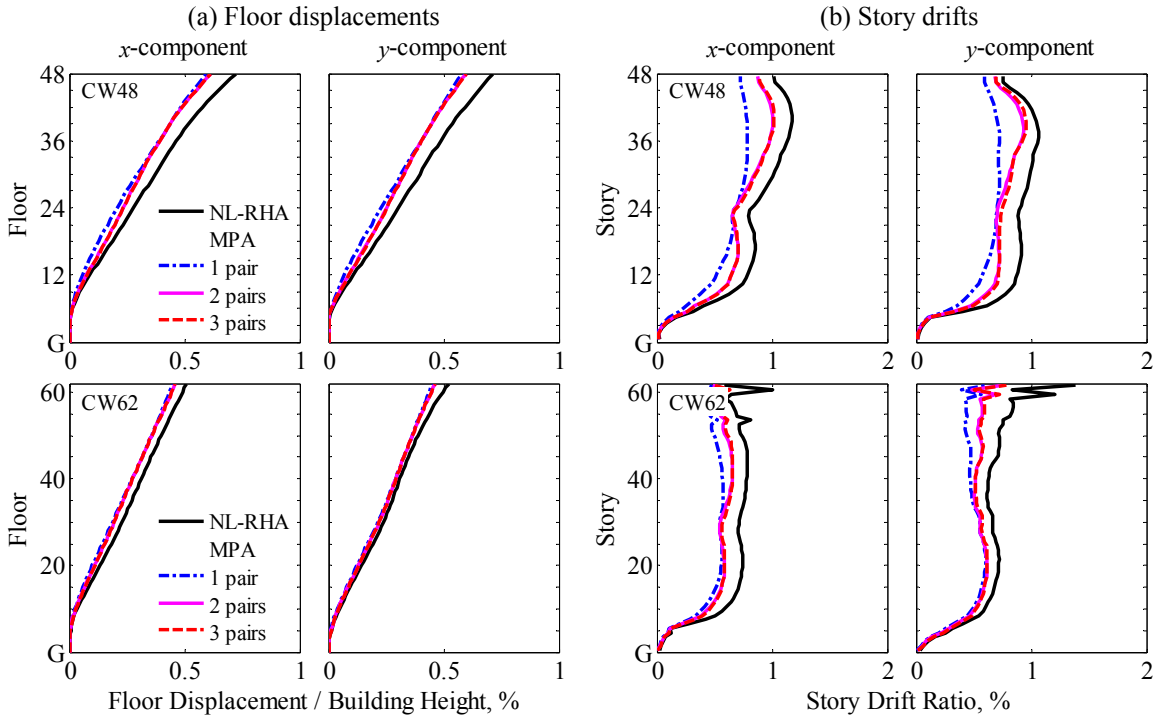

Figure 4.17 Values of median (a) floor displacements, and (b) story drifts at the C.M. of the CW48 (row 1) and CW62 (row 2) buildings determined by nonlinear RHA and MPA, with a variable number of "modes".

4.3.3 Evaluation of Modal Pushover Analysis

MPA underestimates the *x* and *y* components of floor displacements for both buildings; the roof displacement is underestimated by about 16% and 12% for the CW48 and CW62 buildings, respectively. The height-wise average underestimation of story drift is about 15% for the CW48 building, and about 18% for the CW62 building. Notable discrepancies remain for *y*-direction drifts in the upper part of the CW62 building where the underestimation is around 30%; recall that in this direction, the core wall of the building interacts with BRBs and outrigger columns developing plastic hinges at various locations over building height (Section 4.3.1).

4.4 Evaluation of Modified MPA (MMPA)

The results of Figs. 4.15 and 4.16 and their interpretation suggested that the buildings could be treated as linear in estimating contributions of modes higher than the first triplet of "modes" (or first pair of "modes" for a symmetric-plan building) to seismic demands. This observation is utilized in the Modified MPA (MMPA) procedure (Section 3.5), which was implemented to estimate seismic demands for the CW48 and CW62 buildings; torsional modes are ignored because their effective modal mass is negligible for the *x*- and *y*-direction excitations.

Figure 4.18 shows the median values of *x* and *y* components of floor displacements and story drifts at the C.M., determined by nonlinear RHA, MPA and MMPA for both buildings. The seismic demands estimated by MMPA and MPA are very close (Fig. 4.18) implying that it is valid to treat the buildings as linearly elastic in estimating higher-mode contributions to seismic demands.

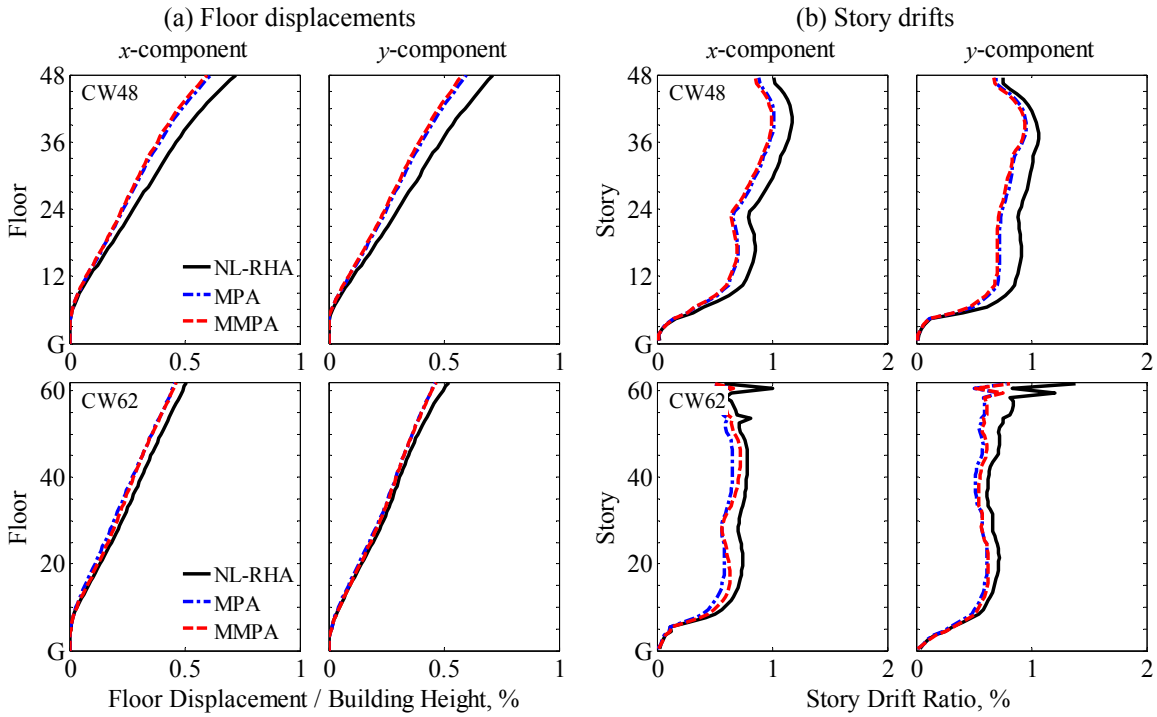

Figure 4.18 Median values of (a) floor displacements and (b) story drifts at the C.M. of the CW48 (row 1) and CW62 (row 2) buildings determined by nonlinear RHA, MPA and MMPA.

4.5 Evaluation of Practical MPA (PMPA)

4.5.1 Floor Displacements and Story Drifts at the C.M.

In implementing the Practical MPA (PMPA) procedure (Section 3.5), the median value of the peak deformation $\hat{D}_n$ of the nth-mode inelastic SDF system was estimated by multiplying the median peak deformation $\hat{D}_{no}$ of the corresponding linear system by the inelastic deformation ratio C_{Rn} (Eq. 3.26); $\hat{D}_{no}$ was determined from the median response spectrum for the ensemble of 30 ground motions corresponding to the modal damping ratios presented in Section 4.1.6. For all modes of these long-period buildings, C_{Rn} was essentially equal to 1.0 (Fig. 3.10).

Figures 4.19 show the median values of the x and y components of floor displacements and story drifts at the C.M., determined by the nonlinear RHA, MPA, and PMPA for both buildings. In general, PMPA provides a larger estimate of seismic demands compared to MPA because $(\hat{D}_n)_{\text{PMPA}}$ determined by Eqs. (3.25) and (3.26) in PMPA is larger than the exact $(\hat{D}_n)_{\text{MPA}}$ determined in MPA (Step 4 of Section 3.4); the ratio of the two for the first pair of "modes" of both buildings is shown in Table 4.3. This is to be expected for some long-period systems because the empirical equation for C_{Rn} does not permit values below 1.0 (Fig. 3.10), whereas the exact data does fall below 1.0 [Chopra and Chintanapakdee, 2004]. Despite this overestimation in one step of PMPA, the method underestimates the seismic demands (Fig. 4.19). The height-wise average underestimation of story drifts is about 16% and 9% for the CW48 and the CW62 buildings, respectively.

The PMPA procedure for concrete buildings subjected to two horizontal components of ground motion, simultaneously, is based on six principal approximations: (1) neglecting the weak coupling of "modes" in computing the peak modal responses r_n to $\mathbf{p}_{eff,n}(t)$; (2) combining the r_n by modal combination rules—known to be approximate—to compute the total response to one component of ground motion; (3) combining the response to individual components of ground motion by multi-component combination rules—known to be approximate—to compute the peak value of the total response; (4) estimating the peak deformation D_n of the nth-mode inelastic SDF system by empirical equations; (5) considering that the structure could be treated as linearly elastic in estimating higher-mode contributions to seismic demand; and (6) ignoring cyclic stiffness degradation of structural elements. Because approximations (2) and (3) are the only

sources of approximation in the widely used response spectrum analysis (RSA) procedure for linear systems, the resulting error in the response of these systems serves as a baseline for evaluating the additional errors in PMPA for nonlinear systems.

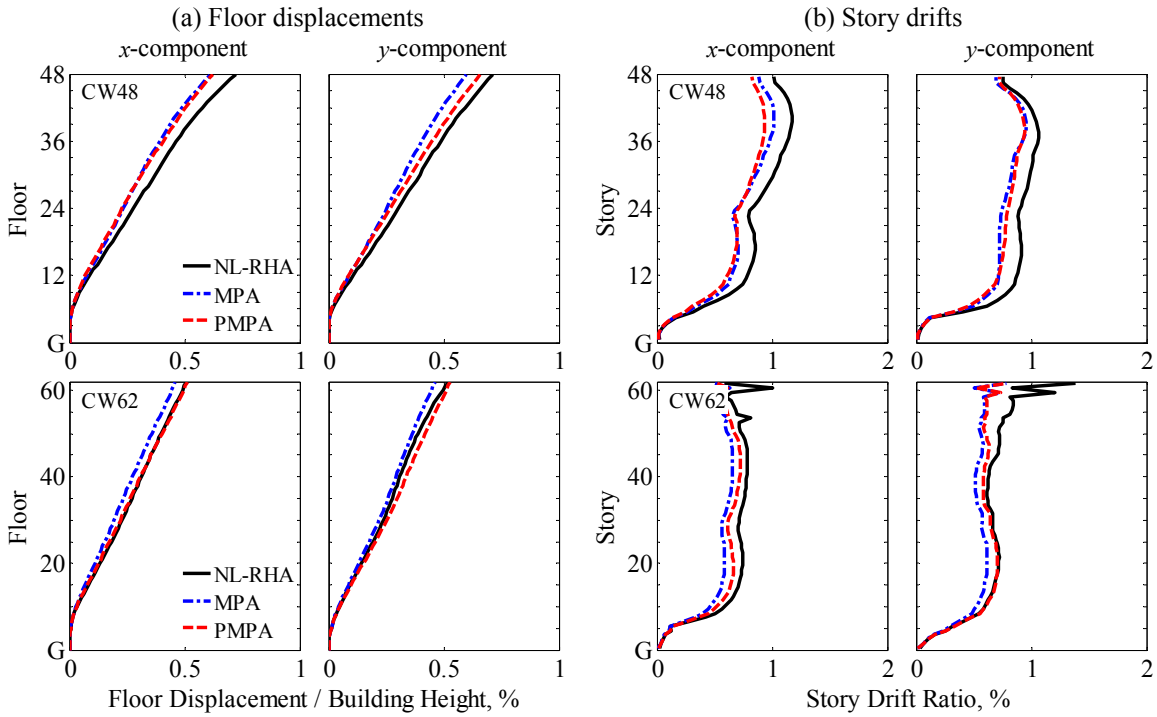

Figure 4.19 Median values of (a) floor displacements and (b) story drifts at the C.M. of the CW48 (row 1) and CW62 (row 2) buildings determined by nonlinear RHA, MPA, and PMPA.

Table 4.3 Peak deformation ratio $(\hat{D}_n)_{\text{PMPA}} \div (\hat{D}_n)_{\text{MPA}}$ for the first pair of modes of the CW48 and CW62 buildings

Building	$(\hat{D}_n)_{\text{PMPA}} \div (\hat{D}_n)_{\text{MPA}}$	
	a-dir (n=1)	b-dir (n=2)
CW48	1.08	1.16
CW62	1.13	1.27

Figure 4.20 compares the accuracy of PMPA in estimating the response of nonlinear systems with that of RSA in estimating the response of linear systems. For each of the two buildings, the results for story drifts at the C.M. are organized in two parts: (a) story drift demands for these buildings treated as linearly elastic systems determined by RSA and RHA procedures, and (b) demands for nonlinear systems determined by PMPA and nonlinear RHA. In implementing the RSA and PMPA procedures, three pairs of "modes" were included for each building.

Observe that the RSA procedure underestimates the median response for both buildings. This underestimation tends to be greater in the upper stories of the buildings, consistent with the height-wise variation of contribution of higher modes to response [Chopra, 2007: Chapter 18]. The height-wise average underestimation in story drifts is 13% and 12% for the CW48 and CW62 buildings, respectively. The additional errors introduced by estimating D_n using empirical equations and by neglecting modal coupling and cyclic stiffness degradation in the PMPA procedure, which are apparent by comparing parts (a) and (b) of Fig. 4.20, are small. PMPA underestimates the story drifts by 16% and 9% (height-wise average error) for the CW48 and the CW62 buildings, respectively; these errors are about the same as those observed in RSA.

For the CW48 building, the principal source of errors in PMPA is due to the underestimation of roof displacement (Fig. 4.19). Suppose we eliminate this underestimation by scaling the PMPA values of D_n to obtain roof displacements equal to the exact values from nonlinear RHA, as shown in Fig. 4.21a. Then, the height-wise average error is reduced from 16% to 5%. Thus, it would be useful to develop improved methods to estimate roof displacement.

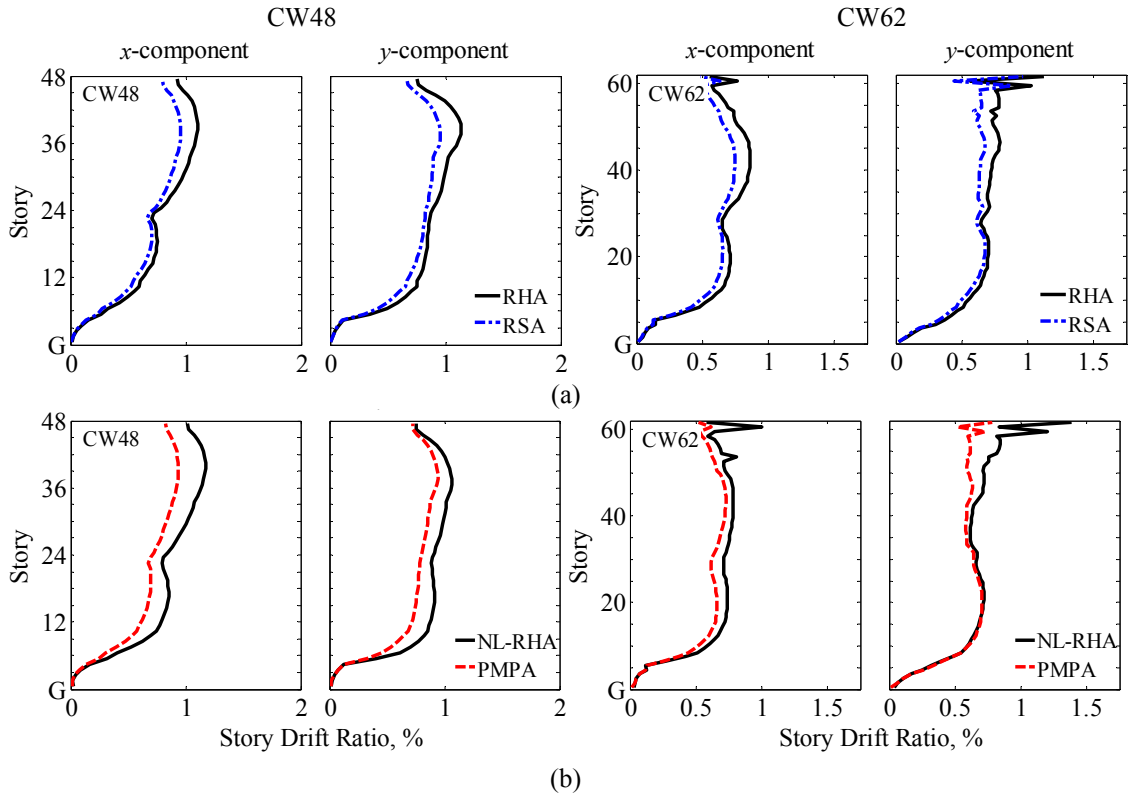

Figure 4.20 Median story drifts at the C.M. for: (a) linearly elastic systems determined by RSA and RHA procedures, and (b) inelastic systems determined by PMPA and nonlinear RHA procedures. Results are for CW48 and CW62 buildings.

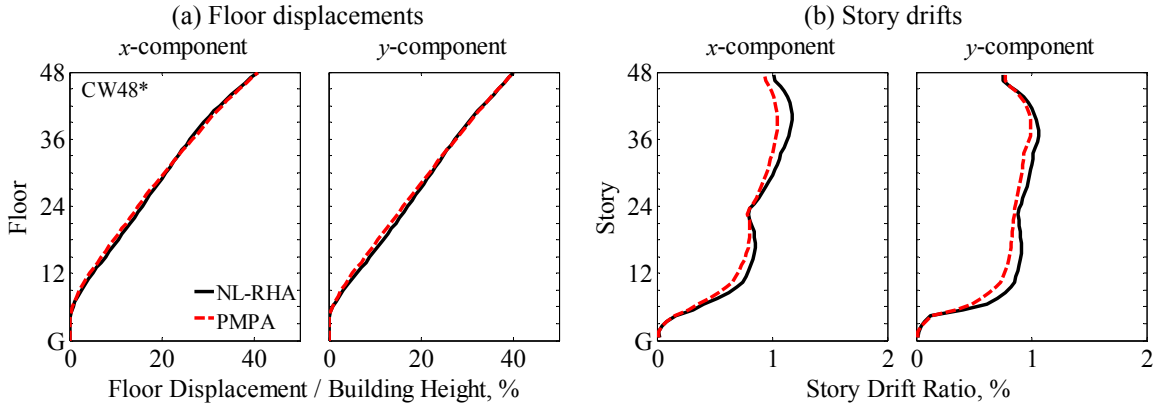

Figure 4.21 Median values of (a) floor displacements and (b) story drifts at the C.M. of the CW48 building determined by nonlinear RHA and PMPA with D_n values scaled to obtain roof displacements equal to those from NLRHA.

The PMPA procedure is an attractive alternative to estimate seismic demands for tall buildings due to two horizontal components of ground motion, simultaneously, not only because it calculates D_n directly from the design spectrum, but also because it leads to a slightly larger estimate of seismic demand, thus reducing the unconservatism (relative to nonlinear RHA) of MPA results.

4.5.2 Other Response Quantities

The member forces and total end rotations corresponding to the median story drifts determined by PMPA (Fig. 4.19b) were estimated by implementing Steps 11 and 12 of the PMPA procedure (Section 3.4). Figure 4.22 presents results for the CW48 building including, bending moments, shear forces, and end rotations in the coupling beams highlighted in Fig. 4.1a, determined by the PMPA and nonlinear RHA procedures. It is apparent that internal forces are estimated accurately, whereas total rotations are underestimated just as the story drifts were underestimated. The error in internal forces is generally smaller than the error in hinge rotations because internal forces vary slowly with hinge rotation for members that deform beyond the elastic limit at both ends. As a result, even a large error in the hinge rotation leads to only small error in the computed internal forces; these observations are consistent with Goel and Chopra [2005].

The forces in the core wall can be estimated to a useful degree of accuracy by the PMPA procedure. Figure 4.23 presents the height-wise variation of bending moments (M_x and M_y) and shear forces (V_x and V_y) in the core wall of the CW48 building including a variable number of "modes" in PMPA superimposed with the results from nonlinear RHA. Figure 4.23 shows that the first pair of "modes" alone is grossly inadequate in estimating internal forces; however, with the second and third pair of

"modes" included, internal forces estimated by PMPA resemble nonlinear RHA results. By including the contributions of all significant modes of vibration, PMPA is able to adequately capture the height-wise variation of shear forces and bending moments in the core shear wall. Thus, PMPA overcomes a well known limitation of pushover procedures with invariant force distribution which are unable to consider the important higher mode effects after formation of local mechanisms [Krawinkler and Seneviratna, 1998].

In summary, based on the results presented in Figs. 4.20, 4.22 and 4.23, the PMPA procedure offers a sufficient degree of accuracy that should make it useful for practical application in estimating seismic demands—floor displacements, story drifts, rotations and internal forces—for tall buildings due to two horizontal components of ground motion applied simultaneously.

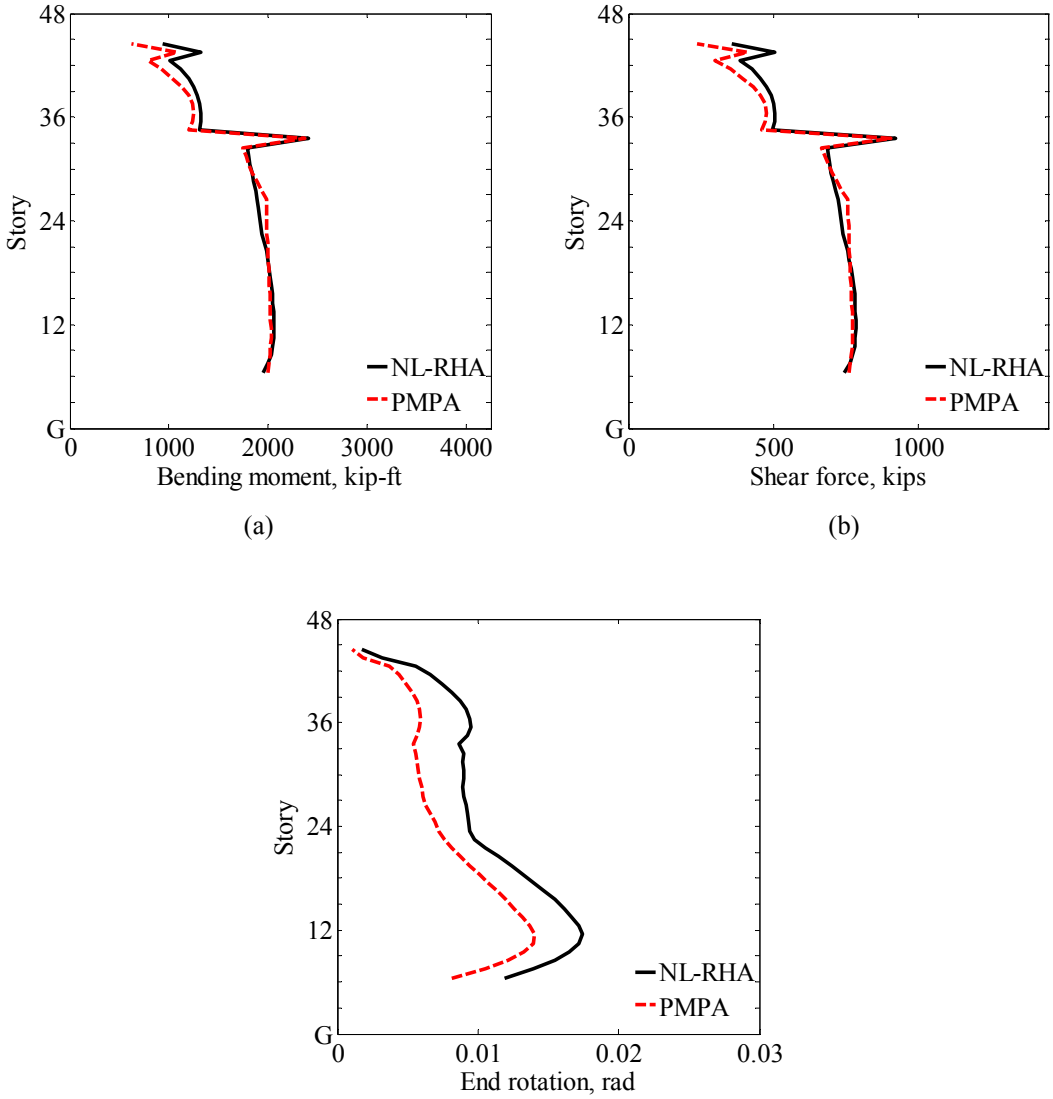

Figure 4.22 (a) Bending moments, (b) shear forces, and (c) total rotations for the coupling beams highlighted in Fig. 4.1a of the CW48 building, determined by nonlinear RHA and PMPA.

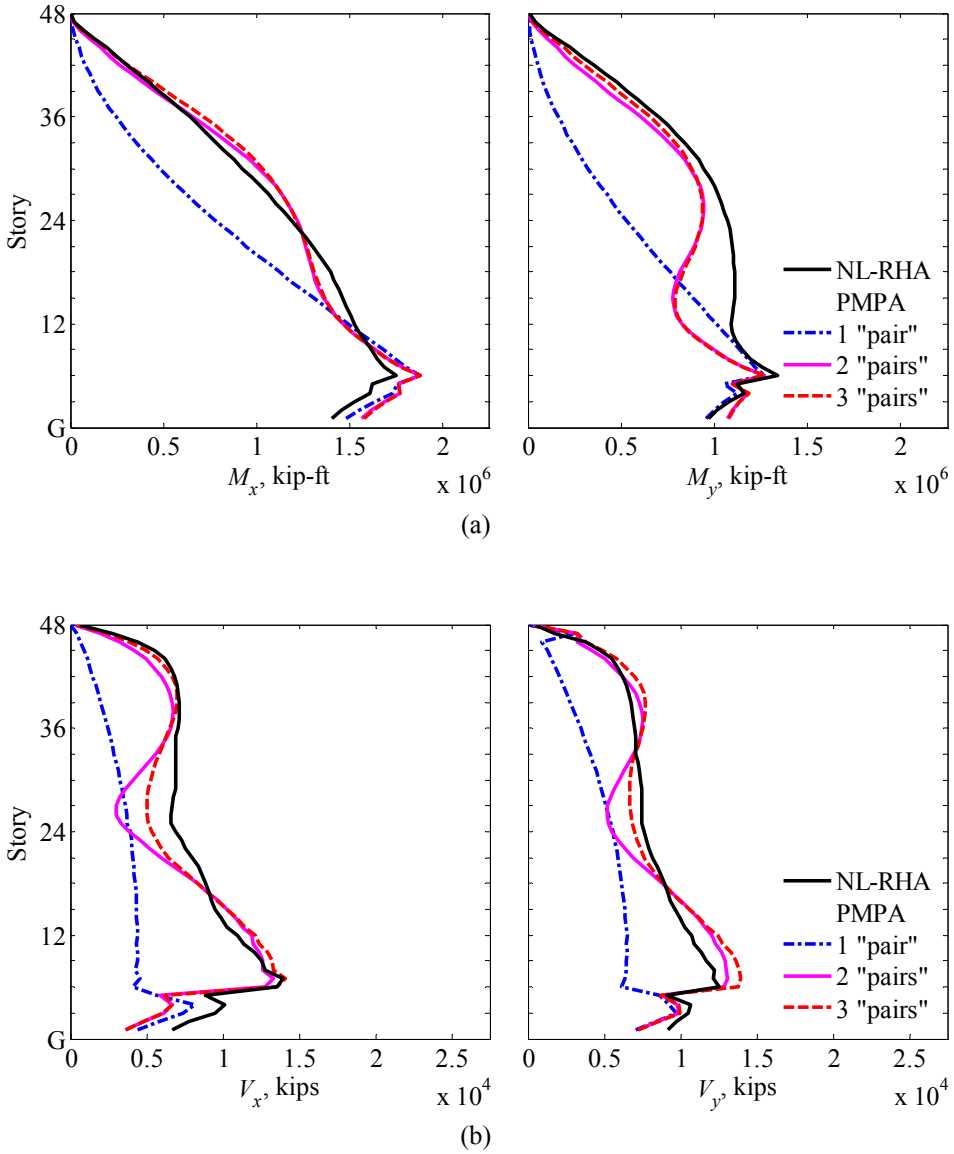

Figure 4.23 (a) Bending moments M_x and M_y, and (b) shear forces V_x and V_y for the core wall of the CW48 building, determined by nonlinear RHA and PMPA.

5 Evaluation of MPA for Unsymmetric-Plan Buildings

This chapter evaluates the accuracy of the MPA, MMPA and PMPA procedures (Chapter 3) for estimating seismic demands for low- and medium-rise unsymmetric-plan buildings with ductile frames. This is followed by a comparative evaluation of the MPA, ASCE41-06 and Eurocode 8 procedures. These investigations are based on seismic demands computed for six buildings due to 39 ground motions acting simultaneously in two orthogonal horizontal directions.

5.1 Selected Structural Systems and Modeling Assumptions

5.1.1 Structural Systems

The structural systems considered are three- and nine-story steel buildings with ductile frames. Four buildings intended to represent some existing buildings were designed according to the 1985 Uniform Building Code (UBC85) while others designs intended to represent new buildings were based on the 2006 International Building Code (IBC06). The plan shapes and frame layouts shown in Fig. 5.1 were considered before selecting the plans showing in Fig. 5.2; moment resisting frames are highlighted in the plans. The buildings are identified by the letters A, B, and C (depending on the plan shape) followed by the number of stories and the design code; plan A is rectangular with two axes of symmetry; plan B is symmetric about the *y* axis, and plan C is unsymmetric about both *x* and *y* axes.

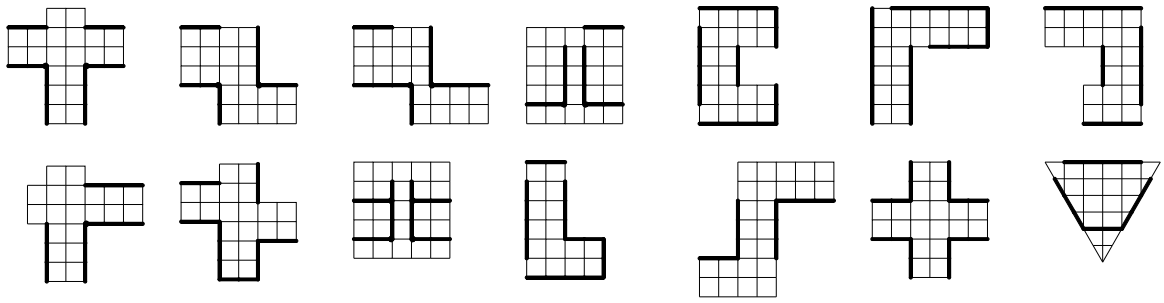

Figure 5.1 Building layouts considered; moment resisting frames are highlighted.

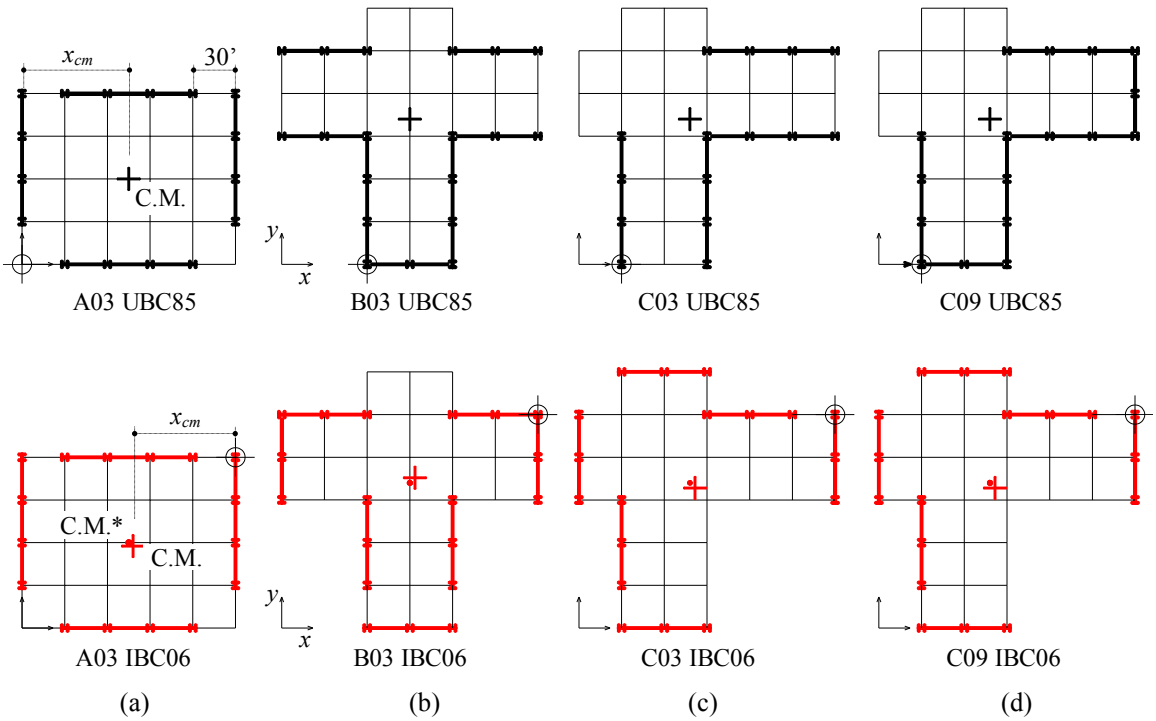

Figure 5.2 Schematic plans of the selected structural systems: (a) A03 buildings, (b) B03 buildings, (c) C03 buildings, and (d) C09 buildings designed according to UBC85 (upper row) and IBC06 (lower row); moment resisting frames are highlighted.

The buildings have similar areas and floor weights with span length 30 ft and story height 13 feet. Design code forces for the buildings, assumed to be located in Bell, CA (33.996N, 118.162 W) were determined, but their member sizes (presented in Appendix B) were governed by drift instead of strength requirements.

5.1.2 Modeling

The buildings were modeled for dynamic analysis, implemented in the PERFORM-3D computer program [CSI, 2006], with the following features: (1) Beams and columns were modeled by a linear element with tri-linear plastic hinges at the ends of the elements that include in-cycle strength deterioration, but not cyclic stiffness degradation (Fig. 4.4a). Axial load-moment interaction in columns is represented by plasticity theory. (2) Panel zones were modeled as four rigid links hinged at the corners with a rotational spring that represents the strength and stiffness of the connection (Fig. 5.3) [Krawinkler, 1978]. (3) Ductility capacities of girders, columns and panel zones were specified according to the ASCE/SEI 41-06 standard [ASCE, 2007]. (4) Columns of moment resisting frames were assumed to be fixed at the base, whereas gravity columns were considered pinned at the base. (5) The geometric nonlinear effects were considered by a standard P-Delta formulation for both moment and gravity frames. (6) Accidental torsion was not considered in the design of the UBC85 buildings, whereas for the IBC06 buildings, the C.M. was shifted from its actual location (C.M.* in Fig. 5.2a) a distance equal to 5% of the maximum dimension of the buildings in the x and y directions (Fig. 5.2). (7) Damping of these buildings was modeled by *Rayleigh damping* with its two constants selected to give 2% damping ratio at the fundamental period of vibration T_1 and a period of $0.2T_1$. Figure 5.4 shows that the damping ratios for the first nine vibration modes of the UBC85 and IBC06 buildings range from 1.5% to 5.2%.

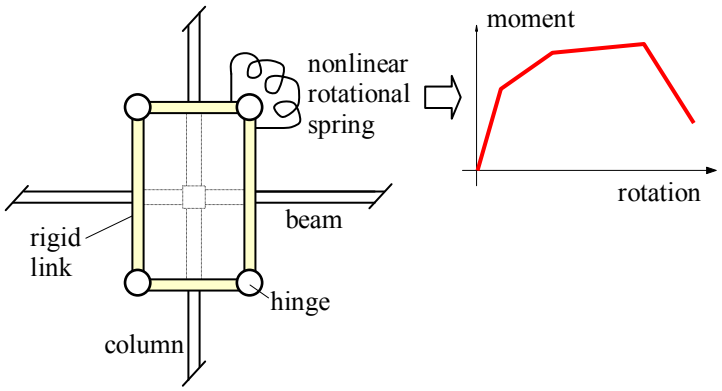

Figure 5.3 Krawinkler model for panel zones; adapted from CSI [2006].

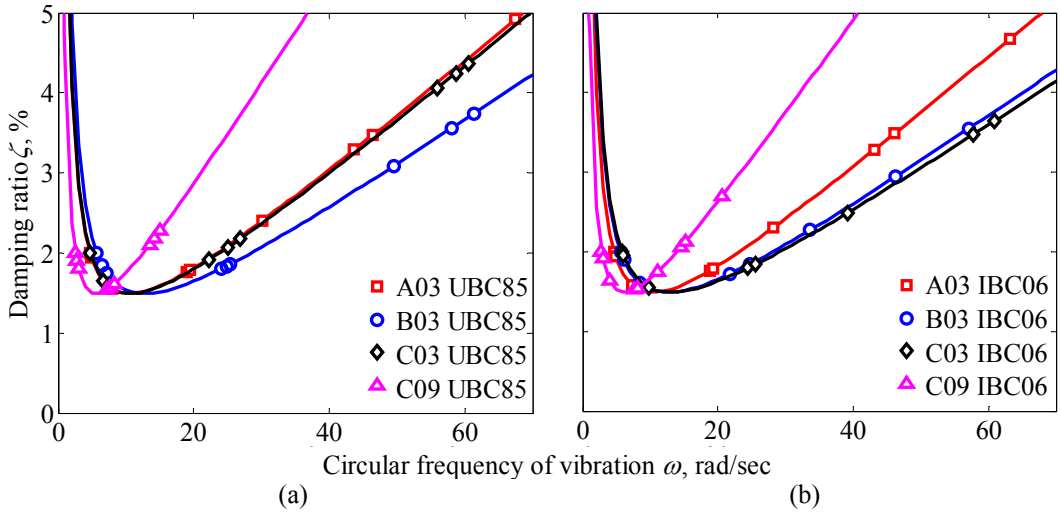

Figure 5.4 Modal damping ratios identified in the damping ratio versus frequency curves for (a) UBC85 buildings and (b) IBC06 buildings.

5.1.3 Natural Vibration Periods and Modes

Figures 5.5 through 5.7 show the natural periods and modes of vibration of the UBC85 buildings; x_{cm} is the distance from the C.M. to a corner of the building (Fig. 5.2). Figure 5.5 shows the height-wise variation of lateral displacements and torsional rotation, whereas Figs. 5.6 and 5.7 show the motion of the roof in plan. The effective modal masses for the first nine modes of vibration are presented in Fig. 5.8.

Figures 5.5 through 5.8 permit the following observations. (1) Lateral displacements dominate motion of the A03 UBC85 building in modes 1 and 2, and in modes 4 and 5, whereas torsion dominates motion in the third and sixth modes, indicating weak coupling between lateral and torsional components of motion. Additionally, the period of the dominantly-torsional mode is much shorter than the periods of the dominantly-lateral modes, a property representative of buildings with moment-resisting frames located along the perimeter of the plan; this system will be referred to as a "torsionally-stiff" system. (2) Torsional rotations dominate motion in the first and fourth modes of the C03 and C09 UBC85 buildings, whereas lateral displacements dominate motion in the second and fifth modes, indicating weak coupling between lateral and torsional motions for these two set of modes. Because the period of the dominantly-torsional modes are longer than that of the dominantly-lateral modes, this system is said to be "torsionally-flexible". (3) Coupled lateral-torsional motions occur in modes 1 and 2, and in modes 4 and 5 of the B03 UBC85 building, which has similar vibration periods. This system will be referred to as a "torsionally-similarly-stiff" system. (4) The higher-mode contributions to forces are expected to be significant for the B03, C03 and C09 UBC85 buildings because the effective mass of the first lateral mode is less than 50% of the total mass (Fig. 5.8).

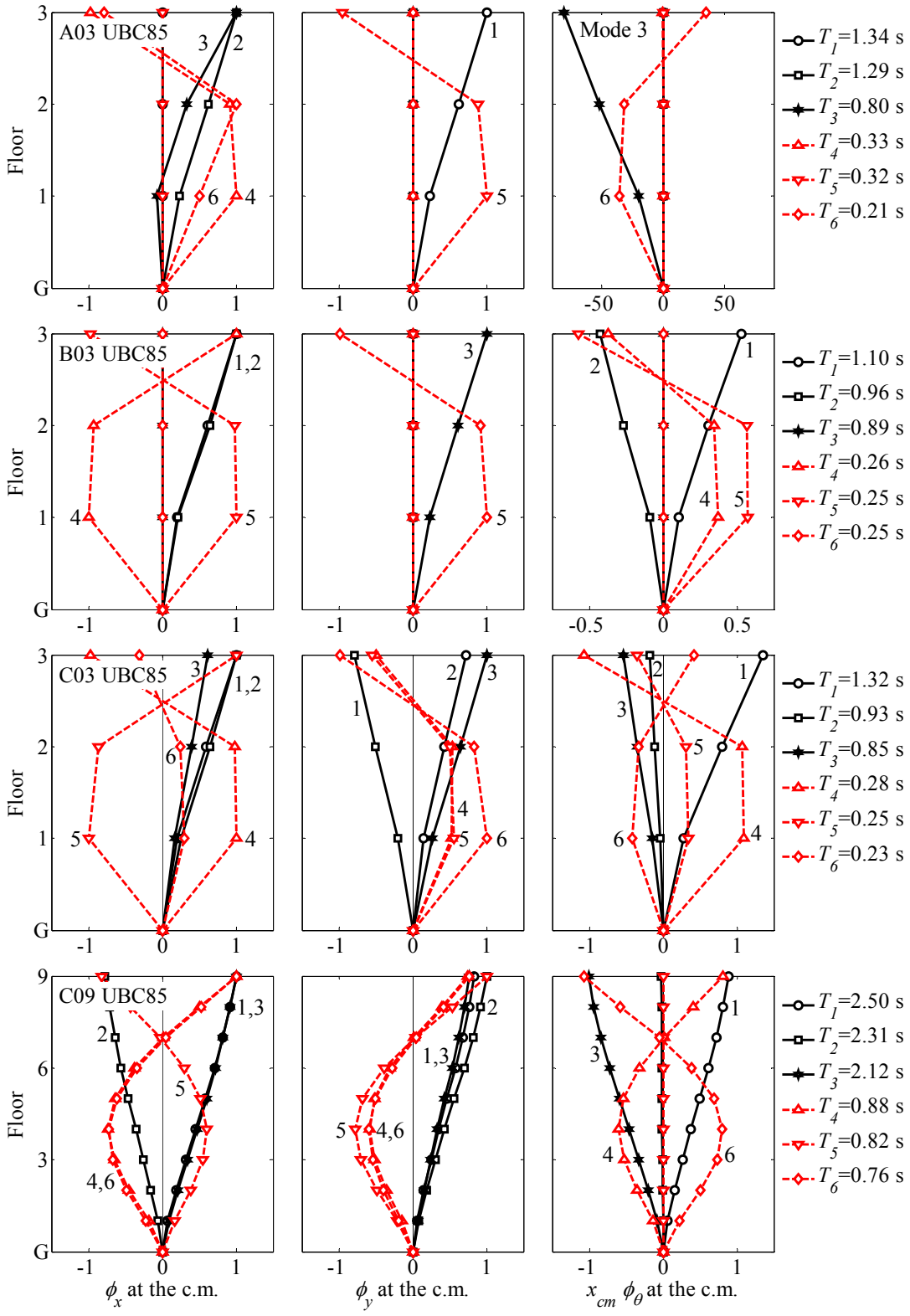

Figure 5.5 First six natural periods and modes of vibration of UBC85 buildings; *x*-lateral, *y*-lateral and torsional motions are shown in the three columns.

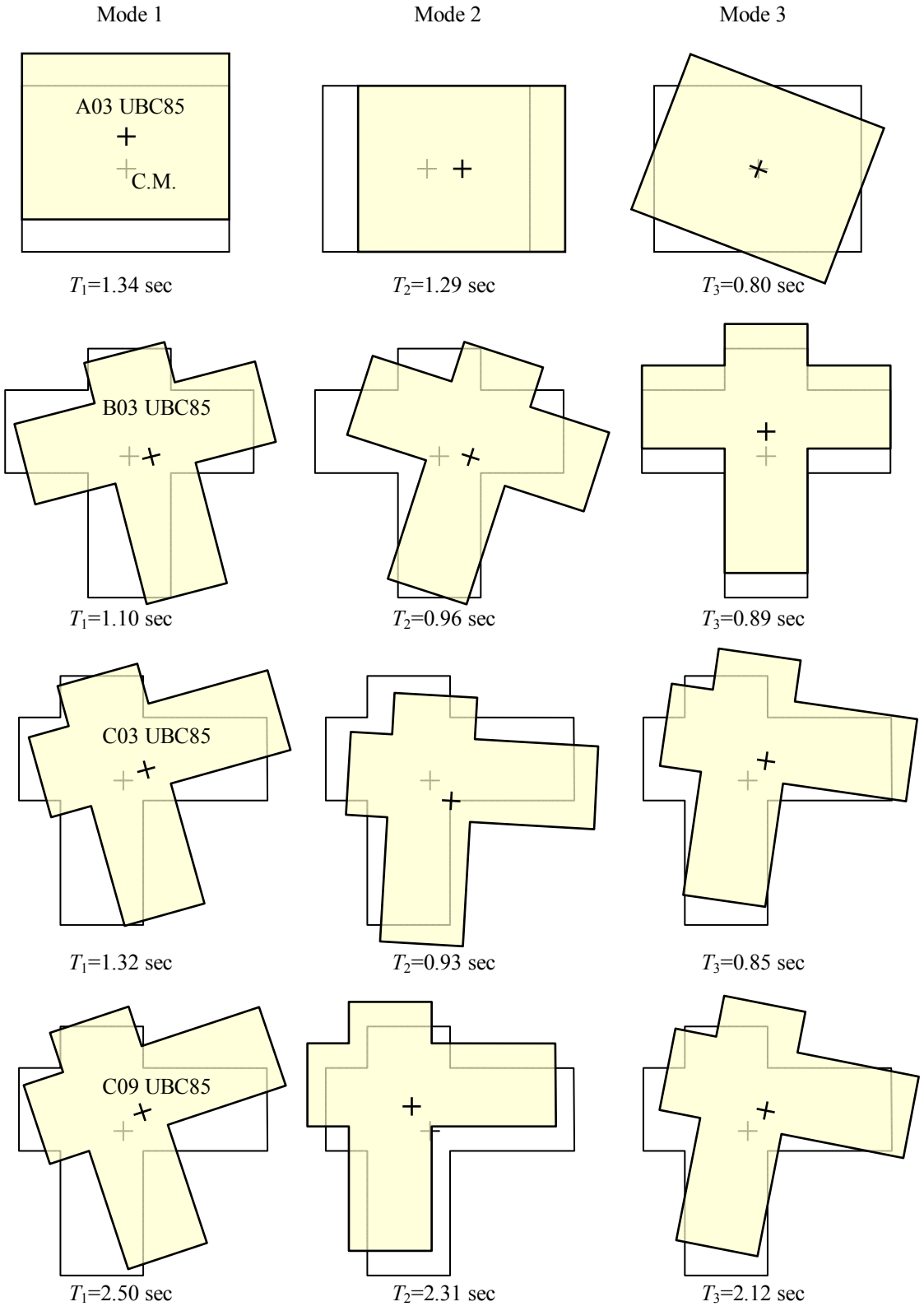

Figure 5.6 First triplet of periods and modes of vibration of UBC85 buildings (only roof motion is shown).

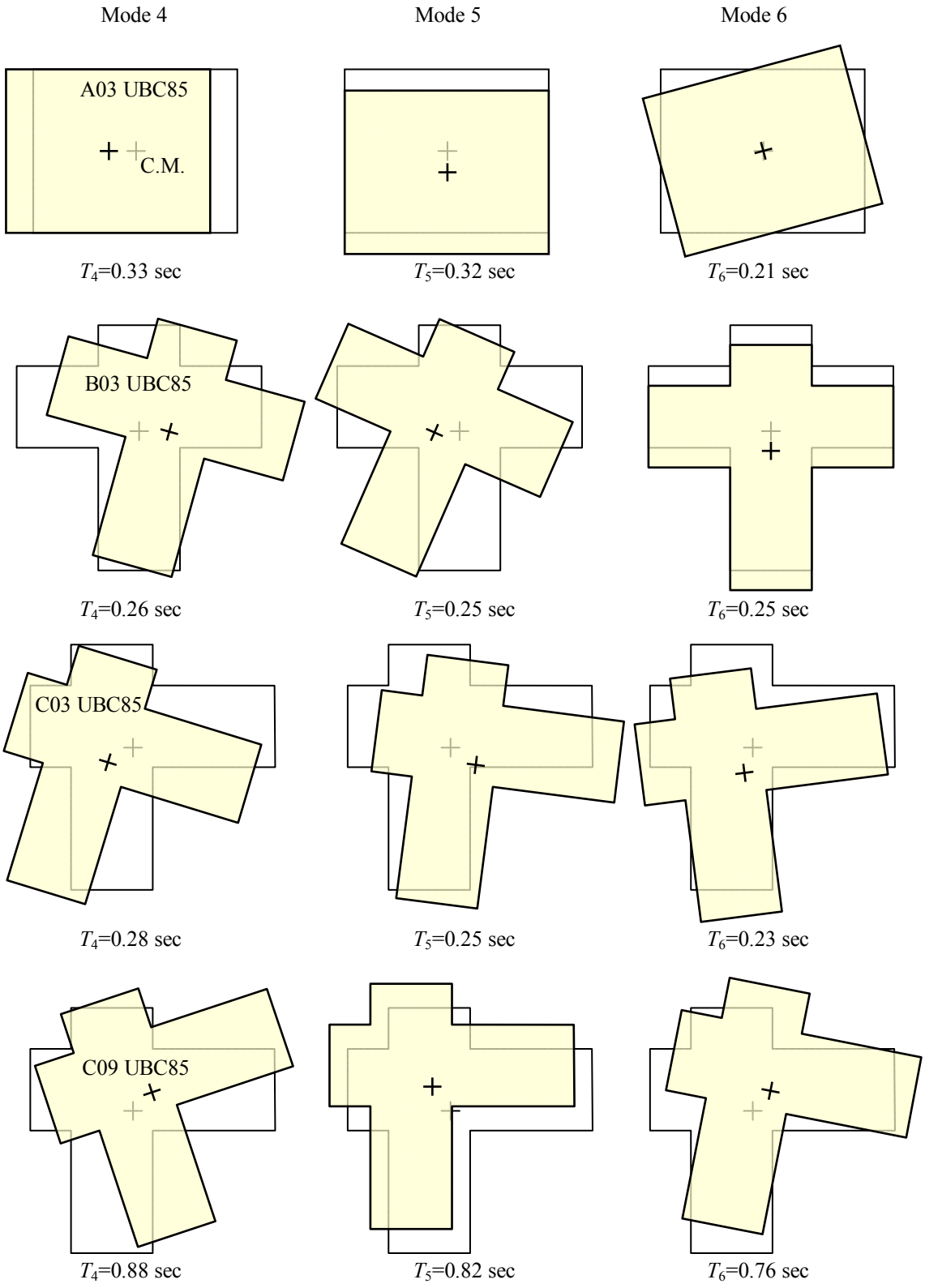

Figure 5.7 Second triplet of periods and modes of vibration of UBC85 buildings (only roof motion is shown).

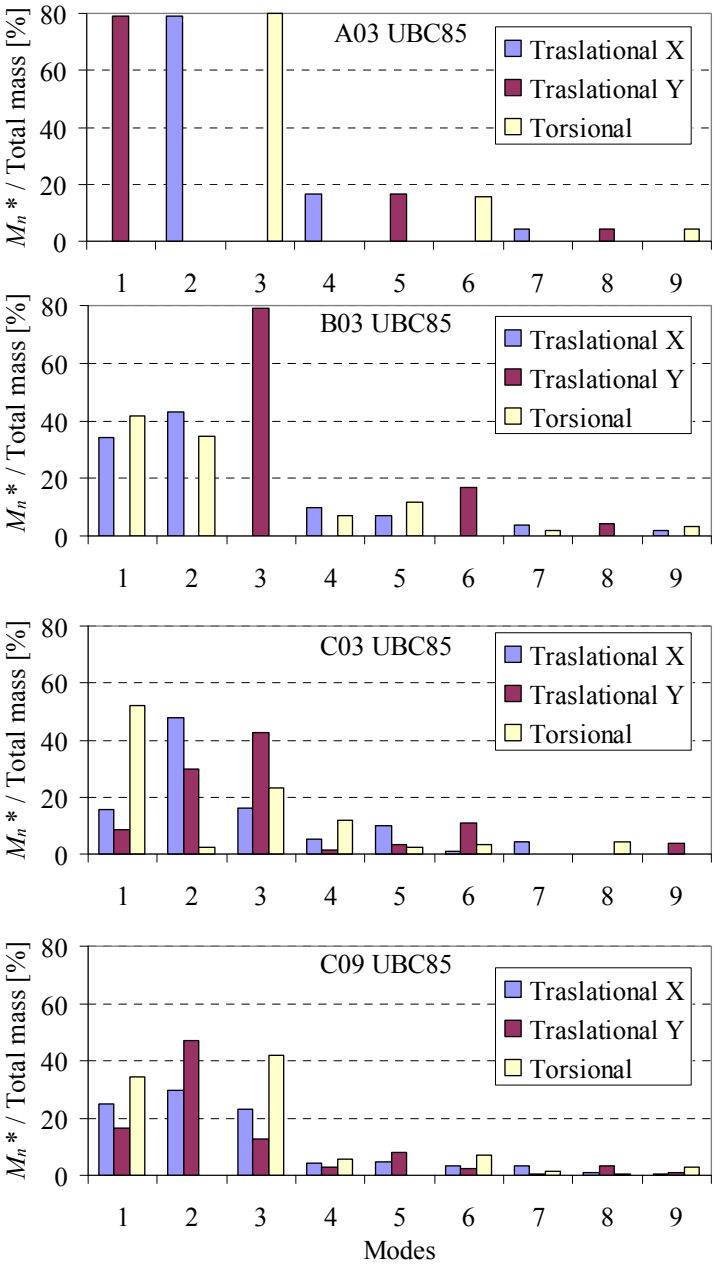

Figure 5.8 Effective modal masses for UBC85 buildings

Figures 5.9 through 5.11 show natural periods and modes of vibration of the IBC06 buildings. Figure 5.9 shows the height-wise variation of lateral displacement and torsional rotations, whereas Figs. 5.10 and 5.11 show the motion of the roof in plan. The effective modal masses for the first nine modes of vibration are presented in Fig. 5.12.

Figures 5.9 through 5.11 permit the following observations. (1) IBC06 is successful in significantly reducing the torsional motions that develop in unsymmetric-plan buildings designed in accordance with UBC85 and other older codes. (2) Lateral displacements dominate motion of all IBC06 buildings in their first two modes, whereas torsional rotations dominate motion in the third mode. (3) The period of the dominantly-torsional mode is much shorter than that of the dominantly-lateral modes, indicating that the modern code provisions result in torsionally-stiff buildings. (4) The vibration periods of the C03 and C09 IBC06 buildings in modes 1 and 2 and in modes 4 and 5 with coupled lateral-torsional motions are very close to each other. (5) The higher-mode contributions to forces are expected to be significant for the C03 and C09 IBC06 buildings because the effective mass of the first lateral mode is less than 60% of the total mass (Fig. 5.12).

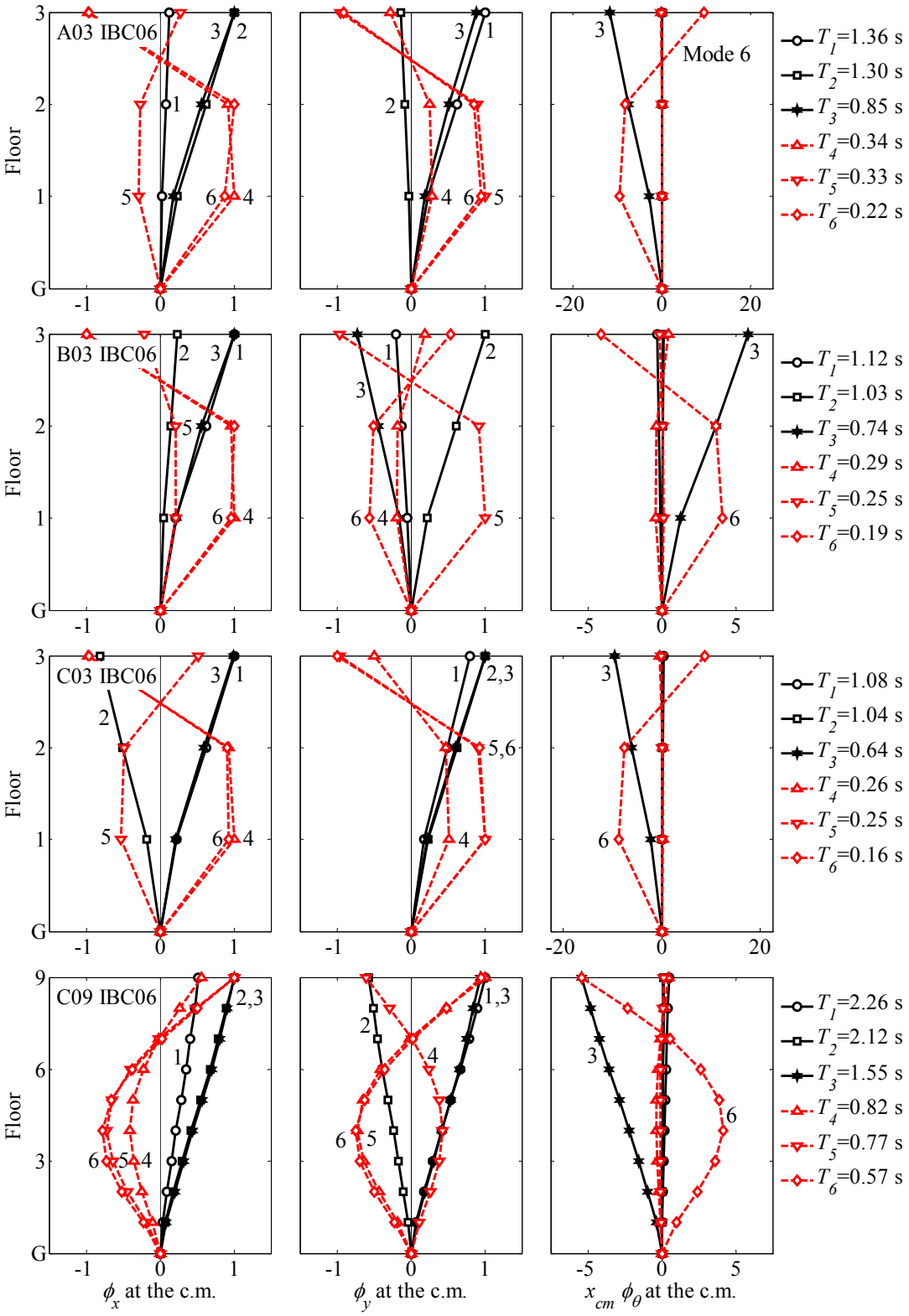

Figure 5.9 First six natural periods and modes of vibration of IBC06 buildings; *x*-lateral, *y*-lateral and torsional motions are shown in the three columns.

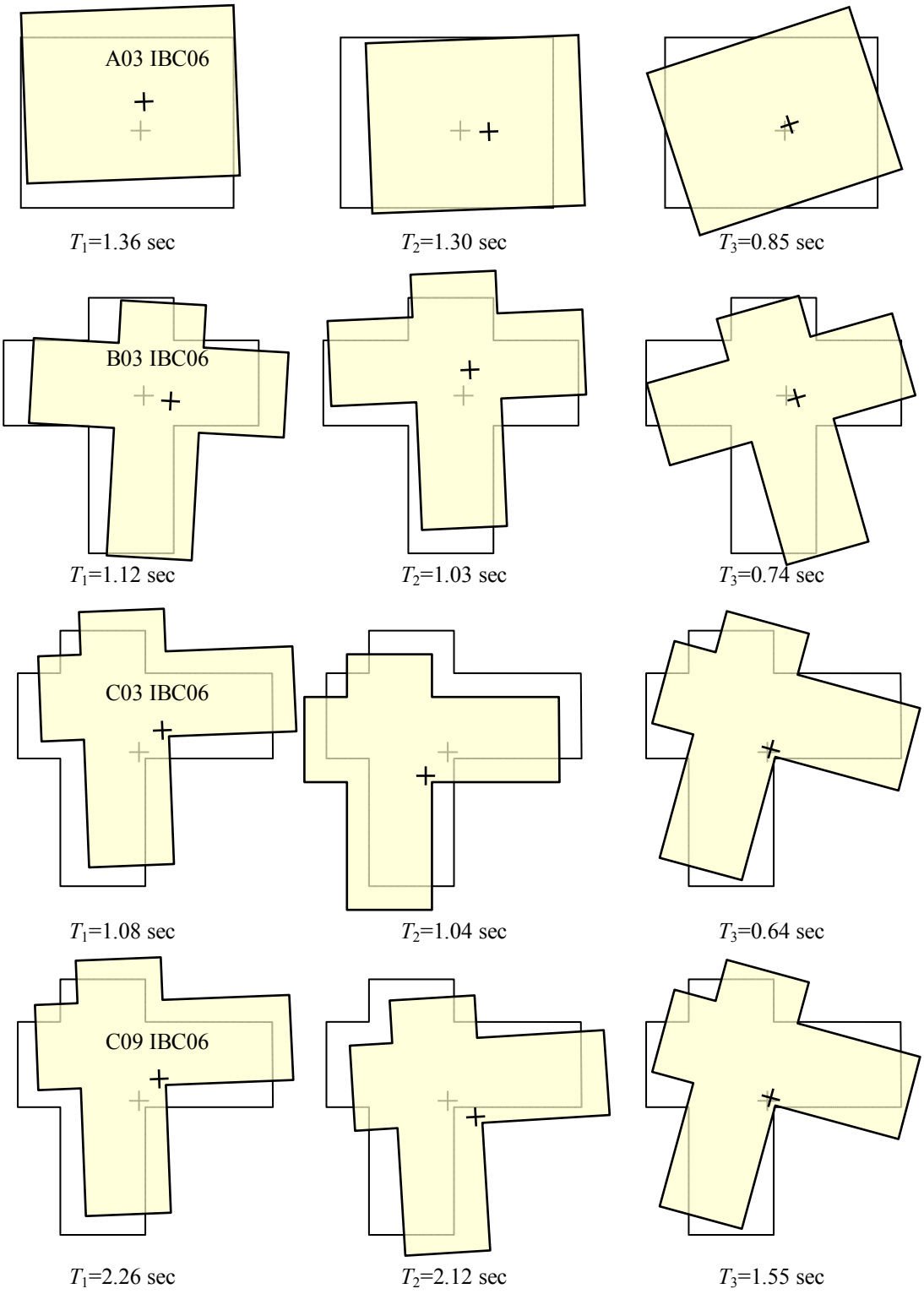

Figure 5.10 First triplet of periods and modes of vibration of IBC06 buildings (only roof motion is shown).

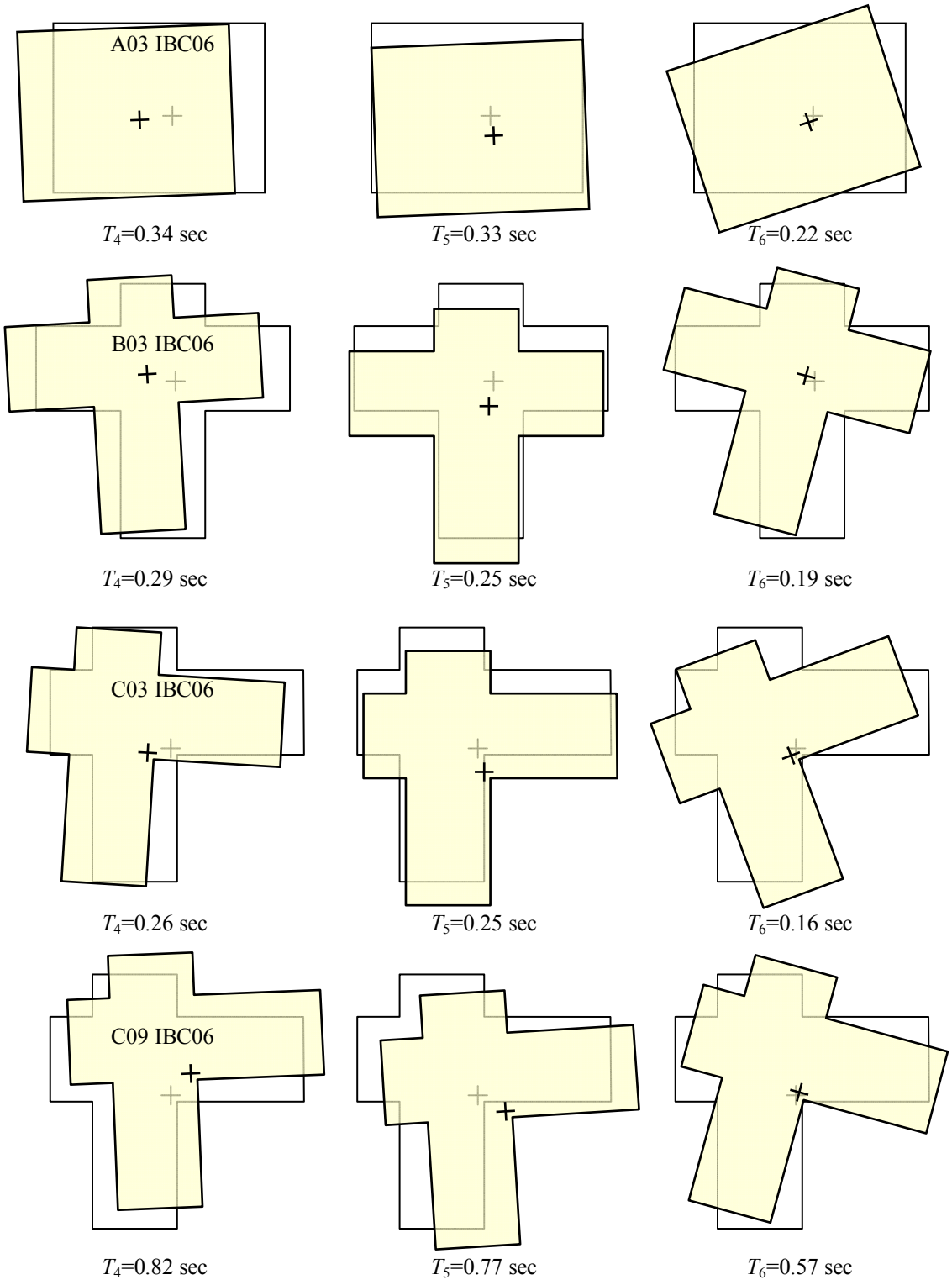

Figure 5.11 Second triplet of periods and modes of vibration of IBC06 buildings (only roof motion is shown).

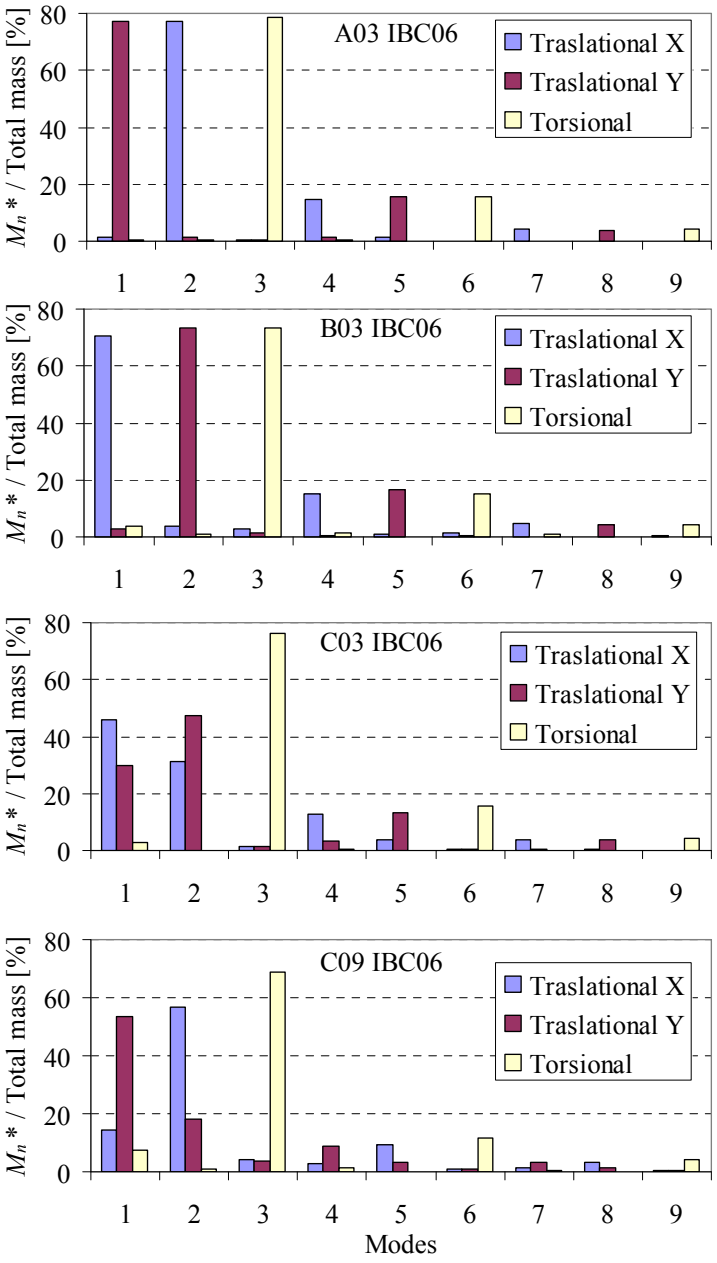

Figure 5.12 Effective modal masses for IBC06 buildings

5.2 Ground Motions

5.2.1 Selected Earthquake Records

A total of 39 ground acceleration records from 14 different earthquakes with magnitudes ranging from 6.5 to 7.6 were selected according to the following criteria [Haselton and Deierlein, 2007]:

- Fault type: strike-slip and thrust faults, consistent with earthquake mechanisms present in California.
- Site class: hard rock to stiff soil, i.e. NEHRP site classes A to D (selected records are all from site classes C or D).
- Peak ground acceleration, PGA > 0.2g, and peak ground velocity, PGV > 15 cm/sec.
- Average shear-wave velocity in upper 30m of soil, $V_{s\text{-}30}$ > 180 cm/sec.
- Lowest useable frequency < 0.25 Hz, to ensure that the low frequency content was not removed by the ground-motion filtering process.
- Limit of six records from a single seismic event.
- No consideration of response spectral shape.

Table 5.1 lists the selected records and their relevant data [PEER, 2007]. Each of the 39 records includes two orthogonal components of horizontal ground motion. Figure 5.13 shows the magnitude-distance distribution for the ensemble of selected records, wherein R_{JB} is the distance of the site to the surface projection of fault rupture, as defined by Joyner and Boore [1981].

Table 5.1 List of 39 ground motion records (†)

Record	Earthquake Name	Mw	Mechanism	Station Name	Vs30 (m/s)	NEHRP Based on Vs30	R_{JB} (km)	Component *a*			Component *b*		
								Comp 1 (deg)	PGA (cm/s^2)	PGV (cm/s)	Comp 2 (deg)	PGA (cm/s^2)	PGV (cm/s)
1	1994 Northridge	6.7	Reverse	Beverly Hills - 14145 Mulhol	355.8	D	9.4	9	407.6	58.9	279	506.3	62.7
2	1994 Northridge	6.7	Reverse	Canyon Country - W Lost Cany	308.6	D	11.4	0	402.0	43.0	270	472.6	45.1
3	1994 Northridge	6.7	Reverse	LA - Saturn St	308.7	D	21.2	20	465.2	34.5	110	430.0	39.0
4	1994 Northridge	6.7	Reverse	Santa Monica City Hall	336.2	D	17.3	90	865.9	41.7	360	362.6	25.1
5	1994 Northridge	6.7	Reverse	Beverly Hills - 12520 Mulhol	545.7	C	12.4	35	604.8	40.8	125	435.7	30.1
6	1999 Duzce, Turkey	7.1	Strike Slip	Bolu	326.0	D	12.0	0	713.4	56.5	90	806.3	62.1
7	1999 Hector Mine	7.1	Strike Slip	Hector	684.9	C	10.4	0	260.4	28.6	90	330.2	41.8
8	1979 Imperial Valley	6.5	Strike Slip	Delta	274.5	D	22.0	262	233.1	26.0	352	344.2	33.0
9	1979 Imperial Valley	6.5	Strike Slip	El Centro Array #11	196.3	D	12.5	140	356.9	34.4	230	372.2	42.1
10	1979 Imperial Valley	6.5	Strike Slip	Calexico Fire Station	231.2	D	10.5	225	269.5	21.2	315	198.0	16.0
11	1979 Imperial Valley	6.5	Strike Slip	SAHOP Casa Flores	338.6	D	9.6	0	281.8	19.4	270	496.1	31.0
12	1995 Kobe, Japan	6.9	Strike Slip	Nishi-Akashi	609.0	C	7.1	0	499.4	37.3	90	492.9	36.7
13	1995 Kobe, Japan	6.9	Strike Slip	Shin-Osaka	256.0	D	19.1	0	238.5	37.8	90	207.8	27.9
14	1995 Kobe, Japan	6.9	Strike Slip	Kakogawa	312.0	D	22.5	0	246.5	18.7	90	338.0	27.7
15	1995 Kobe, Japan	6.9	Strike Slip	KJMA	312.0	D	0.9	0	805.3	81.6	90	586.8	74.5
16	1999 Kocaeli, Turkey	7.5	Strike Slip	Duzce	276.0	D	13.6	180	306.0	58.8	270	350.9	46.4
17	1999 Kocaeli, Turkey	7.5	Strike Slip	Arcelik	523.0	C	10.6	0	214.6	17.7	90	147.0	39.5
18	1992 Landers	7.3	Strike Slip	Yermo Fire Station	353.6	D	23.6	270	240.0	51.5	360	148.6	29.7
19	1992 Landers	7.3	Strike Slip	Coolwater	271.4	D	19.7	0	277.3	25.6	90	408.7	42.3
20	1992 Landers	7.3	Strike Slip	Joshua Tree	379.3	C	11.0	0	268.4	27.5	90	278.5	43.2
21	1989 Loma Prieta	6.9	Reverse Oblique	Capitola	288.6	D	8.7	0	518.2	35.0	90	434.6	29.2
22	1989 Loma Prieta	6.9	Reverse Oblique	Gilroy Array #3	349.9	D	12.2	0	544.2	35.7	90	360.2	44.7
23	1989 Loma Prieta	6.9	Reverse Oblique	Oakland - Outer Harbor Wharf	248.6	D	74.2	0	281.1	40.9	270	263.9	41.8
24	1989 Loma Prieta	6.9	Reverse Oblique	Hollister - South & Pine	370.8	C	27.7	0	363.3	62.3	90	173.9	29.1
25	1989 Loma Prieta	6.9	Reverse Oblique	Hollister City Hall	198.8	D	27.3	90	241.7	38.5	180	210.6	45.0
26	1989 Loma Prieta	6.9	Reverse Oblique	Hollister Diff. Array	215.5	D	24.5	165	263.4	43.8	255	273.4	35.6
27	1990 Manjil, Iran	7.3	Strike Slip	Abbar	724.0	C	12.6	0	504.5	43.2	90	486.6	53.2
28	1987 Superstition Hills	6.5	Strike Slip	El Centro Imp. Co. Cent	192.1	D	18.2	0	350.9	46.3	90	253.3	40.8
29	1987 Superstition Hills	6.5	Strike Slip	Poe Road (temp)	207.5	D	11.2	270	437.6	35.7	360	294.4	32.8
30	1987 Superstition Hills	6.5	Strike Slip	Westmorland Fire Sta	193.7	D	13.0	90	168.5	23.5	180	206.7	31.0
31	1992 Cape Mendocino	7.0	Reverse	Rio Dell Overpass - FF	311.8	D	7.9	270	377.9	43.9	360	538.2	42.1
32	1999 Chi-Chi, Taiwan	7.6	Reverse Oblique	CHY101	258.9	D	10.0	191	346.0	70.6	281	431.5	115.0
33	1999 Chi-Chi, Taiwan	7.6	Reverse Oblique	TCU045	704.6	C	26.0	135	465.1	36.7	225	502.0	39.1
34	1999 Chi-Chi, Taiwan	7.6	Reverse Oblique	TCU095	446.6	C	45.2	195	371.1	62.0	275	697.7	49.1
35	1999 Chi-Chi, Taiwan	7.6	Reverse Oblique	TCU070	401.3	C	19.0	160	250.2	52.1	250	165.4	62.3
36	1999 Chi-Chi, Taiwan	7.6	Reverse Oblique	WGK	258.9	D	10.0	90	327.3	69.0	360	474.3	74.4
37	1999 Chi-Chi, Taiwan	7.6	Reverse Oblique	CHY006	438.2	C	9.8	6	338.5	42.7	276	357.3	55.4
38	1971 San Fernando	6.6	Reverse	LA - Hollywood Stor FF	316.5	D	22.8	90	205.8	18.9	180	170.8	14.9
39	1976 Friuli, Italy	6.5	Reverse	Tolmezzo	424.8	C	15.0	0	344.4	22.0	270	308.7	30.8

(†) Adapted from Haselton and Deierlein [2007]

5.2.2 Ground-Motion Scaling Procedure

All 39 records were scaled by the procedure presented in Section 4.2.2. Table 5.2 lists the values of $A(T_1)$, the pseudo-acceleration at fundamental period T_1, selected to define ground motion ensembles for two intensities: intensity i1 is defined by $A(T_1)_{2\%/50}$ corresponding to the seismic hazard spectrum with 2% probability of exceedance in 50 years (return period of 2475 years) for the selected site (Section 5.1.1) obtained from the

USGS software: *Seismic Hazard Curves and Uniform Hazard Response Spectra* version 5.0.9 [http://earthquake.usgs.gov/research/]; intensity i1 was scaled by factors of 1.5 and 2.0 for the C09 UBC85 and C09 IBC06 buildings, respectively, to define intensity i2.

Figures 5.14 and 5.15 show the median response spectrum for the ensemble of 39 ground motions scaled to match $A(T_1)_{2\%/50}$ for the UBC85 and IBC06 buildings, respectively, and the seismic hazard spectrum corresponding to 2% probability of exceedance in 50 years. As imposed by the scaling criterion, the median pseudo-acceleration of the ensemble at the fundamental period is matched to the seismic hazard spectrum; the match is imperfect because both components of a record were scaled by the same factor selected to match their geometric mean (not the individual values) to the selected seismic hazard. because T_1 differs for each structure, the scaling factors for ground motions and hence the median spectra vary with the building.

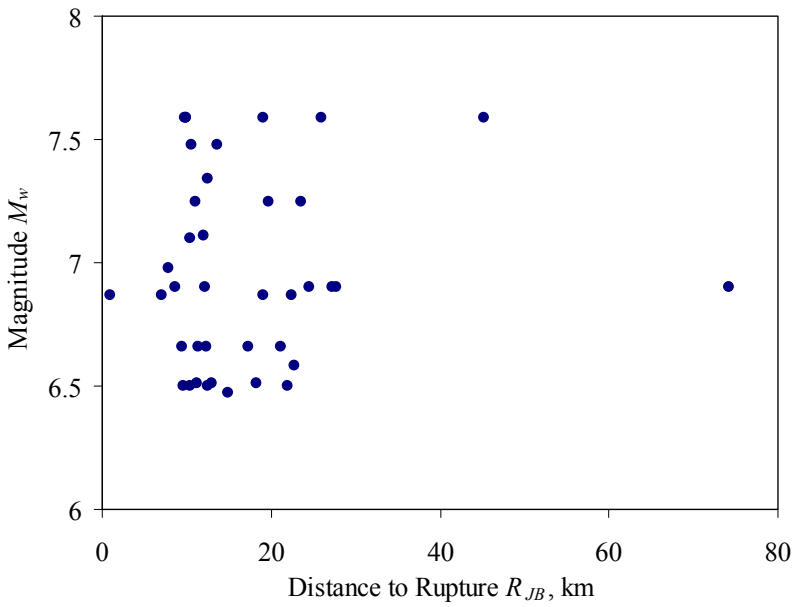

Figure 5.13 Distribution of magnitude, M_w, and distance of site to surface projection of fault rupture, R_{JB}.

Table 5.2 Selected values of $A(T_1)$ corresponding to two ground-motion intensities.

Building	$A(T_1)$ (g)	
	Intensity 1 (i1)	Intensity 2 (i2)
A03 UBC85	0.49	-
B03 UBC85	0.56	-
C03 UBC85	0.50	-
C09 UBC85	0.23	0.34
A03 IBC06	0.49	-
B03 IBC06	0.56	-
C03 IBC06	0.57	-
C09 IBC06	0.25	0.51

Note: Intensity 1 corresponds to the seismic hazard spectrum for 2% probability of exceedance in 50 years.

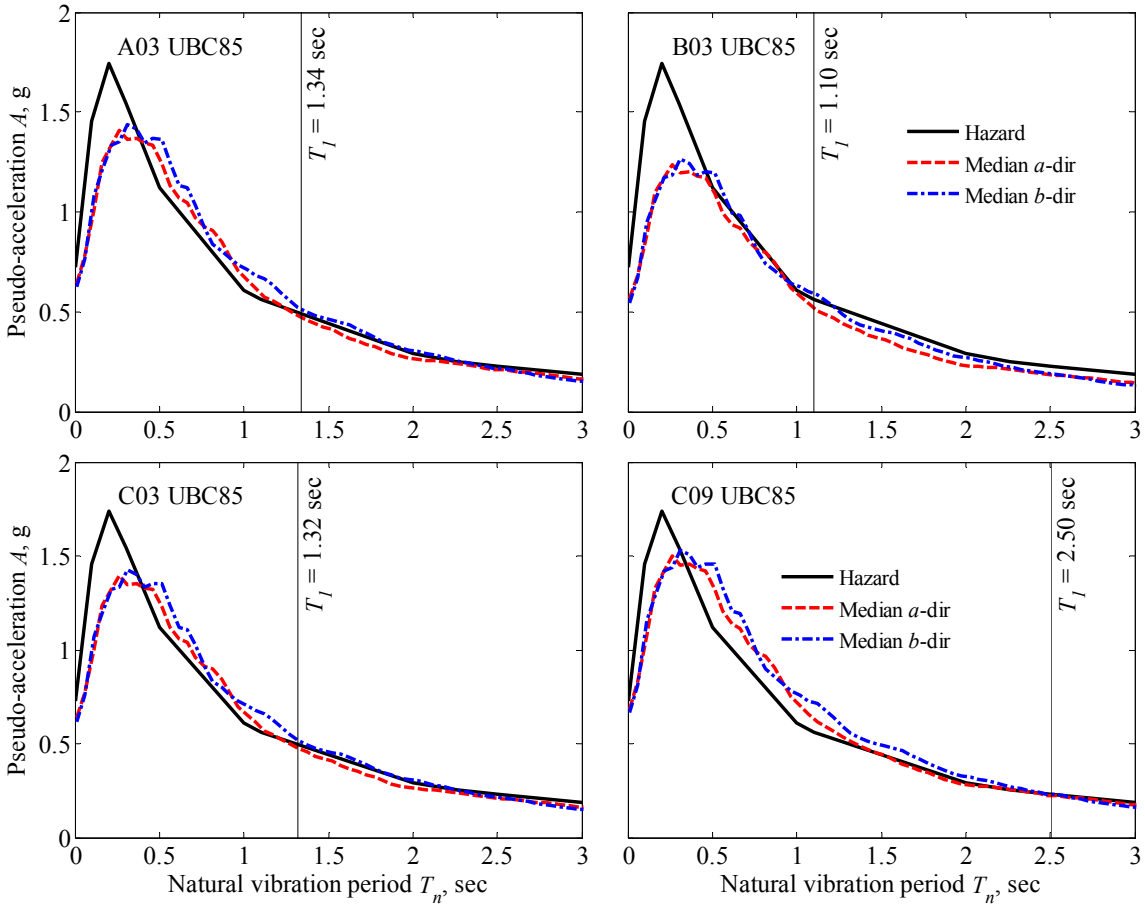

Figure 5.14 Seismic hazard spectrum for building site corresponding to 2% probability of exceedance in 50 years (solid line), and the median response spectra of 39 scaled ground motions in the *a* and *b* directions (dashed lines): A03 UBC85, B03 UBC85, C03 UBC85, and C09 UBC85 buildings.

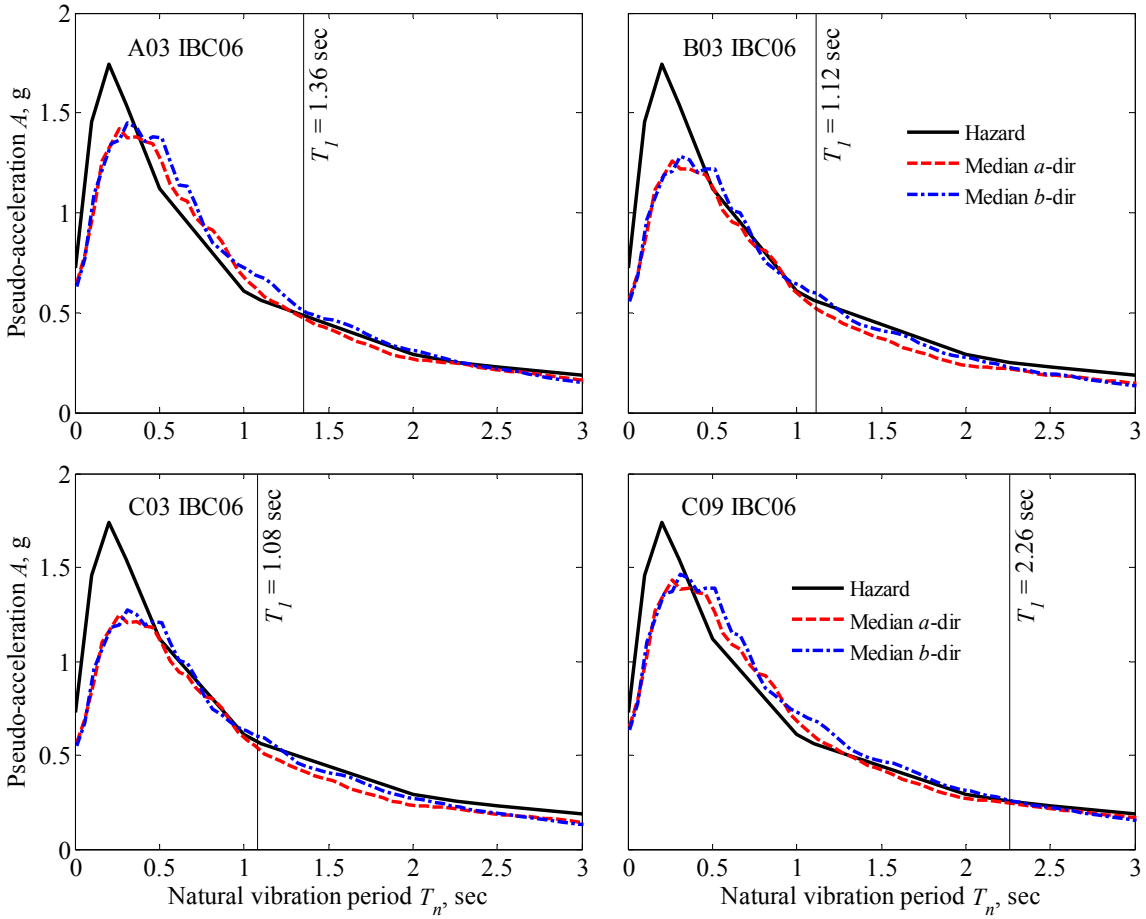

Figure 5.15 Seismic hazard spectrum for building site corresponding to 2% probability of exceedance in 50 years (solid line), and the median response spectra of 39 scaled ground motions in the *a* and *b* directions (dashed lines): A03 IBC06, B03 IBC06, C03 IBC06, and C09 IBC06 buildings.

5.3 Evaluation of MPA

5.3.1 Modal Pushover Curves and Reference Displacements

Figures 5.16 through 5.19 show pushover curves and their tri-linear idealization for the UBC85 and IBC06 buildings associated with their first and second triplets of "modes." Pushover analyses for the first triplet of "modes" of the buildings lead to the following observations (see Fig. 4.16 for definition of u_1, u_2, and u_3). At reference displacements up to u_1, the buildings remain essentially elastic, but some sections begin

to yield. Subsequently at displacements between u_1 and u_2, plastic hinges form at the beam ends and at the base of the first-story columns. From displacements u_2 to u_3 the buildings reach their maximum strength developing a partial or total collapse mechanism. After u_3, in-cycle strength deterioration starts at the base of the first-story columns, resulting in rapid strength degradation. The ductility capacity of the torsionally-similarly-stiff and torsionally-flexible systems is governed by the failure of column sections around the weak axis. This issue is relevant since there is little information available about the nonlinear behavior of steel columns around the weak axis, nor is such information included in the standards of seismic rehabilitation of steel buildings [ASCE, 2007 and British Standards, 2004].

Figures 5.16 through 5.19 also identify the peak modal reference displacement due to each of the 39 scaled ground motions, and their median value $\hat{u}$; these reference displacements were determined in Step 4 of the MPA procedure (Section 3.4). "i1" and "i2" stand for intensity 1 and intensity 2, respectively (Table 5.2). Figure 5.20 presents values of the median ductility factors, defined as $\hat{u}/u_1$. Excluded from the plots are reference displacements due to those ground motions that caused collapse or numerical instability in the response computation of the modal SDF–system: one i1-intensity excitation in case of the A03 UBC85 building, four i2-intensity excitations in case of the C09 UBC85 building, and one i2 excitation in case of the C09 IBC06 building.

Most of the ground motions drive all the UBC85 buildings beyond the first yield displacement u_1 in the first two dominantly-lateral "modes" (Figs. 5.16 to 5.19); the median ductility factor ranges from 1.2 for the C09 building subjected to the i1-intensity ground motions to a maximum of 2.5 for the A03 buildings subjected to the i1-intensity

ground motions, respectively (Fig. 5.20). Fewer than half of the excitations drive the buildings beyond the first yield u_1 in modes 4, 5 and 6, and the median displacement is only slightly larger than the yield displacement u_1.

As in the case of UBC85 buildings, almost all of the excitations drive the IBC06 buildings beyond the first yield displacement u_1 for the dominantly-lateral "modes" (first and second "modes") with ratios $\hat{u} / u_1$ ranging from 1.1 to 2.0 (Fig. 5.20); Only a few of the i1-intensity ground motions drive the buildings beyond the first yield u_1 in "modes" 3, 4, 5, and 6, and the median displacement is smaller than the yield displacement u_1. However, more than half of the i2-intensity ground motions drive the C09 building beyond the first yield u_1 and the median displacement is 1.5 times u_1. These results show that, for most cases, displacements in "modes" higher than the first triplet are either close to or exceed the first yield displacement u_1 only by a modest amount, consistent with results for tall buildings (Chapter 4). Note that these ductility demands due only to one component of ground motion are moderate since the design of the members was governed by drift and not by strength requirements; ductility demands are expect to be larger if the excitation includes both components.

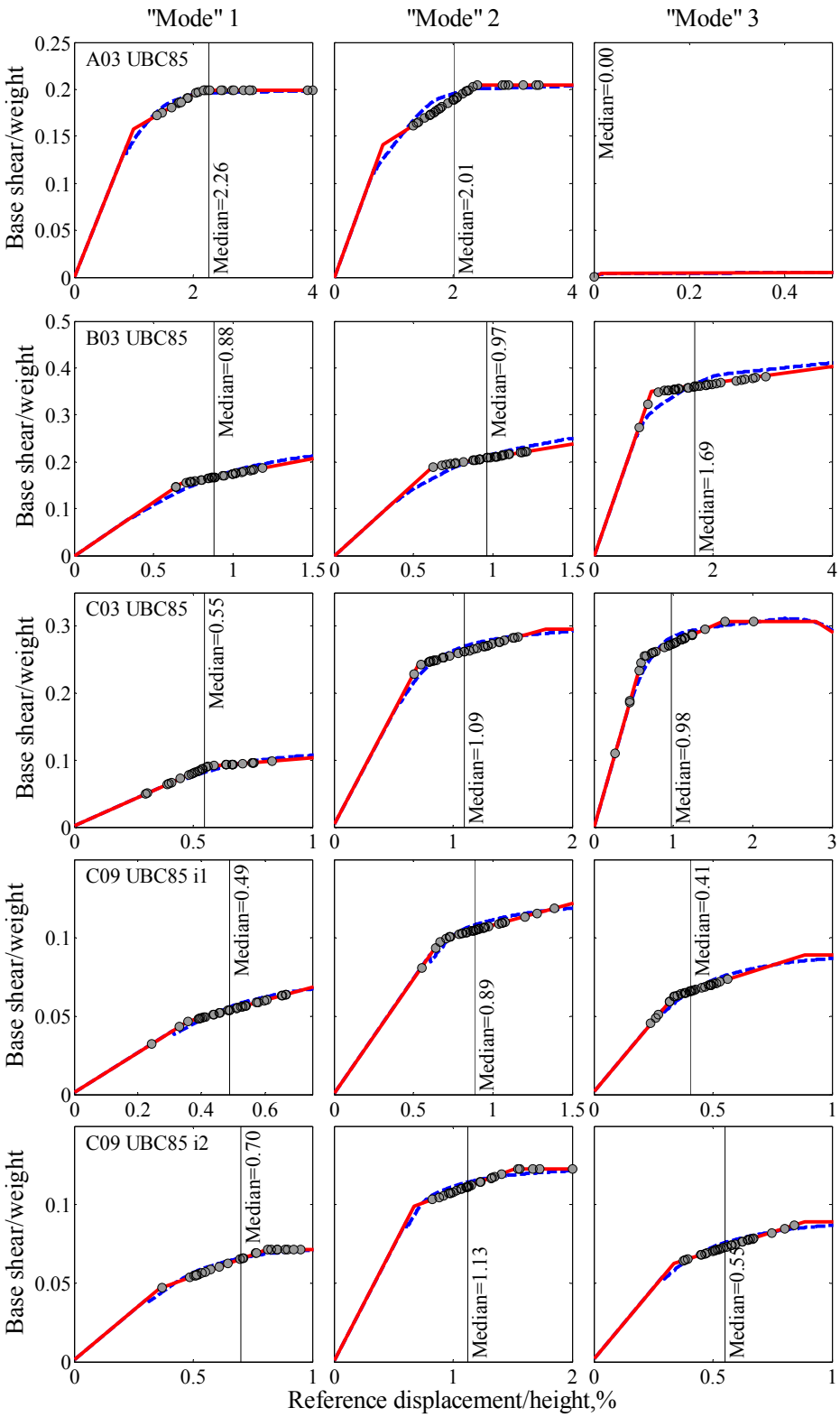

Figure 5.16 First-, second-, and third-"mode" pushover curves for UBC85 buildings. The reference displacement due to 39 ground motions is identified and the median value is also noted. Intensity i2 is considered only for the C09 building.

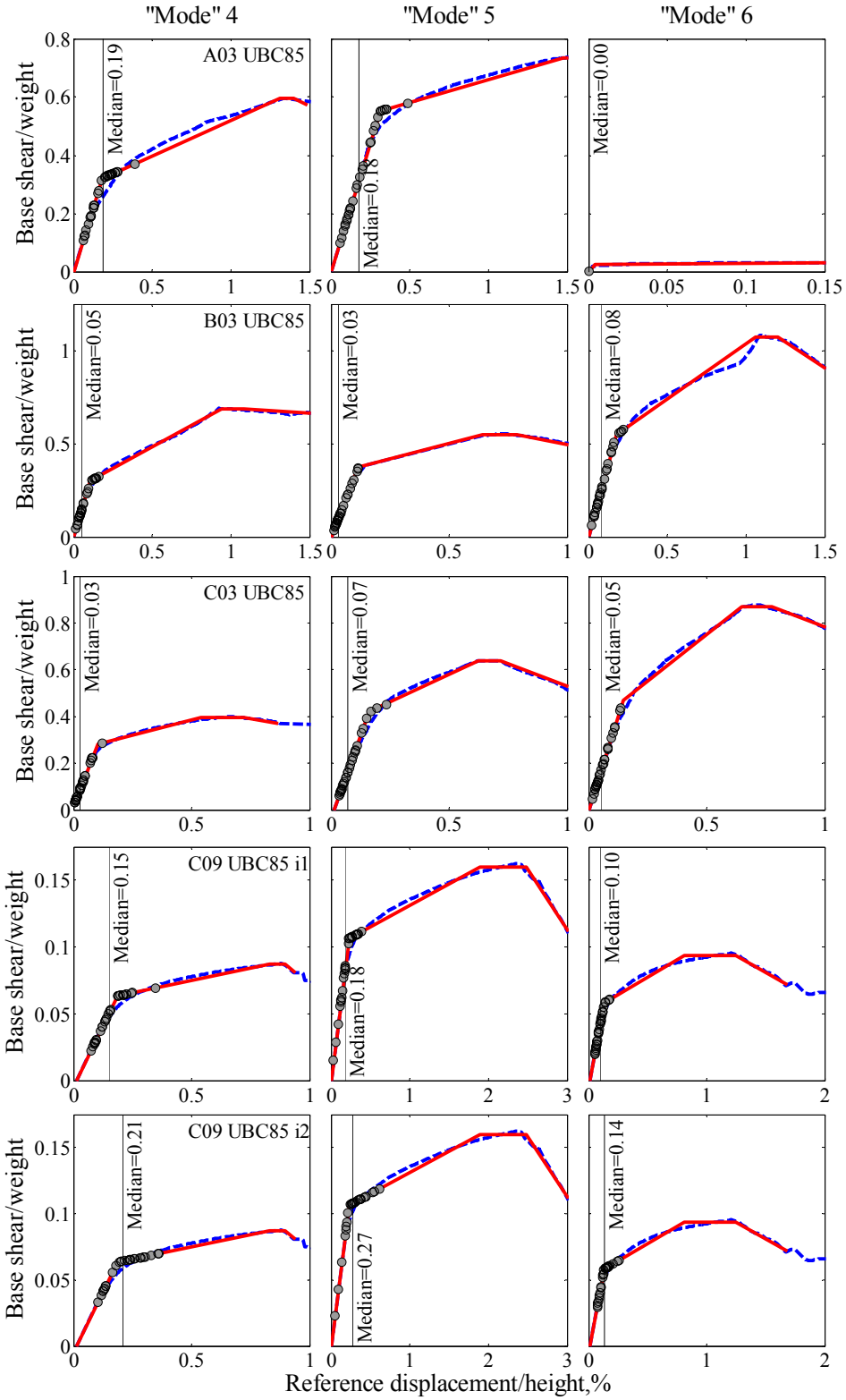

Figure 5.17 Fourth-, fifth-, and sixth-"mode" pushover curves for UBC85 buildings. The reference displacement due to 39 ground motions is identified and the median value is also noted. Intensity i2 is considered only for the C09 building.

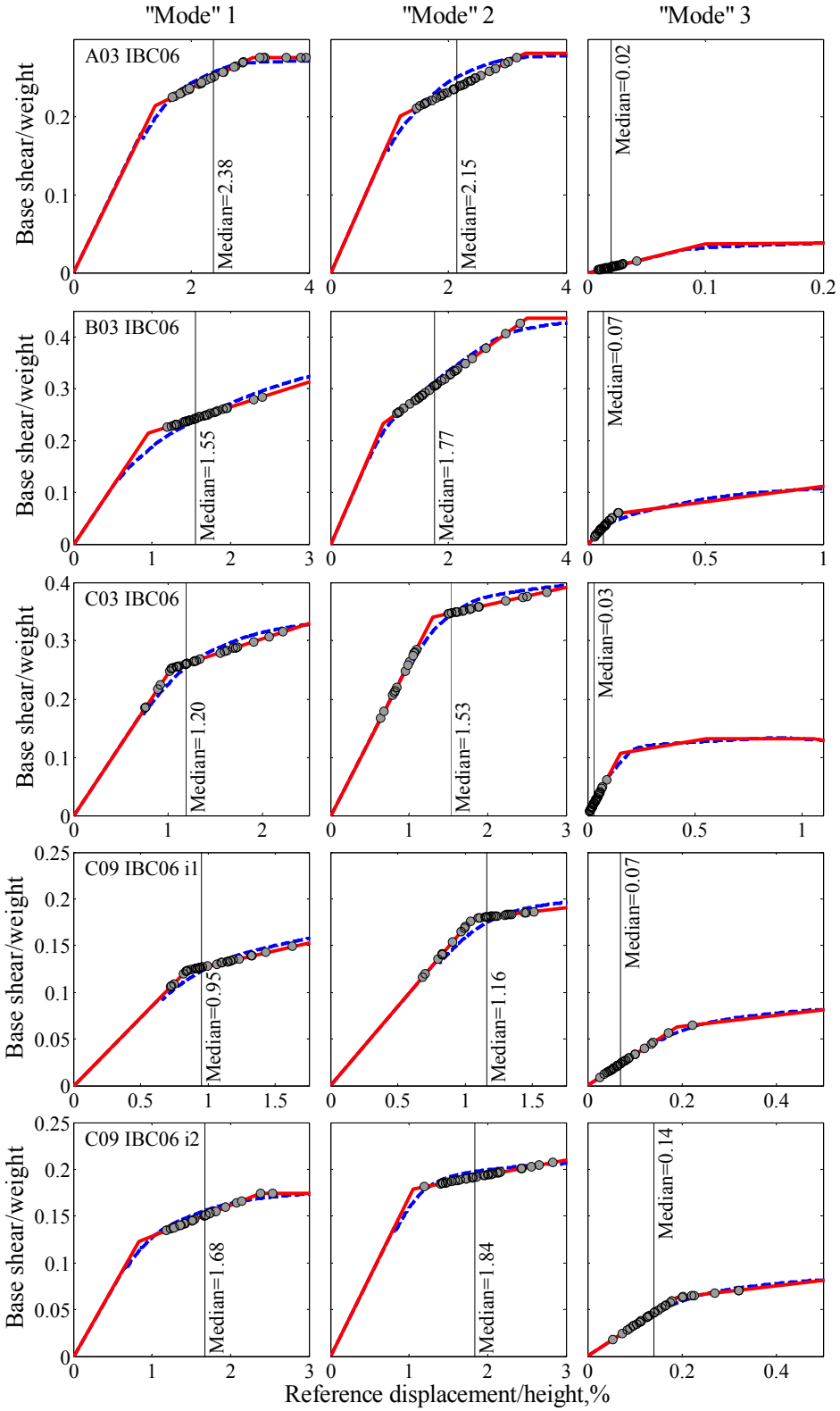

Figure 5.18 First-, second-, and third-"mode" pushover curves for IBC06 buildings. The reference displacement due to 39 ground motions is identified and the median value is also noted. Intensity i2 is considered only for the C09 building.

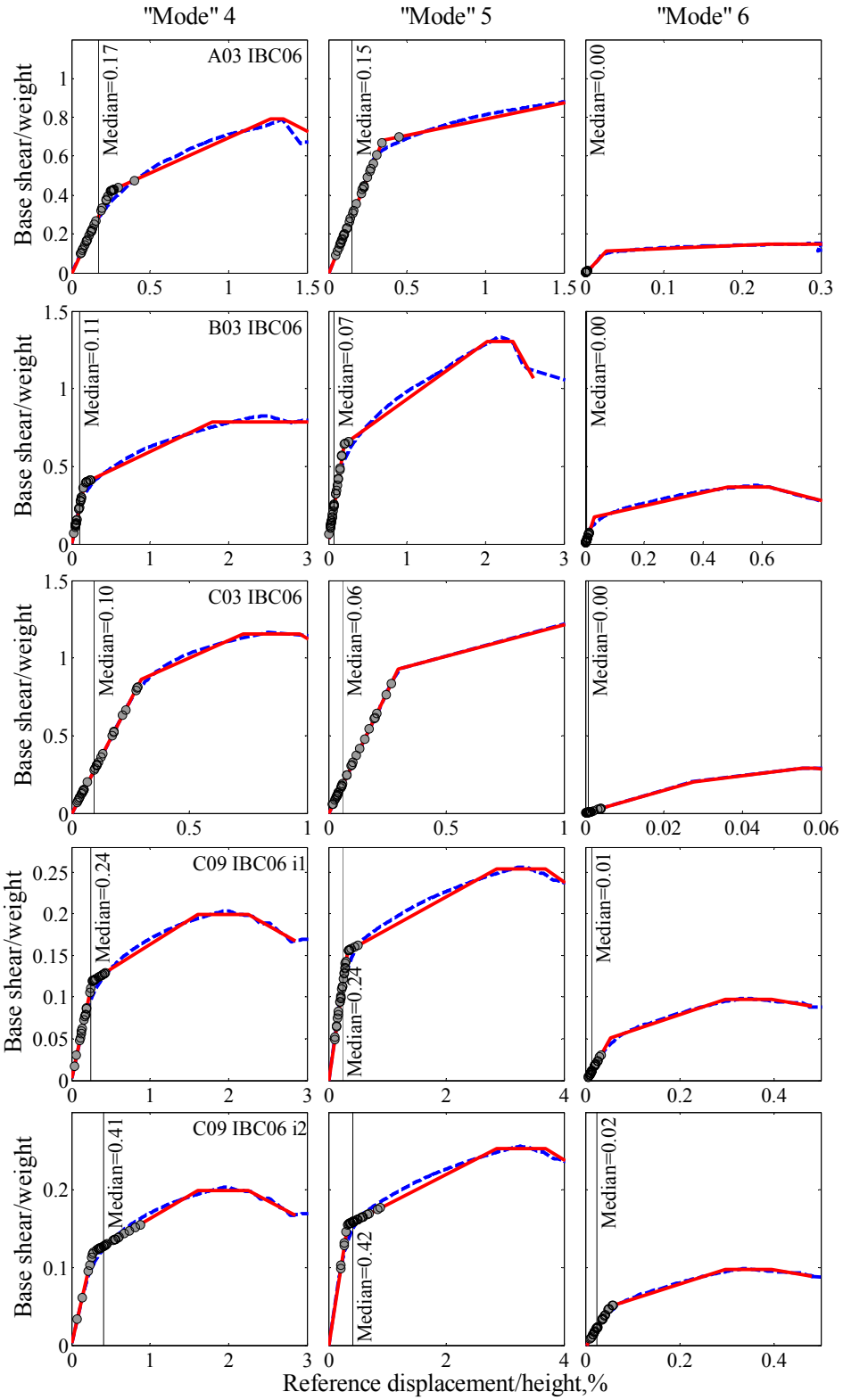

Figure 5.19 Fourth-, fifth-, and sixth-"mode" pushover curves for IBC06 buildings. The reference displacement due to 39 ground motions is identified and the median value is also noted. Intensity i2 is considered only for the C09 building.

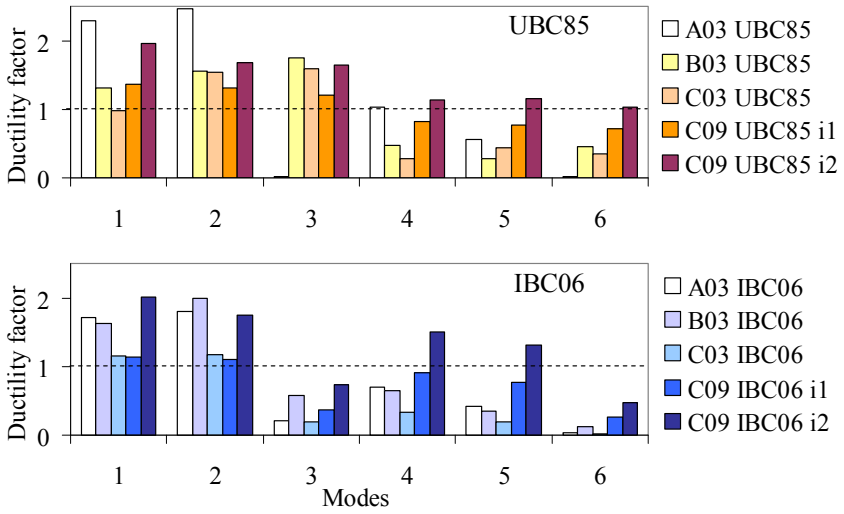

Figure 5.20 Ductility factors calculated as the ratio of the median reference displacement due to 39 ground motions over the first yield displacement for the UBC85 and IBC06 buildings.

5.3.2 Higher Mode Contributions in Seismic Demands

Figures 5.21 and 5.22 show median values of floor displacements and story drifts in the *x*- and *y*-direction at the C.M. including a variable number of "modes" in MPA, superimposed with the "exact" result from nonlinear RHA, for each building subjected to both components of motion, simultaneously; for the C09 buildings, results for two different levels of ground-motion intensity are included.

The first triplet of "modes" is adequate in estimating roof displacements for both groups—UBC85 and IBC06—of buildings; including higher "modes" does not significantly improve this estimate. The first triplet of "modes" alone is adequate in estimating story drifts for the three-story buildings, but it is inadequate in case of the nine-story buildings; in the latter case, with a few "modes" included, story drifts estimated by MPA are much better, and resemble nonlinear RHA results (Figs. 5.21 and 5.22). However, some discrepancies remain for the upper stories of the C09 buildings subjected to i2-intensity ground motions.

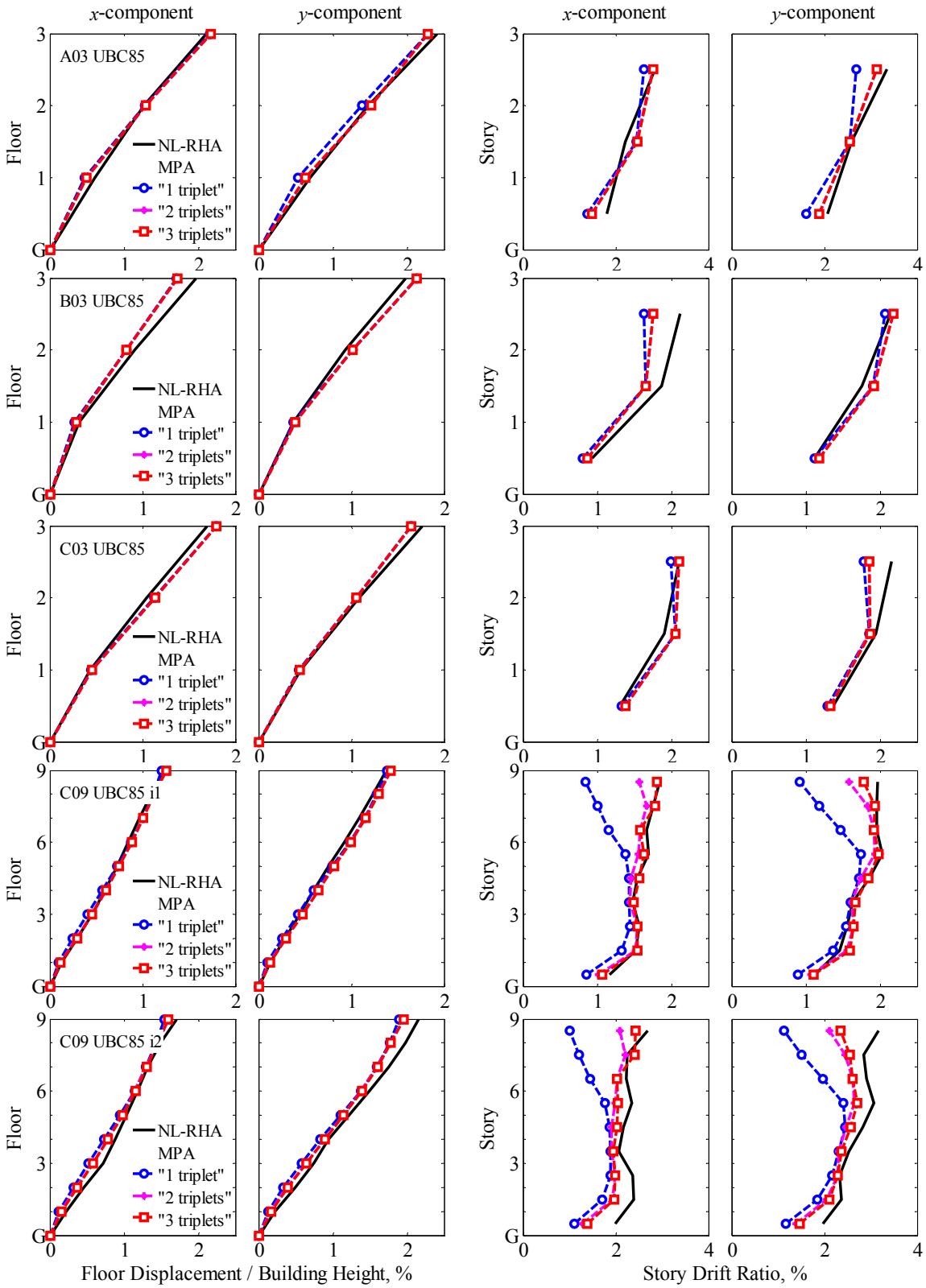

Figure 5.21 Median floor displacements (columns 1 and 2) and story drifts (columns 3 and 4) at the C.M. of the UBC85 buildings determined by nonlinear RHA and MPA, with a variable number of "modes". For the C09 building, ground motions are scaled to two different intensities: i1 and i2.

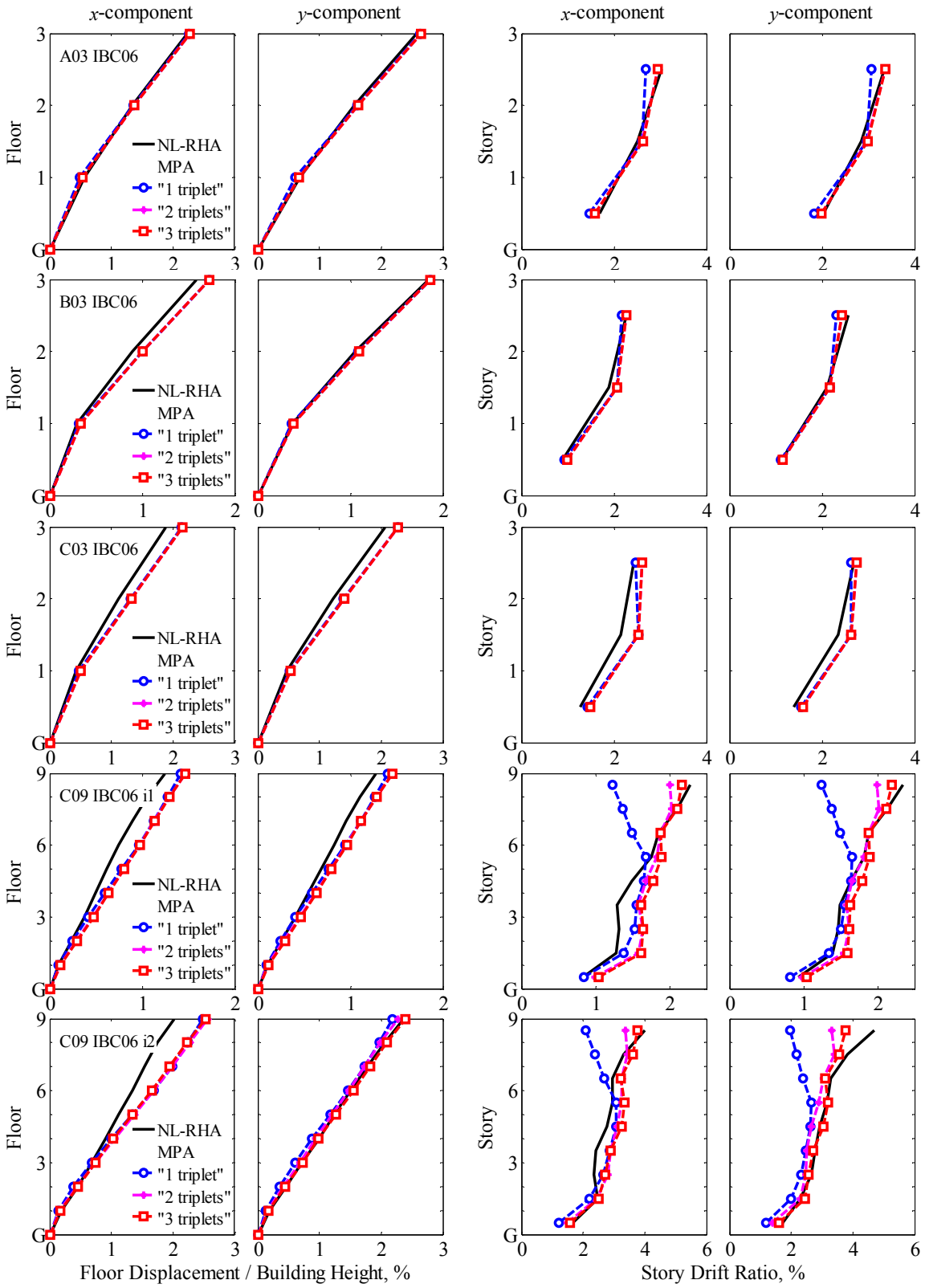

Figure 5.22 Median floor displacements (columns 1 and 2) and story drifts (columns 3 and 4) at the C.M. of the IBC06 buildings determined by nonlinear RHA and MPA, with a variable number of "modes". For the C09 building, ground motions are scaled to two different intensities: i1 and i2.

5.3.3 Evaluation of Modal Pushover Analysis

MPA adequately estimates the *x* and *y* components of floor displacements at the C.M. for the UBC85 buildings; the error in the *x* and *y* components of roof displacement ranges from 3% to 13% and from 4% to 9%, respectively, for all UBC85 buildings. The largest discrepancy in roof displacement is obtained for the B03 UBC85 building, which has close modal periods and strong coupling of the *x*-lateral and torsional motions in each mode of vibration (Fig. 5.3). This discrepancy occurs because the individual 'modal' responses attain their peaks almost simultaneously; a situation for which the CQC modal combination rule is not valid, especially for lightly-damped systems. Floor displacements are conservatively estimated for the IBC06 buildings; the overestimation in the *x* and *y* components of roof displacement ranges from 2% to 27% and from 1% to 14%, respectively.

Figure 5.21 and 5.22 shows that higher 'modal' triplets contribute significantly to the seismic demands for the selected systems and MPA is able to capture these effects. With sufficient number of 'modal' triplets included, the height-wise distribution of story drifts estimated by MPA is generally similar to the 'exact' results from nonlinear RHA, and much superior to the first 'modal' triplet result. The height-wise average errors in the *x* and *y* components of story drifts at the C.M. are 8%, 9%, 6%, 3%, and 13% for the A03, B03, C03, and C09 (intensities i1 and i2) UBC85 buildings, respectively, and 3%, 5%, 12%, 11%, and 10% for the A03, B03, C03, and C09 (intensities i1 and i2) IBC06 buildings, respectively (Figs. 5.21 and 5.22). Although notable discrepancies remain for the C09 buildings in some stories, MPA gives useful estimates of story drifts in most cases. The MPA results are accurate for the B03 and C03 buildings to a similar degree as

they were for the symmetric building (A03) which is apparent by comparing the first three rows of Figs. 5.21 and 5.22. However, the results are less accurate for the C09 buildings, which may be due to stronger coupling between translational and torsional components of motion in modes contributing significantly to the response.

5.4 Evaluation of ASCE41-06 and Eurocode8 procedures

5.4.1 ASCE41-06 Nonlinear Static Procedure

The nonlinear static procedure (NSP) in ASCE/SEI 41-06 [ASCE, 2007] requires development of a pushover curve by nonlinear static analysis of the structure, subjected first to gravity loads, followed by monotonically increasing lateral forces with an invariant height-wise distribution proportional to the first mode of vibration of the structure. The NSP is permitted only for structures that satisfy the following conditions:

1. The strength ratio R, defined by Eq. (5.1), is less than R_{max} calculated in accordance with Eq. (5.2).

$$R = \frac{A_1}{V_{b1y}/w} C_m \tag{5.1}$$

$$R_{max} = \frac{u_{r1}^d}{u_{r1y}} + \frac{|\alpha_e|^{-h}}{4} \tag{5.2}$$

where the various symbols are defined as follows:

A_1: Ordinate of the pseudo-acceleration response spectrum at the fundamental period and damping ratio of the building in the direction under consideration.

V_{b1y}: Yield base shear determined from the idealized first mode pushover analysis (Fig. 5.23).

w: Effective seismic weight of the building including the total dead load and applicable portions of other gravity loads [ASCE, 2007, p. 64].

C_m: Effective modal mass participation factor for the fundamental mode. C_m shall be taken as 1.0 if the fundamental period is greater than 1.0 sec.

u_{r1d}: Lesser of target displacement (explained later) or displacement at the maximum base shear V_{b1u} (Fig. 5.23).

u_{r1y}: Displacement at effective yield strength defined in Fig. 5.23.

h: $1+0.15\,ln(T_e)$ where $T_e = T_1\sqrt{k_i / k_e}$ (parameters defined in Fig. 5.23).

α_e: $\alpha_3 + \lambda(\alpha_2 - \alpha_3)$ where α_2 is the negative post-yield slope ratio that includes P-delta effects, in-cycle degradation and cyclic degradation; α_3 the negative slope ratio caused by P-delta effects; and λ, the near field effect factor defined in the standard.

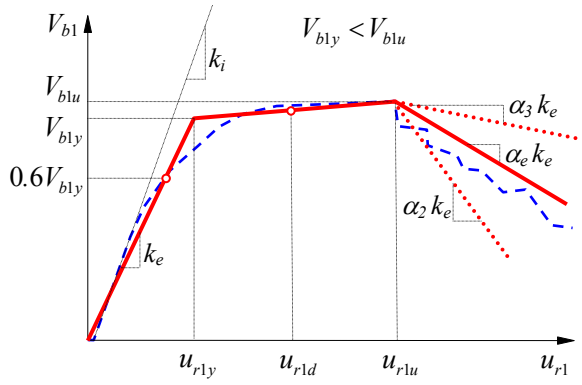

Figure 5.23: Idealized base shear—roof displacement curve for the fundamental mode.

2. Higher mode effects are not significant. According to ASCE/SEI 41-06, "the higher mode effects shall be considered significant if the shear in any story resulting from modal analysis [of the corresponding linear system] considering modes required to obtain 90% mass participation exceeds 130% of the corresponding story shear considering only the first mode response." If the higher modes of vibration contribute significantly to the elastic response of the structure, the NSP must be supplemented by the linear dynamic analysis procedure (LDP), and seismic demands computed by the two procedures are evaluated against their respective acceptance criteria.

Increasing lateral forces proportional to $\mathbf{s}_1^* = \mathbf{M}\phi_1$, the first-mode force distribution, are applied until the roof displacement at the C.M. reaches *the target displacement* (Section 3.3.3.3.2 of ASCE/SEI 41-06). ASCE/SEI 41-06 states that: "the lateral loads shall be applied in both positive and negative directions, and the maximum seismic effects shall be used for design."

The two conditions that restrict the application of the NSP procedure were verified for the two groups—UBC85 and IBC06—of buildings. The first condition is satisfied for all buildings, but the second condition is not satisfied in case of the B03, C03, and C09 UBC85 buildings because higher mode effects are "significant". The ASCE/SEI 41-06 NSP was implemented with one modification: the target displacement was not determined by the equations in ASCE/SEI 41-06, but was taken equal to the MPA value to ensure a meaningful comparison of the two sets of results.

How to consider bidirectional ground motions in estimating seismic demands for unsymmetric-plan buildings is not defined clearly in ASCE/SEI 41-06, and the NSP procedure was implemented using the following interpretations [Heintz, 2008]:

1. To determine the seismic demands due to *a* (or *b*) ground motion, the fundamental mode is defined as the mode with larger effective mass.
2. Only *x* (or *y*) component of lateral forces are included due to ground motion in the *a* (or *b*) direction, as shown in Fig. 5.24, i.e. the y (or x) and θ components of forces are excluded. ASCE *a* and ASCE *b* denote force distributions associated with excitations in the *a* and *b* directions.
3. The NSP procedure is applied to determine the seismic demands due to each horizontal component of ground motion, considered separately, and then, the two sets of demands are combined using the SRSS rule.

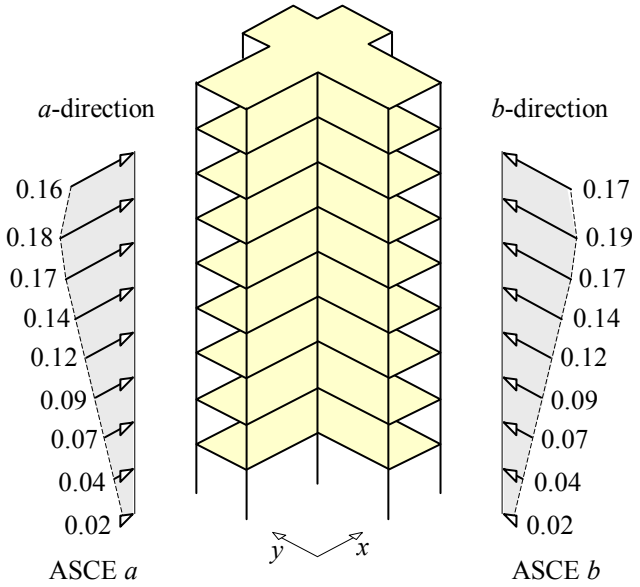

Figure 5.24 ASCE41-06 (first mode pattern) force distributions for the C09 UBC85 building

5.4.2 Eurocode8 Nonlinear Static Analysis

Like the NSP of the ASCE41-06 standard, the Eurocode 8 [British Standards, 2004] requires development of a pushover curve by nonlinear static analysis of the structure subjected first to gravity loads, followed by monotonically increasing lateral forces with a specified invariant height-wise distribution. At least two force distributions must be considered:

- *Uniform pattern* (EURO1): $\mathbf{s}_a^* = \mathbf{M}\boldsymbol{\iota}_a = \begin{bmatrix} \mathbf{m1} \\ \mathbf{0} \\ \mathbf{0} \end{bmatrix}$ $\mathbf{s}_b^* = \mathbf{M}\boldsymbol{\iota}_b = \begin{bmatrix} \mathbf{0} \\ \mathbf{m1} \\ \mathbf{0} \end{bmatrix}$

- *Modal pattern* (EURO2): $\mathbf{s}_a^*$ and $\mathbf{s}_b^*$ are defined by lateral forces back-calculated from (as the difference of) the story shears determined by response spectrum analysis of the structure assumed to be linearly elastic, subjected to *a* and *b* components of ground motion, respectively.

The target displacement was not determined by the equations in the Annex B of Eurocode8, but was taken equal to the MPA value to ensure a meaningful comparison of the two sets of results.

How to consider bidirectional ground motions in estimating seismic demands for unsymmetric-plan buildings is not defined clearly in Eurocode8 provisions, and the NSP was implemented using the following interpretations [Fajfar, 2008]:

1. To determine the seismic demands due to *a* (or *b*) ground motion, the fundamental mode is defined as the mode with larger effective mass.
2. Only *x* (or *y*) component of lateral forces are included due to ground motion in the *a* (or *b*) direction, as shown in Fig. 5.25, i.e. the y (or x) and θ components of forces

are excluded. EURO *a* and EURO *b* denote force distributions associated with excitations in the *a* and *b* directions.

3. The NSP procedure is applied to determine the seismic demands due to each horizontal component of ground motion, considered separately, and then, the two sets of demands are combined using the SRSS rule.

5.4.3 Comparative Evaluation of ASCE41-06, Eurocode8 and MPA

Figures 5.26 and 5.27 show the pushover curves for each building determined for the ASCE, EURO1 and EURO2 lateral force distributions; P-Δ effects due to gravity loads were included. The ASCE and EURO2 force distributions provide similar pushover curves, but the "uniform" force (EURO1) distribution, intended to develop a soft-story mechanism in the lower stories, leads to a pushover curve with higher elastic stiffness, higher yield strength, lower yield displacement, and less displacement capacity.

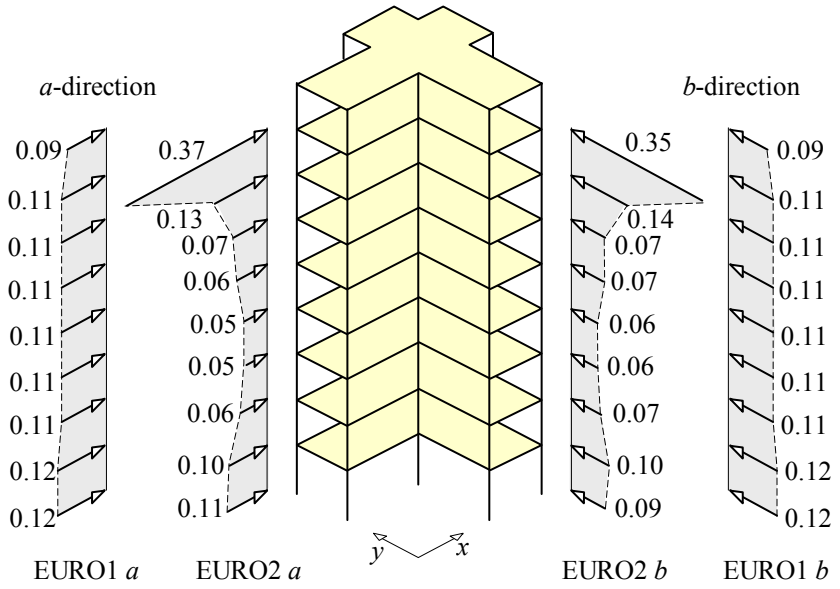

Figure 5.25 Eurocode8 force distributions for the C09 UBC85 building: EURO1 (uniform pattern) and EURO2 (modal pattern).

Figures 5.28 and 5.29 show median values of the *x* and *y* components of story drifts at the C.M. for the UBC85 and IBC06 buildings, respectively, due to the two components of ground motion, simultaneously. For each building the results are organized in two parts. In the left part of the figures, the ASCE41-06 and Eurocode8 estimates of story drifts are compared with the "exact" value determined by nonlinear RHA. In the right part, the MPA estimate (including all significant modes) of seismic demands is compared with the "exact" value.

It is obvious by comparing the left and right parts of Figures 5.28 and 5.29 that MPA provides much superior results for the C03 and C09 UBC85 buildings compared to the codes, and the two provide similar results for the A03 and B03 UBC85 buildings. ASCE41-06 and Eurocode8 force distributions underestimate the story drifts for the C03 and C09 UBC85 buildings, especially in the upper stories (Fig. 5.28, rows 3, 4, and 5). Although the EURO2 force distribution is intended to account for higher-"mode" responses, it does not provide satisfactory estimates of seismic response, even for buildings that deform only modestly into the nonlinear range (Fig. 5.16, rows 3 and 4), e.g. C03 and C09 UBC85 buildings subjected to i1-intensity ground motions (Fig. 5.28, rows 3 and 4). Both ASCE41-06 and Eurocode8 force distributions underestimate the story drifts for all IBC06 buildings, especially in the upper stories (Fig. 5.29, rows 3, 4, and 5). EURO1 force distributions generally overestimate story drifts in lower stories of the C09 IBC06 building and underestimate them in upper stories (Fig. 5.29, rows 4 and 5). In contrast, the MPA procedure provides a much better estimate of story drift demands in the upper stories of these buildings, because it includes all three components of forces and higher-"mode" contributions to the response. Note that these higher-"mode"

contributions are especially noticeable for the nine-story building (Figs. 5.21 and 5.22, rows 4 and 5), and the MPA procedure is able to account for them to provide excellent estimates of story drifts (Fig. 5.28 and 5.29, rows 4 and 5). Because the response of the A03 UBC85, A03 IBC06 and B03 IBC06 buildings is dominated by the first-"mode" (Figs. 5.8 and 5.12), the ASCE41-06 and Eurocode8 force distributions are adequate and MPA does not offer improvement in the demand estimate (Fig 5.28, row 1; and Fig. 5.29, rows 1 and 2).

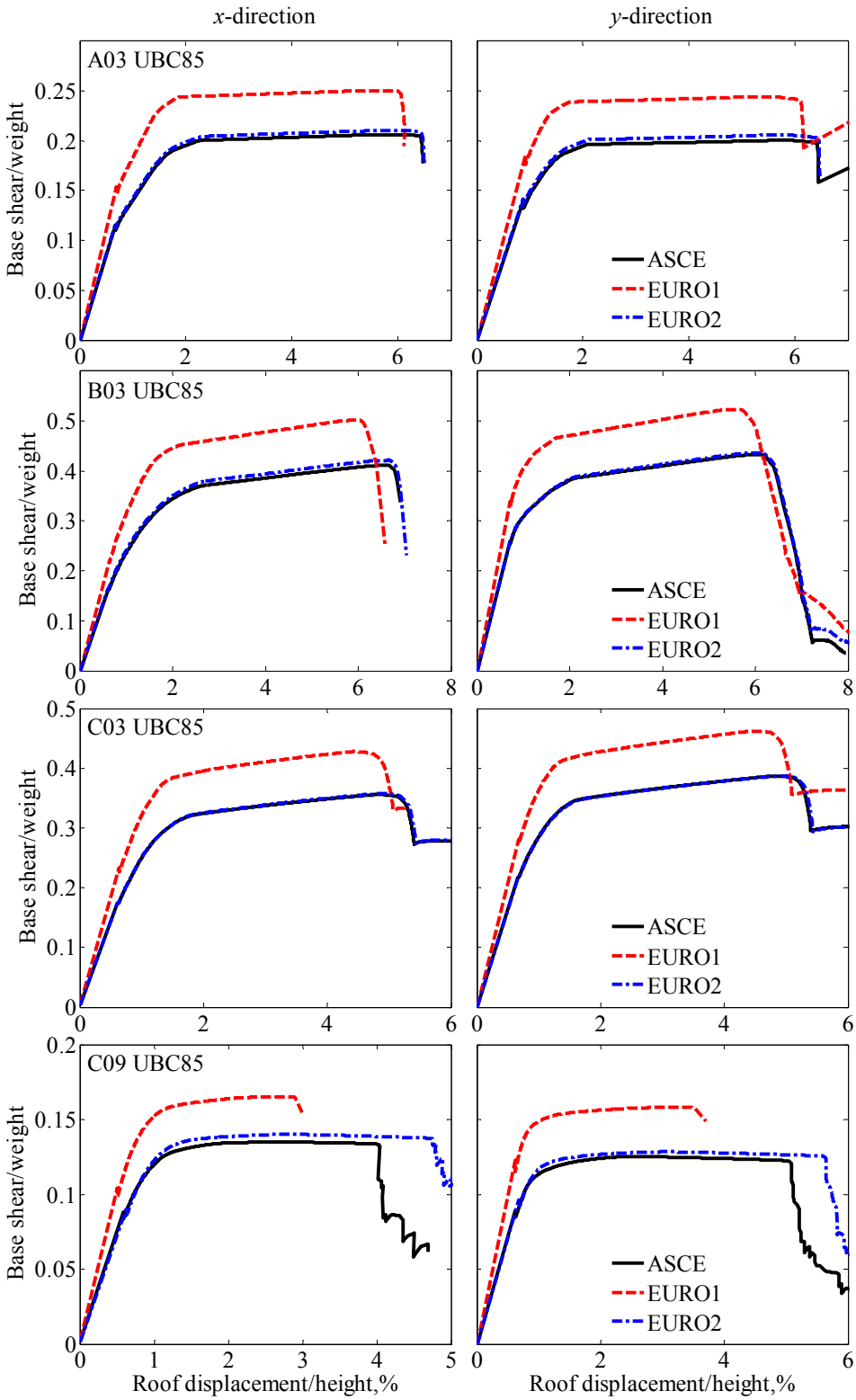

Figure 5.26 Pushover curves for the UBC85 buildings using ASCE41-06 and Eurocode8 force distributions: ASCE (first mode pattern), EURO1 (uniform pattern) and EURO2 (modal pattern).

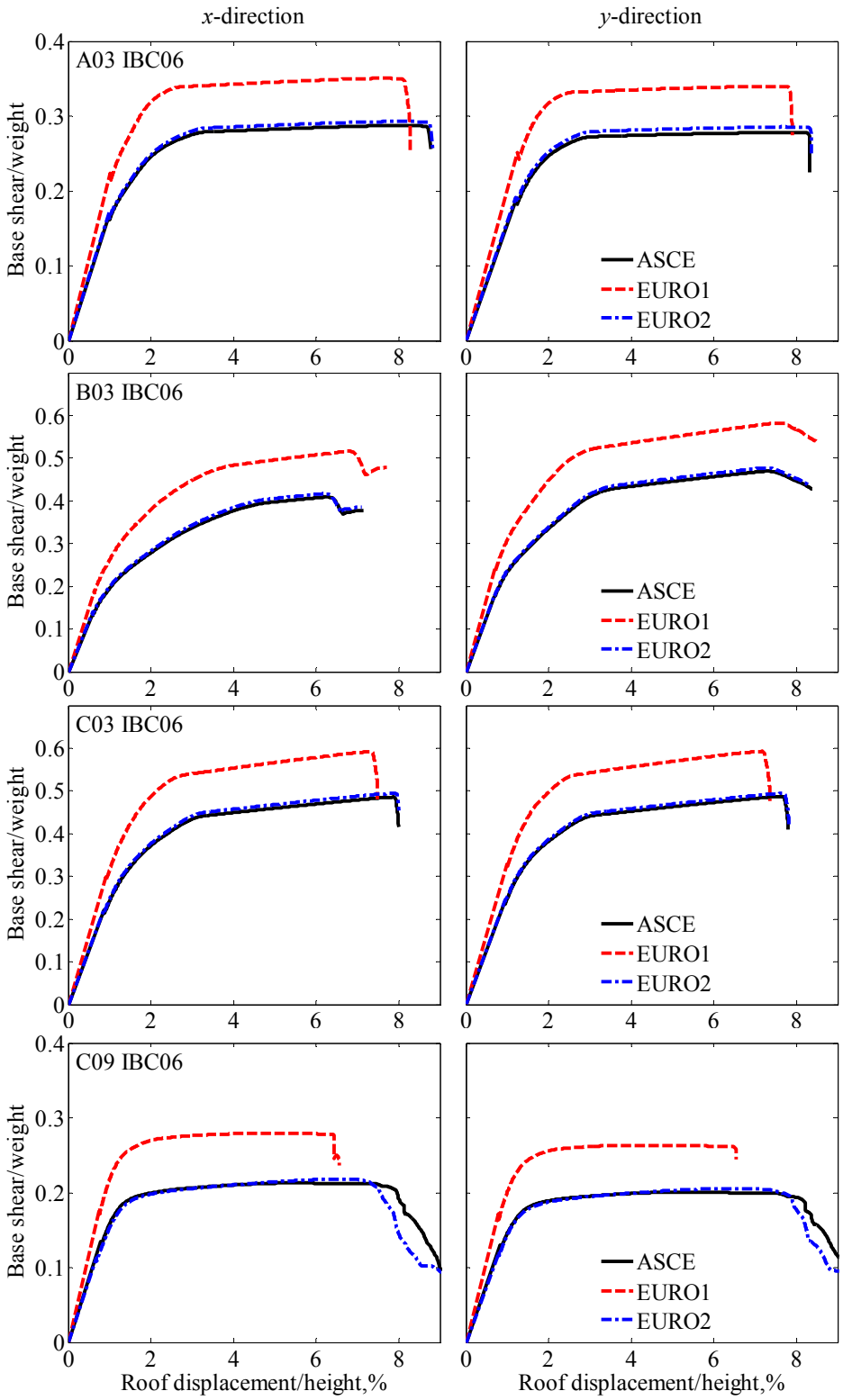

Figure 5.27 Pushover curves for the IBC06 buildings using ASCE41-06 and Eurocode8 force distributions: ASCE (first mode pattern), EURO1 (uniform pattern) and EURO2 (modal pattern).

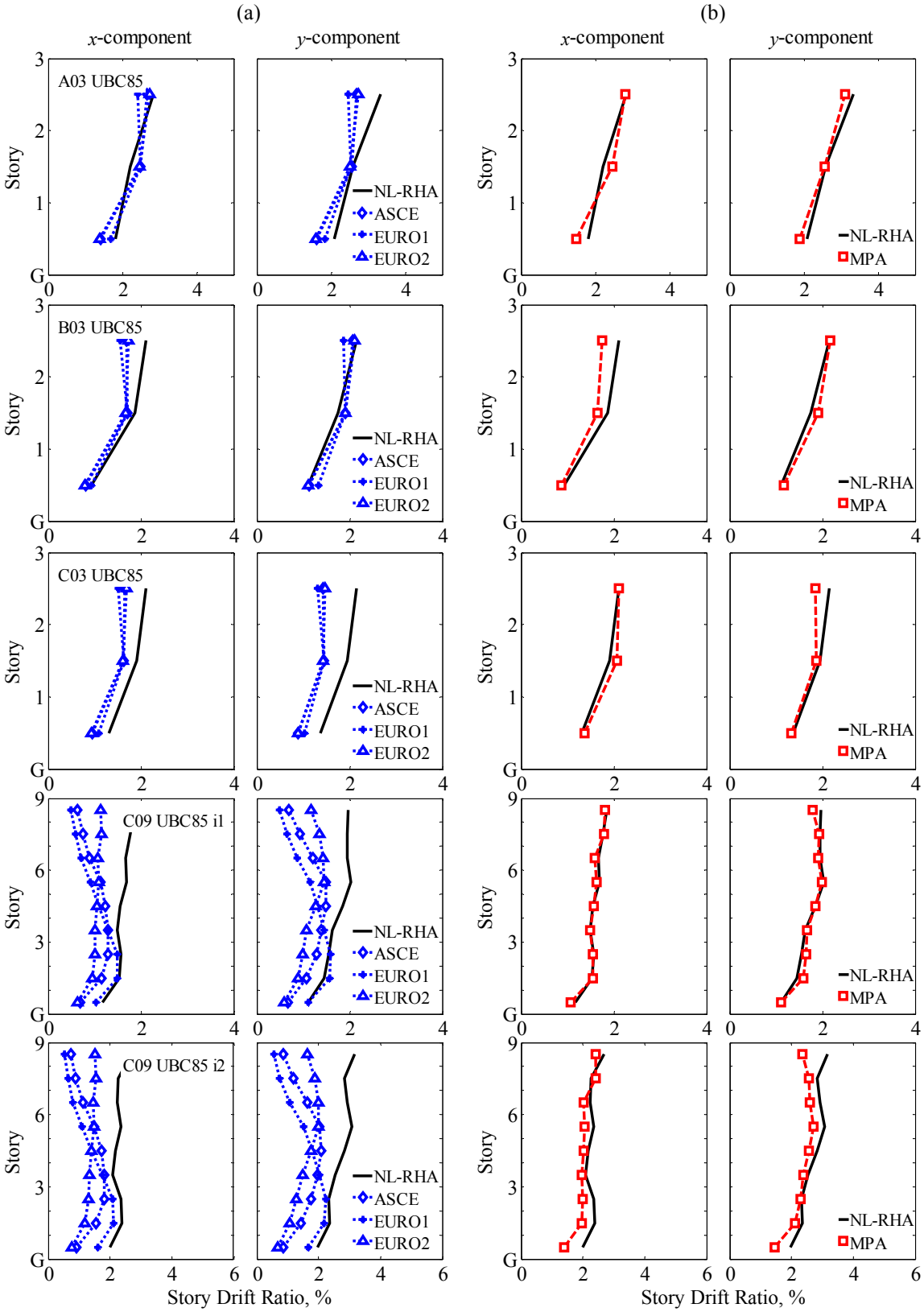

Figure 5.28 Median story drifts at the C.M. for UBC85 buildings determined by three procedures: (1) nonlinear RHA, (2) ASCE, EURO1 and EURO2 force distributions (left side), and (3) MPA (right side). Two ground motion intensities (i1 and i2) are included for the C09 building.

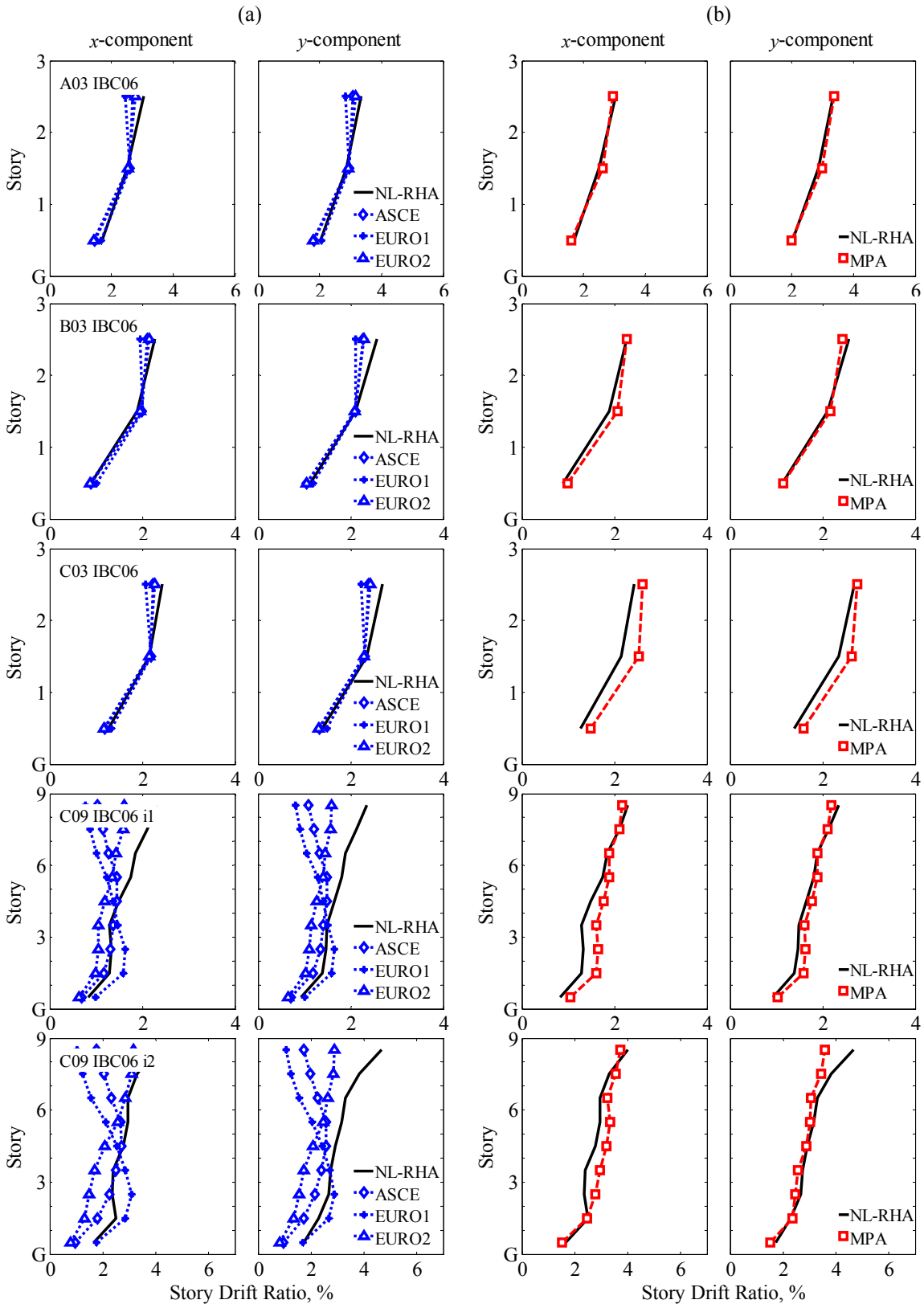

Figure 5.29 Median story drifts at the C.M. for IBC06 buildings determined by three procedures: (1) nonlinear RHA, (2) ASCE, EURO1 and EURO2 force distributions (left side, a), and (3) MPA (right side, b). Two ground motion intensities (i1 and i2) are included for the C09 building.

5.5 Evaluation of Modified MPA (MMPA)

The results of Figs. 5.15 through 5.19 and their interpretation suggested that the buildings could be treated as linear in estimating contributions of modes higher than the first triplet of "modes" to seismic demand. This observation is utilized in the MMPA procedure (Section 3.5), which was implemented to estimate seismic demands for the UBC85 and IBC06 buildings.

Figure 5.30 and 5.31 show median values of the *x*- and *y*-component of floor displacements and story drifts at the C.M. determined by nonlinear RHA, MPA, and MMPA for the UBC85 and IBC06 buildings, respectively. The seismic demands estimated by MMPA and MPA are very close implying that treating the buildings as linearly elastic in estimating higher-mode contributions to seismic demand is valid. Note that MMPA overestimates (relative to MPA) the seismic demands for the buildings, consistent with the results for steel moment resisting frames [Chopra et al, 2004] and for tall buildings (Chapter 4).

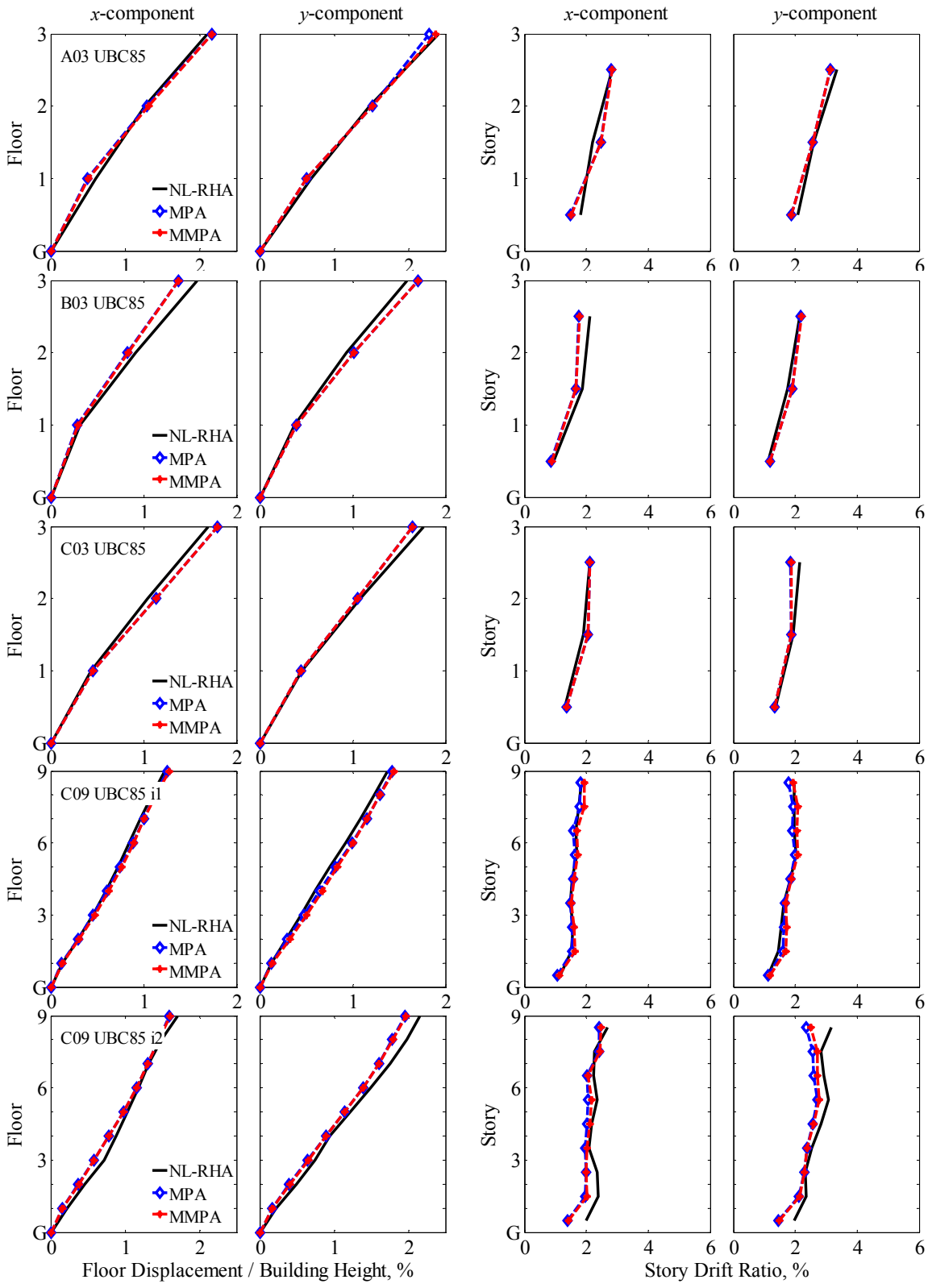

Figure 5.30 Median floor displacements (columns 1-2) and story drifts (columns 3-4) at the C.M. of the UBC85 buildings determined by nonlinear RHA, MPA, and MMPA. Two ground motion intensities (i1 and i2) are included for the C09 building.

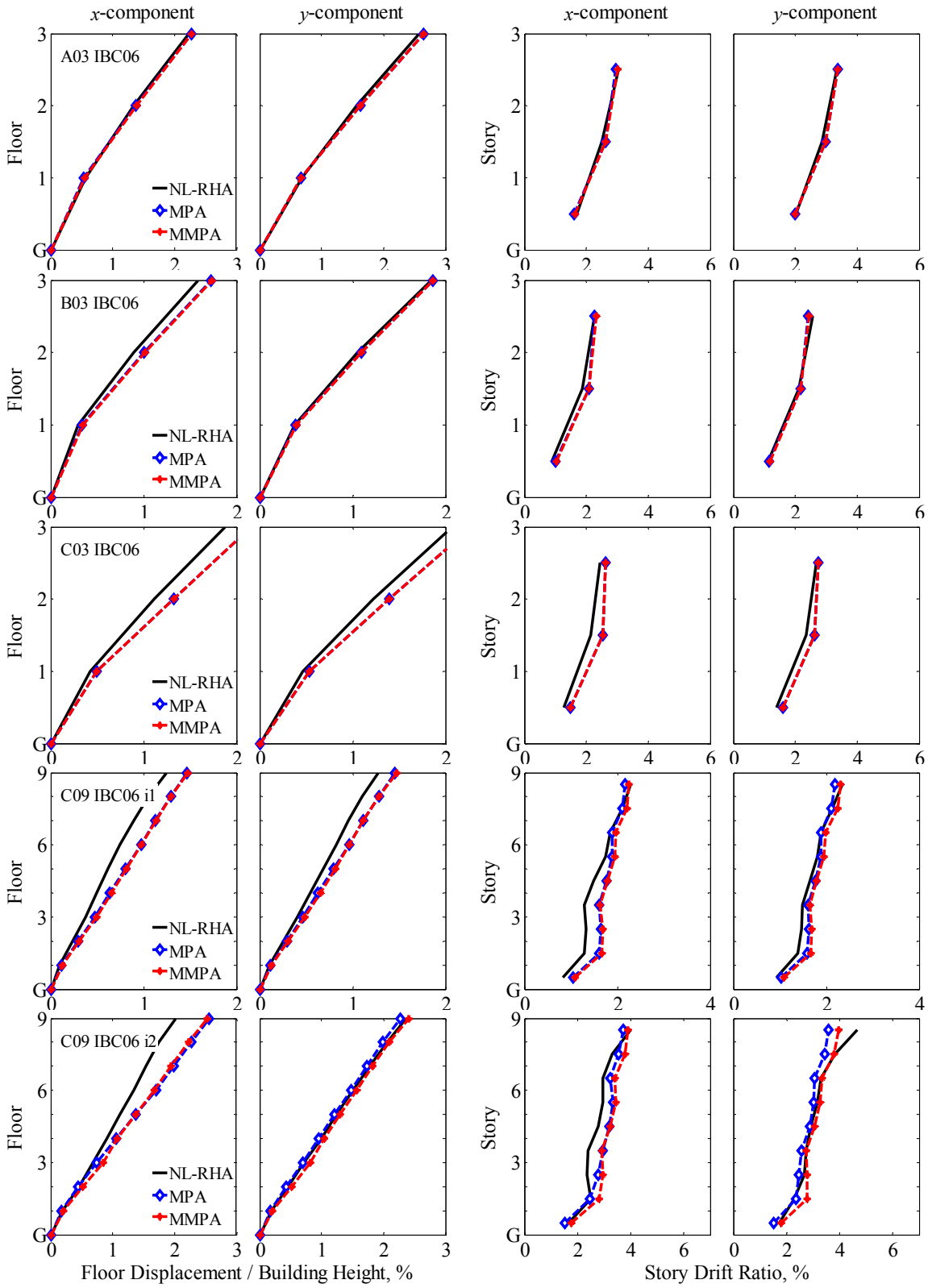

Figure 5.31 Median floor displacements (columns 1-2) and story drifts (columns 3-4) at the C.M. of the IBC06 buildings determined by nonlinear RHA, MPA, and MMPA. Two ground motion intensities (i1 and i2) are included for the C09 building.

5.6 Evaluation of Practical MPA (PMPA)

5.6.1 Floor Displacements and Story Drifts at the C.M.

Figures 5.32 and 5.33 show the median values of floor displacements and story drifts at the C.M., determined by the nonlinear RHA, MPA, and PMPA procedures for the UBC85 and IBC06 buildings, respectively; see section 3.5 for description of the PMPA procedure. Results for two different levels of ground-motion intensity are included for the C09 buildings. In general, PMPA provides a larger estimate of seismic demands compared to MPA because the median value of the peak deformation $(\hat{D}_n)_{\text{PMPA}}$ of the *n*th-mode inelastic SDF system, determined by Eqs. (3.25) and (3.26) in PMPA, is larger than the exact $(\hat{D}_n)_{\text{MPA}}$ determined in MPA (Step 4 of Section 3.4); the ratio of the two for the first pair of lateral "modes" of the UBC85 buildings is shown in Table 5.3. This is to be expected for systems with periods longer than T_c (Fig. 3.9) because the empirical equation for C_{Rn} does not permit values below 1.0 (Fig. 3.10), whereas the exact data does fall below 1.0 [Chopra and Chintanapakdee, 2004]. PMPA generally provided a more accurate estimate of seismic demand for those cases where MPA underestimated demand (relative to nonlinear RHA), but less accurate estimate for cases where MPA already overestimated the demand. For most of the analyzed cases, the PMPA procedure tends to overestimate floor displacements and story drifts, especially for the A03 UBC85, A03 IBC06 buildings subjected to i1-intensity ground motions and C09 IBC06 building subjected to i2-intensity ground motions. The height-wise average discrepancy in story drifts is 27%, 13%, 13%, 5%, 7% for the A03, B03, C03, and C09 (intensities i1 and i2) UBC85 buildings, respectively; and 21%, 25%, 10%, 12%, 20% for the A03, B03, C03, and C09 (intensities i1 and i2) IBC06 buildings, respectively.

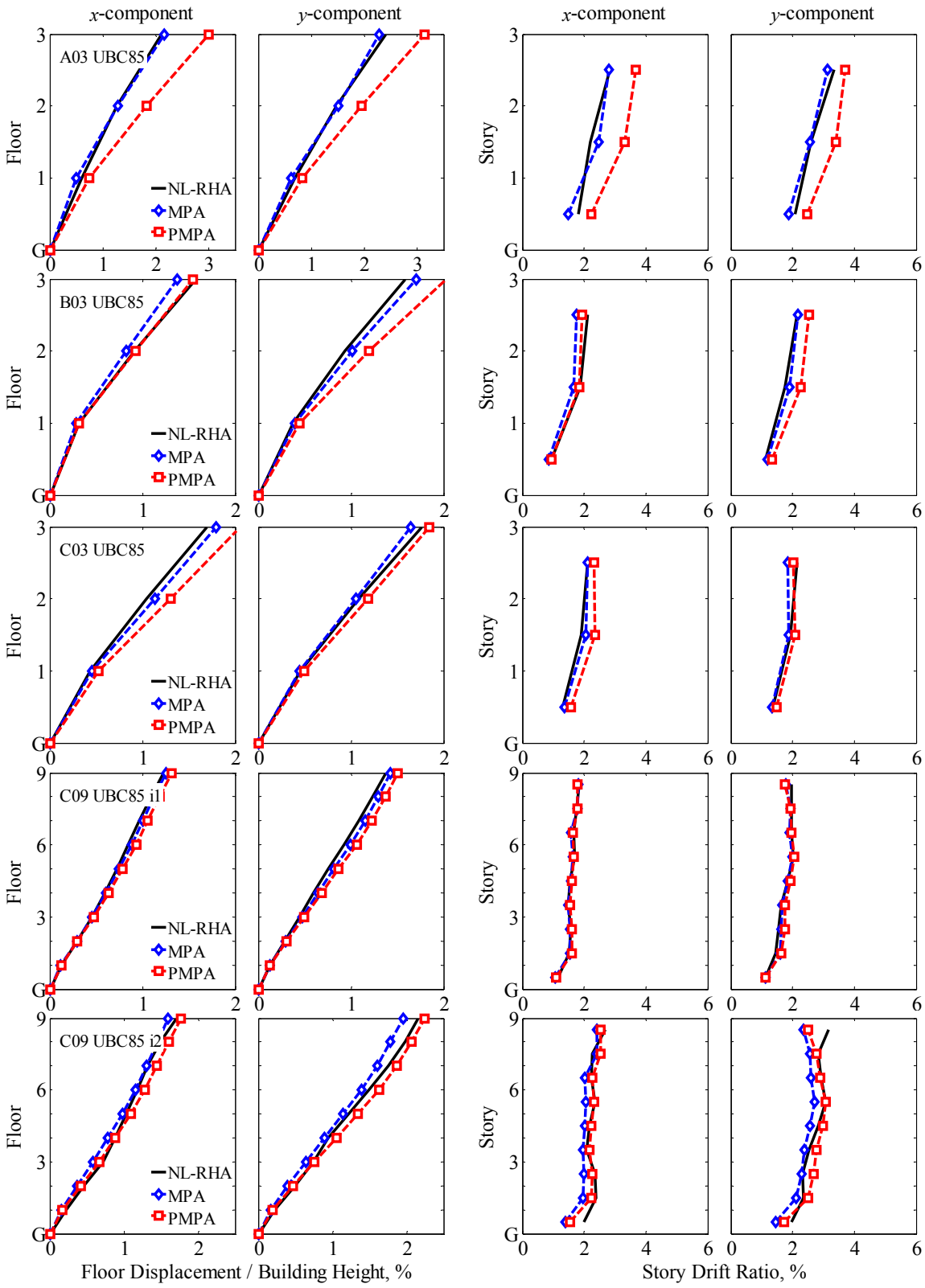

Figure 5.32 Median floor displacements (columns 1-2) and story drifts (columns 3-4) at the C.M. of the UBC85 buildings determined by nonlinear RHA, MPA, and PMPA. Two ground motion intensities (i1 and i2) are included for the C09 building.

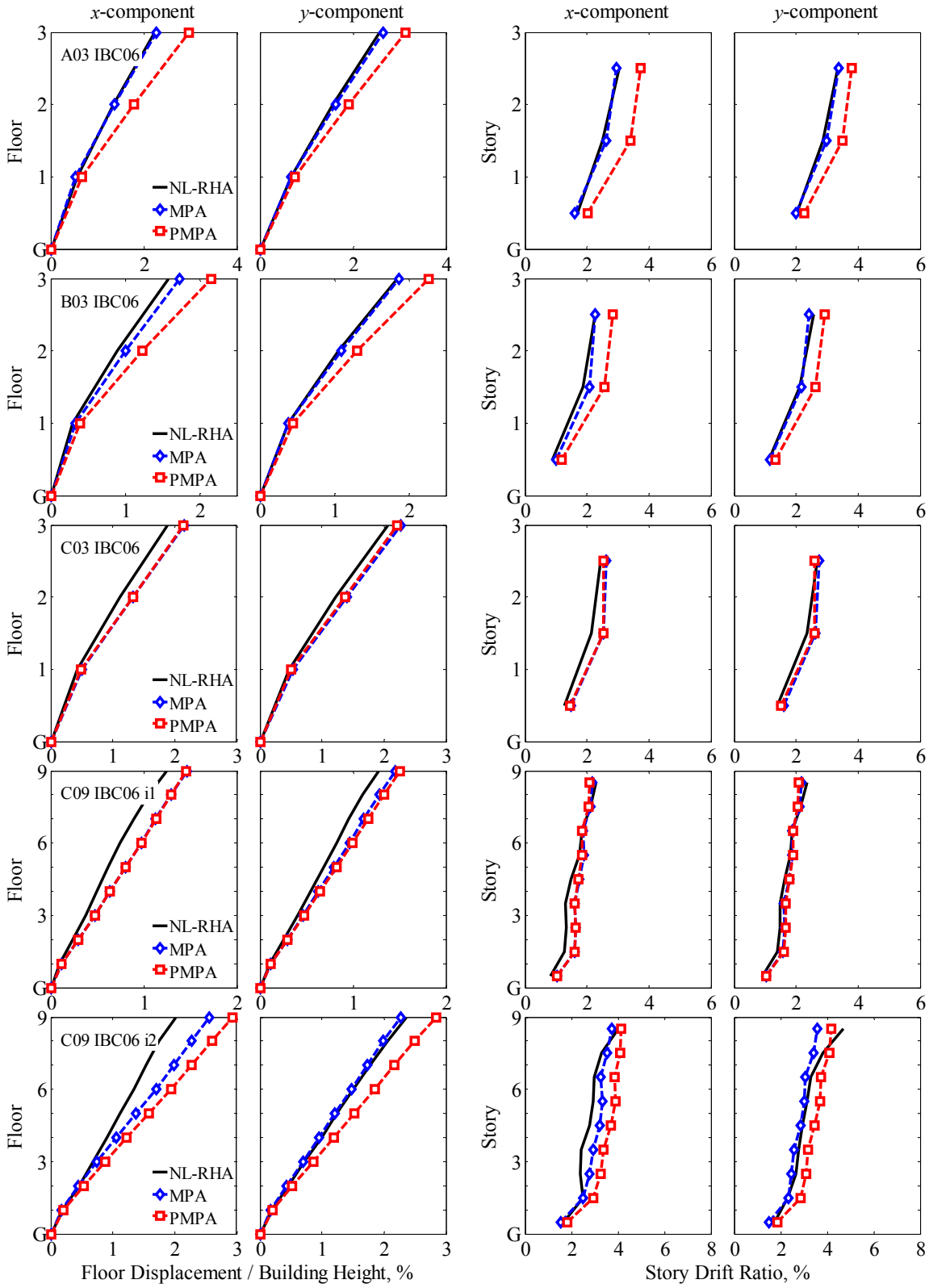

Figure 5.33 Median floor displacements (columns 1-2) and story drifts (columns 3-4) at the C.M. of the IBC06 buildings determined by nonlinear RHA, MPA, and PMPA. Two ground motion intensities (i1 and i2) are included for the C09 building.

Table 5.3 Peak deformation ratio $(\hat{D}_n)_{\text{PMPA}} \div (\hat{D}_n)_{\text{MPA}}$ for the first pair of modes of the UBC85 buildings in the *a*- and *b*-direction

Building	$(\hat{D}_n)_{\text{PMPA}} \div (\hat{D}_n)_{\text{MPA}}$	
	a-dir	b-dir
A03 UBC85	1.37	1.39
B03 UBC85	1.16	1.19
C03 UBC85	1.24	1.19
C09 UBC85 i1	1.10	1.11
C09 UBC85 i2	1.20	1.29

The PMPA procedure for these buildings is based on five principal approximations: (1) neglecting the weak coupling of "modes" in computing the peak modal responses r_n to $\mathbf{p}_{eff,n}(t)$; (2) combining the r_n by modal combination rules, known to be approximate, to compute the total response to one component of ground motion; (3) combining the response to individual components of ground motion by multi-component combination rules, known to be approximate, to compute the peak value of the total response; (4) estimating the peak deformation D_n of the nth-mode inelastic SDF system by empirical equations; and (5) considering that the structure could be treated as linearly elastic in estimating higher-mode contributions to seismic demand. Because approximations (2) and (3) are the only sources of approximation in the widely used response spectrum analysis (RSA) procedure for linear systems, the resulting error in the response of these systems serves as a baseline for evaluating the additional errors in PMPA for nonlinear systems.

Figures 5.34 and 5.35 compare the accuracy of PMPA in estimating the response of nonlinear systems with that of RSA in estimating the response of linearly elastic systems for UBC85 and IBC06 buildings, respectively. For each of the buildings, the results for story drifts at the C.M. are organized in two parts: (a) story drift demands for these buildings treated as linearly elastic systems determined by RSA and RHA procedures, and (b) demands for nonlinear systems determined by PMPA and nonlinear RHA. In implementing RSA and PMPA, three triplets of "modes" were included for each building.

The RSA procedure underestimates the median response of both groups of buildings; this underestimation tends to be greater in the upper stories of the buildings, consistent with the height-wise variation of contribution of higher modes to response [Chopra, 2007: Chapter 18]. The height-wise largest underestimation of drifts is 27% and 22% for the UBC85 and IBC06 buildings, respectively. This underestimation is compensated in the PMPA procedure because the reference displacements are overestimated (Table 5.3), leading to estimates of demand that are close to nonlinear RHA results, or are slightly conservative. Even for the most intense ground motions, the PMPA procedure offers conservative results that should make it useful for practical application in estimating seismic demands for unsymmetric-plan buildings.

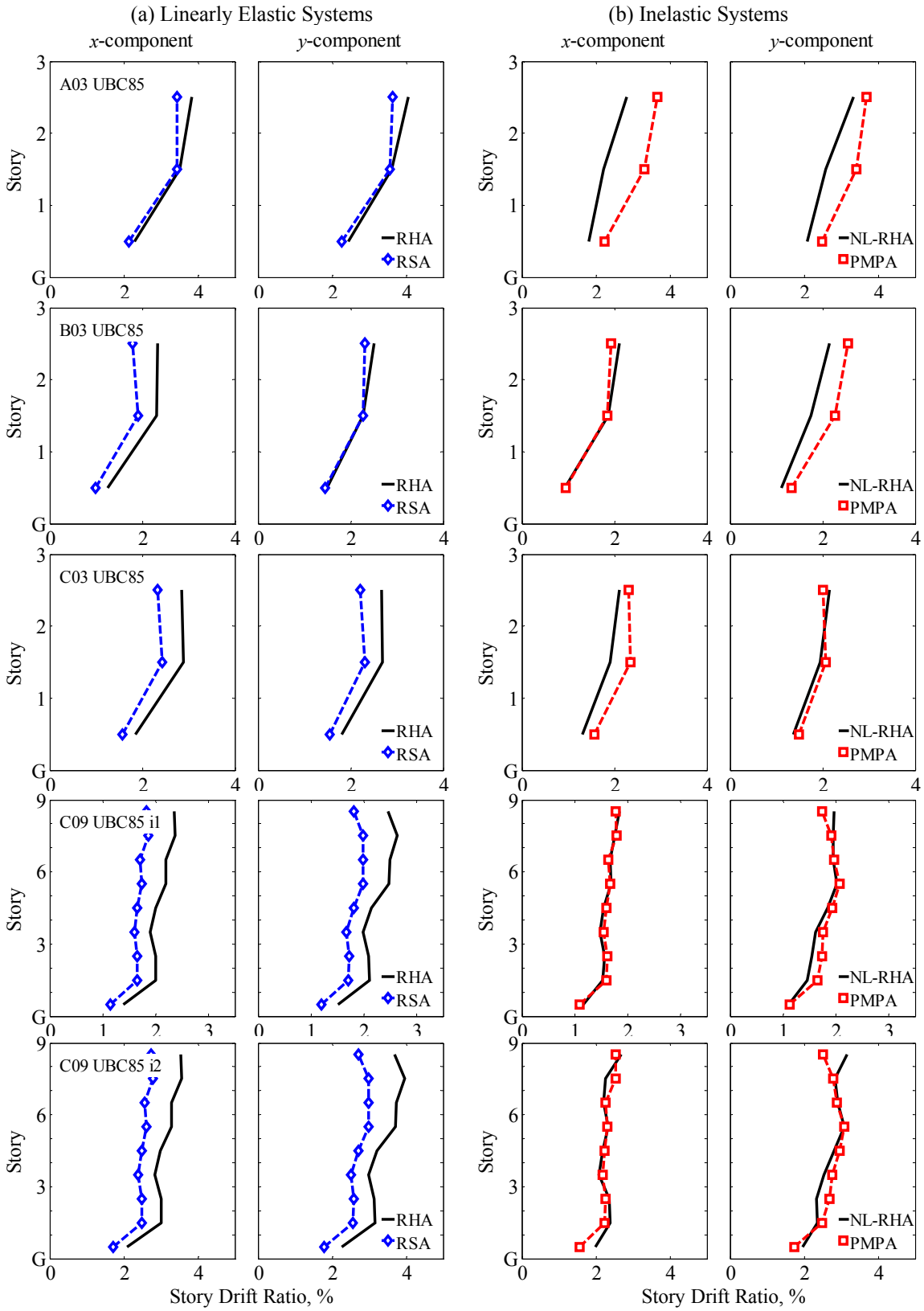

Figure 5.34 Median story drifts at the C.M. of the UBC85 buildings for: (a) linearly elastic systems determined by RSA and RHA procedures, and (b) inelastic systems determined by PMPA and nonlinear RHA procedures. Two ground motion intensities (i1 and i2) are included for the C09 building.

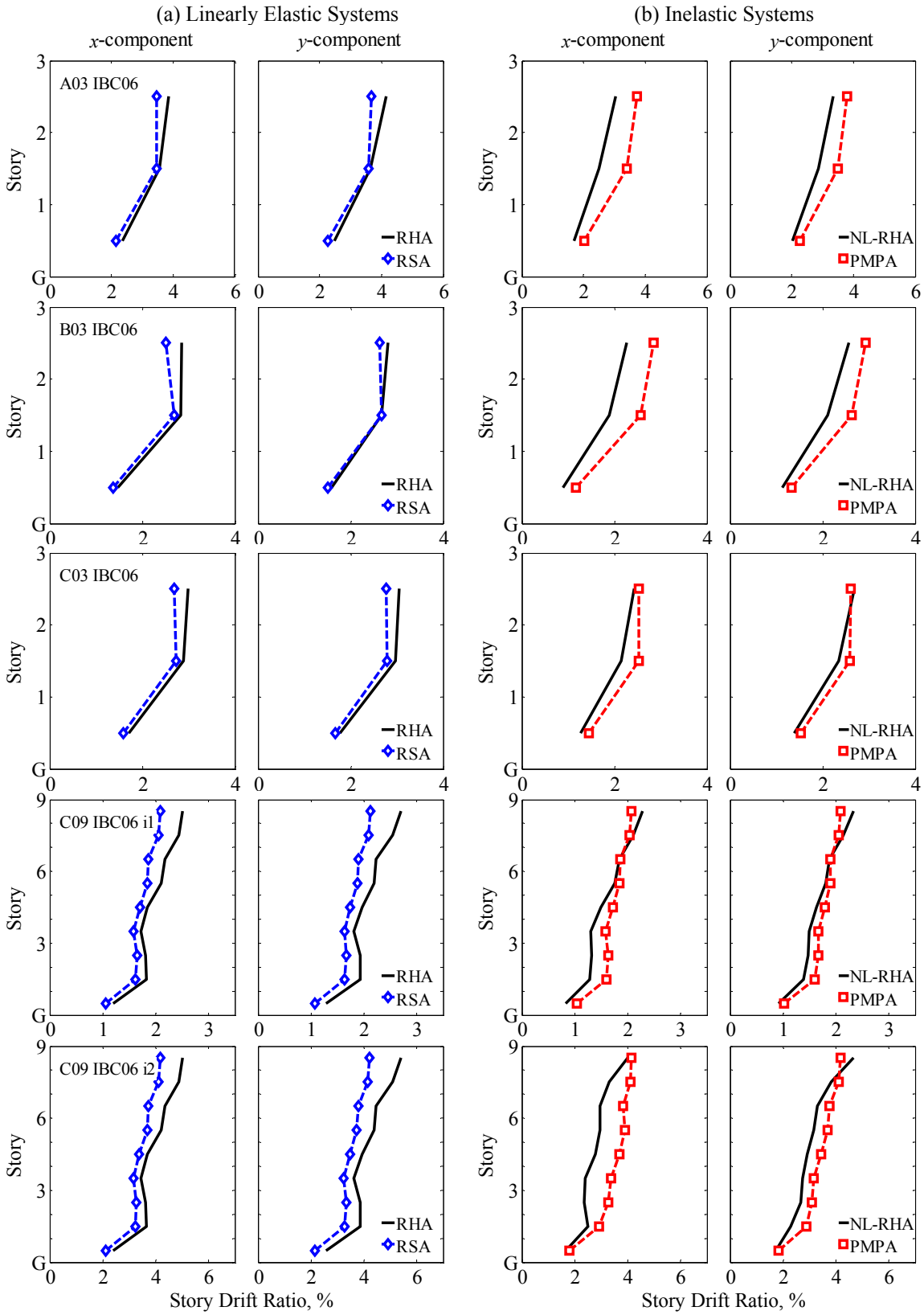

Figure 5.35 Median story drifts at the C.M. of the IBC06 buildings for: (a) linearly elastic systems determined by RSA and RHA procedures, and (b) inelastic systems determined by PMPA and nonlinear RHA procedures. Two ground motion intensities (i1 and i2) are included for the C09 building.

5.6.2 Other Response Quantities

The deformation quantities and member forces corresponding to the story drifts calculated by PMPA (Fig. 5.34b) were estimated by implementing Steps 11 and 12 of the procedure (Section 3.4). As mentioned therein, for unsymmetric-plan buildings, these steps are implemented for four excitations developed by applying the two horizontal components of ground motion in (1) $+x$ and $+y$ directions, (2) $+x$ and $-y$ directions, (3) $-x$ and $+y$, and (4) $-x$ and $-y$ directions. The largest of the four values is taken as the PMPA-estimate of the response. The exact value of response to each of the four excitations was determined by nonlinear RHA, and the largest of the four values is defined as the "exact" result. The median of such values of maximum response over the ensemble of ground motions is defined as the benchmark against which PMPA is judged. Figure 5.37 presents the median story drifts determined by the two procedures at the corner identified in Figure 5.36 for the C09 UBC85 building subjected to i2-intensity ground motions. It is apparent that PMPA provides conservative estimates of story drifts at the corner.

Figure 5.38 presents a similar comparison for shear forces, bending moments, and plastic hinge rotations in the girders identified in Fig. 5.36, determined by NL-RHA and PMPA. It is apparent that internal forces and plastic hinge rotations are estimated accurately. The error in internal forces is generally smaller than the error in hinge rotations because internal forces increase slowly with hinge rotation for members that deform beyond the elastic limit at both ends. As a result, even a large error in the hinge rotation leads to only small error in the computed internal forces; these observations are consistent with Goel and Chopra [2005].

Figure 5.39 shows the height-wise variation of the shear forces, bending moments, and plastic hinge rotations around the strong axis at the bottom of the columns identified in Fig. 5.36. It is apparent that the internal forces and plastic hinge rotations in these columns can be estimated to a useful degree of accuracy by the PMPA procedure.

In summary, based on the results presented in Figs. 5.37 through 5.39, PMPA for low and medium rise unsymmetric-plan buildings subjected to ground motion along two horizontal components applied simultaneously leads to accurate estimates of seismic demands; thus, PMPA should be useful for practical application in estimating seismic demands for evaluating such existing buildings or proposing designs of new buildings.

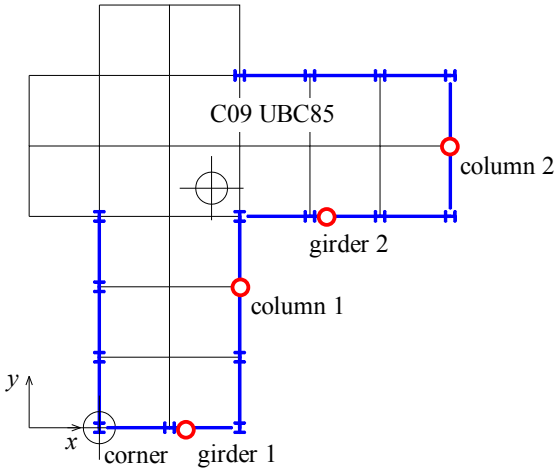

Figure 5.36 Schematic plan view of the C09 UBC85 building with girder 1, girder 2, column 1 and column 2 noted.

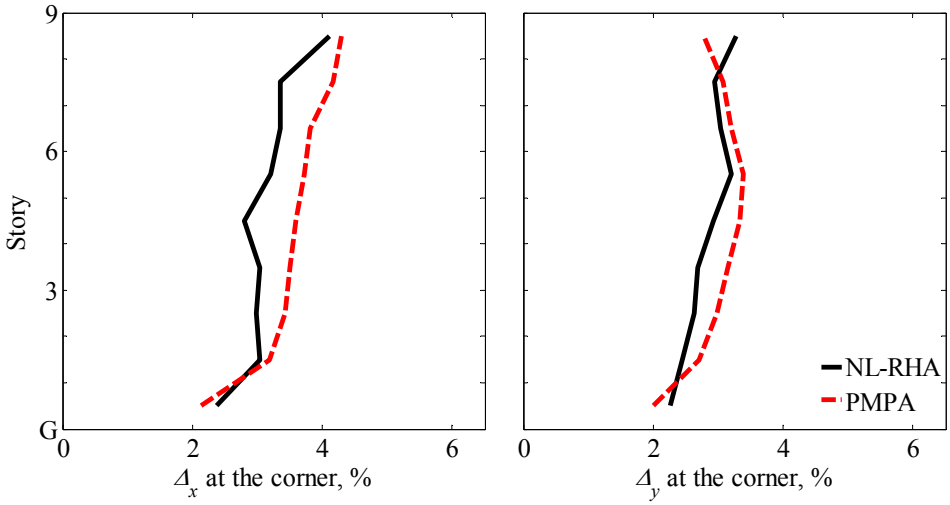

Figure 5.37 Median story drifts at the corner (identified in Fig. 5.36) of the C09 UBC85 building determined by nonlinear RHA, and PMPA. Ground motions are scaled to intensity i2.

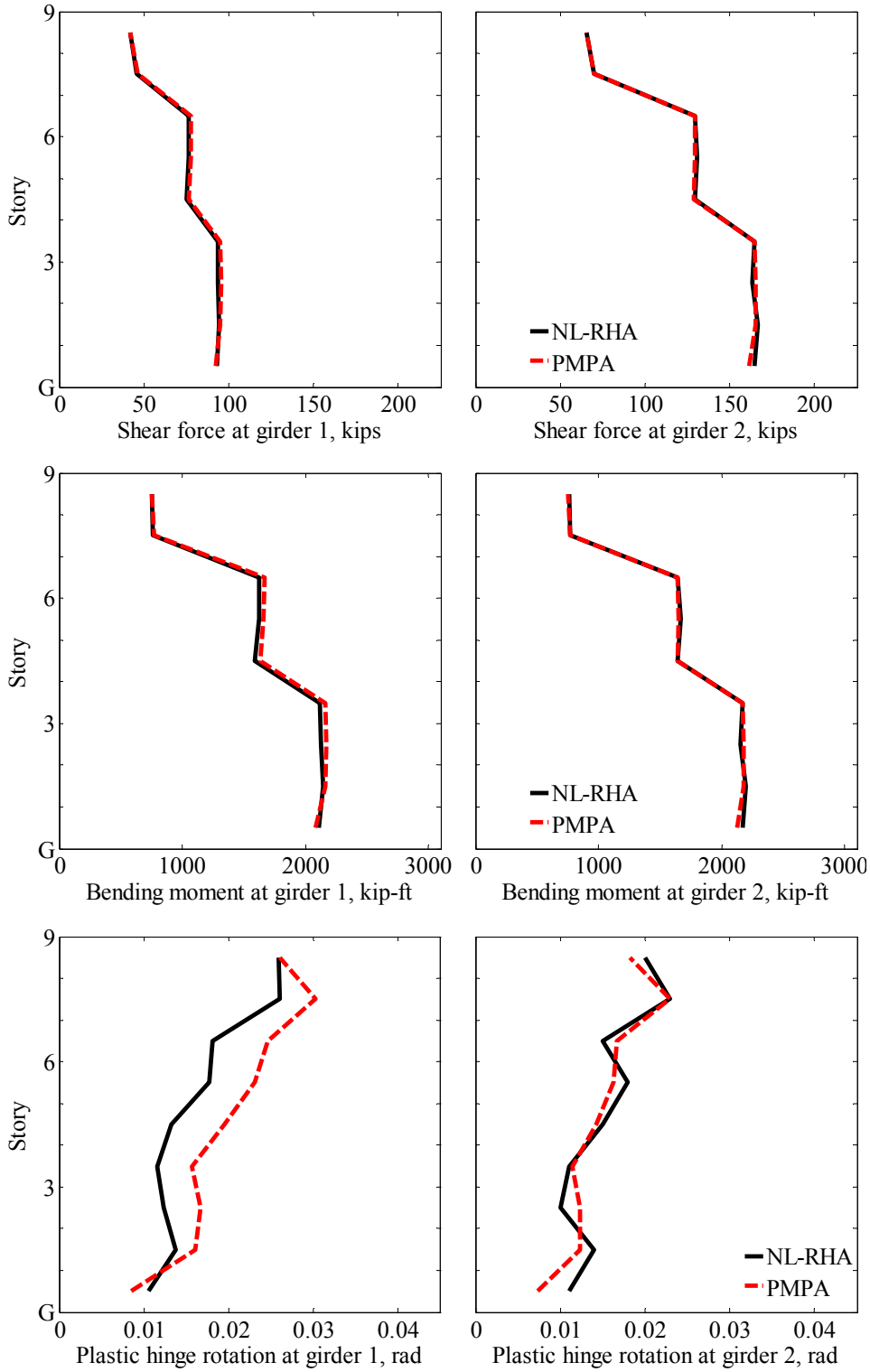

Figure 5.38 Median shear force, bending moment, and plastic hinge rotation for girders 1 and 2 (identified in Fig. 5.36) of the C09 UBC85 building determined by nonlinear RHA, and PMPA. Ground motions are scaled to intensity i2.

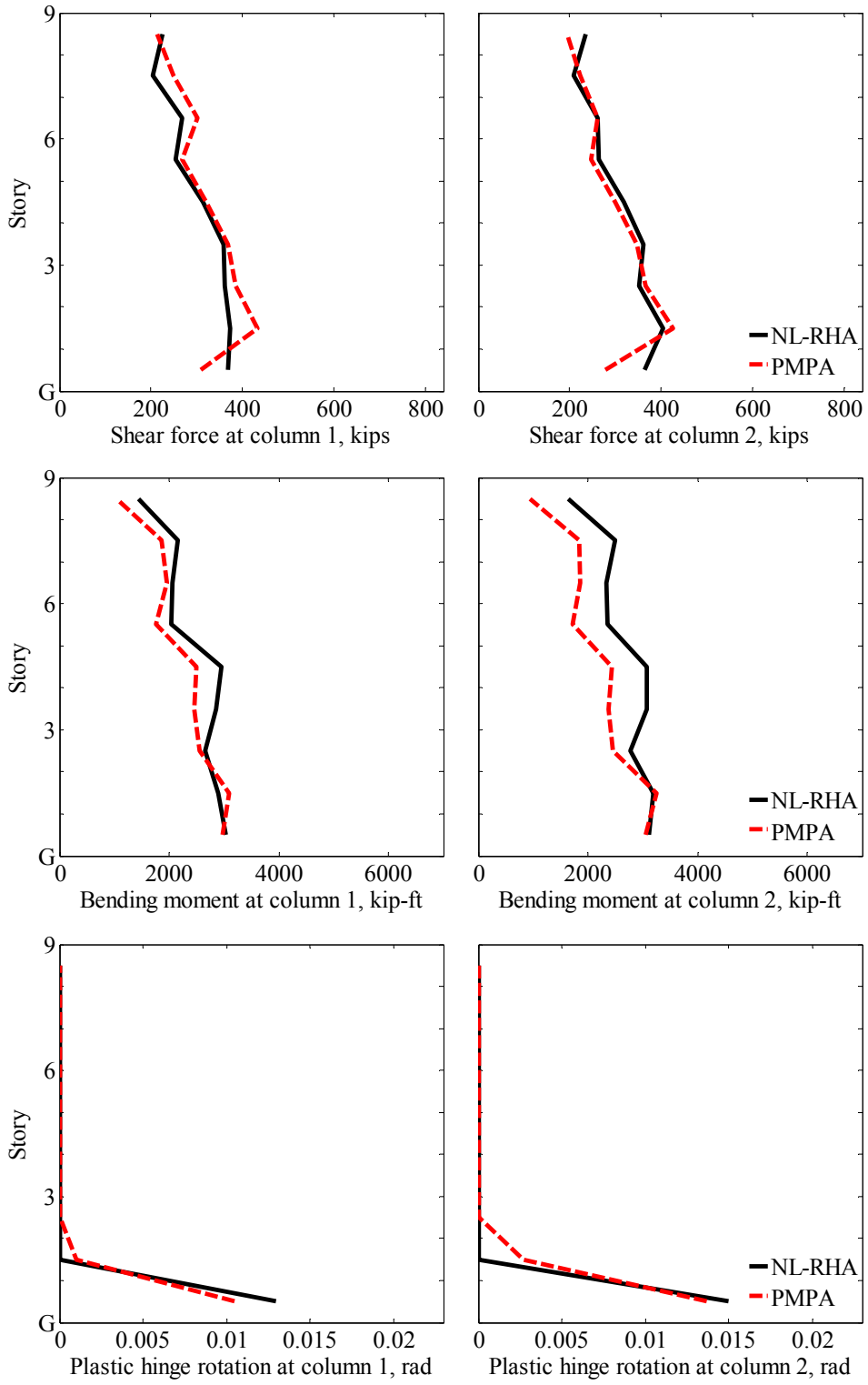

Figure 5.39 Median shear force, bending moment, and plastic hinge rotation for columns 1 and 2 (identified in Fig. 5.36) of the C09 UBC85 building determined by nonlinear RHA, and PMPA. Ground motions are scaled to intensity i2.

6 Modal-Pushover-Based-Scaling of Ground Motions

This chapter extends the original MPS procedure [Kalkan and Chopra, 2010] for one component of ground motion to two horizontal components, and investigates the accuracy and efficiency of the extended MPS procedure for nonlinear RHA of three-dimensional buildings. In addition, the accuracy and efficiency of the scaling procedure recommended in the ASCE/SEI 7-05 standard [ASCE, 2005] is evaluated. This investigation is based on seismic demands computed for medium-rise symmetric- and unsymmetric-plan buildings with ductile frames subjected to 28 ground motions.

6.1 MPS Procedure

In the MPS procedure for one component of ground motion, each record is scaled by a factor selected to match the resulting deformation of the first-"mode" inelastic SDF system—established from the first-"mode" pushover curve for the building—to a target value [Kalkan and Chopra, 2010]. Defined as the median deformation of the first-"mode" inelastic SDF system due to a large ensemble of unscaled ground motions compatible with the site-specific seismic hazard, the target deformation may be estimated by either: (1) nonlinear RHA of the first-"mode" inelastic SDF system to obtain the peak deformation due to each ground motion, and then compute the median of the resulting response values, or (2) multiplying the median peak deformation of the corresponding linear SDF system, known from the elastic design spectrum, by the inelastic deformation ratio (Section 3.5); empirical equations for the inelastic deformation ratio are available in FEMA-356 [FEMA, 2000]; Ruiz-Garcia and Miranda [2003]; Chopra and Chintanapakdee [2004]; and ASCE/SEI 41-06 [ASCE, 2007]. The final set of records are

selected by ranking the scaled ground motions based on the difference between the peak deformation of the second-"mode" SDF system, treated as elastic, and the target deformation for that mode; the record with the smallest difference is ranked the highest.

The MPS procedure may be extended to scale two components of ground motion by implementing the original scaling procedure for each component (*a* and *b*), independently, resulting in different scaling factors SF_a and SF_b; such a procedure is presented in Section 6.1.1. Recognizing that seismologists may prefer a single scaling factor for both components of a ground motion record, i.e. $SF_a = SF_b$, an MPS procedure with this constraint is developed in Section 6.1.2 and its limitations are discussed.

6.1.1 MPS Procedure: Different Scaling Factors for Two Components

The original MPS procedure is implemented to independently scale the *a* and *b* components of ground motion. Thus, Steps 1 to 9 in the following summary are to be implemented separately for each component of ground motion. Based on Kalkan and Chopra [2009a], this summary is presented in a form that is applicable to three-dimensional analysis of multistory buildings, including those that are unsymmetric in plan.

1. For the given site, define the target pseudo-acceleration response spectrum $\hat{A}(T)$ as the median pseudo-acceleration spectrum for a large ensemble of (unscaled) earthquake records compatible with the site-specific seismic hazard conditions.
2. Compute the natural frequencies ω_n (periods T_n) and modes ϕ_n of the first few modes of linearly elastic vibration of the building. For each ground motion component direction (*a* or *b*), identify the first and second modes as the two modes with the largest effective modal mass.

First-mode Dominated Structures

3. Develop the base shear-roof displacement, $V_{b1} - u_{r1}$, relation or pushover curve by non-linear static analysis of the building subjected to the first-"mode" force distribution:

$$\mathbf{s}_n^* = \begin{bmatrix} \mathbf{m}\phi_{xn} \\ \mathbf{m}\phi_{yn} \\ \mathbf{I}_O\phi_{\theta n} \end{bmatrix} \tag{6.1}$$

where **m** is a diagonal matrix of order N with $m_{jj} = m_j$, the mass lumped at the jth floor level; $\mathbf{I}_O$ is a diagonal matrix of order N with $I_{O\,jj} = I_{O\,j}$, the moment of inertia of the jth floor diaphragm about a vertical axis through the C.M. Gravity loads are applied before the lateral forces causing roof displacement u_{rg}.

4. Idealize the $V_{b1} - u_{r1}$ pushover curve as a bilinear or trilinear curve, as appropriate. Starting with this initial loading curve, define the unloading and reloading branches appropriate for the structural system and material being considered [Han and Chopra, 2006; Bobadilla and Chopra, 2007].

5. Convert the idealized pushover curve to the force-deformation, $F_{s1}/L_1 - D_1$, relation for the first-"mode" inelastic SDF system by utilizing Eq. (3.22), repeated for convenience:

$$\frac{F_{s1}}{L_1} = \frac{V_{b1}}{M_1^*} \qquad D_1 = \frac{u_{r1} - u_{rg}}{\Gamma_1 \phi_{r1}}$$

where

$$\Gamma_1 = \frac{L_1}{M_1} = \frac{\phi_1^T \mathbf{M}\boldsymbol{\iota}}{\phi_1^T \mathbf{M}\phi_1} \qquad \mathbf{M} = \begin{bmatrix} \mathbf{m} & \mathbf{0} & \mathbf{0} \\ \mathbf{0} & \mathbf{m} & \mathbf{0} \\ \mathbf{0} & \mathbf{0} & \mathbf{I}_O \end{bmatrix} \qquad \boldsymbol{\iota}_a = \begin{bmatrix} \mathbf{1} \\ \mathbf{0} \\ \mathbf{0} \end{bmatrix}, \quad \boldsymbol{\iota}_b = \begin{bmatrix} \mathbf{0} \\ \mathbf{1} \\ \mathbf{0} \end{bmatrix}$$

1 and **0** are vectors of dimension N with all elements equal to one and zero, respectively; ϕ_{r1} is the value of ϕ_1 at the roof.

6. Compute the peak deformation $D_1 = \max|D_1(t)|$ of the first-"mode" inelastic SDF system defined by the force deformation relation developed in Steps 4 and 5, and damping ratio ζ_1. For an SDF system with known T_1 and ζ_1, D_1 can be computed by nonlinear RHA of the system due to each of the unscaled ground motions $\ddot{u}_g(t)$ by solving

$$\ddot{D}_1(t) + 2\zeta_1\omega_1 \dot{D}_1(t) + \frac{F_{s1}}{L_1} = -\ddot{u}_g(t) \tag{6.2}$$

Define the target value of deformation $\hat{D}_1$ as the median of the response values due to all ground motions.

7. By nonlinear RHA, compute the peak deformation $D_1 = \max|D_1(t)|$ of the first-"mode" inelastic SDF system due to one of the selected ground motions $\ddot{u}_g(t)$ multiplied by a scale factor SF to be determined in Step 8, by solving Eq. (6.2) with the right side equal to $-(SF)\,\ddot{u}_g(t)$.

8. Compare the normalized difference between D_1 (Step 7) and the target value $\hat{D}_1$ (Step 6) against a specified tolerance, ε_{MPS}

$$\left(D_1 - \hat{D}_1\right) / \hat{D}_1 = \varepsilon_{\text{MPS}} \tag{6.3}$$

Determine the scale factor SF such that the scaled record, $(SF)\,\ddot{u}_g(t)$, satisfies the criterion of Eq. (6.3). Because Eq. (6.2) is nonlinear, SF cannot be determined a priori, but requires an iterative procedure starting with an initial guess. Starting with $SF = 1.0$, Steps 7 and 8 are implemented and repeated with modified values of SF

until Eq. (6.3) is satisfied. Successive values of SF may be chosen by trial and error, but preferably by a convergence algorithm, e.g., Quasi-Newton methods. For a given ground motion, if Eq. (6.3) is satisfied by more than one value of SF, the SF closest to one is chosen.

9. Repeat Steps 7 and 8 for as many records as deemed necessary; obviously the scaling factor SF will be different for each record. It will be demonstrated later that these scaling factors are appropriate for structures that respond dominantly in the first-mode.

At the end of steps 1 to 9, implemented separately for the *a* and *b* components of a ground motion record, scaling factors SF_a and SF_b have been determined for the two components, respectively, of each ground motion.

Higher Mode Considerations

10. Establish target values of deformation of higher-mode SDF systems, treated as elastic systems, directly from the target spectrum in the *a* and *b* directions $\hat{D}_n = (2\pi / T_n)^2 \hat{A}_n$; where the mode number n = 2. We have found that considering only the second-mode is usually adequate for most buildings.

11. By linear RHA, calculate the peak deformation $D_2 = \max|D_2(t)|$ of the second-mode elastic SDF system due to a selected ground motion $\ddot{u}_g(t)$ multiplied by its scale factor determined in Step 9.

12. Compute the difference between the peak deformation D_2 determined in Step 11 and the target value $\hat{D}_2$ determined in Step 10 for each component of ground motion. Define the normalized error

$$E_2 = \frac{\left| D_{2a} - \hat{D}_{2a} \right| + \left| D_{2b} - \hat{D}_{2b} \right|}{\hat{D}_{2a} + \hat{D}_{2b}} \tag{6.4}$$

and rank the scaled records based on their E_2 value; the record with the lowest value of E_2 is ranked the highest.

13. From the ranked list, select the final set of records with their scale factors determined in Step 9 to be used in nonlinear RHA of the structure.

The preceding procedure differs from the original MPS procedure for one component of ground motion [Kalkan and Chopra, 2010] in three aspects. (1) Instead of multiplying the median peak deformation of the corresponding linear system by the inelastic deformation ratio, the target deformation (Step 6) is computed as the median value of the peak deformations of the first-"mode" inelastic SDF system due to an ensemble of unscaled records determined by nonlinear RHA. (2) Steps 1 to 9 are implemented to scale both components of ground motion independently. (3) Higher mode effects in response due to both components of ground motion are considered in Steps 10 to 12.

6.1.2 MPS Procedure: Same Scaling Factor for Two Components

Seismologists prefer to scale all components of a ground motion record by the same factor to preserve focal mechanism and wave propagation effects [Dreger, 2009]. To satisfy this constraint, the following alternatives were analyzed:

1. Scaling both components of a record by the same factor selected to minimize the absolute sum of the differences between the peak deformation D_1 and the target deformation $\hat{D}_1$ due to the *a* and *b* components of ground motion, i.e.,

$$\min_{SF} \left[\frac{\left| D_{1a} - \hat{D}_{1a} \right| + \left| D_{1b} - \hat{D}_{1b} \right|}{\hat{D}_{1a} + \hat{D}_{1b}} \right] \tag{6.5}$$

where the peak deformations $D_{1a} = \max|D_{1a}(t)|$ and $D_{1b} = \max|D_{1b}(t)|$ are obtained by solving Eq. (6.2) for *a* and *b* components of ground motion with the right side equal to $-(SF)\,\ddot{u}_g(t)$. This approach was found to be inadequate because satisfying Eq. (6.5) may introduce large discrepancies between the peak deformation D_{1b} and the corresponding target value $\hat{D}_{1b}$ for the *b* component, but match perfectly D_{1a} to $\hat{D}_{1a}$ for the *a* component. This is demonstrated schematically in Fig. 6.1a where the force-deformation curves for the first vibration "mode" associated with each of the *a* and *b* directions are shown together with the peak deformations due to unscaled and scaled versions of the *a* and *b* components of ground motion. For each component, note that the deformation due to the unscaled ground motion is larger than the target deformation. The scaling factor determined to satisfy Eq. (6.5) may results in matching the target value for one component with significant discrepancies remaining for the second component.

2. Modifying Eq. (6.3) to simultaneously consider both components of ground motion, i.e.,

$$\left[\left(D_{1a} - \hat{D}_{1a}\right) + \left(D_{1b} - \hat{D}_{1b}\right)\right] / \left(\hat{D}_{1a} + \hat{D}_{1b}\right) = \varepsilon_{\text{MPS}} \qquad (6.6)$$

For the example of Fig. 6.1, the criterion of Eq. (6.6) will lead to a scaling factor such that the peak deformation D_1 due to a scaled ground motion will overestimate the target value $\hat{D}_1$ for one component, but will underestimate for the other component. This is demonstrated schematically in Fig. 6.1b where the force-deformation curves for the first vibration "mode" associated with each of the *a* and *b* directions are shown together with the peak deformations due to unscaled and scaled

versions of the *a* and *b* components of ground motion; for each component, note that the deformation due to the unscaled ground motion is larger than the target deformation.

To implement the latter approach, Steps 8 and 9 are modified as follows:

8. Compare the sum of the normalized differences between D_1 (Step 6) and target values of the deformation $\hat{D}_1$, defined by Eq. (6.6), against a specified tolerance ε_{MPS}.

   Determine the scale factor SF such that the scaled records $(SF)\,\ddot{u}_{ga}(t)$ and $(SF)\,\ddot{u}_{gb}(t)$ satisfy the criterion of Eq. (6.6). Because Eq. (6.2) is nonlinear, SF cannot be determined a priori, but requires an iterative procedure starting with an initial guess. Starting with $SF = 1.0$, Steps 7 and 8 are implemented and repeated with modified values of SF until Eq. (6.6) is satisfied. Successive values of SF are chosen by trial and error or by a convergence algorithm, e.g., Quasi-Newton methods. For a given ground motion, if Eq. (6.6) is satisfied by more than one value of SF, the SF closest to one is chosen.

9. Repeat Steps 7 and 8 for as many records as deemed necessary; obviously the scaling factor SF will be different for each record.

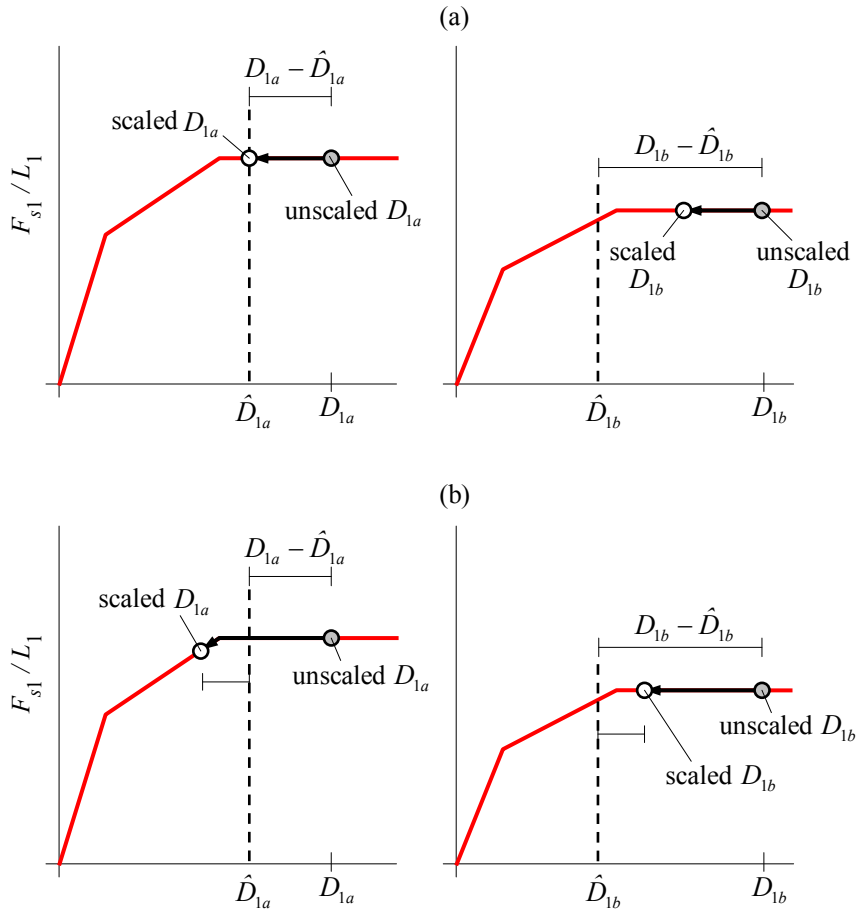

Figure 6.1 Schematic explanation of the MPS procedure with SF_a=SF_b, shown implications of the criterion of (a) Eq. (6.5) and (b) Eq. (6.6).

6.2 ASCE/SEI 7-05 Procedure

6.2.1 One Component of Ground Motion

The criteria for selecting and procedures for scaling ground motions in the 2006 International Building Code (IBC06) and the 2007 California Building Code (CBC07) for use in nonlinear RHA of buildings are based on the ASCE/SEI 7-05 standard [ASCE 2005]. In the ASCE/SEI 7-05 (abbreviated to ASCE7) procedure, earthquake records are to be selected from events of magnitudes, fault distances, and source mechanisms consistent with the maximum considered earthquake. For two dimensional (or planar)

analyses of "regular" structures, the ground motions should be scaled such that the average value of the 5%-damped response spectra for the set of scaled motions is not less than the design spectrum over the period range from $0.2T_1$ to $1.5T_1$. The design value of an engineering demand parameter (EDP)—member forces, member deformations, story drifts, etc—is specified as the average value of the EDP over a set of seven ground motions, or the maximum value over 3 ground motions.

Various combinations of scaling factors for the individual ground motions can satisfy the requirement that the average spectrum of scaled records exceeds the design spectrum over the specified period range [Kalkan and Chopra, 2010]. To achieve the desirable goal of scaling each record by the smallest possible factor, we implemented the ASCE7 procedure as follows:

1. Obtain the target pseudo-acceleration spectrum $\hat{A}(T)$ for the building site as described in Step 1 of the MPS procedure. Define $\hat{\mathbf{A}}$ as a vector of spectral values $\hat{A}_i$ at, say, 100 different periods T_i over the period range from $0.2T_1$ to $1.5T_1$.
2. Select seven ground motions appropriate for the site, based on the criteria specified in ASCE7.
3. Calculate the 5%-damped response spectrum $A(T)$ and the vector $\mathbf{A}$ of spectral values at the same periods for each ground motion.
4. Estimate the scaling factor SF_1 to minimize the difference between the target spectrum (Step 1) and the response spectrum (Step 3) by solving the following minimization problem for each ground motion: $\underset{SF_1}{min} \left\| \hat{\mathbf{A}} - SF_1 \times \mathbf{A} \right\| \Rightarrow SF_1$ where $\|\cdot\|$ is the Euclidean norm**.** Required for this purpose is a numerical method to

minimize scalar functions of one variable; such methods are available in textbooks on numerical optimization. This minimization ensures that the scaled response spectrum is as close as possible to the target spectrum, as shown schematically in Fig. 6.2.

5. Determine the vector $\hat{\mathbf{A}}_{\text{scaled}}$ for the mean scaled spectrum defined as the mean of the scaled spectra ($SF_1 \times \mathbf{A}$) of the set of records. The ordinates of this mean scaled spectrum could be smaller than the ordinates of the target spectrum at the same periods.

6. Calculate the maximum normalized difference $\varepsilon_{\text{ASCE}}$ (Fig. 6.3a) between the target spectrum $\hat{\mathbf{A}}$ and the mean scaled spectrum $\hat{\mathbf{A}}_{\text{scaled}}$, over the period range from $0.2T_1$ to $1.5T_1$; i.e., $\varepsilon_{\text{ASCE}} = \max_{0.2T_1 \le T_i \le 1.5T_1} (\hat{A}_i - \hat{A}_{\text{scaled},i}) \div \hat{A}_i$, where $\hat{A}_i$ and $\hat{A}_{\text{scaled},i}$ are the ordinates of the target and the mean scaled pseudo-acceleration spectra at vibration period T_i, respectively. Define the scale factor $SF_2 = 1/\,1 - \varepsilon_{\text{ASCE}}$ if $\varepsilon_{\text{ASCE}} > 0$; otherwise, $SF_2 = 1.0$.

7. Determine the final scale factor $SF = SF_1 \times SF_2$ for each ground motion. Scaling ground motions by the scaling factor SF ensures that the average value of the response spectra for the set of scaled motions is not less than the target spectrum over the period range from $0.2T_1$ to $1.5T_1$ (Fig. 6.3b).

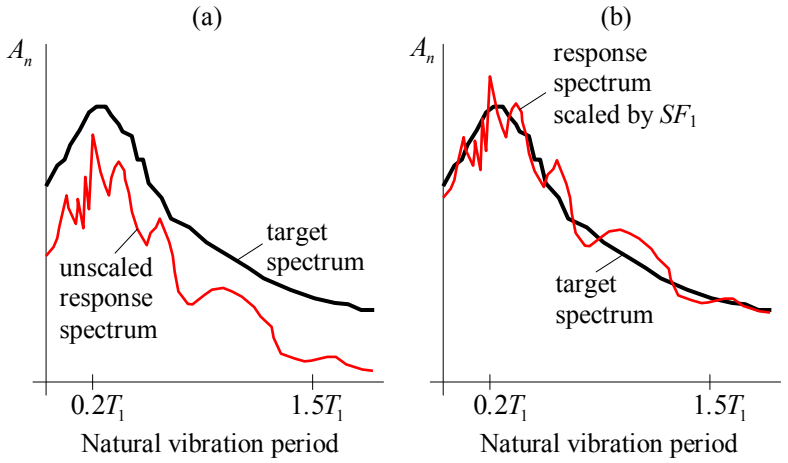

Figure 6.2 Schematic illustration of Step 4 of the ASCE7 scaling procedure.

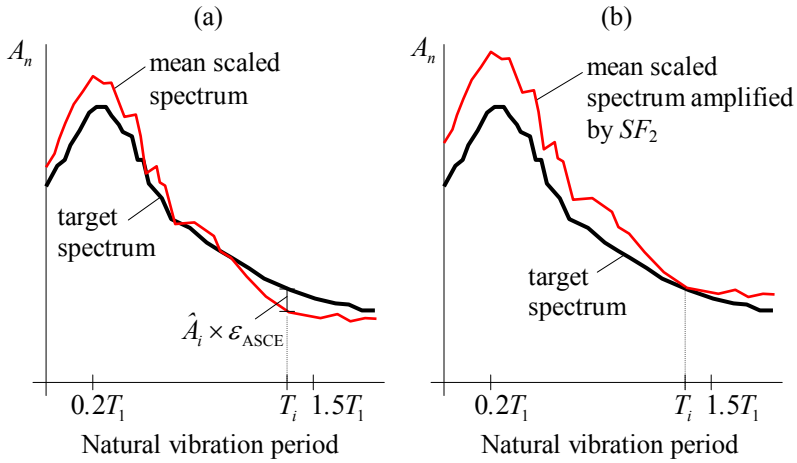

Figure 6.3 Schematic illustration of Step 6 of the ASCE7 scaling procedure.

6.2.2 Two Components of Ground Motion

ASCE7 requires that the ground motions are scaled such that the average of the SRSS spectra from all ground motions does not fall below 1.3 times the target spectrum by more than 10 percent over the period range $0.2T_1$ to $1.5T_1$. The SRSS spectrum for each ground motion is constructed by calculating the square-root-of-sum-of-squares (SRSS) of the 5%-damped response spectra for the two horizontal components of the scaled ground motion, with both components scaled by the same factor.

The preceding implementation of scaling of ground motions for two-dimensional (planar) analysis of structures can be extended for three-dimensional analysis as follows:

1. Obtain the target pseudo-acceleration spectra $\hat{A}_a(T)$ and $\hat{A}_b(T)$ for the *a* and *b* components of ground motion for the building site, as described in Step 1 of the MPS procedure. Define $\hat{\mathbf{A}}_a$ and $\hat{\mathbf{A}}_b$ as vectors of spectral values $\hat{A}_i$ at different periods T_i over the period range from $0.2T_1$ to $1.5T_1$.
2. Calculate the amplified target spectrum $\hat{\mathbf{A}} = 1.3\left(\hat{\mathbf{A}}_a + \hat{\mathbf{A}}_b\right)/2$.
3. Select seven ground motions appropriate for the site, based on the criteria specified in ASCE7.
4. Calculate the 5%-damped response spectra $A_a(T)$ and $A_b(T)$, and the vectors $\mathbf{A}_a$ and $\mathbf{A}_b$ of spectral values at the same periods (as in Step 1) for the *a* and *b* components of ground motion.
5. Compute the SRSS spectrum $\mathbf{A}_{\text{SRSS}}$ of each ground motion: $A_{SRSS,i} = \sqrt{\left(A_{a,i}\right)^2 + \left(A_{b,i}\right)^2}$ where $A_{SRSS,i}$, $A_{a,i}$ and $A_{b,i}$ are the *i*th components of the vectors $\mathbf{A}_{\text{SRSS}}$, $\mathbf{A}_a$, and $\mathbf{A}_b$, respectively.
6. Estimate the scaling factor SF_1 to minimize the difference between the amplified target spectrum (Step 2) and the SRSS spectrum (Step 5) by solving the following minimization problem for each ground motion: $\underset{SF_1}{min} \left\| \hat{\mathbf{A}} - SF_1 \times \mathbf{A}_{\text{SRSS}} \right\| \Rightarrow SF_1$

   where $\|\cdot\|$ is the Euclidean norm**.** Required for this purpose is a numerical method to minimize scalar functions of one variable; such methods are available in textbooks on numerical optimization.

7. Determine the mean scaled SRSS spectrum $\hat{\mathbf{A}}_{\text{SRSS}}$ defined as the average of the scaled SRSS spectra ($SF_1 \times \mathbf{A}_{\text{SRSS}}$) for the set of records.

8. Calculate the maximum normalized difference $\varepsilon_{\text{ASCE}}$ between the target spectrum $\hat{\mathbf{A}}$ and the mean scaled SRSS spectrum $\hat{\mathbf{A}}_{\text{SRSS}}$ over the period range from $0.2T_1$ to $1.5T_1$; i.e. $\varepsilon_{\text{ASCE}} = \max_{0.2T_1 \le T_i \le 1.5T_1} (\hat{A}_i - \hat{A}_{\text{SRSS},i}) \div \hat{A}_i$, where $\hat{A}_i$ and $\hat{A}_{\text{SRSS},i}$ are the ordinates of the target and the mean of the scaled SRSS pseudo-acceleration spectra at vibration period T_i, respectively. Define the scale factor $SF_2 = 0.9/\,1 - \varepsilon_{\text{ASCE}}$ if $\varepsilon_{\text{ASCE}} > 0.1$; otherwise, $SF_2 = 1.0$

9. Determine the final scale factor $SF = SF_1 \times SF_2$ for each ground motion.

6.3 Ground motions

The twenty eight ground motion records selected for this investigation are listed in Table 6.1 with their relevant data [PEER, 2007]. Each of the 28 records includes two orthogonal components of horizontal ground motion. Figure 6.4 shows the magnitude-distance distribution for the ensemble of selected records, wherein R_{JB} is the distance of the site to the surface projection of fault rupture, as defined by Joyner and Boore [1981].

An initial investigation indicated that the 28 ground motions selected are not intense enough to drive the buildings considered in this research significantly into the nonlinear range. Therefore, the ground motions were amplified by a factor of 3.0; the resulting 28 ground motions are treated as "unscaled" motions for this investigation. Figure 6.5 shows the 5%-damped median response spectrum for components *a* and *b* of the "unscaled" ground motions.

Table 6.1 List of 28 ground motion records

Record	Earthquake Name	M_w	Mechanism	Station Name	V_{s30} (m/s)	NEHRP Based on Vs30	R_{JB} (km)	Component *a*			Component *b*		
								Comp 1 (deg)	PGA (cm/s^2)	PGV (cm/s)	Comp 2 (deg)	PGA (cm/s^2)	PGV (cm/s)
1	1994 Northridge	6.7	Reverse	Canyon Country - W Lost Cany	308.6	D	11.4	0	402.0	43.0	270	472.6	45.1
2	1994 Northridge	6.7	Reverse	LA - Saturn St	308.7	D	21.2	20	465.2	34.5	110	430.0	39.0
3	1994 Northridge	6.7	Reverse	Santa Monica City Hall	336.2	D	17.3	90	865.9	41.7	360	362.6	25.1
4	1999 Duzce, Turkey	7.1	Strike Slip	Bolu	326.0	D	12.0	0	713.4	56.5	90	806.3	62.1
5	1999 Hector Mine	7.1	Strike Slip	Hector	684.9	C	10.4	0	260.4	28.6	90	330.2	41.8
6	1979 Imperial Valley	6.5	Strike Slip	Delta	274.5	D	22.0	262	233.1	26.0	352	344.2	33.0
7	1979 Imperial Valley	6.5	Strike Slip	El Centro Array #11	196.3	D	12.5	140	356.9	34.4	230	372.2	42.1
8	1979 Imperial Valley	6.5	Strike Slip	Calexico Fire Station	231.2	D	10.5	225	269.5	21.2	315	198.0	16.0
9	1979 Imperial Valley	6.5	Strike Slip	SAHOP Casa Flores	338.6	D	9.6	0	281.8	19.4	270	496.1	31.0
10	1995 Kobe, Japan	6.9	Strike Slip	Nishi-Akashi	609.0	C	7.1	0	499.4	37.3	90	492.9	36.7
11	1995 Kobe, Japan	6.9	Strike Slip	Shin-Osaka	256.0	D	19.1	0	238.5	37.8	90	207.8	27.9
12	1995 Kobe, Japan	6.9	Strike Slip	Kakogawa	312.0	D	22.5	0	246.5	18.7	90	338.0	27.7
13	1999 Kocaeli, Turkey	7.5	Strike Slip	Duzce	276.0	D	13.6	180	306.0	58.8	270	350.9	46.4
14	1992 Landers	7.3	Strike Slip	Yermo Fire Station	353.6	D	23.6	270	240.0	51.5	360	148.6	29.7
15	1992 Landers	7.3	Strike Slip	Coolwater	271.4	D	19.7	0	277.3	25.6	90	408.7	42.3
16	1992 Landers	7.3	Strike Slip	Joshua Tree	379.3	C	11.0	0	268.4	27.5	90	278.5	43.2
17	1989 Loma Prieta	6.9	Reverse Oblique	Capitola	288.6	D	8.7	0	518.2	35.0	90	434.6	29.2
18	1989 Loma Prieta	6.9	Reverse Oblique	Gilroy Array #3	349.9	D	12.2	0	544.2	35.7	90	360.2	44.7
19	1989 Loma Prieta	6.9	Reverse Oblique	Hollister City Hall	198.8	D	27.3	90	241.7	38.5	180	210.6	45.0
20	1989 Loma Prieta	6.9	Reverse Oblique	Hollister Diff. Array	215.5	D	24.5	165	263.4	43.8	255	273.4	35.6
21	1990 Manjil, Iran	7.3	Strike Slip	Abbar	724.0	C	12.6	0	504.5	43.2	90	486.6	53.2
22	1987 Superstition Hills	6.5	Strike Slip	El Centro Imp. Co. Cent	192.1	D	18.2	0	350.9	46.3	90	253.3	40.8
23	1987 Superstition Hills	6.5	Strike Slip	Poe Road (temp)	207.5	D	11.2	270	437.6	35.7	360	294.4	32.8
24	1987 Superstition Hills	6.5	Strike Slip	Westmorland Fire Sta	193.7	D	13.0	90	168.5	23.5	180	206.7	31.0
25	1992 Cape Mendocino	7.0	Reverse	Rio Dell Overpass - FF	311.8	D	7.9	270	377.9	43.9	360	538.2	42.1
26	1999 Chi-Chi, Taiwan	7.6	Reverse Oblique	TCU070	401.3	C	19.0	160	250.2	52.1	250	165.4	62.3
27	1999 Chi-Chi, Taiwan	7.6	Reverse Oblique	CHY006	438.2	C	9.8	6	338.5	42.7	276	357.3	55.4
28	1971 San Fernando	6.6	Reverse	LA - Hollywood Stor FF	316.5	D	22.8	90	205.8	18.9	180	170.8	14.9

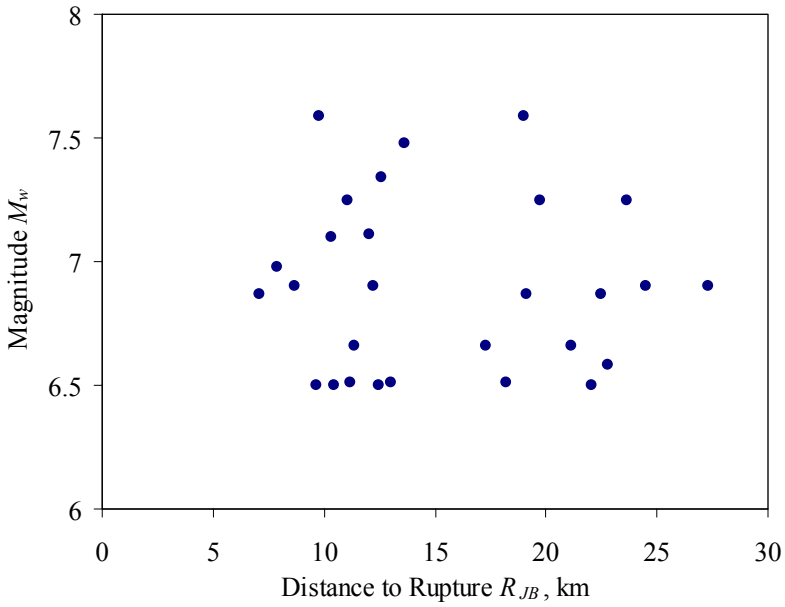

Figure 6.4 Distribution of magnitude, M_w, and distance of site to surface projection of fault rupture, R_{JB}.

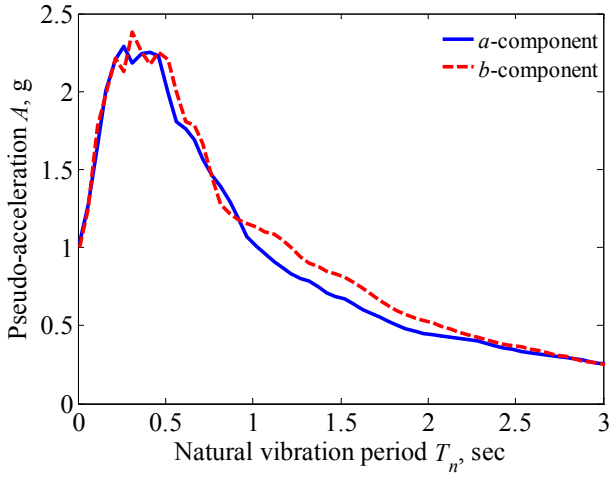

Figure 6.5 Median response spectra of 28 ground motions in the *a* and *b* directions; damping ratio 5%. Recorded ground motions were amplified by a factor of 3.0.

To evaluate the MPS and ASCE7 scaling procedures, two sets of seven ground motions each are selected from the ensemble of earthquakes presented in Table 6.1. The data set of 28 values of deformation of the first-"mode" inelastic SDF system to the 28 unscaled ground motions are sorted in ascending order and the seven ground motions that lead to the smallest deformations are grouped as set 1, whereas the seven ground motions that drive the SDF system to the largest deformations are defined as set 2; obviously, these sets depend on the building and represent a very severe test of the scaling procedures. The accuracy of the scaling procedures is evaluated by comparing the median (or geometric mean)† values of the EDPs for a selected building due to each set against the benchmark values, defined as the median values of the EDPs due to the 28 unscaled

† The median $\hat{x}$ of the n_{EQ} observed values (x_i=1,2,…n_{EQ}) of a random variable *x,* are defined as: $\hat{x} = exp\left[\sum_{i=1}^{n_{EQ}} \ln x_i \div n_{EQ}\right]$ [Benjamin and Cornell, 1970].

ground motions. The efficiency of the scaling procedures is evaluated by computing the dispersion† of the responses for each set of scaled ground motions; small dispersion indicates that the scaling procedure is efficient.

6.4 Modeling of the Symmetric-Plan Building

6.4.1 Structural System

The symmetric-plan structure considered is an existing 9-story steel building with ductile frames located in Aliso Viejo, CA (Fig. 6.6). The west elevation of the building and the plan of floors 3 to 8 are shown in Fig. 6.7. The lateral load resisting system consists of two ductile steel moment frames in the longitudinal and transverse directions (Fig. 6.7b) with SSDA beam slot connections (U.S. patent No. 5680738, 6237303 and 7047695); all structural members are standard I-sections and the typical floors are 3" metal deck with 3¼" of light weight concrete fill. The building façade consists of concrete panels and glass (Fig. 6.6), and the building has a helistop on the roof (Fig. 6.7a).

The selected building was designed as an office building according to 2001 California Building Code (CBC01) for zone 4 and soil profile S_d. The earthquake forces were determined by linear response spectrum analysis (RSA) of the building with the design spectrum reduced by a response modification factor of 8.5.

† The dispersion measure δ of the n_{EQ} observed values (x_i=1,2,…n_{EQ}) of a random variable x, are defined as: $\delta = \left\{ \left[\sum_{i=1}^{n_{EQ}} \left(\ln x_i - \ln \hat{x} \right)^2 \right] \div \left(n_{EQ} - 1 \right) \right\}^{\frac{1}{2}}$ [Benjamin and Cornell, 1970].

Figure 6.6 9-story symmetric-plan building in Aliso Viejo, CA.

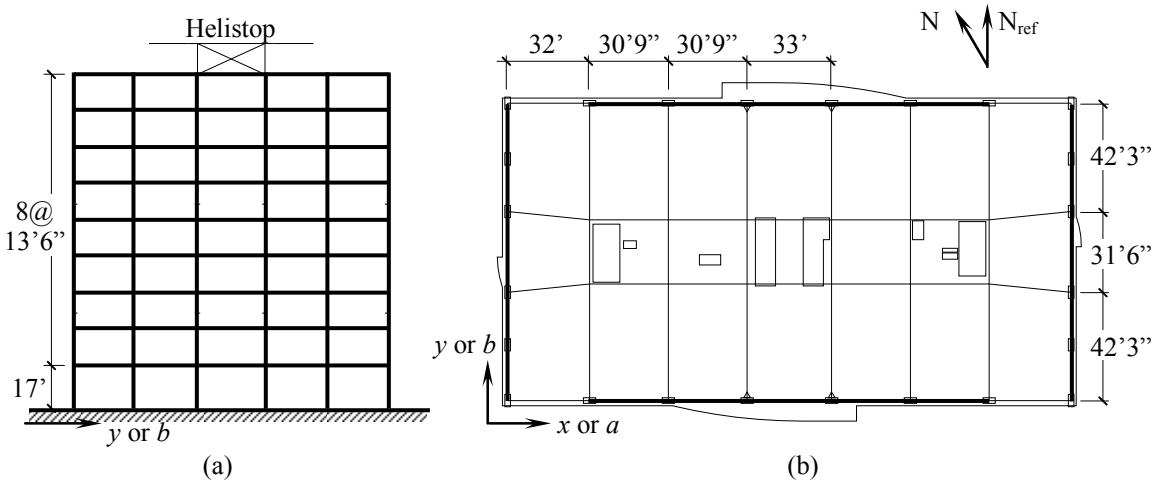

Figure 6.7 (a) West elevation; (b) typical floor plan of the selected 9-story symmetric-plan building.

The location and orientation of the fifteen sensors installed in the building to record its motions during an earthquake are shown in Fig. 6.8. All eight sensors in the *y*-direction and only two in the *x*-direction (9 and 13) recorded reliable data during the magnitude 5.4 Chino-Hills earthquake (2008) centered at a distance of 40 km. The acceleration records are shown in Fig. 6.9, wherein the peak values are noted. The horizontal acceleration of 0.026g at the ground was amplified to 0.042g at the roof of the building; this earthquake did not cause any observable damage.

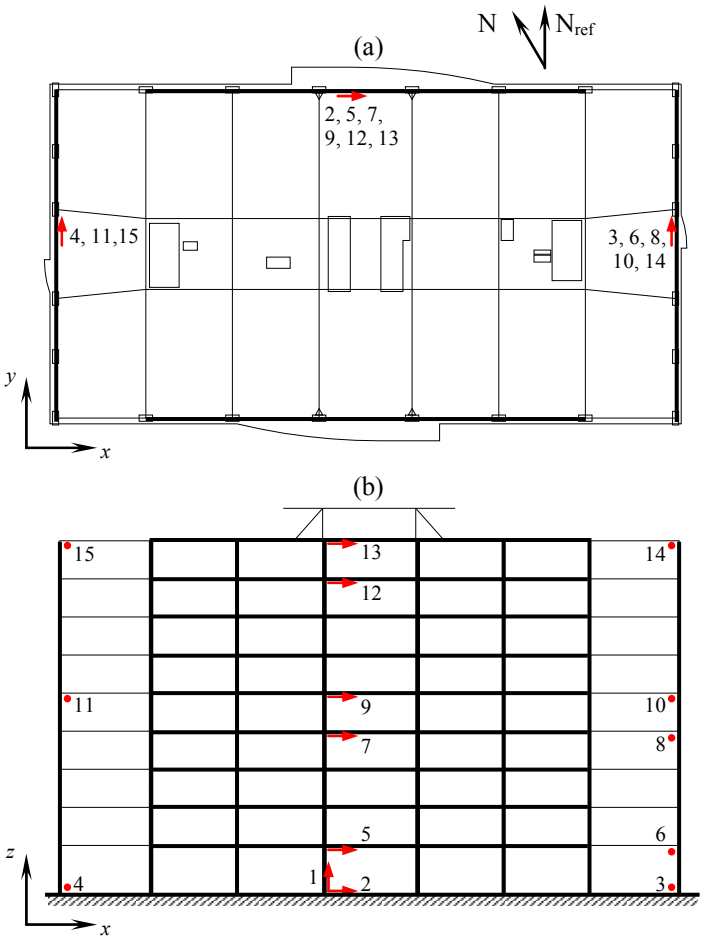

Figure 6.8 Locations of sensors in the 9-story symmetric-plan building: (a) plan view, and (b) south elevation.

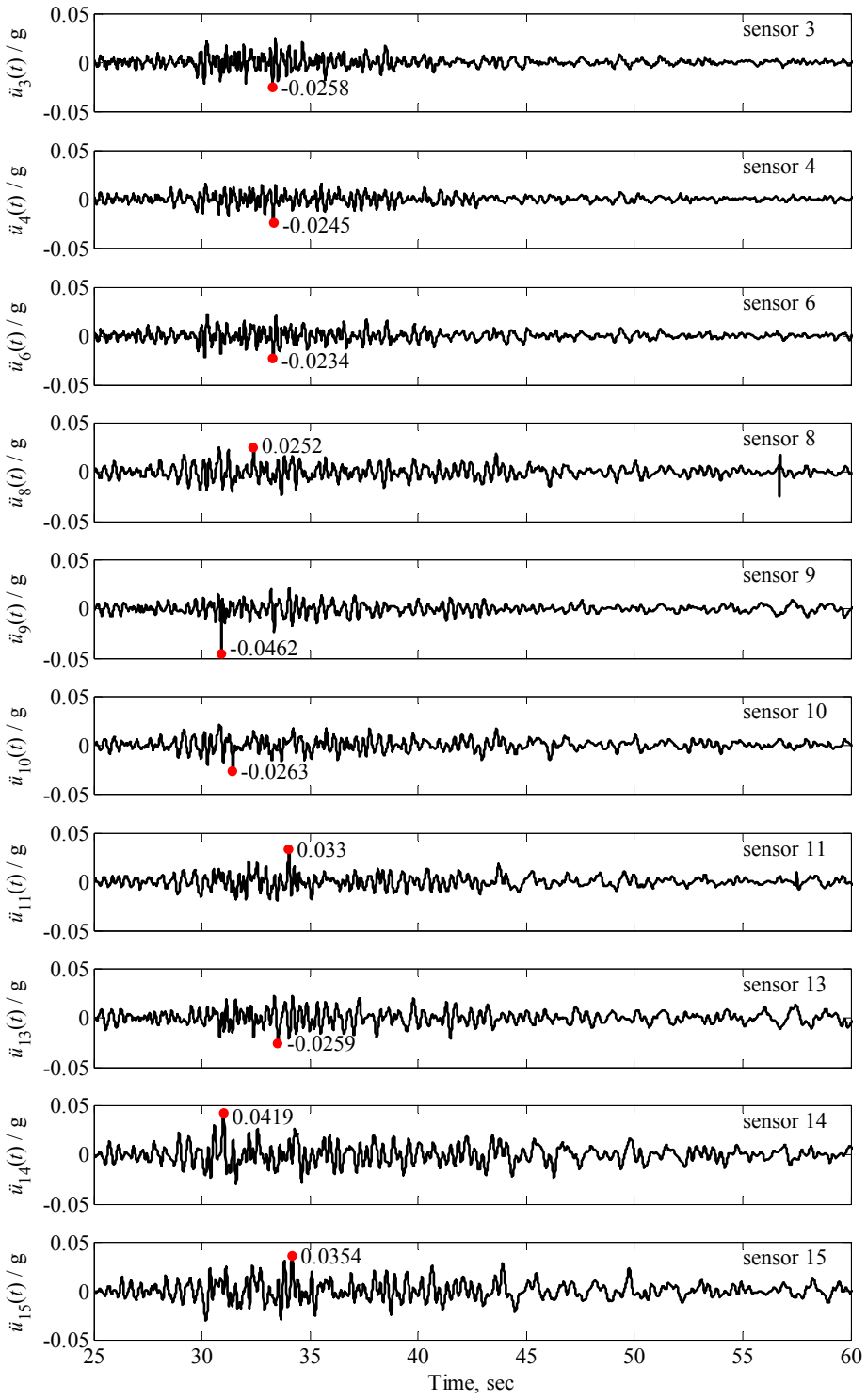

Figure 6.9 Floor accelerations recorded by the sensors showed in Fig. 6.8 during the magnitude 5.4 Chino-Hills earthquake (2008).

6.4.2 Modeling

The building is modeled for dynamic analysis, implemented by the PERFORM-3D computer program [CSI, 2006], with the following features: (1) Beams and columns are modeled by a linear element with tri-linear plastic hinges at the ends of the elements that can include in-cycle strength deterioration, but not cyclic stiffness degradation (Fig. 4.4a). The bending stiffness of the beams is modified to include the effect of the slab. Axial load-moment interaction in columns is based on plasticity theory. (2) The braces below the helistop are modeled using fiber sections that can model buckling behavior. (3) Panel zones are modeled as four rigid links hinged at the corners with a rotational spring that represents the strength and stiffness of the connection (Fig. 5.3) [Krawinkler, 1978]. (4) The tab connections are modeled using rigid-perfectly-plastic hinges that can include in-cycle and cyclic degradation. (5) The contribution of non-structural elements is modeled by adding four shear columns located close to the perimeter of the building with their properties obtained from simplified models of the façade and partitions. Nonlinear behavior of these elements is represented using rigid-plastic shear hinges. (6) Ductility capacities of girders, columns and panel zones are specified according to the ASCE/SEI 41-06 standard [ASCE, 2007]. (7) Columns of moment resisting frames and the gravity columns are assumed to be clamped at the base. (8) A standard P-Delta formulation is used to approximate effects of nonlinear geometry at large deformations for both moment and gravity frames.

6.4.3 System Identification and Response Prediction

Vibration properties—natural periods, natural modes, and modal damping ratios—of the building are determined from recorded motions (Fig. 6.9) by two system

identification methods: the combined deterministic-stochastic subspace (DSS) method and the peak-picking (PP) method. DSS algorithms are both user-friendly and highly robust to sensor noise [Giraldo et al, 2009], but, they need a complete input from all sensors to get reliable results. Because the motions recorded in the *x*-direction are incomplete, the DSS method is used only to identify vibration properties in *y*-direction. Additional information about DSS methods can be found in Van Overschee and De Moor [1996]. The PP method estimates natural vibration frequencies from the ratio of power spectral densities (PSD) of recorded floor and ground accelerations. Because sensor 2 did not record ground acceleration in the *x*-direction, vibration frequencies for this direction are estimated directly from the PSD of floor accelerations.

Figure 6.10 shows power spectral densities of the motions recorded in *x*-direction at the 5th and 9th floors, and the floor-to-ground ratio of PSDs for motions in *y*-direction recorded at various floors; also included are the natural vibration periods identified by PP method. The periods of the first two modes of lateral vibration are 1.46 and 0.50 sec for motion in the *x*-direction; and 1.58 and 0.55 sec for motion in the *y*-direction. The periods of torsion vibration modes are 1.08 and 0.38 sec, which appear in both parts (a) and (b) of Fig. 6.10. Table 6.2 compares values of natural vibration periods identified by PP and DSS methods with the computed periods of the building model. Figure 6.11 compares natural modes of vibration identified by the DSS method with calculated modes of the computer model. Remarkably good agreement between calculated and identified values of vibration periods and modes is achieved.

The damping ratios determined by the DSS method are 4.30, 3.30, 3.96 and 3.22 percent for the first, third, fourth and sixth modes of vibration. Based on these data,

energy dissipation in the building was modeled by *Rayleigh damping* with its two constants selected to give 4.30% and 3.96% damping ratio at the vibration periods of the first and fourth modes, respectively. The resulting damping ratios for the first nine vibration modes of the buildings are shown in Fig. 6.12.

Nonlinear RHA of the computer model with these modal damping ratios subjected to the ground motion recorded during the 2008 Chino Hills earthquake led to the floor displacements shown in Fig. 6.13, where these computed responses are compared with the recorded motion. The good agreement between calculated and recorded floor displacements indicates that the computer model is adequate.

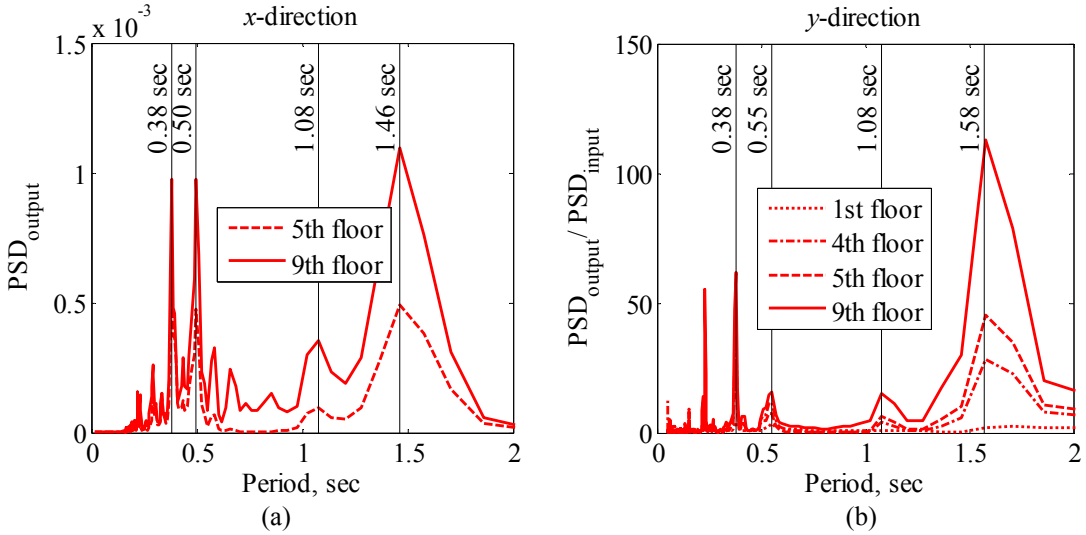

Figure 6.10 Identification of natural periods of vibration in the (a) *x*-direction and (b) *y*-direction by the peak-picking (PP) method.

Table 6.2 Natural periods of vibration obtained from the peak-picking (PP) method, the combined deterministic-stochastic subspace (DSS) method, and the computer model.

Mode	Direction	Identified Period [sec]		Computer Model Period [sec]
		PP method	DSS method	
1	translational *y*	1.58	1.53	1.53
2	translational *x*	1.46	-	1.46
3	torsional	1.08	1.07	1.02
4	translational *y*	0.55	0.49	0.54
5	translational *x*	0.50	-	0.50
6	torsional	0.38	0.36	0.36

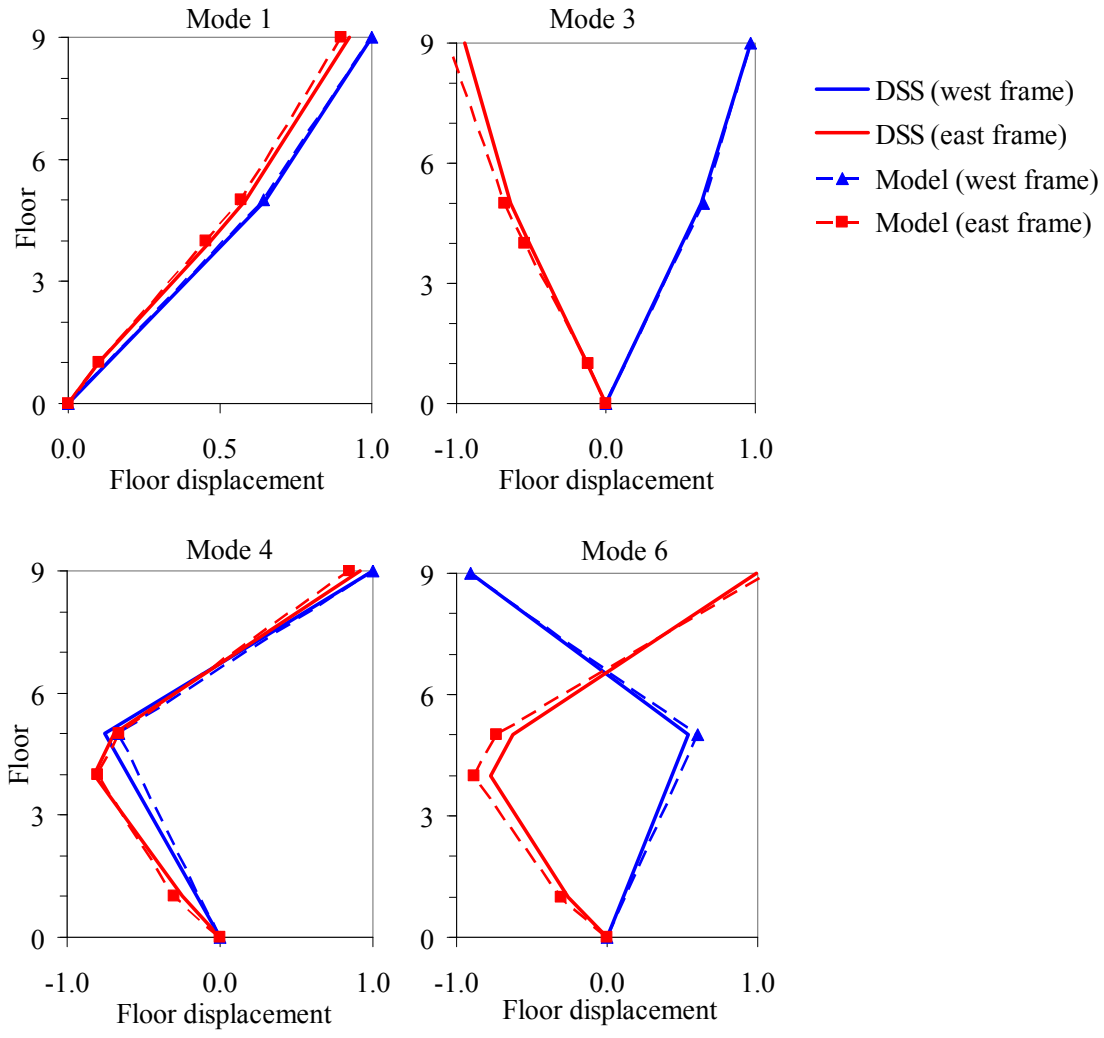

Figure 6.11 Comparison of natural vibration modes identified by the DSS method with modes of the computer model.

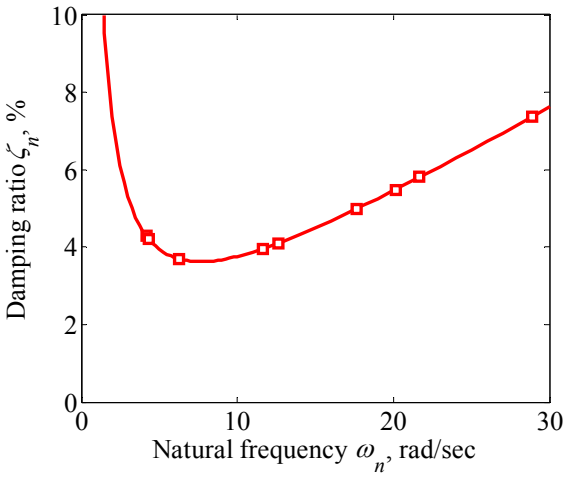

Figure 6.12 Modal damping ratios shown in the damping ratio versus frequency curve

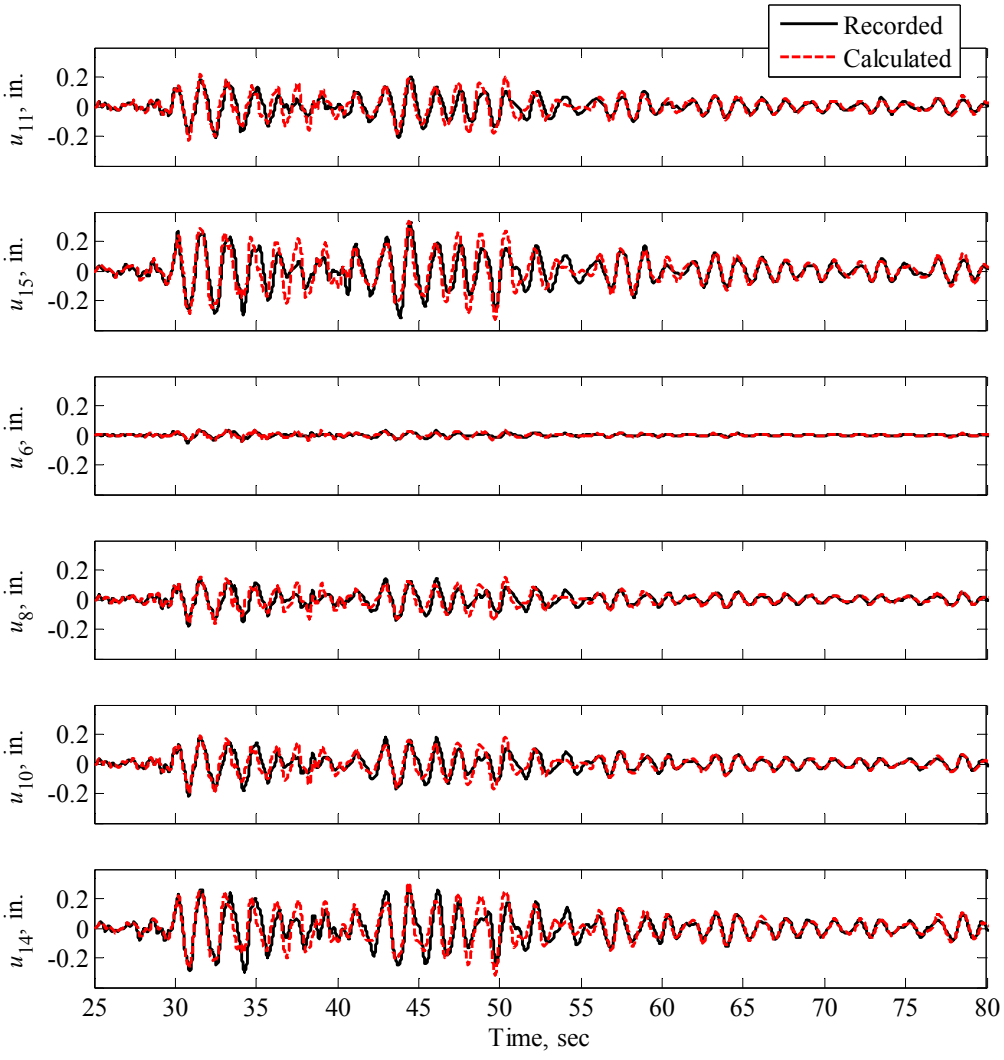

Figure 6.13 Comparison of recorded and computed floor displacements at the sensor locations (Fig. 6.8). Recorded data is from the Chino Hills earthquake (2008).

6.5 Evaluating Scaling Procedures: One Component of Ground Motion

6.5.1 Benchmark Responses

Benchmark values of the EDPs were determined by conducting nonlinear RHA of the symmetric-plan building described in Section 6.4 subjected to each of the 28 unscaled ground motions, and computing the median value of the data set. Figure 6.14 shows the benchmark values of roof displacements and story drifts in *y*-direction associated with the *b*-component of ground motion. Responses to individual ground motions are also included to demonstrate their large dispersion; roof displacements vary from 0.3% to 2.1% of the building height, and second-story drift ratios range from 0.6% to 3.7%. The median roof displacement is 17.3 in. (1.15% of the building height), and the height-wise largest median story drift ratio is 1.7%.

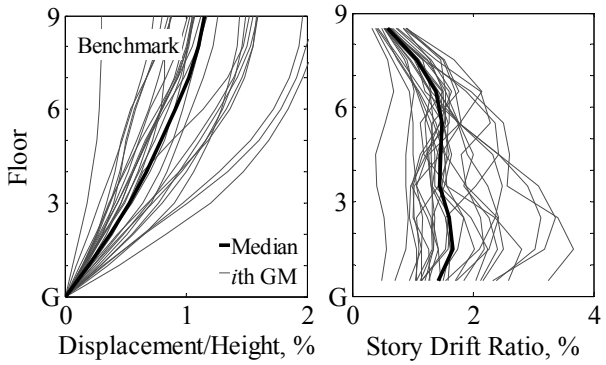

Figure 6.14 Median values of EDPs determined by nonlinear RHA of the building subjected to one component of 28 unscaled ground motions; results for individual ground motions are also included.

6.5.2 Evaluation of One-mode MPS Procedure

Figure 6.15a shows the force-deformation curve for the first-"mode" inelastic SDF system (Step 5 of the procedure) and its tri-linear idealization, wherein the peak values of inelastic deformations due to each of the 28 unscaled ground motions are identified together with their median value, which defines the target deformation required in the scaling procedure. Most ground motions drive the building well into the nonlinear range, and the median deformation exceeds the yield deformation by a factor of 3.1. Recall that the recorded ground motions were amplified by a factor of 3.0, and the resulting ground motions are treated as "unscaled" motions.

The MPS scaling procedure presented in Section 6.1 is implemented for the symmetric-plan building described in Section 6.4 subjected to the *b*-component of ground motion (Table 6.1) applied in the *y*-direction (Fig. 6.7b). Steps 7 to 9 of the MPS procedure were implemented using a numerical method to solve the nonlinear equation (6.3) with the tolerance ε_{MPS} set equal to 10^{-6}. The resulting scaling factors for the 28 ground motions, shown in Fig. 6.16, range from 0.4 to 3.2; the peak deformation of the first-"mode" inelastic SDF system due to each scaled ground motion is identical to the target deformation, as shown in Fig. 6.15b.

Figure 6.17 shows the median values of floor displacements and story drifts in the *y*-direction due to sets 1 and 2 of seven ground motions[†] scaled by the factors in Fig. 6.16, with the benchmark responses presented in Fig. 6.14. Also included are the responses due

[†] Set 1 includes records 7, 8, 11, 17, 20, 25, and 28 (Table 6.1). Set 2 include records 6, 13, 16, 18, 19, 21, and 27.

to each of the scaled ground motions to show that dispersion of the responses to scaled ground motions is much smaller than to unscaled excitations (Fig. 6.14). It is apparent that the MPS procedure provides good estimates of the *y*-component floor displacements and story drifts; in particular, the median roof displacement is overestimated by less than 14% and 0.1% by the scaled ground motions in sets 1 and 2, respectively; and the story drift ratios in the lower and intermediate stories are overestimated by less than 18% for set 1 and underestimated by less than 17% for set 2. However, larger discrepancies are noted for drifts in the upper stories, where the discrepancy is as much as 34% and 28% for sets 1 and 2, respectively, indicating that neither set includes the most appropriate records for this building; which is to be expected because these sets were chosen to provide the most severe test of the MPS procedure. The most appropriate records for this building will be identified in Section 6.5.4 after considering higher modes effects.

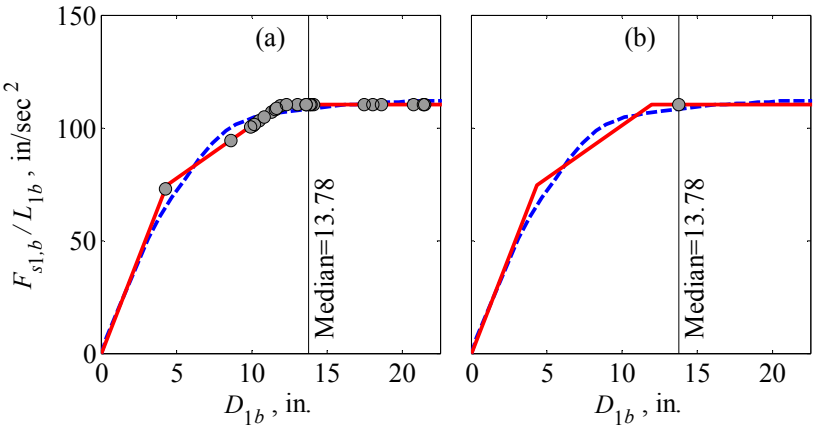

Figure 6.15: Force-deformation curve for the first "mode" inelastic SDF system and its tri-linear idealization. Peak deformations due to (a) unscaled and (b) scaled ground motions are identified.

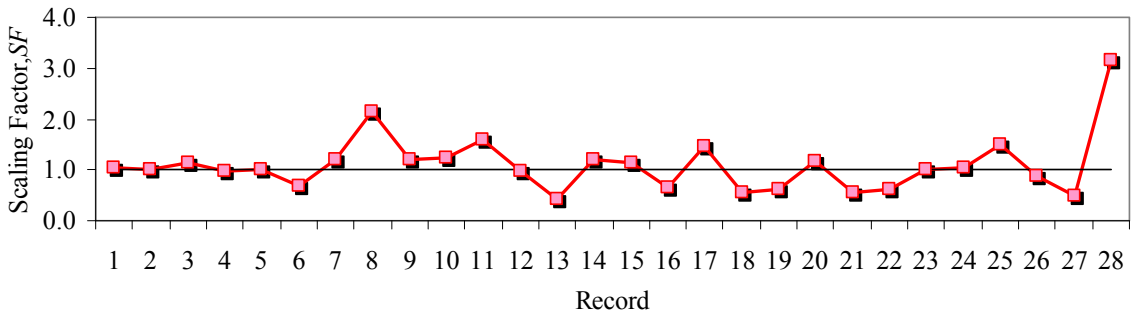

Figure 6.16 Scaling factors determined by the MPS procedure for the records of Table 6.1.

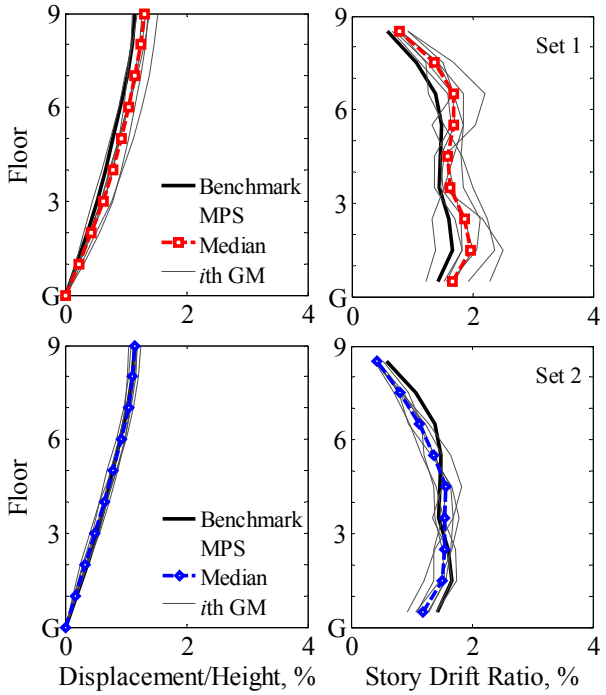

Figure 6.17 Comparison of median EDPs for ground motion sets 1 and 2 scaled according to one-mode MPS procedure with benchmark EDPs; individual results for the seven scaled ground motions are also presented.

Figure 6.18 shows the dispersion for the *y*-component of floor displacements and story drifts due to sets 1 and 2 scaled according to the MPS procedure, and compares them with the dispersion of the benchmark responses. The MPS method significantly reduces dispersion of the EDPs; for example, dispersion is reduced from 0.39 to 0.10 for roof displacement and from 0.44 to 0.18 for drift in the third story.

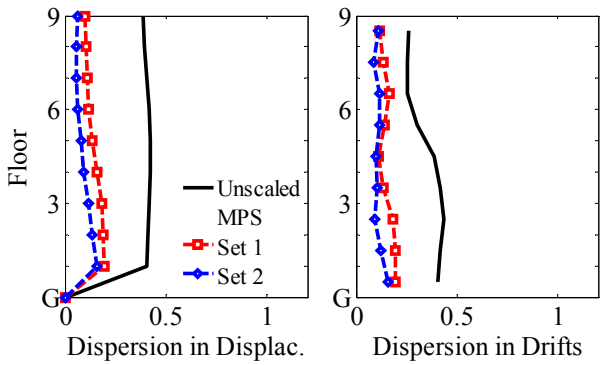

Figure 6.18 Dispersion of EDPs for ground motion sets 1 and 2 scaled according to the MPS procedure and dispersion of EDPs due to 28 unscaled ground motions.

6.5.3 Comparative Evaluation of MPS and ASCE7 Scaling Procedures

The ASCE7 scaling procedure presented in Section 6.2.1 is implemented for the symmetric-plan building described in Section 6.4 subjected to the *b*-component of ground motion (Table 6.1) applied in the *y*-direction (Fig. 6.7b). Figure 6.19 presents the median values of the *y*-component of floor displacements and story drifts due to sets 1 and 2 scaled according to the ASCE7 procedure, and compares them with the benchmark values presented in Fig. 6.14. Also included are the responses due to each of the scaled ground motions to show dispersion of the responses.

It is obvious by comparing Figs. 6.17 and 6.19 that the MPS procedure provides much superior estimates of the EDPs compared to the ASCE7 method. The latter method overestimates floor displacements and story drifts considerably, exceeding 100% in case of set 2. Figure 6.20 compares the dispersion for the *y*-component of floor displacements and story drifts associated with sets 1 and 2 scaled according to the ASCE7 scaling procedures with the dispersion values of the benchmark responses. Dispersion in the ASCE7 method for floor displacements due to set 1 is unacceptably large, exceeding even the dispersion of the benchmark responses. It is evident by comparing Figs. 6.18

and 6.20 that the MPS scaling method leads to much smaller dispersion values than the ASCE7 procedure.

The MPS scaling procedure provides good estimates of the median values of EDPs for the building considered subjected to one component of ground motion, and reduces their dispersion, whereas the ASCE7 scaling procedure grossly overestimates the median EDPs with unacceptably large dispersion. This conclusion provides yet another example building in addition to the five buildings previously considered [Kalkan and Chopra, 2009 and 2010], for which the MPS procedure is much superior than the ASCE7 scaling method.

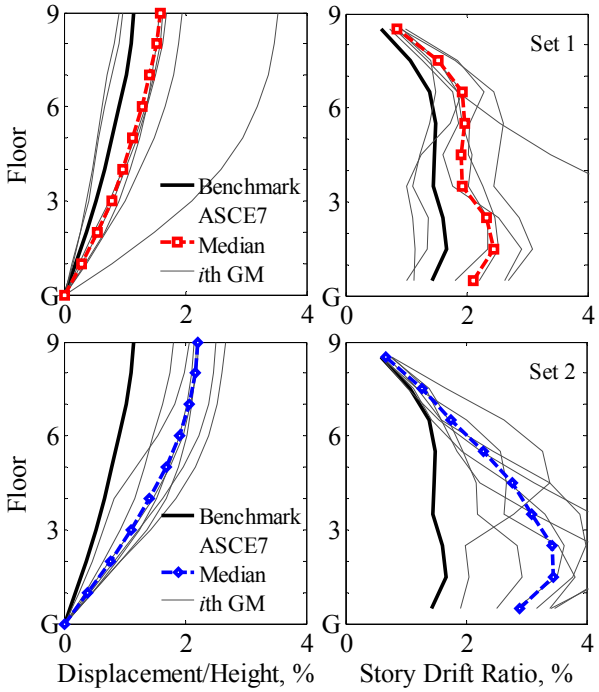

Figure 6.19 Comparison of median EDPs for ground motion sets 1 and 2 scaled according to ASCE7 procedure with benchmark EDPs; individual results for the seven scaled ground motions are included.

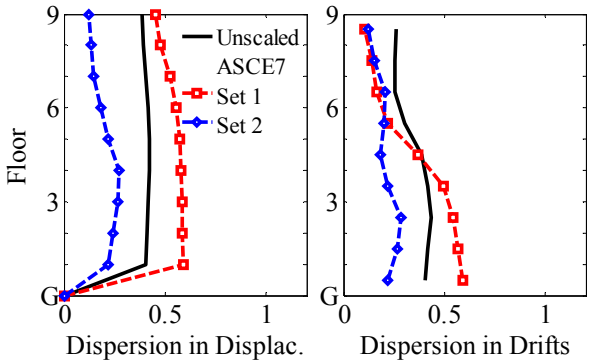

Figure 6.20 Dispersion of EDPs for ground motion sets 1 and 2 scaled according to the ASCE7 procedure and dispersion of EDPs due to 28 unscaled ground motions..

6.5.4 Higher Mode Considerations

The 28 records scaled based only on the first-mode response (scaling factors were presented in Fig. 6.16) are ranked by considering their accuracy in estimating the second mode response (Steps 10 to 13 of the MPS procedure). Among the 14 records in sets 1 and 2, the 7 records with the highest rank (according to Step 12) were defined as ground motion set 3.

Considering the second mode in selecting the ground motions in the MPS method provides accurate estimates of the median EDPs and reduces the record-to-record variability (compared to the results associated with ground motion sets 1 and 2). This improvement in accuracy and efficiency is demonstrated in Figs. 6.21 and 6.22 where the median and dispersion values of the *y*-component of floor displacements and story drifts due to set 3 are shown together with the benchmark values. It is evident by comparing Figs. 6.21-6.22 with 6.17-6.18 that this new set leads to significantly reduced dispersion and much more accurate estimates of median demands compared to sets 1 and 2; the discrepancy in drift ratios in the lower and intermediate stories is reduced from 18% (set 1) to less than 5%; the error in story drifts in the upper stories is reduced from 34% (set

1) to less than 10%. Thus, the MPS method considering higher mode contributions to response provides a set of scaled records that provide highly accurate estimates of EDPs, which are even more superior to the ASCE7 procedure than it was possible with ground motion sets 1 and 2 where higher modes were not considered.

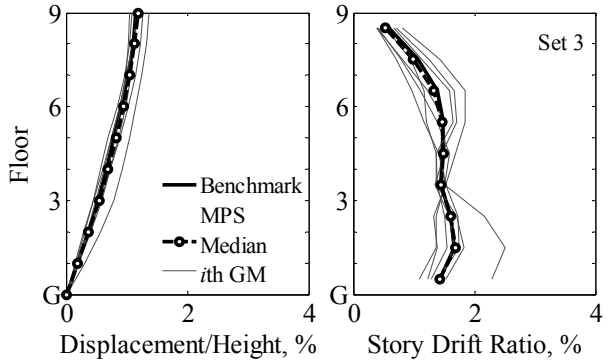

Figure 6.21 Comparison of median EDPs for ground motion set 3 scaled by the MPS procedure (considering higher modes) with benchmark EDPs; individual results for the seven scaled ground motions are also presented.

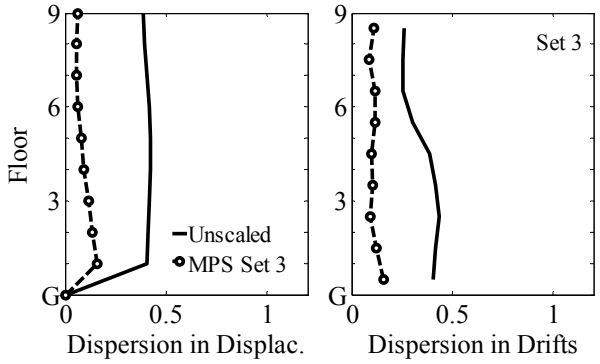

Figure 6.22 Comparison of dispersion of EDPs due to ground motion set 3 scaled by the MPS procedure (considering higher modes) against dispersion of 28 unscaled records.

6.6 Evaluating Scaling Procedures: Symmetric-Plan Building Subjected to Two Components of Ground Motion

6.6.1 Benchmark Responses

Benchmark values of the EDPs were determined by conducting nonlinear RHA of the symmetric-plan building described in Section 6.4 subjected simultaneously to both horizontal components of the 28 unscaled ground motions, and computing the median value of the data set. Figure 6.23 shows the benchmark values of roof displacements and story drifts in x and y directions. Responses to individual ground motions are also included to demonstrate their large dispersion; roof displacements vary from 0.4% to 1.7% of building height in the x-direction and from 0.3% to 2.0% in the y-direction; second-story drift ratios range from 0.7% to 3.6% and from 0.6% to 3.3% in the x and y directions, respectively. Although the building is now subjected to both components of ground motion, simultaneously, median responses for floor displacements and story drifts in y-direction are similar to those shown in Fig. 6.14 due to one component of ground motion, which seems intuitively reasonable for symmetric-plan buildings. Maximum story drifts in x-direction are concentrated at the bottom stories, whereas story drifts in y-direction, which has the shorter bay widths (Fig. 6.7b), tend to be more uniformly distributed over the height of the building.

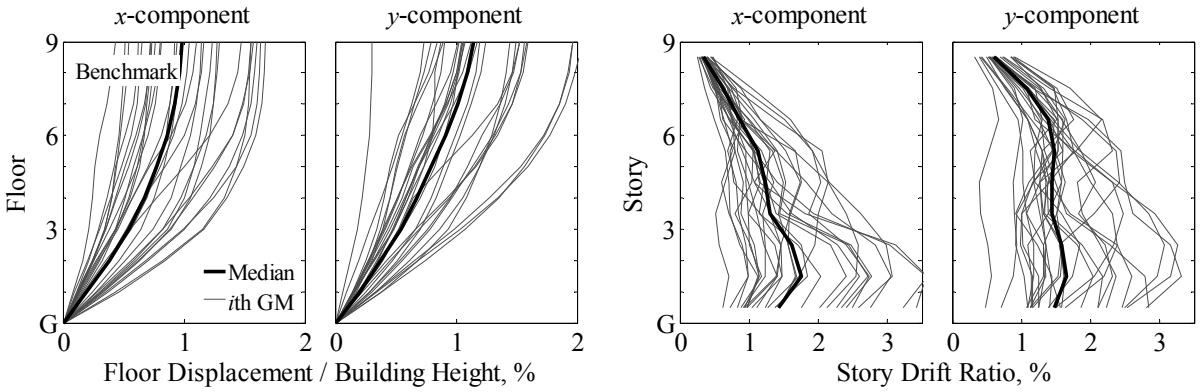

Figure 6.23 Median values of EDPs determined by nonlinear RHA of the building subjected to two components, simultaneously, of 28 unscaled records; individual results for the 28 excitations are included.

6.6.2 One-Mode MPS Procedure: Same Scaling Factors

For each lateral direction, Fig. 6.24 shows the force-deformation curve for the first-"mode" inelastic SDF system (Step 5 of the procedure) and its trilinear idealization, wherein the peak values of inelastic deformation due to each of the unscaled 28 ground motions are identified together with the median value, which defines the target deformation required in the scaling procedure. Most ground motions drive the building well into the nonlinear range; the median deformation exceeds the yield deformation by a factor of 3.5 and 3.1 in the *a* and *b* directions of ground motion, respectively.

The MPS scaling procedure using a single scaling factor for both components of ground motion, i.e., $SF_a = SF_b$, presented in Section 6.1.2 is implemented for the symmetric-plan building described in Section 6.4 subjected to both components of motion, simultaneously. Steps 7 to 9 of the MPS procedure were implemented using a numerical method to solve the nonlinear equation (6.6) with the tolerance ε_{MPS} set equal to 10^{-6}, resulting in the scaling factors shown in Fig. 6.25; they range from 0.6 to 2.5. Scaling both components of ground motions by the same scaling factor does not ensure

that the peak deformations of the first-"mode" inelastic SDF systems to each scaled ground motion matches the target value, as demonstrated in Fig. 6.26, where peak values of inelastic deformation due to each of the scaled ground motions are identified. In contrast, each scaled one-component ground motion provided the target value (Fig. 6.15b). Comparing Figs. 6.24 and 6.26 indicates that the dispersion in the peak deformations of the inelastic SDF systems is not reduced significantly.

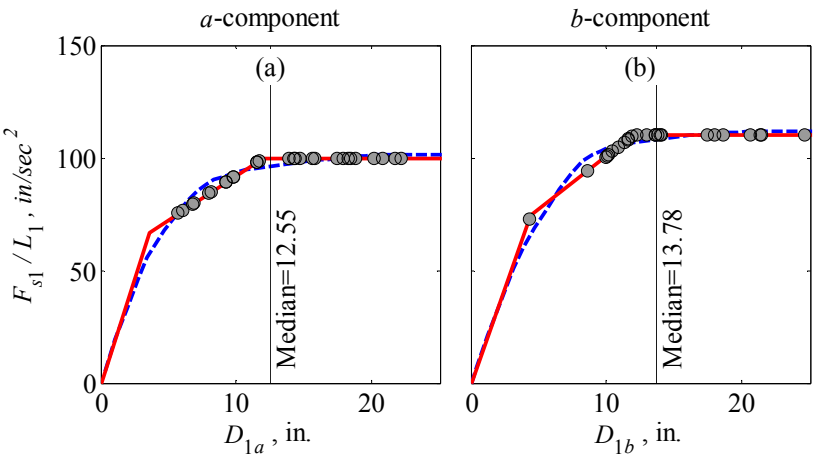

Figure 6.24 Force-deformation curves for the first "modes" of lateral vibration of the building in *a* and *b* directions and their tri-linear idealization. Peak deformations due to 28 unscaled ground motions are identified.

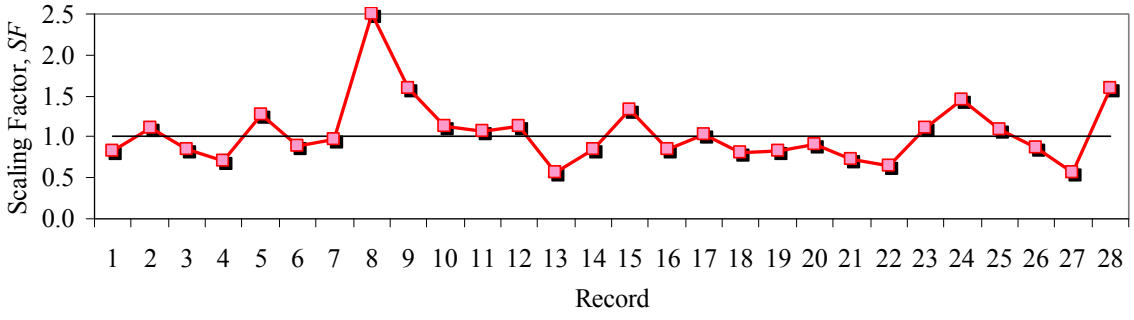

Figure 6.25 Single scaling factor for both components of ground motion determined by the MPS procedure.

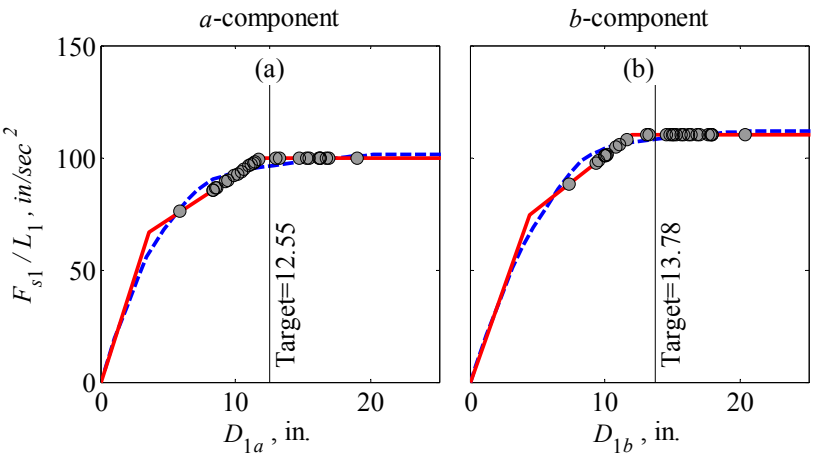

Figure 6.26 Force-deformation curves for the first "modes" of lateral vibration of the building in *a* and *b* directions and their tri-linear idealization. Peak deformations due to 28 ground motions scaled by the one-mode MPS procedure with the same scaling factor for both components are identified.

If the intensities of the two horizontal components of ground motion are considerably different, perhaps no scaling procedure with a single scaling factor for both components can lead to accurate values of EDPs in both *x* and *y* directions, simultaneously. This is demonstrated in Fig. 6.27 where the values of EDPs due to ground motion number 28 (Table 6.1) scaled according to the MPS scaling procedure are shown together with the benchmark EDPs. This scaled ground motion overestimates EDPs in the *x*-direction, but underestimates them in the *y*-direction. Thus, no single scaling factor would lead to accurate values of EDPs in both *x* and *y* directions, simultaneously.

The MPS procedure using a single scaling factor for both components of ground motion leads to inaccurate estimates of the median EDPs accompanied by large record-to-record variability of the responses. This is demonstrated in Fig. 6.28 where the median values of EDPs due to the seven scaled ground motions of earlier sets 1 and 2 are shown together with the benchmark EDPs; also included are the EDPs due to each of the seven

scaled ground motions to show the dispersion of the EDP values due to individual ground motions. The height-wise maximum discrepancy is 34% and 37% in the x and y components of the responses, respectively. The inefficiency of the procedure is demonstrated in Fig. 6.29 that shows the large dispersion of the EDP values due to the seven scaled records, especially in the y-direction where it is almost as large as it was for the unscaled ground motions.

Based on these results, we conclude that, in general, it may not be possible to achieve accurate estimates of EDPs if both horizontal components of ground motion are to be scaled by the same factor. This difficulty could possibly be overcome by selecting only those ground motions that satisfy the requirement that both components lead to a peak deformation of the first-"mode" inelastic SDF system that is close to the target deformation—within certain tolerance. However, such restrictions will reduce the number of available ground motions, in particular, eliminate near fault ground motions because their fault-normal and fault-parallel components are very different due to directivity effects and fling. Furthermore, such restrictions may not be practical if the target deformations in the two directions are very different (e.g., because the lateral-force-resisting systems are different). To overcome these restrictions, we may consider two different scaling factors for the two components of ground motion. Seismologists may consider this liberal approach to be unacceptable because it does not preserve focal mechanism and wave travel path effects, inherent in recorded motions. However, we believe that it can be justified because the goal of any scaling procedure is to estimate the EDPs accurately, where the benchmark values are determined from a large set of unscaled records, which obviously preserve all the seismological features.

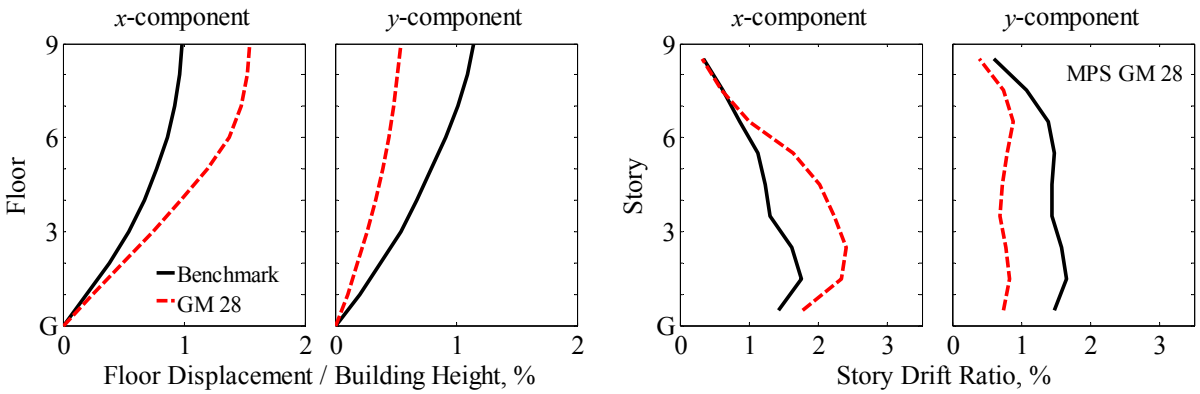

Figure 6.27 Comparison of EDPs due to GM 28 (Table 6.1) scaled by the one-mode MPS procedure with the same scaling factor for both components of ground motion against benchmark values.

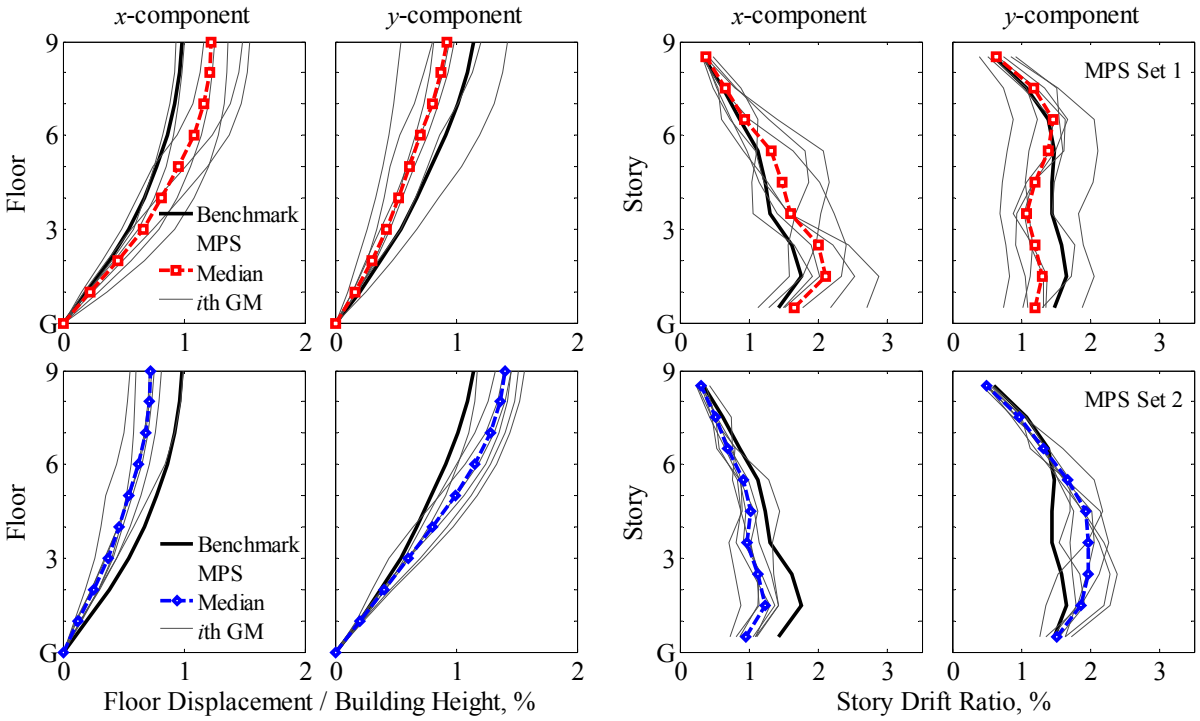

Figure 6.28 Median values of EDPs due to ground motion sets 1 and 2 scaled by the one mode MPS procedure with the same scaling factor for both components of ground motion and the benchmark values of EDPs.

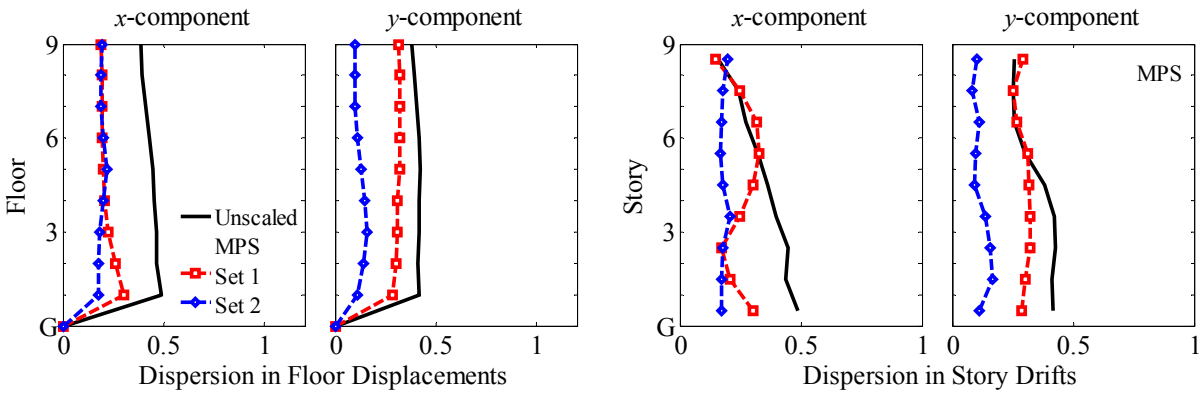

Figure 6.29 Dispersion of EDPs due to ground motion sets 1 and 2 scaled according to the one-mode MPS procedure with the same scaling factor for both components of ground motion and dispersion of EDPs due to unscaled records.

6.6.3 One-Mode MPS Procedure: Different Scaling Factors

For each component of ground motion, Fig. 6.30 shows the force-deformation curve for the first-"mode" inelastic SDF system (Step 5 of the procedure) and its trilinear idealization, wherein the peak values of inelastic deformation due to each of the unscaled 28 ground motions are identified together with the median value, which defines the target deformation required in the scaling procedure.

The MPS scaling procedure allowing for different scaling factors for the *a* and *b* components of ground motion, i.e., $SF_a \neq SF_b$, presented in Section 6.1.1 is implemented for the symmetric-plan building described in Section 6.4 subjected to both components of motion, simultaneously. Steps 7 to 9 of the MPS procedure were implemented using a numerical method to solve the nonlinear equation (6.3) with the tolerance ε sets equal to 10^{-6}. The resulting scaling factors for each horizontal component of ground motion, shown in Fig. 6.31; range from 0.5 to 2.7 and from 0.4 to 3.2 for the *a* and *b* components, respectively. The scaling procedure is effective in the sense that the peak deformation of the first-"mode" inelastic SDF system due to each scaled ground motion is identical to the target deformation, as shown in Fig. 6.32.

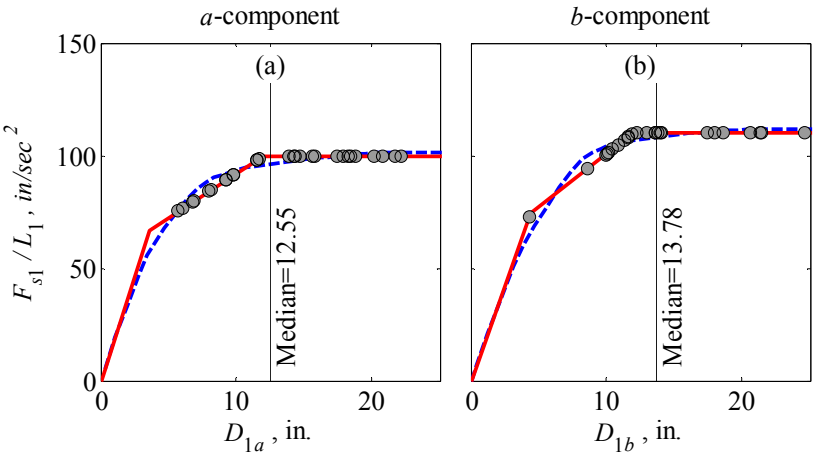

Figure 6.30 Force-deformation curves for the first "modes" of lateral vibration of the building in *a* and *b* directions and their tri-linear idealization. Peak deformations due to 28 unscaled ground motions are identified.

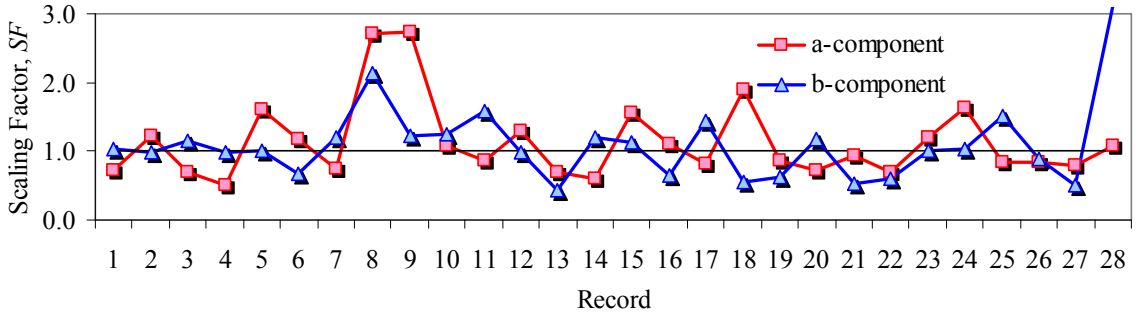

Figure 6.31 Scaling factors for the two components of ground motion scaled by the one-mode MPS procedure.

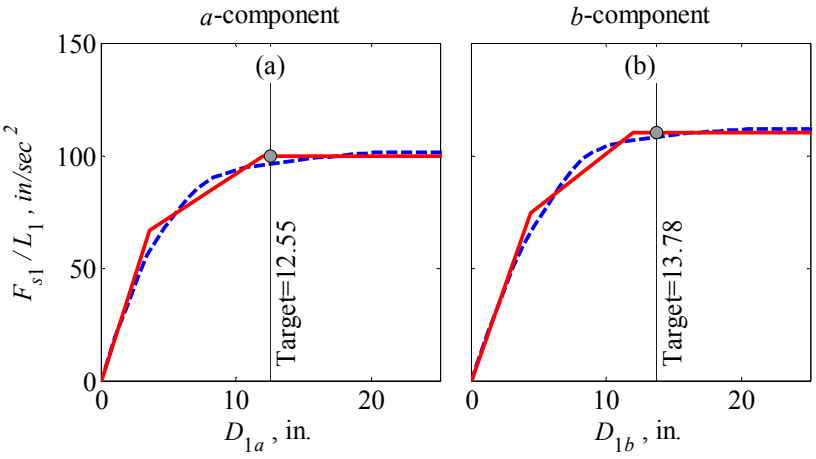

Figure 6.32 Force-deformation curves for the first "modes" of lateral vibration of the building in *a* and *b* directions and their tri-linear idealization. Peak deformations due to 28 ground motions scaled by the one-mode MPS procedure are identified.

The MPS procedure for scaling two components of ground motion provides an accurate estimate of the median EDPs and reduces the record-to-record variability of the responses. This is demonstrated in Fig. 6.33 where the median values of EDPs due to the seven scaled ground motions of sets 1 and 2 (ground motions in these sets are as before) are shown together with the benchmark EDPs; also included are the EDPs due to each of the seven scaled ground motions to show the dispersion of the EDP values. It is apparent that the median values of EDPs are close to the benchmark results determined for a set of 28 unscaled ground motions in Fig. 6.23. Although the height-wise maximum discrepancy in the *x*-component of floor displacements and story drifts is less than 10% and the discrepancy in the *y*-component of story drifts in the upper stories reaches 30%, the discrepancies in most floors and stories is much smaller. This discrepancy will be greatly reduced when response in the second "mode" of vibration is considered in ranking and selecting ground motions (Section 6.6.5).

The efficiency achieved by the MPS procedure is evaluated in Fig. 6.34, wherein the dispersion of the EDPs due to scaled ground motions is compared with the dispersion of the responses to unscaled ground motions. It is apparent that the dispersion in the EDP values due to the seven scaled records around the median value is much smaller; in particular, dispersion is reduced from 0.39 to 0.12 and from 0.49 to 0.26 for the *x*-component of roof displacement and first-story drift. However, this reduction is less for EDPs in the upper floors, indicating that higher-mode contributions to structural response should also be considered in selecting the most appropriate scaled ground motions.

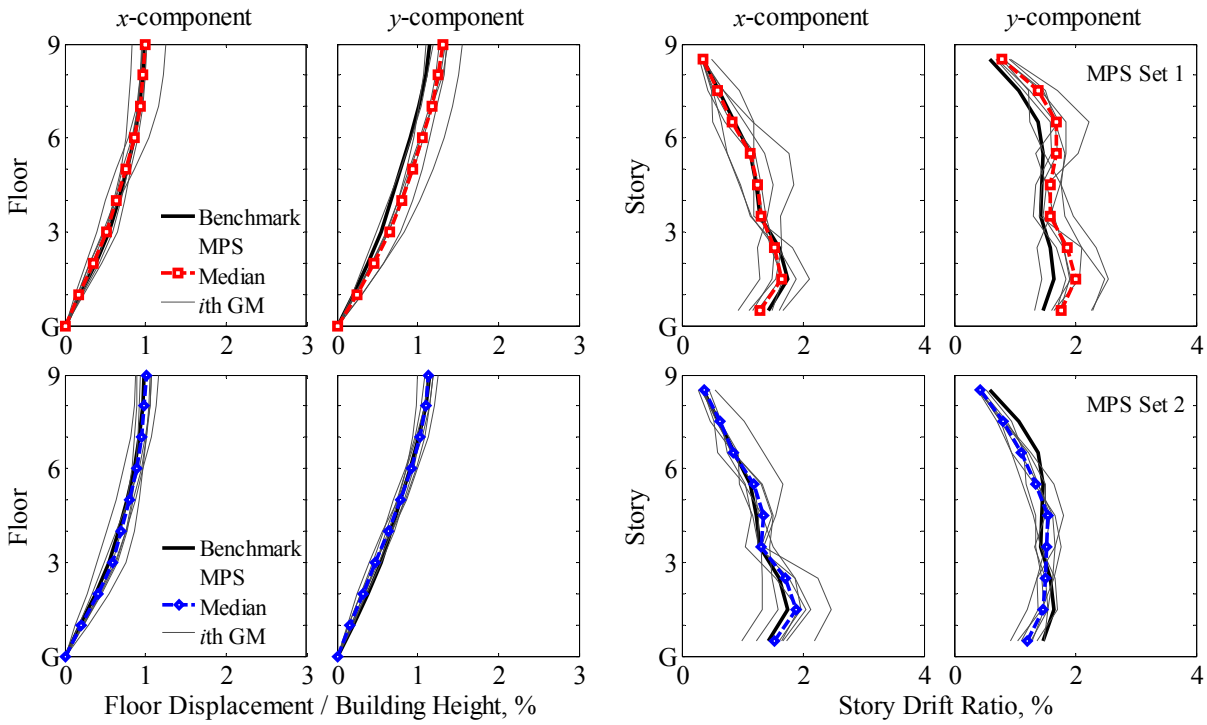

Figure 6.33 Comparison of EDPs due to ground motion sets 1 and 2 scaled according to the one-mode MPS procedure and the benchmark EDPs; individual results for seven scaled ground motions are included.

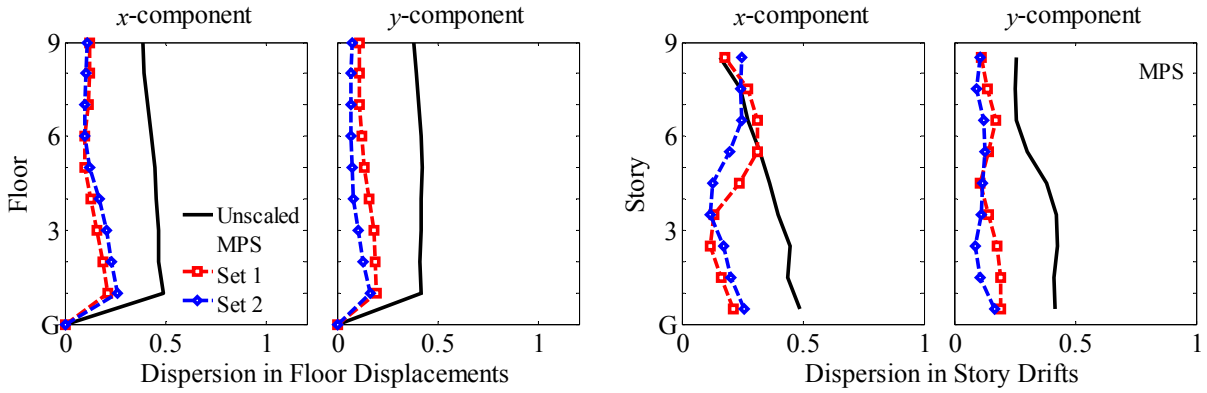

Figure 6.34 Dispersion of EDPs due to ground motion sets 1 and 2 scaled according to the one-mode MPS procedure and dispersion of EDPs due to unscaled records.

6.6.4 Comparative Evaluation of MPS and ASCE7 Scaling Procedures

The ASCE7 scaling procedure presented in Section 6.2.2 is implemented for the symmetric-plan building described in Section 6.4 subjected to both horizontal components of ground motion, simultaneously. Figures 6.35 and 6.36 show the median values of EDPs and the dispersion of the EDPs due to ground motion sets 1 and 2 scaled according to the ASCE7 procedure and compares them with the benchmark values presented in Fig. 6.23. These results together with the previous results for the one-mode-based MPS procedure demonstrate that the MPS procedure is much superior compared to the ASCE7 procedure for scaling ground motions. This superiority is evident in two respects. First, for each ground motion set, the ground motions scaled according to the MPS procedure provide median values of EDPs that are much closer to the benchmark values than is achieved by the ASCE7 procedure. The discrepancy of 36% (set 2) in roof displacements determined by scaling records according to the ASCE7 procedure is reduced to 14% when records are scaled by the MPS procedure; likewise, the error in drift ratios in the lower and intermediate stories is reduced from 53% (set 2) to less than 20%. Second, the dispersion in the EDPs due to the seven scaled records (or record-to-record variability) around the median value is much smaller when the records are scaled by the MPS procedure compared to the ASCE7 scaling procedure; for example, dispersion is reduced from 0.43 (set 1) to 0.12 for roof displacement and from 0.61 (set 1) to 0.21 for drift in the first story. However, the reduction in dispersion achieved by the MPS procedure in the drifts in the higher stories is less significant, suggesting that higher-mode responses should also be considered in identifying the “best” scaled records.

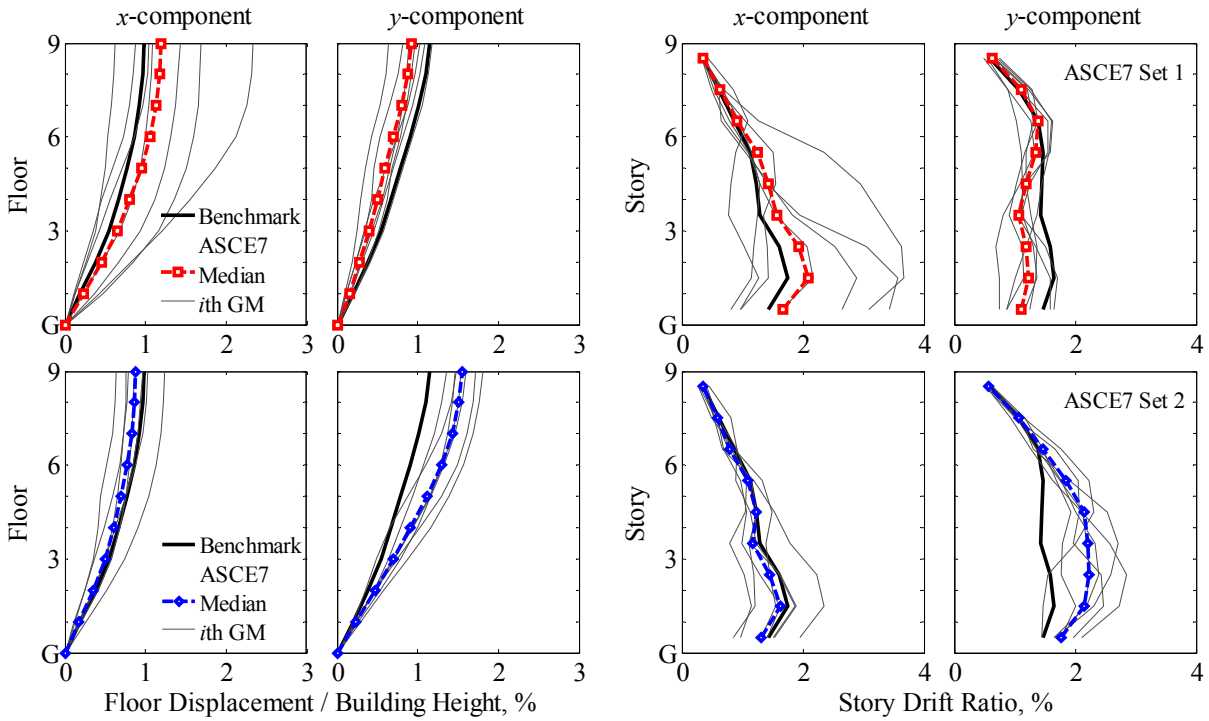

Figure 6.35 Comparison of EDPs due to ground motion sets 1 and 2 scaled by the ASCE7 procedure against benchmark values; individual results for seven scaled ground motions are included.

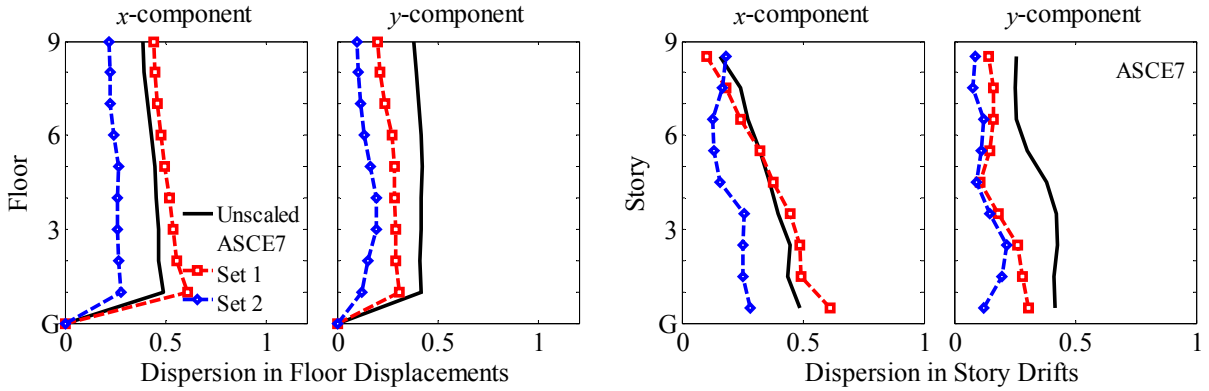

Figure 6.36 Dispersion of EDPs due to ground motion sets 1 and 2 scaled by the ASCE7 procedure and dispersion of EDPs due to 28 unscaled records.

6.6.5 Higher Mode Considerations

The 28 records scaled based only on the first-mode response (scaling factors were presented in Fig. 6.31) are ranked by considering their accuracy in estimating the second mode response (Steps 10 to 13 of the MPS procedure). Among the 14 records in sets 1 and 2, the seven records with the highest rank (according to Step 12) were defined as ground motion set 3.

Considering the second mode in selecting the ground motions in the MPS method provides accurate estimates of the median EDPs and reduces the record-to-record variability (compared to the results associated with ground motion sets 1 and 2). This improvement in accuracy and efficiency is demonstrated in Figs. 6.37 and 6.38 where the median and dispersion values of the *x* and *y* components of floor displacements and story drifts due to set 3 are shown together with the benchmark values. It is evident by comparing Figs. 6.37-6.38 with Figs. 6.33-6.34 that this new set leads to reduced dispersion and much more accurate estimates of median demands compared to sets 1 and 2; the discrepancy in drift ratios in the lower and intermediate stories is reduced from 20% (set 1) to less than 5%; the error in story drifts in the upper stories is reduced from more than 30% (set 1) to less than 10%. Thus, the MPS method considering higher mode contributions to response provides a set of scaled records that provide highly accurate estimates of EDPs, which are even more superior to the ASCE7 procedure than it was possible with ground motion sets 1 and 2 where higher modes were not considered.

Comparing Figs. 6.37-6.38 with Figs. 6.21-6.22, it is clear that the accuracy and efficiency of the MPS procedure does not degrade when the building is subjected simultaneously to both components of ground motion.

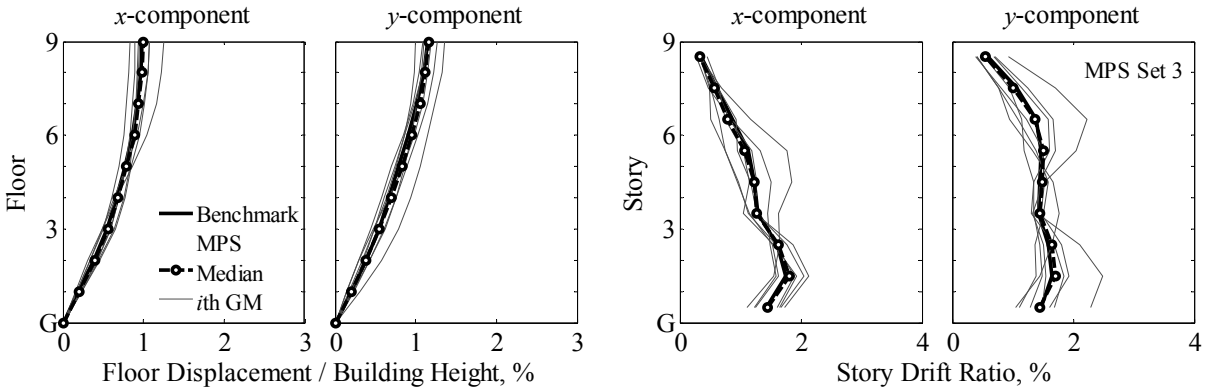

Figure 6.37 Comparison of median EDPs for ground motion set 3 scaled by the MPS procedure (considering higher modes) with benchmark EDPs; individual results for the seven scaled ground motions are included.

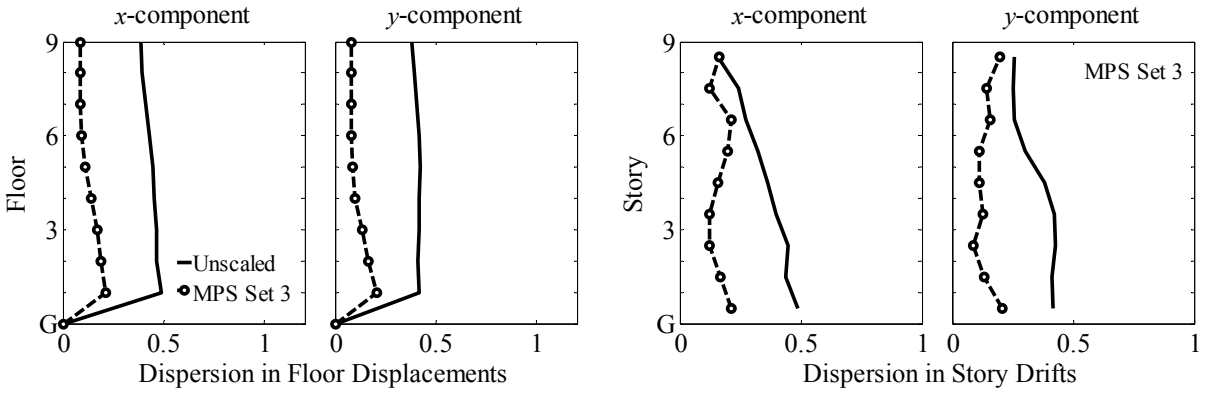

Figure 6.38 Comparison of dispersion of EDPs due to ground motions set 3 scaled by the MPS procedure (considering higher modes) against dispersion of 28 unscaled records.

6.7 Evaluating Scaling Procedures: Unsymmetric-Plan Buildings Subjected to Two Components of Ground Motion

The scaling procedures presented in Sections 6.2.1 and 6.3.2 are implemented for the unsymmetric-plan buildings C09 IBC06 and C09 UBC85 described in Section 5.1 subjected to two horizontal components of ground motion, simultaneously. Figure 6.39 shows the typical floor plans of these buildings, wherein the moment resisting frames are highlighted. Free vibration characteristics of the buildings were presented in Section 5.1.3, and their computer models in Section 5.1.2; in this section, the structural elements are modeled without including strength loss to avoid possible complications associated with local numerical instabilities.

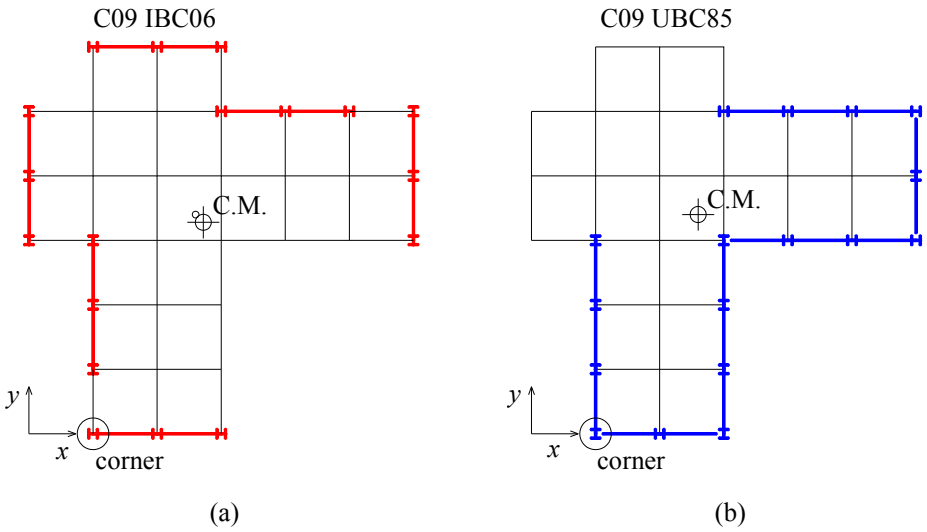

Figure 6.39 Schematic plan view of the (a) C09 IBC06 and (b) C09 UBC85; moment resisting frames are highlighted.

6.7.1 Benchmark Responses

Benchmark values of the EDPs were determined by conducting nonlinear RHA of the buildings subjected simultaneously to both horizontal components of the 28 unscaled ground motions, and computing the median value of the data set. Recall that the ground motions were amplified by a factor of 3.0, and the resulting ground motions are treated as "unscaled" motions for this investigation. Figures 6.40 and 6.41 show the benchmark values of roof displacements and story drifts in x and y directions at the center of mass (C.M.) and at the corner identified in Fig. 6.39, respectively. Responses for individual ground motions are also included to demonstrate their dispersion. Comparing Figs. 6.40-6.41 with Fig. 6.23, it is obvious that the dispersion of the EDPs is much larger for unsymmetric-plan buildings than for symmetric-plan buildings. Although median roof displacement ratios are around 2% of building height and story drift ratios are around 2-3% for both buildings, EDPs due to individual ground motions vary over a wide range, e.g., roof displacement ratios at the C.M. of the C09 IBC06 building ranges from 1% to 4.8% and top-story drift ratios from 1.3% to 6.3%.

6.7.2 Evaluation of One-Mode MPS Procedure

For each component of ground motion, Fig. 6.42 shows the force-deformation curve for the first-"mode" inelastic SDF system (Step 5 of the procedure) and its trilinear idealization, wherein the peak values of inelastic deformation for both buildings due to each of the unscaled 28 ground motions are identified together with the median value. Many of the ground motions drive both building significantly into the nonlinear range. The target deformation is about 1.8 times the yield deformation for both buildings.

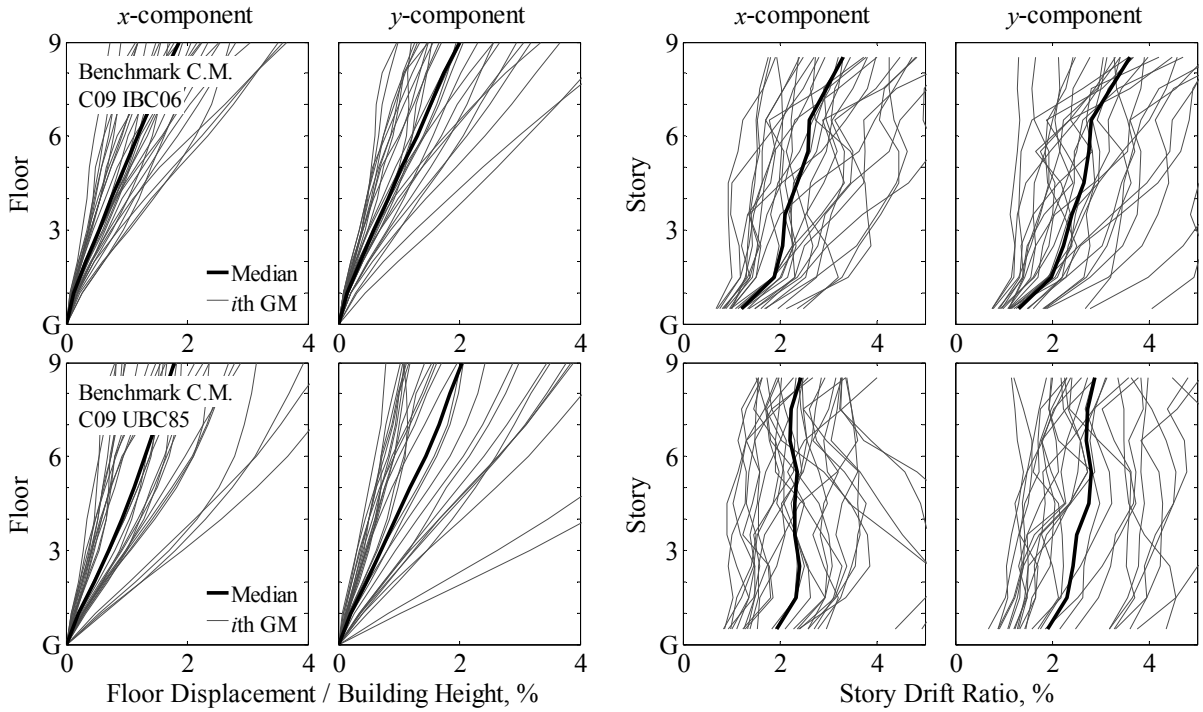

Figure 6.40 Median values of EDPs at the C.M. determined by nonlinear RHA of the C09 IBC06 and UBC85 buildings subjected to two components, simultaneously, of each of the 28 unscaled records; individual results for the 28 excitations are included.

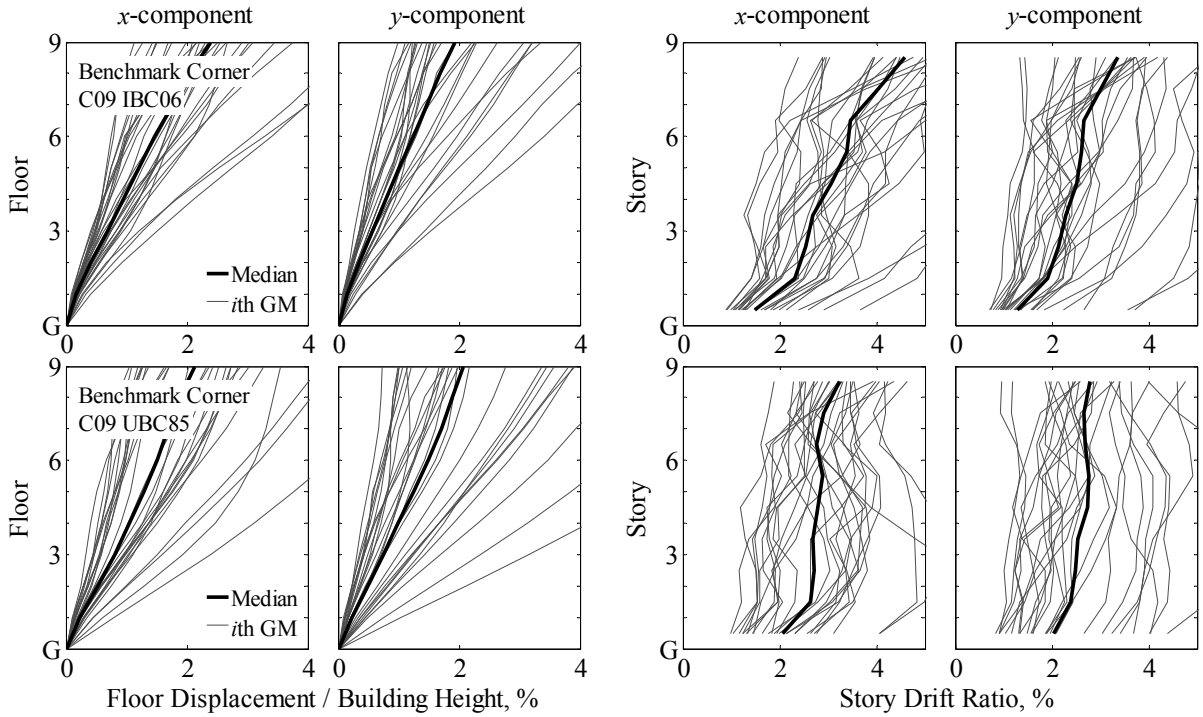

Figure 6.41 Median values of EDPs at the corner determined by nonlinear RHA of the C09 IBC06 and UBC85 buildings subjected to two components, simultaneously, of each of the 28 unscaled records; individual results for the 28 excitations are included.

The MPS scaling procedure allowing for different scaling factors for the a and b components of ground motion, i.e., $SF_a \neq SF_b$, presented in Section 6.1.1 is implemented. Steps 7 to 9 of the MPS procedure were implemented using a numerical method to solve the nonlinear equation (6.3) independently for each component of ground motion with the tolerance ε set equal to 10^{-6}. The resulting scaling factors for each horizontal component of ground motion, shown in Fig. 6.43, range from 0.4 to 2.7 and from 0.3 to 3.1 for the C09 IBC06 and UBC85 buildings, respectively. The scaling procedure is effective in the sense that the peak deformation of the first-"mode" inelastic SDF system due to each scaled ground motion is identical to the target deformation, as demonstrated in Fig. 6.44.

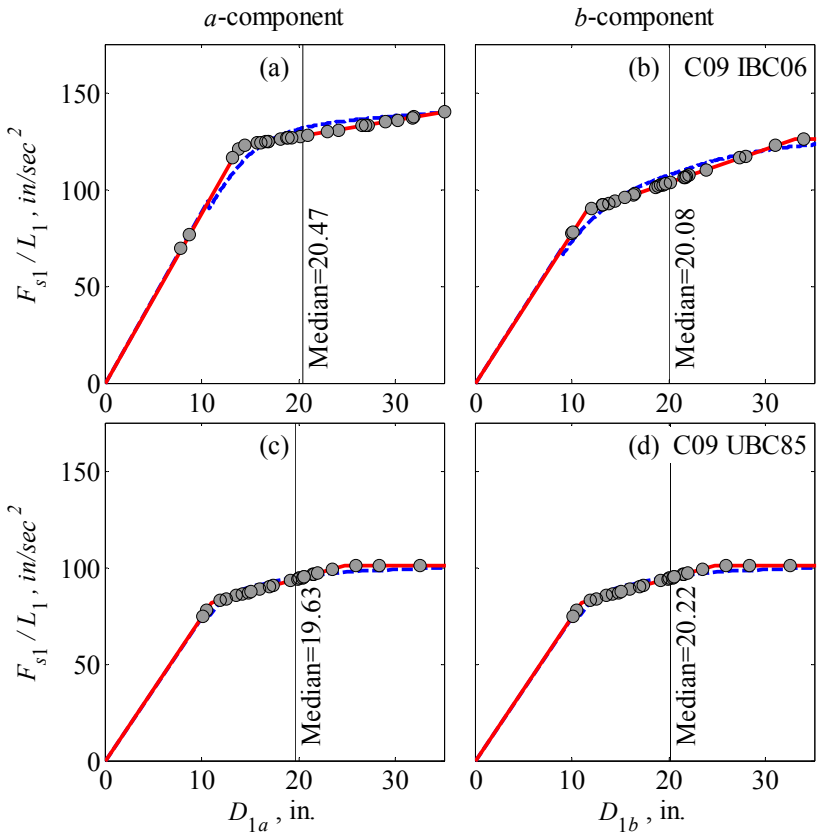

Figure 6.42 Force-deformation curves for the first "modes" of lateral vibration of the C09 IBC06 and UBC85 buildings in a and b directions and their tri-linear idealization. Peak deformations due to 28 unscaled ground motions are identified.

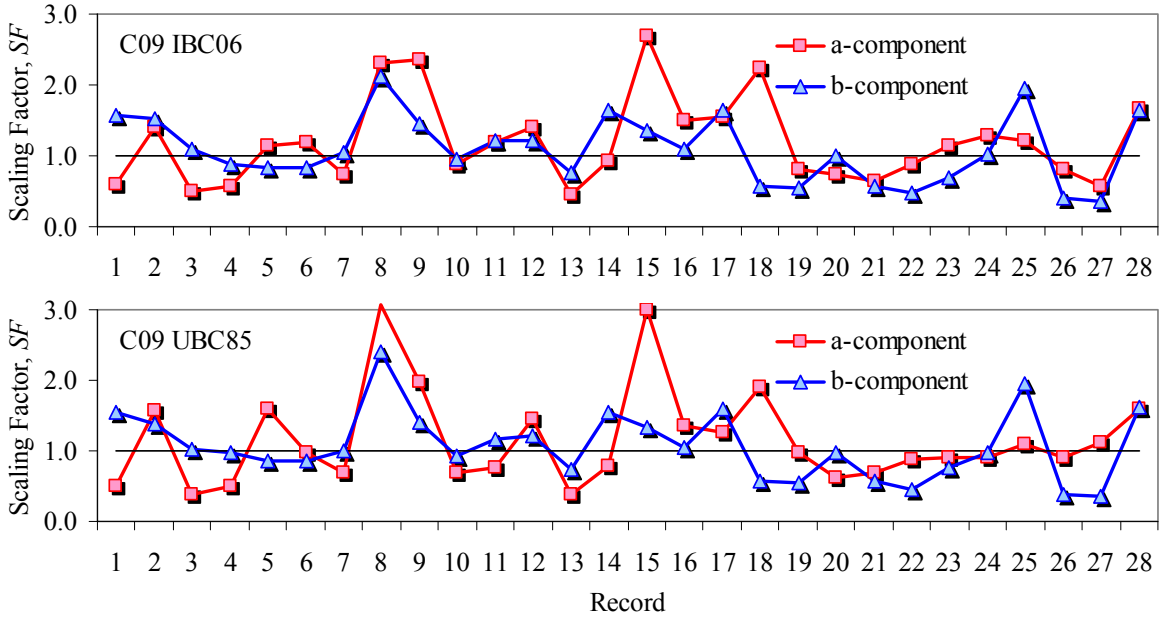

Figure 6.43 Scaling factors for the two components of ground motion scaled by the one-mode MPS procedure: C09 IBC06 and UBC85 buildings.

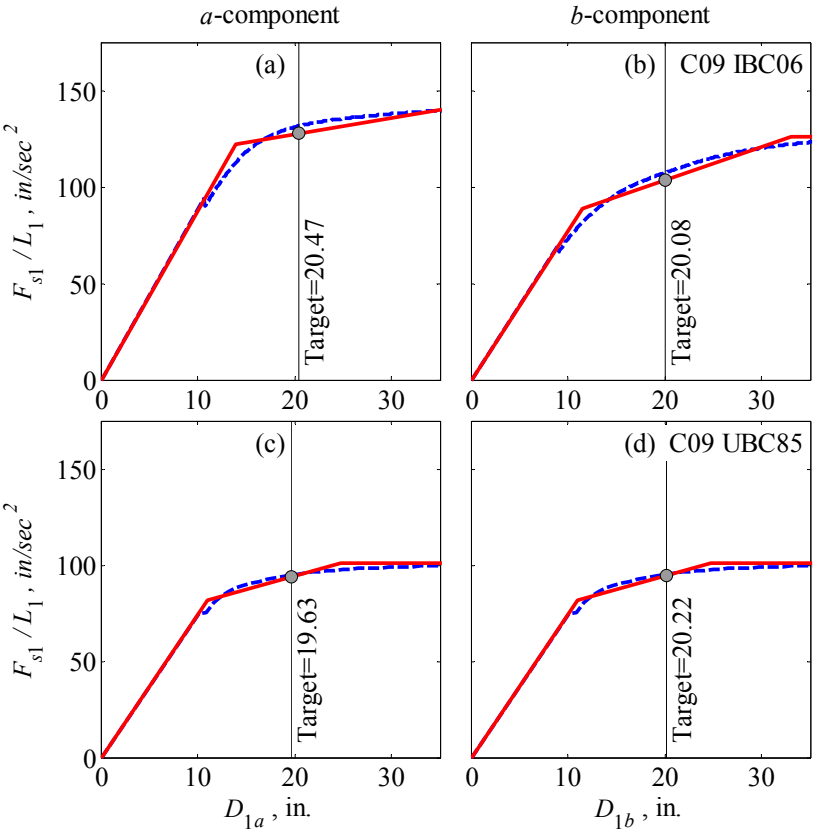

Figure 6.44 Force-deformation curves for the first "modes" of lateral vibration of the C09 IBC06 and UBC85 buildings in *a* and *b* directions and their tri-linear idealization. Peak deformations due to 28 ground motions scaled by the one-mode MPS procedure are identified.

The MPS procedure for the C09 IBC06 building subjected to two components of ground motion provides accurate estimate of the median EDPs and reduces the record-to-record variability. This is demonstrated in Figs. 6.45 and 6.46 where the median values of EDPs determined by nonlinear RHA of the building due to the seven scaled records of sets 1 and 2[†] (see Section 6.3) are shown together with the benchmark EDPs; also included are the EDPs due to each of the seven scaled records to show their dispersion. It is apparent that the median values of EDPs are close to the benchmark results determined for a set of 28 unscaled records in Figs. 6.40 and 6.41. The height-wise maximum discrepancy in floor displacements and story drifts due to record set 2 is less than 15%; the discrepancy in story drifts due to record set 1 is less than 22%, except for the first story. This discrepancy will be significantly reduced when response in the second "mode" of vibration is considered in ranking and selecting ground motions (Section 6.7.4).

The accuracy of the MPS procedure for the C09 UBC85 building is evaluated in Figs. 6.47 and 6.48, where median values of EDPs due to record sets 1 and 2 are shown together with the benchmark EDPs. Comparing Figs. 6.47-6.48 with Figs. 6.45-6.46, it is observed that the accuracy of the MPS procedure deteriorates for this building; the height-wise maximum overestimation in median displacements and story drifts is 24% and 34%, respectively, in case of record set 1, and the underestimation in *x*-component of story drifts exceeds 20% for set 2. Deterioration in the one-mode based MPS procedure is

[†] Set 1 includes records 2, 8, 9, 15, 16, 18, and 28 (Table 6.1) for the C09 IBC06 building, and 2, 5, 8, 9, 15, 18, and 28 for the UBC85 building. Set 2 includes records 1, 3, 7, 13, 19, 20, and 27 for the C09 IBC06 building, and 1, 3, 7, 13, 14, 20, and 21 for the C09 UBC85 building.

not surprising for this torsionally-flexible building with strong coupling between lateral and torsional motions, because the effective mass in the first mode is less than 50% of the total mass (Figs. 5.5 through 5.8), implying that higher mode contributions to the demand are expected to be large. When higher mode responses are considered in ranking and selecting ground motions, the accuracy of the MPS procedure improves (Section 6.7.4).

Efficiency of the MPS procedure for both buildings is evaluated in Figs. 6.49 and 6.50, wherein the dispersion of the EDPs due to seven scaled records is compared with the dispersion of the responses to 28 unscaled ground motions. It is apparent that the dispersion in the EDP values to the seven scaled records around the median value is significantly smaller; for the C09 UBC85 building, dispersion is reduced from 0.61 to 0.27 and from 0.65 to 0.42 for the *y*-direction of roof displacement and first-story drift. However, this reduction is comparatively less for story drifts at the corner of the C09 IBC06 building.

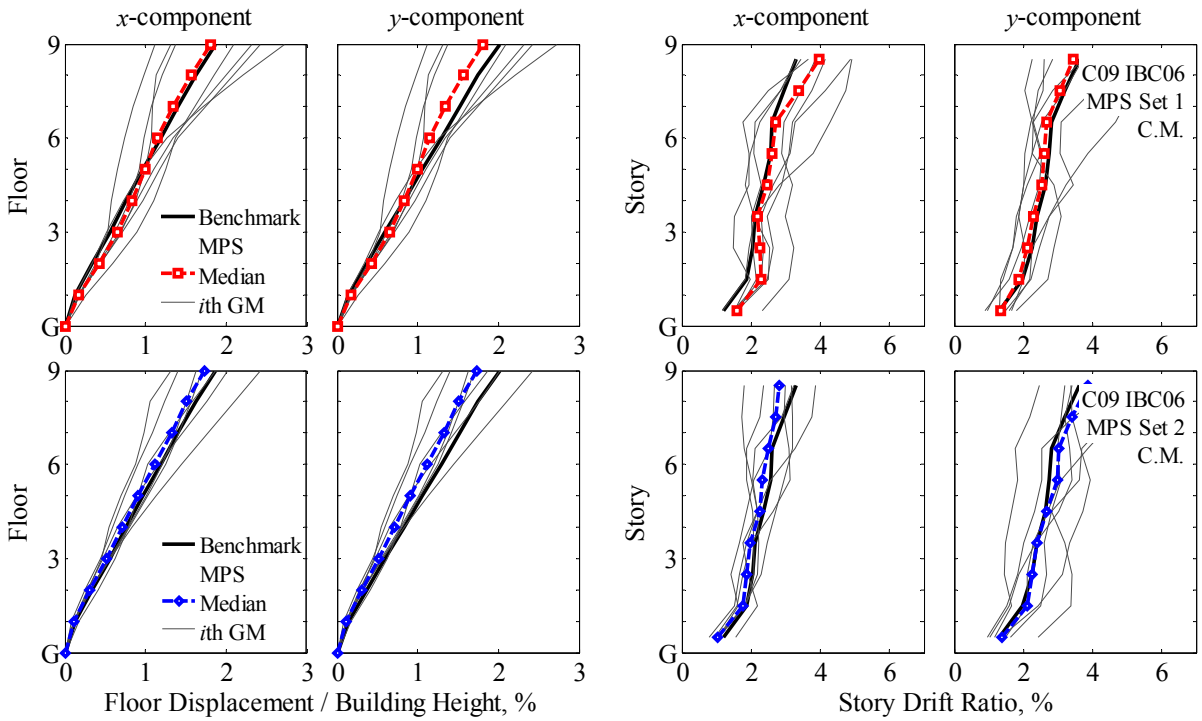

Figure 6.45 Comparison of EDPs at the C.M. for the C09 IBC06 building due to ground motion sets 1 and 2 scaled by the one-mode MPS procedure against benchmark values; individual results for seven scaled ground motions are included.

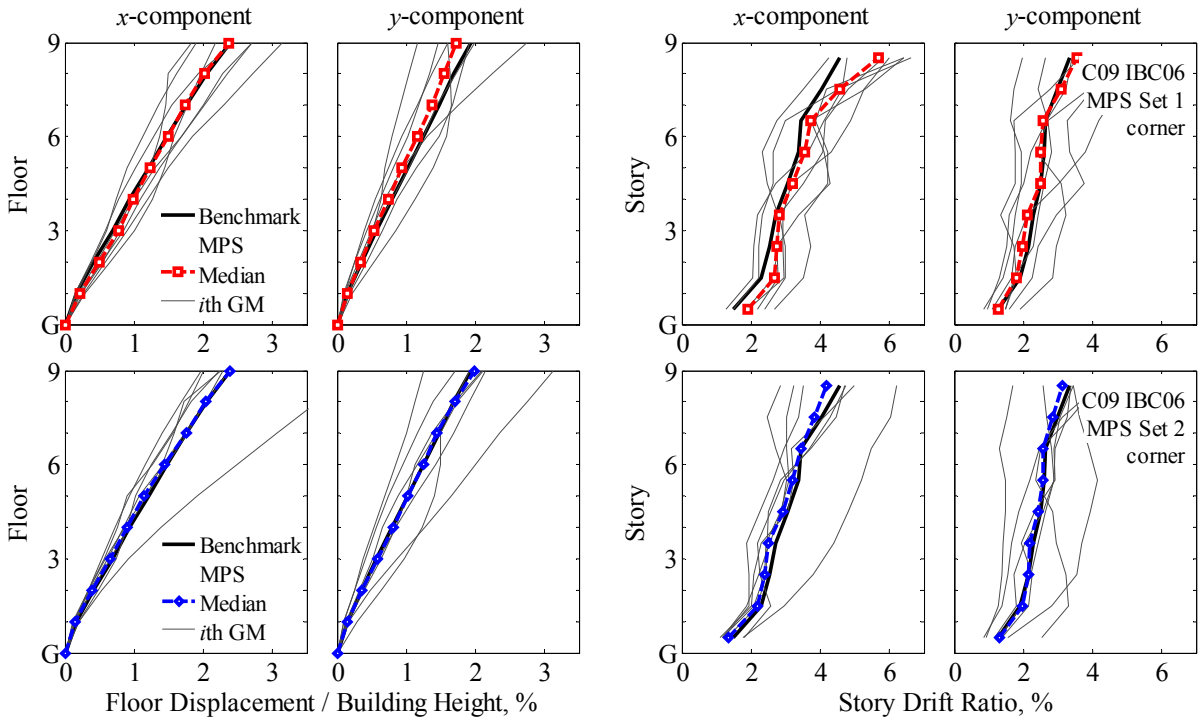

Figure 6.46 Comparison of EDPs at the corner for the C09 IBC06 building due to ground motion sets 1 and 2 scaled by the one-mode MPS procedure against benchmark values; individual results for seven scaled ground motions are included.

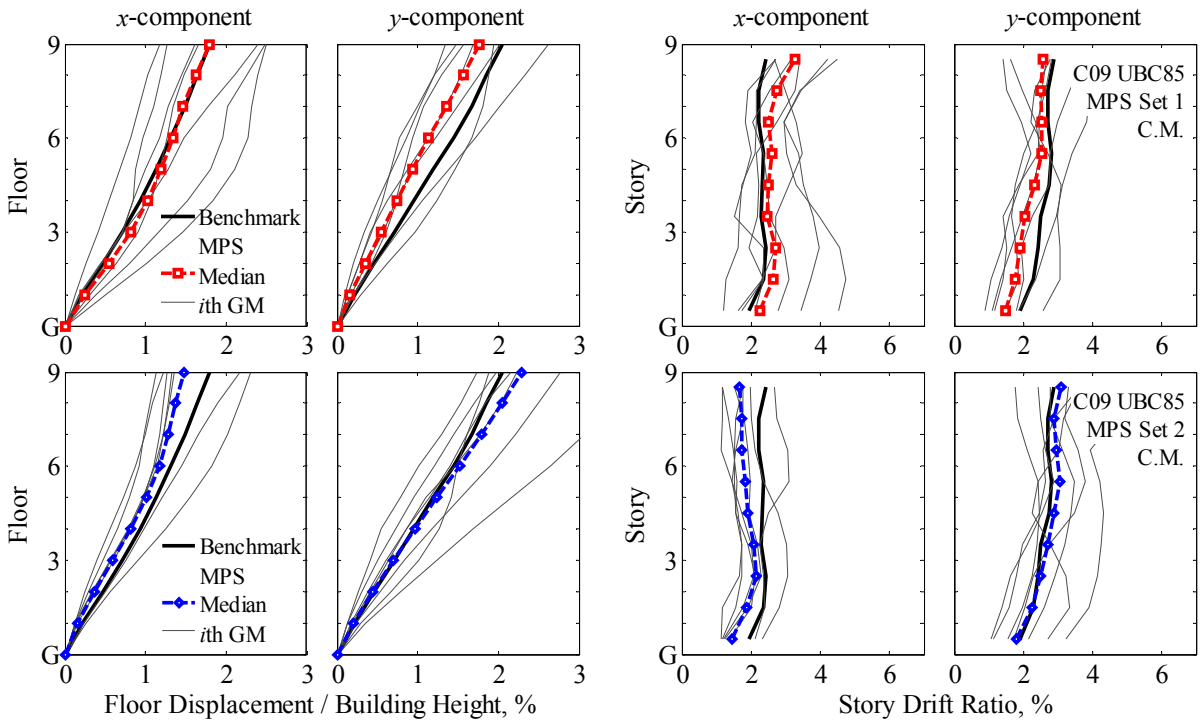

Figure 6.47 Comparison of EDPs at the C.M. for the C09 UBC85 building due to ground motion sets 1 and 2 scaled by the one-mode MPS procedure against benchmark values; individual results for seven scaled ground motions are included.

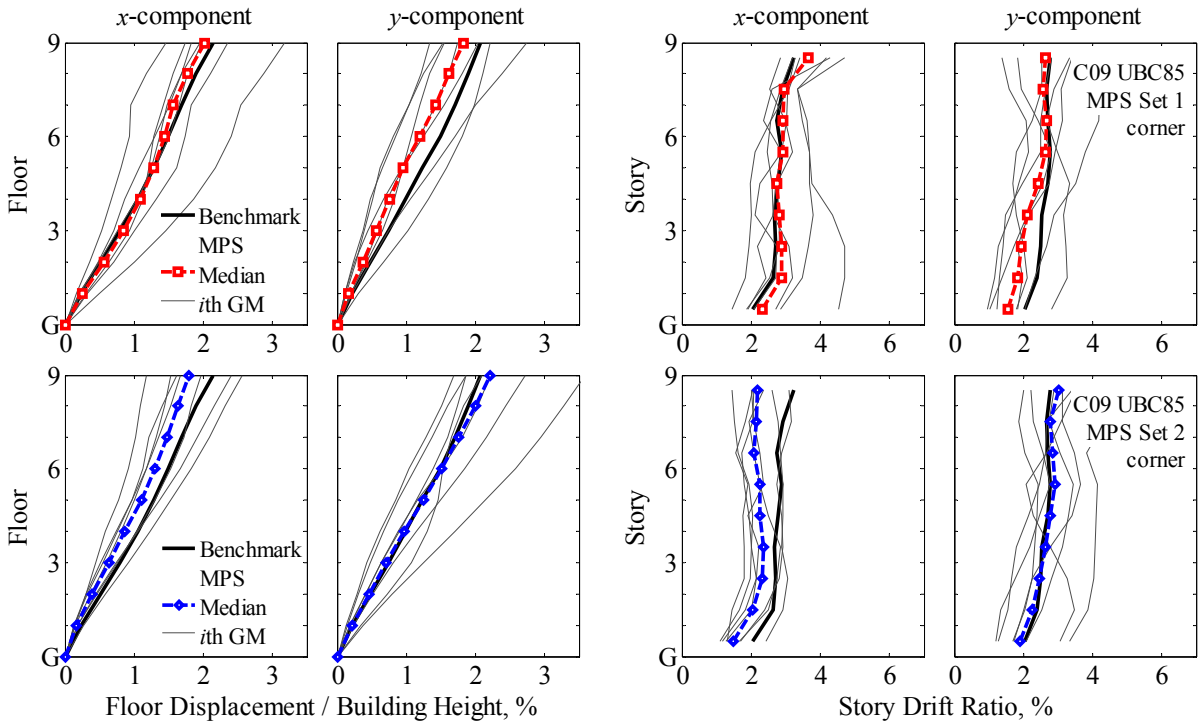

Figure 6.48 Comparison of EDPs at the corner for the C09 UBC85 building due to ground motion sets 1 and 2 scaled by the one-mode MPS procedure against benchmark values; individual results for seven scaled ground motions are included.

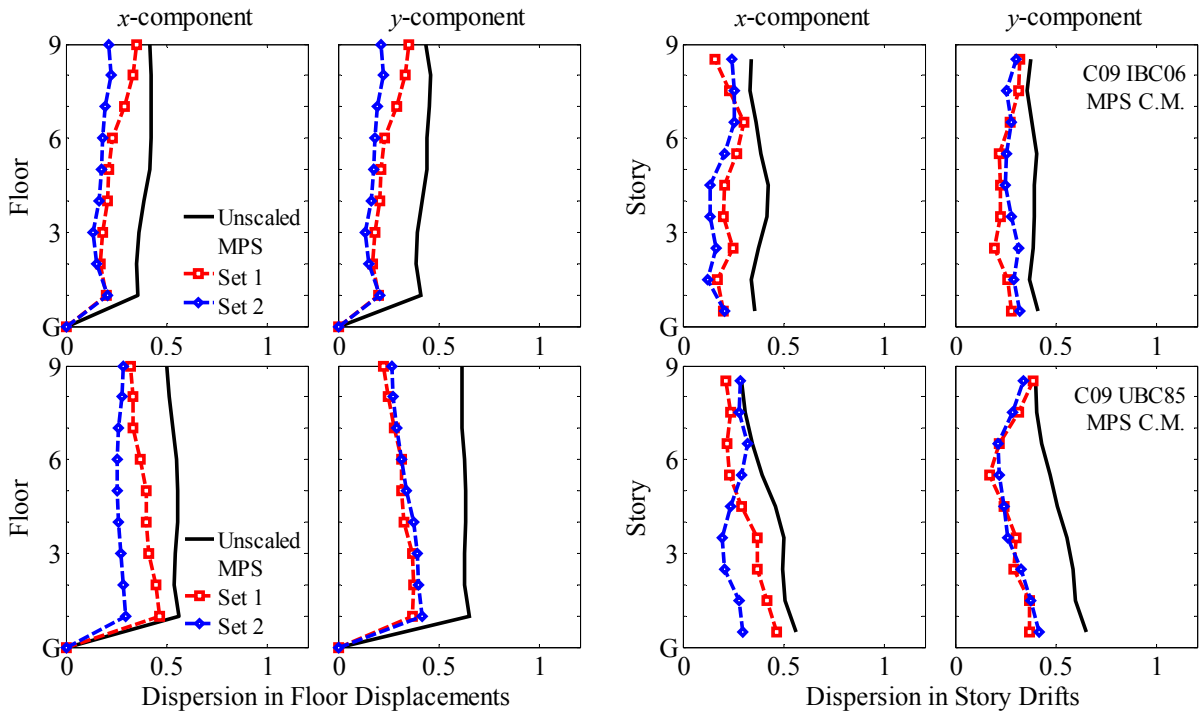

Figure 6.49 Dispersion of EDPs at the C.M. due to ground motion sets 1 and 2 scaled by the one-mode MPS procedure and dispersion of EDPs due to 28 unscaled records.

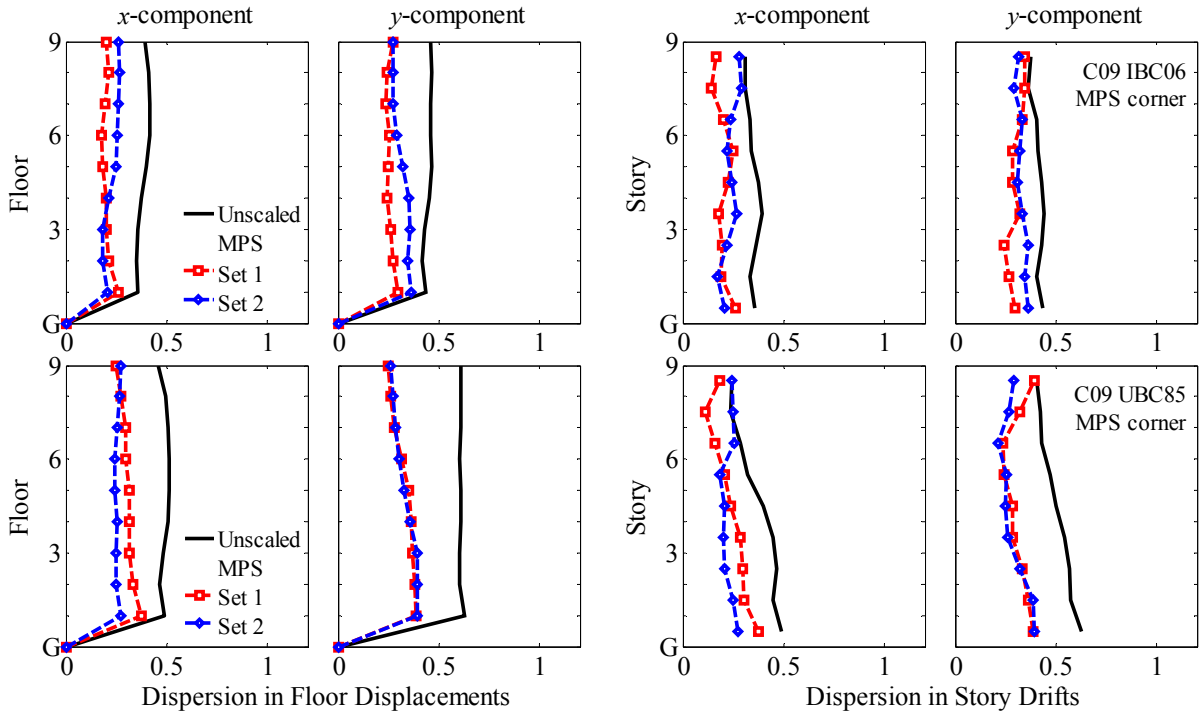

Figure 6.50 Dispersion of EDPs at the corner due to ground motion sets 1 and 2 scaled by the one-mode MPS procedure and dispersion of EDPs due to 28 unscaled records..

6.7.3 Comparative Evaluation of MPS and ASCE7 Scaling Procedures

The ASCE7 scaling procedure presented in Section 6.2.2 is implemented for the C09 IBC06 and UBC85 buildings subjected to both horizontal components of ground motion, simultaneously. Figures 6.51 through 6.56 show the median and dispersion values of EDPs for both buildings due to ground motion sets 1 and 2 scaled according to the ASCE7 procedure and compares them with the benchmark values presented in Figs. 6.40 and 6.41. These results together with the previous results for the one-mode based MPS procedure demonstrate that the MPS procedure is superior compared to the ASCE7 procedure for scaling ground motions. This superiority is evident in two respects. First, for each ground motion set, the ground motions scaled according to the MPS procedure provide median values of EDPs that are much closer to the benchmark values than is achieved by the ASCE7 procedure. For the C09 IBC06 building, the height-wise maximum error of 38% in the floor displacements determined by scaling record set 2 according to the ASCE7 procedure is reduced to 15% when record set 2 is scaled by the MPS procedure. Likewise, the height-wise maximum error in story drifts reduces from 36% to 15% in case of record set 2; however, this reduction is comparatively less for EDPs due to record set 1. For the C09 UBC85 building, the height-wise maximum discrepancy in floor displacements and story drifts reduces from 43% to 28% and from 40% to 34%, respectively. Second, the record-to-record variability around the median value is smaller when the records are scaled by the MPS procedure (Figs. 6.45-6.48) compared to the ASCE7 scaling procedure (Figs. 6.51-6.54). For the C09 IBC06 building, the height-wise maximum value of dispersion is reduced from 0.48 (set 2) to 0.36 for floor displacements and from 0.47 (set 2) to 0.36 for story drifts. However, the

reduction in dispersion achieved by the MPS procedure in story drifts at the corner for the IBC06 building is less significant.

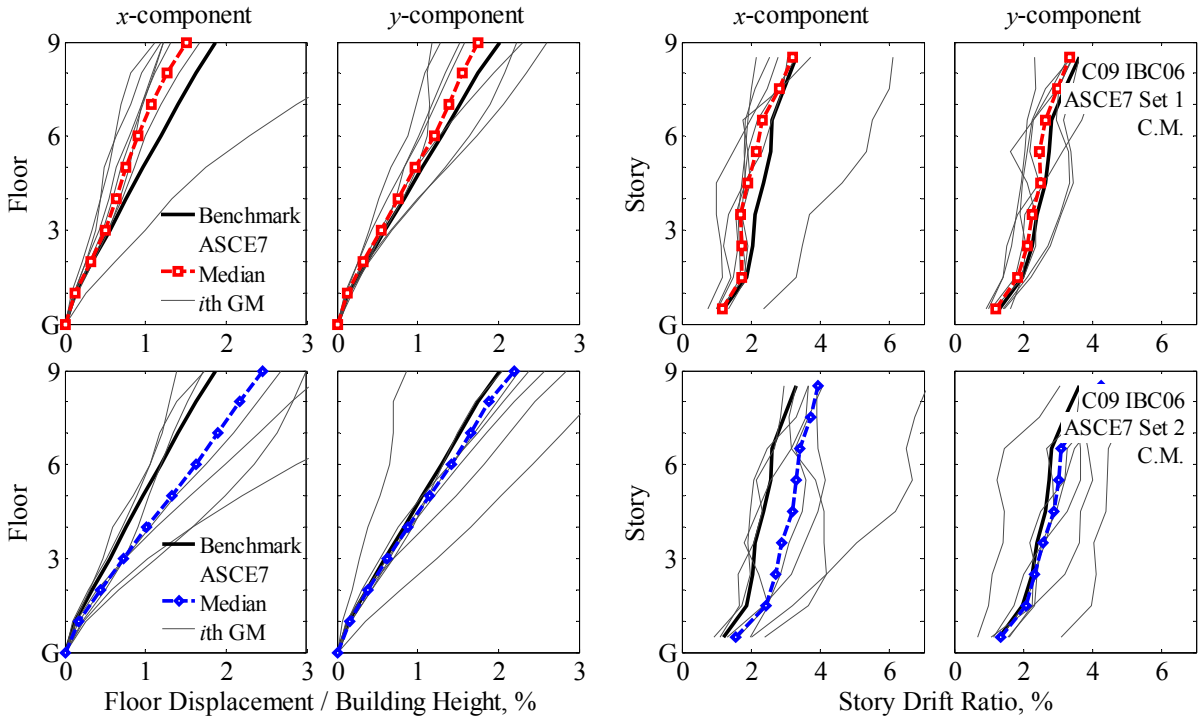

Figure 6.51 Comparison of EDPs at the C.M. for the C09 IBC06 building due to ground motion sets 1 and 2 scaled by the ASCE7 procedure against benchmark values; individual results for seven scaled ground motions are included.

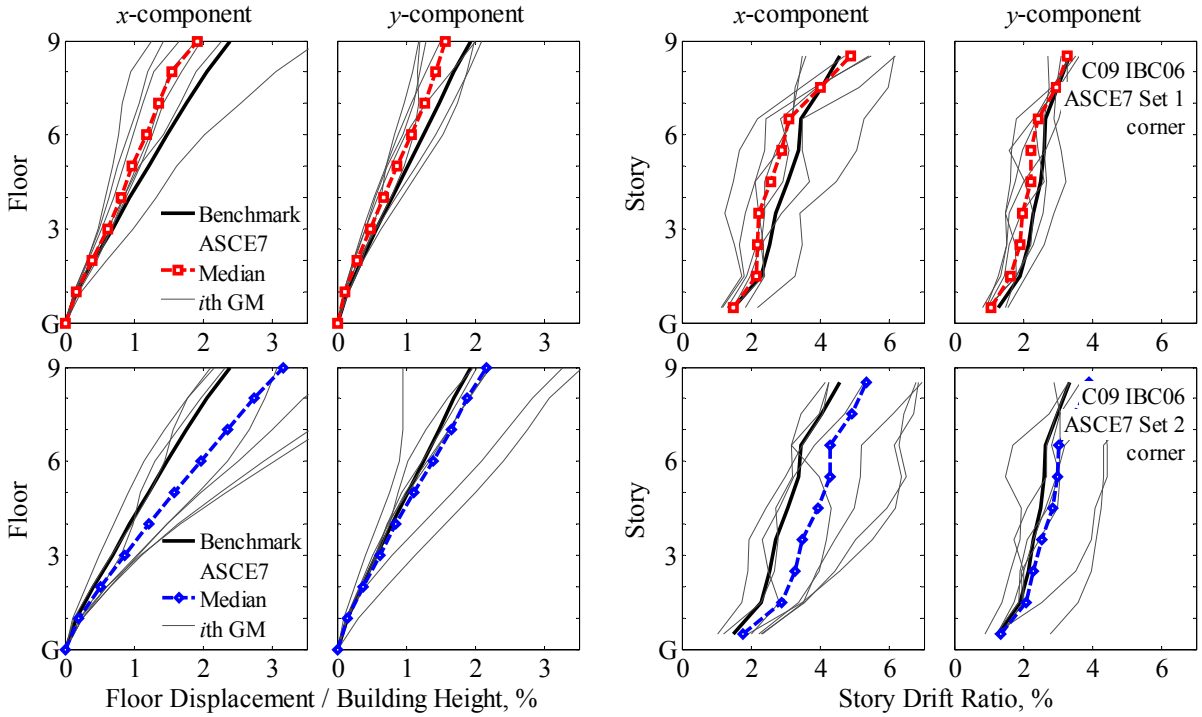

Figure 6.52 Comparison of EDPs at the corner for the C09 IBC06 building due to ground motion sets 1 and 2 scaled by the ASCE7 procedure against benchmark values; individual results for seven scaled ground motions are included.

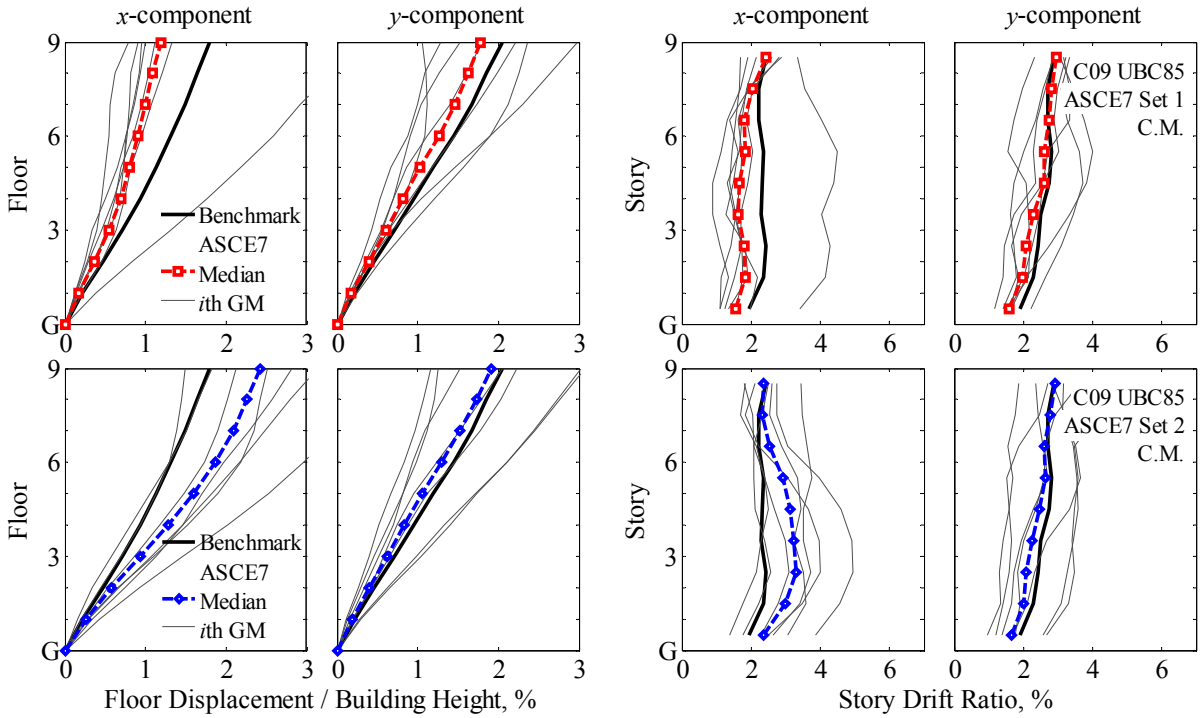

Figure 6.53 Comparison of EDPs at the C.M. for the C09 UBC85 building due to ground motion sets 1 and 2 scaled by the ASCE7 procedure against benchmark values; individual results for seven scaled ground motions are included.

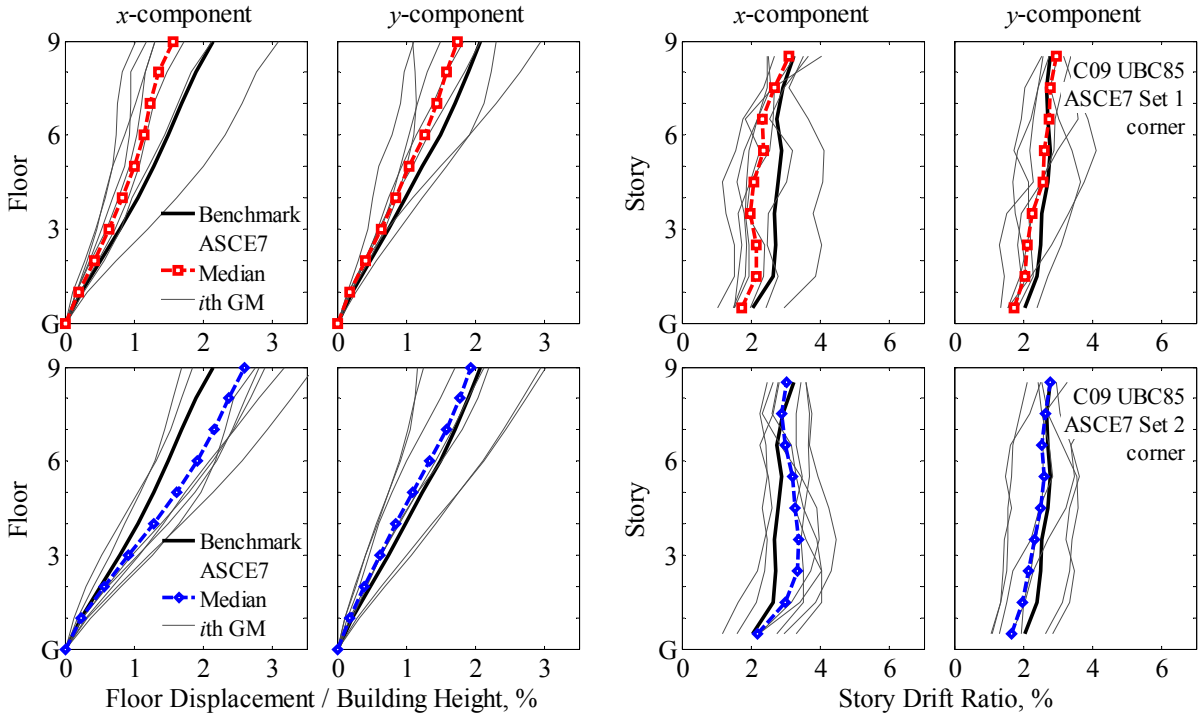

Figure 6.54 Comparison of EDPs at the corner for the C09 UBC85 building due to ground motion sets 1 and 2 scaled by the ASCE7 procedure against benchmark values; individual results for seven scaled ground motions are included.

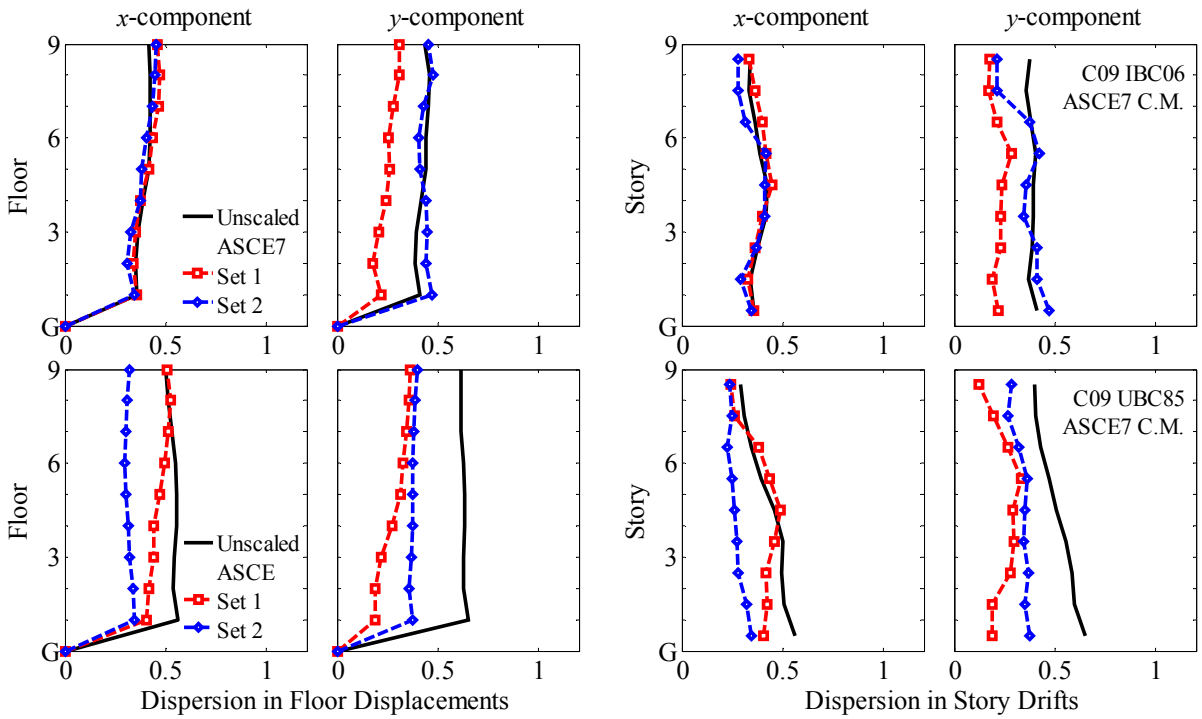

Figure 6.55 Dispersion of EDPs at the C.M. due to ground motion sets 1 and 2 scaled by the ASCE7 procedure and dispersion of EDPs due to 28 unscaled records.

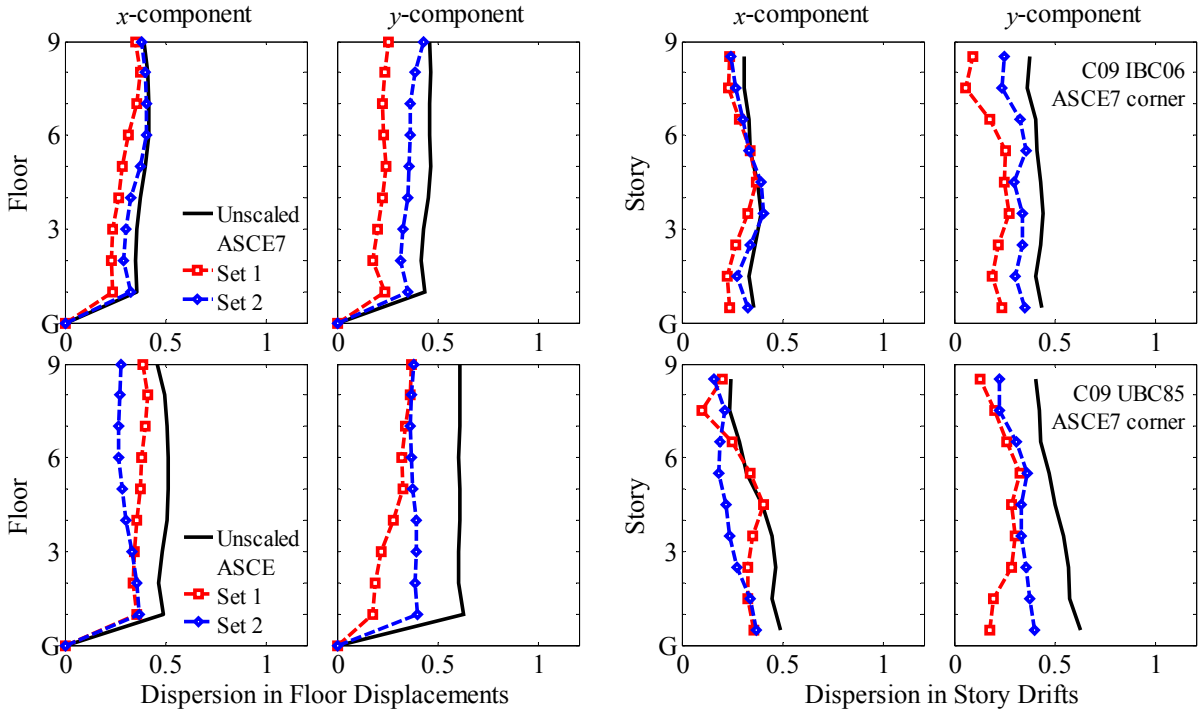

Figure 6.56 Dispersion of EDPs at the corner due to ground motion sets 1 and 2 scaled by the ASCE7 procedure and dispersion of EDPs due to 28 unscaled records.

6.7.4 Higher Mode Considerations

The 28 records scaled based only on the first-mode response (scaling factors were presented in Fig. 6.43) are ranked by considering their accuracy in estimating the second mode response (Steps 10 to 13 of the MPS procedure). Among the 14 records in sets 1 and 2, the seven records with the highest rank (according to Step 12) were defined as ground motion set 3.

Considering the second mode in selecting the ground motions in the MPS method provides accurate estimates of the median EDPs and generally reduces the record-to-record variability (compared to the results associated with ground motion sets 1 and 2). This improvement in accuracy and efficiency is demonstrated in Figs. 6.57 through 6.60 where the median and dispersion values of the *x* and *y* components of floor displacements and story drifts at the C.M. and at the corner for both buildings due to set 3 are shown together with the benchmark values. It is evident that this new set leads to better estimates of median demands compared to sets 1 and 2 (Figs. 6.45-6.48); the height-wise maximum discrepancy in drift ratios is reduced from 31% to less than 20%, and from 34% to less than 26% for the C09 IBC06 and UBC85 buildings, respectively. However, the dispersion in EDPs due to ground motion set 3 (Figs. 6.59 and 6.60) is not significantly reduced, indicating that the MPS procedure is less efficient—implying record-to-record variability remains large—for unsymmetric-plan buildings. This may be because of two reasons: strong coupling between translational and torsional components of motion, and relatively small effective mass in the first mode—less than 60% of the total mass (Figs. 5.8 and 5.12).

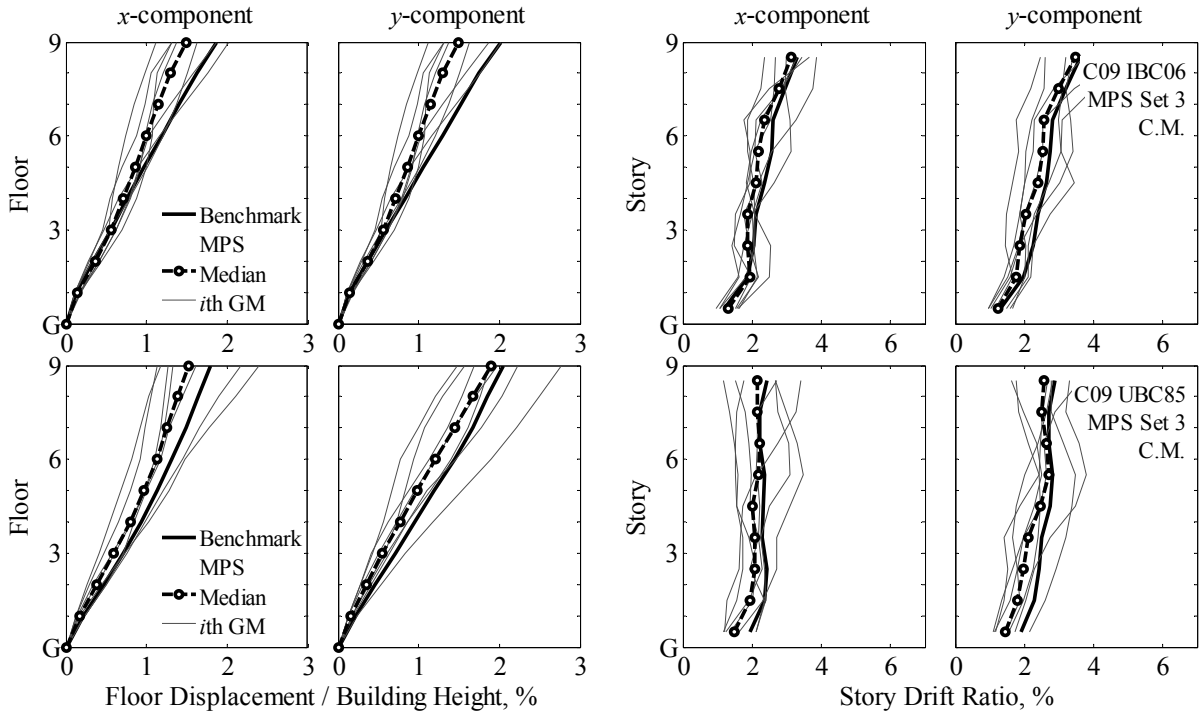

Figure 6.57 Comparison of median EDPs at the C.M. for ground motion set 3 scaled by the MPS procedure (considering higher modes) with benchmark EDPs; individual results for the seven scaled ground motions are included.

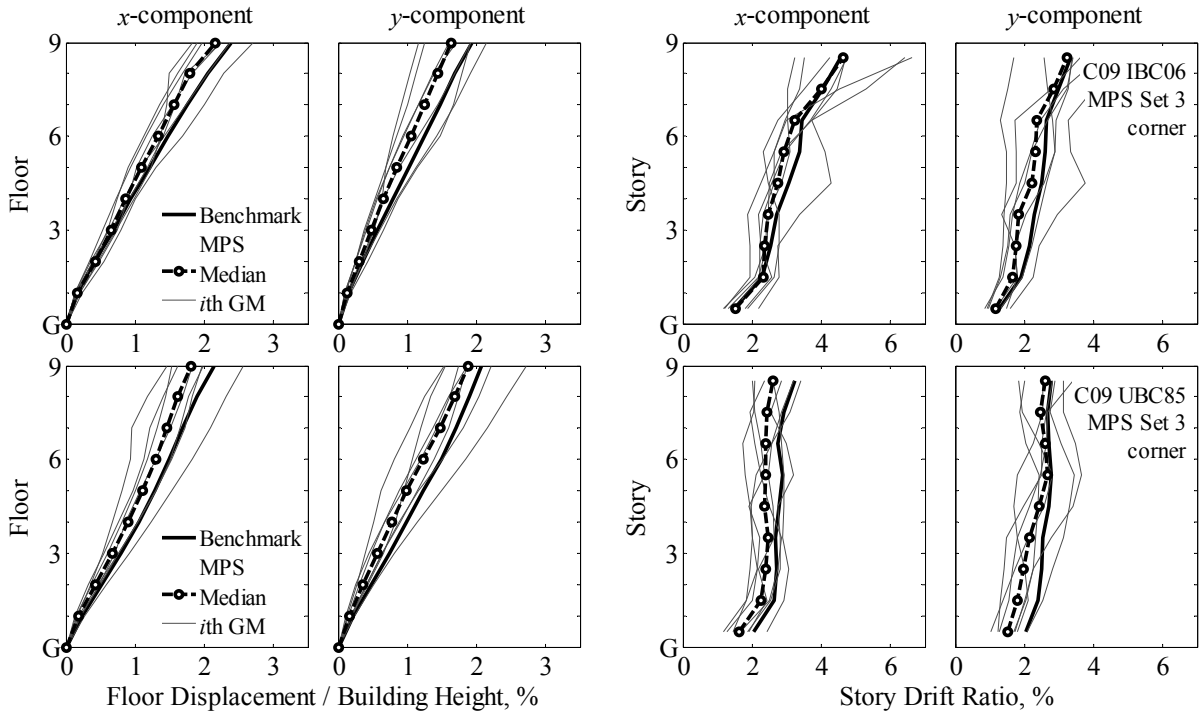

Figure 6.58 Comparison of median EDPs at the corner for ground motion set 3 scaled by the MPS procedure (considering higher modes) with benchmark EDPs; individual results for the seven scaled ground motions are included.

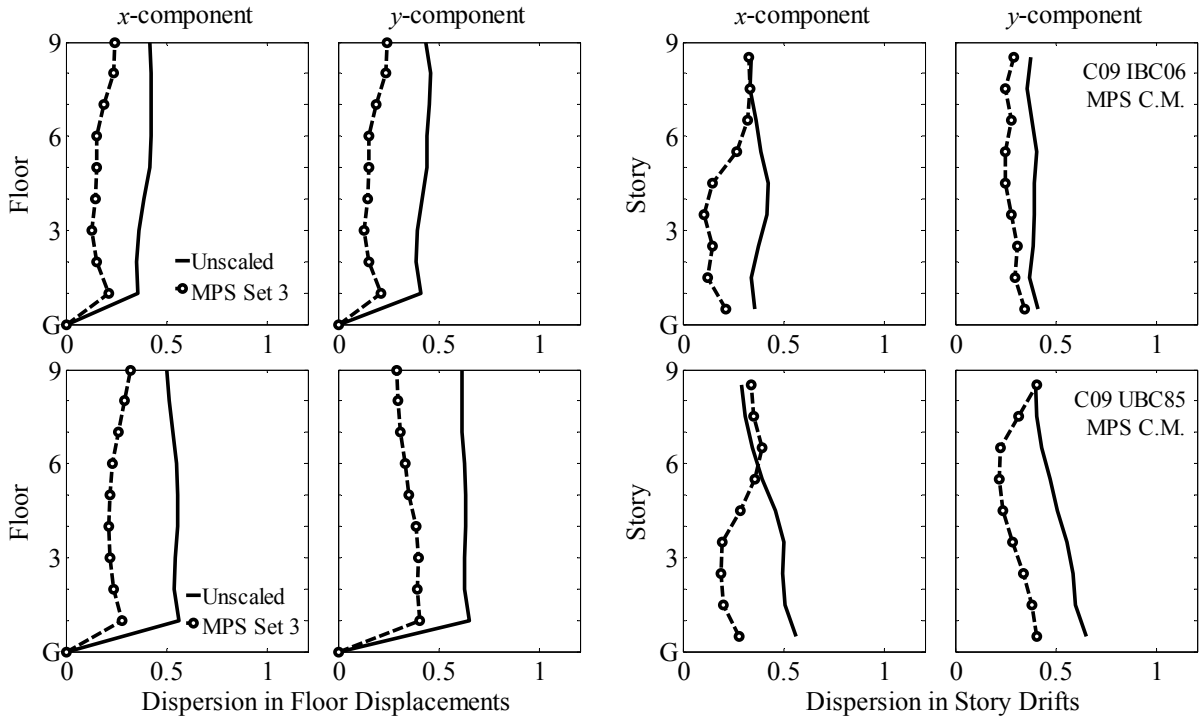

Figure 6.59 Comparison of dispersion of EDPs at the C.M. due to ground motions set 3 scaled by the MPS procedure (considering higher modes) against dispersion of 28 unscaled records.

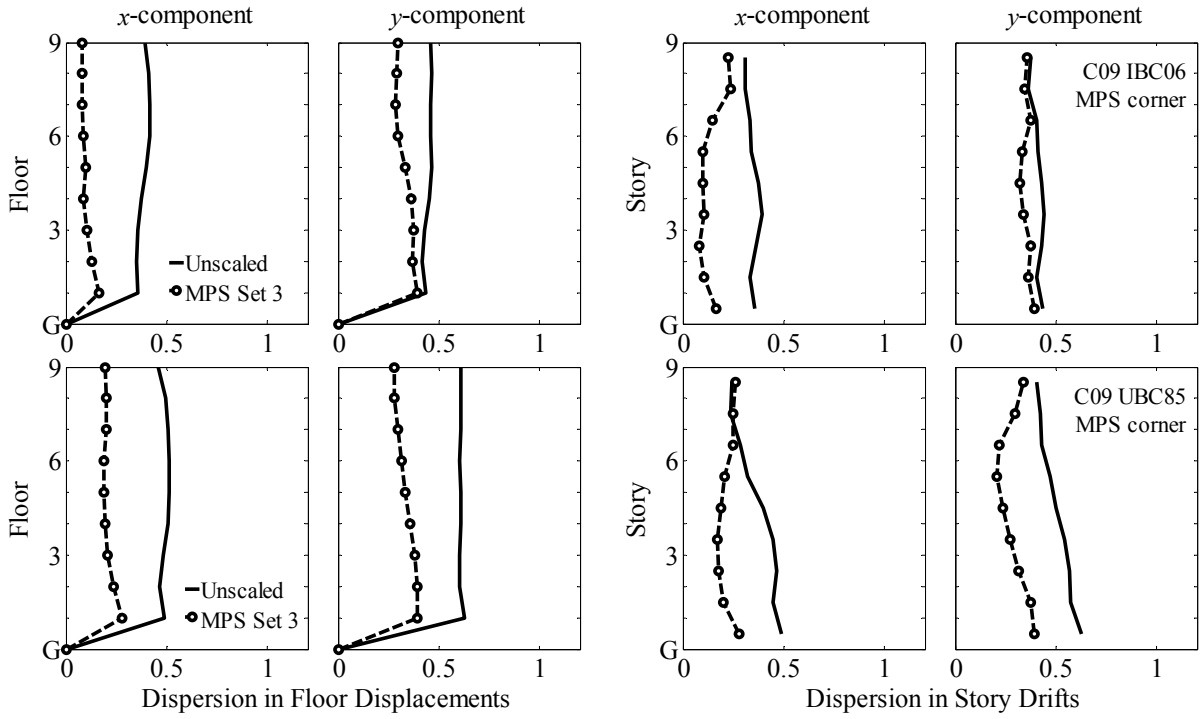

Figure 6.60 Comparison of dispersion of EDPs at the corner due to ground motions set 3 scaled by the MPS procedure (considering higher modes) against dispersion of 28 unscaled records.

7 Conclusions

The modal pushover analysis (MPA) procedure for estimating seismic demands has been extended to three dimensional analyses of buildings subjected to two components of ground motion. Rooted in structural dynamics theory, the extended MPA procedure retains the conceptual simplicity of current pushover procedures with invariant force distribution now common in structural engineering practice. However, it includes the contributions of all significant "modes" of vibration, thus making it suitable in estimating seismic demands for tall buildings and unsymmetric-plan buildings.

A version of MPA that is especially convenient for practical application, called the Practical MPA (PMPA), has been developed to compute seismic demands directly from the earthquake response (or design) spectrum. This procedure is based on two simplifications: (1) the structure is treated as linearly elastic in estimating higher-"mode" contributions to seismic demand; and (2) the median deformation of the *n*th-mode inelastic SDF system is estimated directly from the design spectrum using an empirical equation for the inelastic deformation ratio.

Evaluation of the accuracy of the MPA procedure in estimating seismic demands for existing 48- and 62-story symmetric-plan buildings with ductile concrete core walls—designed to comply with current codes—due to an ensemble of 30 ground motions (Chapter 4) has led to the following conclusions:

1. Although the first "mode" of lateral vibration in the *x* and *y* directions is inadequate in estimating story drifts, with the second "mode" of lateral vibration included, the discrepancies (relative to nonlinear RHA results) reduce greatly and story drifts estimated by MPA resemble nonlinear RHA results.

2. The MPA procedure may be simplified by treating the building as linearly elastic in estimating higher-"mode" contributions to seismic demands. This approximation has been demonstrated to be valid.
3. The modal combination and multi-component combination approximations used in the response spectrum analysis (RSA) procedure for linearly elastic systems may—a standard tool in structural engineering practice—lead to significant underestimation of story drift demands, especially in upper stories, for tall buildings.
4. Although additional errors are induced by estimating deformations of modal SDF systems directly from the median response spectrum and by neglecting modal coupling and cyclic stiffness degradation, the PMPA procedure for inelastic systems is almost as accurate as RSA is for linearly elastic systems.
5. The PMPA procedure offers a sufficient degree of accuracy that should make it useful for practical application in estimating seismic demands—floor displacements, story drifts, rotations and internal forces—for tall buildings due to two horizontal components of ground motion applied simultaneously.

Evaluation of the accuracy of the MPA procedure in estimating seismic demands for six low- and medium-rise, unsymmetric-plan steel moment-resisting frame buildings designed according to the UBC85 and IBC06 codes, due to an ensemble of 38 ground motions (presented in Chapter 5) has led to the following conclusions:

1. The first triplet of "modes" alone is adequate in estimating story drifts for the three-story unsymmetric-plan buildings, but it is inadequate in case of the nine-story

buildings; in the latter case, with the second triplet of "modes" included, story drifts estimated by MPA are much better, and resemble nonlinear RHA results.

2. The MPA procedure may be simplified by treating the building as linearly elastic in estimating higher-"mode" contributions to seismic demands. This approximation has been demonstrated to be valid.
3. The modal combination and multi-component combination approximations used in the response spectrum analysis (RSA) procedure for linearly elastic systems may lead to significant underestimation of story drift demands, especially in upper stories, for unsymmetric-plan buildings.
4. The PMPA procedure for low- and medium-rise unsymmetric-plan buildings subjected to ground motion along two horizontal components applied simultaneously leads to conservative, but generally not overly conservative, estimates of seismic demands—floor displacements, story drifts, rotations and internal forces; thus, PMPA should be useful for practical application in estimating seismic demands for evaluating existing buildings or proposing designs of new buildings.
5. As a side, pushover analysis of buildings revealed that the ductility capacity of low-rise torsionally-similarly-stiff and torsionally-flexible systems is governed by the failure of column sections around the weak axis. Unfortunately, there is little information available about the nonlinear behavior of steel columns around the weak axis, and the standards of seismic rehabilitation of steel buildings do not include such information.

Comparative evaluation of MPA and the nonlinear static procedure (NSP) of the ASCE/SEI 41-06 standard [ASCE, 2007] and the Eurocode 8 [British Standards, 2004] for low and medium-rise unsymmetric-plan buildings has led to the following conclusions:

1. Both ASCE/SEI 41-06 and Eurocode8 force distributions significantly underestimate drifts at the upper stories of low and medium-rise torsionally-flexible buildings, even for buildings that deform only modestly into the nonlinear range. In contrast, the MPA procedure provides a much better estimate of seismic demands in the upper stories of these buildings, because it includes all three components of forces and higher-"mode" contributions to the response. In particular, for the 9-story building designed according to the UBC85 code, the discrepancy (relative to the nonlinear RHA result) of 73% in the *x*-component of drift in the ninth story determined by the nonlinear static procedure (NSP) of the ASCE/SEI 41-06 standard is reduced to 10% when the MPA procedure is implemented.
2. For structures that respond dominantly in the first-"mode", the ASCE41-06 and Eurocode8 force distributions are adequate and MPA does not offer improvement in the demand estimate.

With the goal of developing effective procedures for selection and scaling of multi-component ground motions to be used in nonlinear RHA, a modal-pushover-based-scaling (MPS) procedure has been developed in this investigation. The objective of this amplitude scaling procedure is to determine scale factors for a small number of records such that the scaled records provide an accurate estimate of median structural responses,

and, at the same time, are efficient, i.e. reduce the record-to-record variability of response. The developed MPS procedure is an extension of the original MPS procedure for one component of ground motion to two horizontal components [Kalkan and Chopra, 2010].

The accuracy of the extended MPS procedure was evaluated by comparing the median values of the engineering demand parameters (EDPs) for a selected building due to a set of seven ground motions scaled according to the MPS procedure against the benchmark values, defined as the median values of the EDPs due to 28 unscaled ground motions. The efficiency of the scaling procedures was evaluated by computing the dispersion of the responses to the seven scaled ground motions; small dispersion indicates that the scaling procedure is efficient. Selected for this investigation is an actual 9-story symmetric-plan building with its computer model calibrated against its motions recorded during an earthquake. This evaluation of the MPS procedure has led to the following conclusions:

1. Even for the most intense near-fault ground motions, which represent a severe test, the MPS scaling procedure for one component of ground motion provides good estimates of the median values of engineering demand parameters (EDPs), and reduces their dispersion; in particular, the discrepancy in drift ratios relative to the benchmark values is less than 10%.
2. The one-mode MPS procedure using a single scaling factor for both components of ground motion was judged to be unacceptable because it led to unacceptably inaccurate estimates of the median EDPs accompanied by large record-to-record variability of the responses.

3. The MPS procedure allowing for different scaling factors for the *a* and *b* components of ground motion provides an accurate estimate of the median EDPs and reduces the record-to-record variability of the responses; in particular, the discrepancy in drift ratios relative to the benchmark values is less than 10%.

Comparative evaluation of the MPS and ASCE7 [ASCE, 2005] procedures in estimating EDPs for the 9-story symmetric-plan building has led to the following conclusions:

1. The MPS procedure provides much superior estimates of the EDPs due to one component of ground motion compared to the ASCE7 method. The latter method grossly overestimates floor displacements and story drifts with unacceptably large dispersion, with discrepancies exceeding 100% and dispersion values exceeding even the dispersion of the benchmark responses.
2. The MPS procedure is superior compared to the ASCE7 procedure for scaling two components of ground motions. This superiority is evident in two respects. First, the ground motions scaled according to the MPS procedure provide median values of EDPs that are much closer to the benchmark values than is achieved by the ASCE7 procedure. The discrepancy of 53% in drift ratios relative to the benchmark values determined by scaling records according to the ASCE7 procedure is reduced to less than 10% when records are scaled by the MPS procedure. Second, the dispersion in the EDPs due to seven scaled records (or record-to-record variability) around the median is much smaller when records are scaled by the MPS procedure compared to the ASCE7 scaling procedure.

Evaluation of the accuracy and efficiency of the MPS and the ASCE7 scaling procedures in estimating EDPs for 9-story unsymmetric-plan buildings designed according to the IBC06 and UBC85 codes has led to the following conclusions:

1. The one-mode MPS procedure allowing for different scaling factors for the *a* and *b* components of ground motion for the IBC06 building subjected to two components of ground motion provides good estimates of the median EDPs and reduces considerably the record-to-record variability. By considering the second "mode" in ranking and selecting the "best" ground motions, the median EDPs are within about 15% of the benchmark value.
2. The accuracy of the one-mode MPS procedure deteriorates for the building designed according to the UBC85 code. Deterioration in the one-mode based MPS procedure is not surprising for this torsionally-flexible building with strong coupling between lateral and torsional motions, because the effective mass in the first mode is less than 50% of the total mass, implying that higher-"mode" contributions to the demand are expected to be large.
3. The dispersion in EDPs determined by scaling records according to the MPS procedure is not significantly reduced compared with the dispersion of responses to 28 unscaled records, indicating that the MPS procedure is less efficient—implying record-to-record variability remains large—for unsymmetric-plan buildings. This may be because of two reasons: strong coupling between translational and torsional components of motion, and relatively small effective mass in the first mode—less than 60% of the total mass.

4. The MPS procedure provides superior estimates of the EDPs compared to the ASCE7 method for both unsymmetric-plan buildings. The discrepancies in the latter method exceed 40% with unacceptably large dispersion.

8 Bibliography

Abrahamson, N. A. [1992], "Non-stationary Spectral Matching," Seismological Research Letters 63(1), 30.

Abrahamson N. and Silva W. [2008], "Summary of the Abrahamson & Silva NGA Ground-Motion Relations," Earthquake Spectra, 24(1), pp. 67-97.

Alavi, B. and Krawinkler, H. [2000], "Consideration of Near-Fault Ground Motion Effects in Seismic Design," Proceedings of the 12th World Conference on Earthquake Engineering, Paper No. 2665, Auckland, New Zealand.

Alavi, B. and Krawinkler, H. [2004], "Behavior of Moment-Resisting Frame Structures Subjected to Near-Fault Ground Motions," Earthquake Engineering and Structural Dynamics, Vol. 33, No. 6, pp. 687-706.

ASCE [2005], "Minimum Design Loads for Buildings and Other Structures," SEI/ASCE 7-05, Reston, VA.

ASCE [2007], "Seismic Rehabilitation of Existing Buildings," ASCE/SEI 41-06, Reston, VA.

Aydinoglu, M. N. [2003], "An Incremental Response Spectrum Analysis Procedure Based on Inelastic Spectral Displacements for Multi-Mode Seismic Performance Evaluation," Bulletin of Earthquake Engineering, 1(1), pp. 3-36.

Báez, J. I. and Miranda, E. [2000], "Amplification factors to estimate inelastic displacement demands for the design of structures in the near field," Proceedings of the Twelfth World Conference on Earthquake Engineering, Paper No. 1561, Auckland, New Zealand.

Baker, J. W. and Cornell, A. C. [2006], "Spectral Shape, Epsilon and Record Selection," Earthquake Engineering and Structural Dynamics, Vol. 35, No. 9, pp. 1077-1095.

Bazzurro, P. [1998], "Probabilistic Seismic Demand Analysis," Ph.D. dissertation, Stanford University, CA.
(Available online at http://www.stanford.edu/group/rms/Thesis/index.html; last accessed on 10/2009).

Beyer, K. and Bommer, J. J. [2007], "Selection and Scaling of Real Accelerograms for Bi-Directional Loading: A Review of Current Practice and Code Provisions," Journal of Earthquake Engineering, 11:1, pp. 13-45.

Benjamin, J. R. and Cornell, C. A. [1970], Probability, Statistics, and Decision for Civil Engineers, McGraw-Hill, New York, pp. 684.

Bobadilla, H. and Chopra, A. K. [2007], "Modal Pushover Analysis for Seismic Evaluation of Reinforced Concrete Special Moment Resisting Frame Buildings," Earthquake Engineering Research Center UCB/EERC-2007/01, University of California, Berkeley, CA.

Bobadilla, H. and Chopra, A. K. [2008], "Evaluation of the MPA Procedure for Estimating Seismic Demands: RC-SMRF Buildings," Earthquake Spectra, 24(4), pp. 827-845.

Bommer, J. J. and Acevedo, A. B. [2004], "The Use of Real Earthquake Accelerograms as Input to Dynamic Analysis," Journal of Earthquake Engineering 8 (Special Issue 1), pp. 43-91.

Boore D. M. and Atkinson G. M. [2008], "Ground-Motion Prediction Equations for the Average Horizontal Component of PGA, PGV, and 5%-Damped PSA at Spectral Periods between 0.01 s and 10.0 s," Earthquake Spectra, 24(1), pp. 99-138.

Bozorgnia, Y. and Mahin, S. A. [1998], "Ductility and Strength Demands of Near-Fault Ground Motions of the Northridge Earthquake," Proceedings of the 6th U.S. National Conference on Earthquake Engineering, Seattle, WA.

Bracci, J. M., Kunnath, S. K., Reinhorn, A. M. [1997], "Seismic Performance and Retrofit Evaluation for Reinforced Concrete Structures," Journal of Structural Engineering, 123(1), pp. 3-10.

British Standards, [2004], "Eurocode 8: Design of Structures for Earthquake Resistance," BS-EN1998:2004, UK.

Joyner, W. B. and Boore, D. M. [1981], "Peak Horizontal Acceleration and Velocity from Strong-Motion Records Including Records from the 1979 Imperial Valley, California, Earthquake," Bulletin of the Seismological Society of America, 71, pp. 2011–2038.

Campbell, K. W. and Bozorgnia Y. [2008], "NGA Ground Motion Model for the Geometric Mean Horizontal Component of PGA, PGV, PGD and 5% Damped Linear Elastic Response Spectra for Periods Ranging from 0.01 to 10 s," Earthquake Spectra, 24(1), pp. 139-171.

Chintanapakdee, C. [2002], "Evaluation of the Modal Pushover Analysis Procedure Using Vertically 'Regular' and Irregular Generic Frames," Ph.D. dissertation, University of California, Berkeley, CA.

Chopra, A. K., and Goel, R. K. [2002], "A Modal Pushover Analysis Procedure for Estimating Seismic Demands for Buildings," Earthquake Engineering and Structural Dynamics, 31(3), pp. 561–582.

Chopra, A. K., and Chintanapakdee, C. [2004], "Inelastic Deformation Ratios for Design and Evaluation of Structures: Single-Degree-of-Freedom Bilinear Systems," Journal of Structural Engineering, ASCE, 130, pp. 1309–1319.

Chopra, A. K., and Goel, R. K. [2004], "A Modal Pushover Analysis Procedure to Estimate Seismic Demands for Unsymmetric-plan Buildings," Earthquake Engineering and Structural Dynamics, 33, pp. 903-927.

Chopra, A. K., Goel, R. K., and Chintanapakdee, C. [2004], "Evaluation of a Modified MPA Procedure Assuming Higher Modes as Elastic to Estimate Seismic Demands," Earthquake Spectra, 20(3), pp. 757-778.

Chopra, A. K. [2007], Dynamics of Structures, Theory and Applications to Earthquake Engineering, 3rd ed., Pearson, Prentice Hall, Upper Saddle River, NJ.

Chung, W. and Campbell, S.D. [2007], "Implicit Pseudo-dynamic Algorithm with an Event-to-Event Solution Scheme," Engineering Structures, 29, pp. 640-648.

Computers and Structures (CSI), Inc., [2006], PERFORM 3D, User Guide v4, Non-linear Analysis and Performance Assessment for 3D Structures, Computers and Structures, Inc., Berkeley, CA.

Computers and Structures (CSI), Inc., [2006], PERFORM 3D, Components & Elements v4, Defining the Standard for Practical Performance Based Design, Computers and Structures, Inc., Berkeley, CA.

De Stefano M., and Rutenberg, A. [1998], "Predicting the Dynamic Response of Asymmetric Multistorey Wall-Frame Structures by Pushover Analysis: Two Case Studies. Proceedings of the 11th European Conference on Earthquake Engineering, Balkema, Rotterdam.

Der Kiureghian, A. [1981], "A Response Spectrum Method for Random Vibration Analysis of MDF Systems," Earthquake Engineering and Structural Dynamics, 9, pp. 419-435.

Dreger, D. [2009], Personal Communications.

Elnashai, A. S. [2001], "Advanced Inelastic Static (Pushover) Analysis for Earthquake Applications," Structural Engineering and Mechanics, 12(1), pp. 51-69.

Faella, G. and Kilar, V. [1998], "Asymmetric Multistorey R/C Frame Structures: Push-over Versus Nonlinear Dynamic Analysis," Proceedings of the 11th European Conference on Earthquake Engineering, Balkema, Rotterdam.

Fajfar, P. [2002], "Structural Analysis in Earthquake Engineering – A Breakthrough of Simplified Non-linear Methods." Proceedings of the 12th European Conference on Earthquake Engineering, London, UK.

Fajfar, P. [2008], Personal Communications.

FEMA [2000], "Pre-standard and Commentary for the Seismic Rehabilitation of Buildings", FEMA-356, Washington, D.C.

FEMA [2005], "Improvement of Non-linear Static Seismic Analysis Procedures", FEMA-440, Washington, D.C.

Giraldo, D. F., Song, W., Dyke, S. J. and Caicedo, J. M. [2009], "Modal Identification through Ambient Vibration: Comparative Study," Journal of Engineering Mechanics, ASCE, Vol. 135, No. 8, pp. 759-770.

Goel, R. K. and Chopra A. K. [2004], "Evaluation of Modal and FEMA Pushover Analyses: SAC Buildings," Earthquake Spectra, 20(1), pp. 225-254.

Goel, R. K. and Chopra A. K. [2005], "Extension of Modal Pushover Analysis to Compute Member Forces," Earthquake Spectra, 21(1), pp. 125-139.

Gupta, A., and Krawinkler, H. [1999], "Seismic Demands for Performance Evaluation of Steel Moment Resisting Frame Structures (SAC Task 5.4.3)," Report No. 132, John A. Blume Earthquake Engineering Center, Stanford University, CA.

Gupta, B., Kunnath, S. K. [2000], "Adaptive Spectra-Based Pushover Procedure for Seismic Evaluation of Structures," Earthquake Spectra, 16(2), pp. 367-391.

Han, S. W. and Chopra, A. K. [2006], "Approximate Incremental Dynamic Analysis Using the Modal Pushover Analysis Procedure," Earthquake Engineering and Structural Dynamics, 35, pp. 1853-1873.

Hancock, J., Watson-Lamprey, J., Abrahamson, N. A., Bommer, J. J., Markatis, A., McCoy, E., and Mendis R. [2006], "An Improved Method of Matching Response Spectra of Recorded Earthquake Ground Motion Using Wavelets," Journal of Earthquake Engineering, Vol. 10, Special Issue 1, pp. 67-89.

Heintz, J. A. [2008], Personal Communications.

Haselton, C. B. [2006], "Assessing Seismic Collapse Safety of Modern Reinforced Concrete Moment Frame Buildings," Ph.D. dissertation, Stanford University, CA.

Haselton, C. B., Deierlein, G. G. [2007], "Assessing Seismic Collapse Safety of Modern Reinforced Concrete Moment-Frame Buildings," Report No. 156, John A. Blume Earthquake Engineering Center, Stanford University, CA.

PEER Ground Motion Selection and Modification Working Group, [2009], "Evaluation of Ground Motion Selection and Modification Methods: Predicting Median Interstory Drift Response of Buildings," Haselton C. B. (editor), PEER Report 2009/01, University of California, Berkeley, CA.

International Conference of Building Officials [1985], "1985 Uniform Building Code", International Conference of Building Officials, USA.

International Code Council [2006], "2006 International Building Code", International Code Council, Inc., USA.

Kalkan E. and Chopra A. K. [2009], "Modal Pushover-Based Ground Motion Scaling Procedure for Nonlinear Response History Analysis of Structures," SEAOC 2009 Convention Proceedings, San Diego, CA.

Kalkan E. and Chopra A. K. [2010], "Modal-Pushover-Based Ground Motion Scaling Procedure," ASCE Journal of Structural Engineering, (in-press).

Kalkan E. and Kunnath, S. K. [2004], "Method of Modal Combinations for Pushover Analysis of Buildings," Proceedings of the 13th World Conference on Earthquake Engineering, Paper No. 2713, Vancouver, Canada.

Kennedy, R. P., Short, S. A., Merz, K. L., Tokarz, F. J., Idriss, I. M., Power, M. S., and Sadigh, K. [1984], "Engineering Characterization of Ground Motion-task 1: Effects of Characteristics of Free-Field Motion on Structural Response," NUREG/CR-3805, U.S. Regulatory Commission, Washington, D.C.

Kilar V. and Fajfar P. [1997], "Simple Push-over Analysis of Asymmetric Buildings," Earthquake Engineering and Structural Dynamics, 26, pp. 233–249.

Kim, S., and D'Amore, E. [1999], "Pushover Analysis Procedure in Earthquake Engineering," Earthquake Spectra, 15, pp. 417-434.

Krawinkler, H. [1978], "Shear in Beam-Column Joints in Seismic Design of Frames," Engineering Journal, v15, n3, American Institute of Steel Construction, Chicago, IL.

Krawinkler, H. and Seneviratna, G. D. P. K. [1998], "Pros and Cons of a Pushover Analysis of Seismic Performance Evaluation," Engineering Structures, Vol. 20, No. 4-6, pp. 452-464.

Kurama, Y. and Farrow, K. [2003], "Ground Motion Scaling Methods for Different Site Conditions and Structure Characteristics," Earthquake Engineering and Structural Dynamics, Vol. 32, No. 15, pp. 2425-2450.

Lilhanand, K. and Tseng, W. S. [1987], "Generation of Synthetic Time Histories Compatible with Multiple-Damping Design Response Spectra," Transactions of the 9th International Conference on Structural Mechanics in Reactor Technology, Lausanne, K1, pp. 105-110.

Lilhanand, K. and Tseng, W. S. [1988], "Development and Application of Realistic Earthquake Time Histories Compatible with Multiple-Damping Design Spectra," Proceedings of the 9th World Conference on Earthquake Engineering, Tokyo Japan, II, pp. 819-824.

Luco, N. and Cornell, A. C. [2007], "Structure-Specific Scalar Intensity Measures for Near-Source and Ordinary Earthquake Ground Motions," Earthquake Spectra, 23(2), pp. 357-392.

Malhotra, P. K. [2003], "Strong-Motion Records for Site-Specific Analysis," Earthquake Spectra, Vol. 19, No. 3, pp. 557-578.

Mehanny, S. S. F. [1999], "Modeling and Assessment of Seismic Performance of Composite Frames with Reinforced Concrete Columns and Steel Beams," Ph.D. dissertation, Stanford University, CA.

Menun, C. and Der Kiureghian A. D. [1998], "A Replacement for the 30%, 40% and SRSS Rules for Multicomponent Seismic Analysis," Earthquake Spectra, 14(1), pp. 153-163.

Moehle, J. P. [2007], "The Tall Buildings Initiative for Alternative Seismic Design," The Structural Design of Tall and Special Buildings, 16, pp. 559-567.

Moghadam, A. S., and Tso, W-K. [1998], "Pushover Analysis for Asymmetrical Multistorey Buildings," Proceedings of the 6th U.S. National Conference on Earthquake Engineering, EERI, Oakland, CA.

Newmark, N. M. [1976], "Vibration of Structures Induced by Ground Motion," Shock and Vibration Handbook, 2nd ed., McGraw Hill, New York.

Nau, J., and Hall, W. [1984], "Scaling Methods for Earthquake Response Spectra," Journal of Structural Engineering (ASCE), 110, pp. 91-109.

Naeim, F., Alimoradi, A., and Pezeshk, S. [2004], "Selection and Scaling of Ground Motion Time Histories for Structural Design Using Genetic Algorithms," Earthquake Spectra, 20(2), pp. 413-426.

Naeim F., and Lobo R. M. [1998], "Common Pitfalls in Pushover Analysis," Proceedings of the SEAOC Annual Convention, Reno, NV.

Nocedal, J. and Stephen J. W. [2006], "Numerical Optimization," 2nd ed., Springer Series in Operations Research, Springer, USA.

PEER. [2007], "Pacific Earthquake Engineering Research Center: PEER NGA Database," University of California, Berkeley, CA.

Poursha, M., Khoshnoudian, F., and Moghadam A. S. [2009], "A Consecutive Modal Pushover Procedure for Estimating the Seismic Demands of Tall Buildings," Journal of Engineering Structures, 31, pp. 591-599.

Post, N. M. [2008], "A Sleek Skyscraper in San Francisco Raises the Profile of Performance-Based Design," McGraw-Hill Construction, Continuing Education Center. (Available online at http://continuingeducation.construction.com/; last accessed on 10/2009)

Rosenblueth, E. and Contreras, H. [1977], "Approximate Design for Multicomponent Earthquakes," Journal of the Engineering Mechanics Division, ASCE, 103, pp. 881-893.

Ruiz-Garcia, J. and Miranda E. [2003], "Inelastic Displacement Ratios for Evaluation of Existing Structures," Earthquake Engineering and Structural Dynamics, 32, pp. 1237-1258.

Sasaki, K. K., Freeman, S. A., Paret, T. F. [1998], "Multimode Pushover Procedure (MMP) - A Method to Identify the Effects of Higher Modes in a Pushover Analysis," Proceedings of the 6th U.S. National Conference of Earthquake Engineering, Seattle, WA.

Shome, N. and Cornell, A. C. [1998], "Normalization and Scaling Accelerograms for Nonlinear Structural Analysis," Prof. of the 6th U.S. National Conf. on Earthquake Engineering, Seattle, WA.

Shome, N., Cornell, C. A., Bazzurro, P., and Carballo, J. E. [1998], "Earthquakes, Records, and Nonlinear Responses," Earthquake Spectra, 14(3), pp. 469-500.

Shome, N., and Cornell, C. A. [1999], "Probabilistic Seismic Demand Analysis of Nonlinear Structures," Reliability of Marine Structures Program, Report No. RMS-35, Department of Civil and Environmental Engineering, Stanford University, CA. (Available online at http://www.stanford.edu/group/rms/Thesis/index.html; last accessed on 06/2008).

Simons, J. W. and Powell, G. H. [1982], "Solution Strategies for Statically Loaded Nonlinear Structures," Earthquake Engineering Research Center UCB/EERC-82/22, University of California, Berkeley, CA.

Smeby, W. and Der Kiureghian A. D. [1985], "Modal Combination Rules for Multicomponent Earthquake Excitation," Earthquake Engineering and Structural Dynamics, 13, pp. 1-12.

Tothong, P. and Cornell, A. C. [2008], "Structural Performance Assessment Under Near-Source Pulse-Like Ground Motions Using Advanced Ground Motion Intensity Measures," Earthquake Engineering and Structural Dynamics, Vol. 37, No. 7, pp. 1013-1037.

Van Overschee P. and De Moor B. [1996], Subspace Identification for Linear Systems. Kluwer Academic Publishers, Boston/London/Dordrecht.
(Available online at http://homes.esat.kuleuven.be/~smc/sysid/software/; last accessed on 10/2009)

Youngs, R., Power, M., Wang, G., Makdisi, F., and Chin, C. C. [2007], "Design Ground Motion Library (DGML) – Tool for Selecting Time History Records for Specific Engineering Applications (Abstract)," SMIP07 Seminar on Utilization of Strong-Motion Data, pp. 109 – 110.
(Available online at http://www.conservation.ca.gov/cgs/smip/docs/seminar/SMIP07/Pages/Paper8_Youngs.aspx; last accessed on 10/2009).

Appendix A: Implementation of Step 11 of MPA

As mentioned in Chapter 2, member forces in those elements that deform into the inelastic range; and deformation quantities such as plastic hinge rotations, and drifts at point other than the C.M. can be estimated from the total member deformations. Such procedure to compute member forces and deformations can be implemented by imposing on the C.M. a set of displacements compatible with the drifts calculated in Step 10 (Section 3.6). In computer programs that do not allow imposing displacements, a model combining lateral forces with bidirectional "gap" elements at each floor could be implemented as follows (Figure A.1):

- Estimate the *j*th floor displacements $u'_{jx} = \sum_{i=1}^{j} \Delta_{jx}^{T}$ and $u'_{jy} = \sum_{i=1}^{j} \Delta_{jy}^{T}$ from the total drifts estimate in Step 10 (Section 3.6).
- Create bidirectional "gap" elements with openings at the *j*th floor equal to u'_{jx} and u'_{jy}. The model should account for nonlinear geometric effects. In PERFORM-3D the inelastic component called *Seismic Isolator, Rubber Type* could be used specifying initial stiffness close to zero, and large deformation stiffening.
- Apply gravity loads
- Push the structure applying monotonically increasing lateral forces $f'_{jx} = \sum_{i=1}^{j} \Delta_{jx}^{T}$ and $f'_{jy} = \sum_{i=1}^{j} \Delta_{jy}^{T}$ until the openings close.
- Extract from the model the desired response quantities.

This procedure has the following disadvantages:

- Path-independent models should be used to conduct the analysis. The implementation of this procedure using path-dependent models could generate bias in the final results.
- The large stiffness values assigned to the gap elements after the openings close could cause some numerical problems.

Step 11 Other response quantities

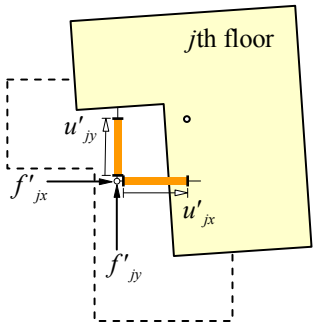

gap element

- Include bidirectional "gap" elements into the model. The openings of these elements at the *j*th floor are:

$$u'_{jx} = \sum_{i=1}^{j} \Delta_{jx}^{T}$$

$$u'_{jy} = \sum_{i=1}^{j} \Delta_{jy}^{T}$$

- Apply gravity loads
- Push the structure applying monotonically increasing lateral forces f'_{jx} and f'_{jy} until the openings close.

$$f'_{jx} = \sum_{i=1}^{j} \Delta_{jx}^{T}$$

$$f'_{jy} = \sum_{i=1}^{j} \Delta_{jy}^{T}$$

Figure A.1 Implementation of Step 11 of the MPA procedure.

Appendix B: Unsymmetric-Plan Buildings (Member Sizes)

Table B.1 Member sizes for the moment resisting frames of the UBC85 buildings

Moment Resisting Frames A03 UBC85					
Story	Columns	Girders EW	Panel EW†	Girders NS	Panel NS†
1	W14x257	W21x62	-	W18x65	-
2	W14x257	W21x62	-	W18x65	-
3	W14x257	W21x44	-	W18x50	-
Moment Resisting Frames B03 UBC85					
Story	Columns	Girders EW	Panel EW†	Girders NS	Panel NS†
1	W14x398	W21x68	-	W27x102	0.8750
2	W14x398	W21x68	-	W27x102	0.8750
3	W14x398	W21x62	-	W21x62	-
Moment Resisting Frames C03 UBC85					
Story	Columns	Girders	Panel EW†	Girders NS	Panel NS†
1	W14x398	W27x94	0.5625	W27x94	0.5625
2	W14x398	W27x94	0.5625	W27x94	0.5625
3	W14x398	W24x68	-	W24x68	-
Moment Resisting Frames C09 UBC85					
Story	Columns	Girders EW	Panel EW†	Girders NS	Panel NS†
1	W14x426	W36x150	0	W33x141	1.5
2	W14x426	W36x150	0	W33x141	1.5
3	W14x426	W36x150	0	W33x141	1.5
4	W14x426	W36x150	0	W33x141	1.5
5	W14x426	W30x132	0	W30x99	1.5
6	W14x370	W30x132	1.75	W30x99	0.75
7	W14x370	W30x132	1.75	W30x99	0.75
8	W14x370	W24x76	0.4375	W24x76	0.4375
9	W14x370	W24x76	0.4375	W24x76	0.4375

† only in interior joints

Table B.2 Member sizes for the moment resisting frames of the IBC06 buildings

Moment Resisting Frames A03 IBC06					
Story	Columns	Girders EW	Panel EW†	Girders NS	Panel NS†
1	W14x257	W21x62	0.375	W18x65	3/8
2	W14x257	W21x62	0.375	W18x65	3/8
3	W14x257	W21x44	-	W18x50	-
Moment Resisting Frames B03 IBC06					
Story	Columns	Girders EW	Panel EW†	Girders NS	Panel NS†
1	W14x398	W21x68	-	W21x68	-
2	W14x398	W21x68	-	W21x68	-
3	W14x398	W21x62	-	W21x62	-
Moment Resisting Frames C03 IBC06					
Story	Columns	Girders	Panel EW†	Girders NS	Panel NS†
1	W14x398	W21x73	-	W21x73	-
2	W14x398	W21x73	-	W21x73	-
3	W14x398	W21x68	-	W21x68	-
Moment Resisting Frames C09 IBC06					
Story	Columns	Girders EW	Panel EW†	Girders NS	Panel NS†
1	W14x426	W30x132	1.75	W30x132	1.75
2	W14x426	W30x132	1.75	W30x132	1.75
3	W14x426	W30x132	1.75	W30x132	1.75
4	W14x426	W30x132	1.75	W30x132	1.75
5	W14x426	W27x94	0	W27x94	0
6	W14x426	W27x94	0	W27x94	0
7	W14x426	W27x94	0	W27x94	0
8	W14x426	W21x50	0	W21x50	0
9	W14x426	W21x50	0	W21x50	0

† only in interior joints

Table B.3 Member sizes for the gravity frames of the IBC06 buildings

Gravity Frames A03 UBC85 and IBC06			
Story	Columns	Beams EW	Beams NS
1	W14x68	W18x50	W16x26
2	W14x68	W18x50	W16x26
3	W14x68	W18x50	W16x26
Gravity Frames B03 UBC85 and IBC06			
Story	Columns	Beams EW	Beams NS
1	W14x68	W18x50	W16x26
2	W14x68	W18x50	W16x26
3	W14x68	W18x50	W16x26
Gravity Frames C03 UBC85 and IBC06			
Story	Columns	Beams EW	Beams NS
1	W14x68	W18x50	W16x26
2	W14x68	W18x50	W16x26
3	W14x68	W18x50	W16x26
Gravity Frames C09 UBC85 and IBC06			
Story	Columns	Beams EW	Beams NS
1	W14x193	W18x50	W16x26
2	W14x193	W18x50	W16x26
3	W14x193	W18x50	W16x26
4	W14x145	W18x50	W16x26
5	W14x145	W18x50	W16x26
6	W14x145	W18x50	W16x26
7	W14x82	W18x50	W16x26
8	W14x82	W18x50	W16x26
9	W14x82	W18x50	W16x26

Appendix C: Notation

List of Acronyms and Abbreviations

A03	three-story building with plan shape A
ASCE7	ASCE/SEI 7-05 standard
ASCE	nonlinear static procedure of ASCE/SEI 41-06 standard
B03	three-story building with plan shape B
BRBs	buckling restrained braces
C03	three-story building with plan shape C
C09	nine-story building with plan shape C
C.M.	center of mass
CQC	complete quadratic combination
CW48	48-story building with concrete walls
CW62	62-story building with concrete walls
DBE	design basis earthquake
DOF	degree of freedom
EDPs	engineering demand parameters
EURO1	nonlinear static procedure of Eurocode-8 (2004) standard using uniform force distribution
EURO2	nonlinear static procedure of Eurocode-8 (2004) standard using "modal" force distribution
GM	ground motion
MCE	maximum considered earthquake
MDF	multiple-degree-of-freedom

MMPA	modified modal pushover analysis
MPA	modal pushover analysis
MPS	modal-pushover-based scaling
NGA	next generation of ground-motion attenuation models
NL-RHA	nonlinear response history analysis
NSP	nonlinear static procedure
PGA	peak ground acceleration
PGV	peak ground velocity
PMPA	practical MPA
PP	peak-picking identification
PSD	power spectral density
RHA	response history analysis
RSA	response spectrum analysis
SDF	single-degree-of-freedom
SFBF	2001 San Francisco Building Code
SRSS	square root of the sum of the squares
DSS	combined deterministic-stochastic subspace identification
UBC85	1985 Uniform Building Code
IBC06	2006 International Building Code
UMRHA	uncoupled modal response history analysis

Notation List

Roman symbols

a , b	components of ground motion
$\mathbf{a}$, $\mathbf{b}$	constants in Newmark's method
$\mathbf{A}$	vector of pseudo-acceleration values for various periods
$\mathbf{A}_a$, $\mathbf{A}_b$	vector of pseudo-acceleration values due to $\ddot{u}_{ga}(t)$ and $\ddot{u}_{gb}(t)$ for various periods
$\mathbf{A}_{\text{SRSS}}$, $A_{\text{SRSS},i}$	see Section 6.2.2 (Step 5)
$A(T)$	pseudo-acceleration spectrum ordinate at period T
A_i	pseudo-acceleration spectrum ordinate at period T_i and damping ratio ζ_i
$\hat{\mathbf{A}}$	vector of target pseudo-acceleration values for various periods
$\hat{\mathbf{A}}_a$, $\hat{\mathbf{A}}_b$	vector of target pseudo-acceleration values in a and b directions for various periods
$\hat{\mathbf{A}}_{\text{scaled}}$, $\hat{A}_{\text{scaled},i}$	see Section 6.2.1 (Step 5)
$\hat{\mathbf{A}}_{\text{SRSS}}$, $\hat{A}_{\text{SRSS},i}$	see Section 6.2.2 (Step 7)
$\hat{A}_n$	target pseudo-acceleration spectrum ordinate at period T_n
$\hat{A}_{na}$, $\hat{A}_{nb}$	target pseudo-acceleration spectrum ordinate at period T_n in a and b directions
$\mathbf{c}$	damping matrix
C_n	generalized damping, nth "mode"

C_m effective modal mass participation factor for the fundamental mode, as defined in ASCE/SEI 41-06

C_{Rn} inelastic deformation ratio

$C_{Rn,a}$, $C_{Rn,b}$ inelastic deformation ratio in a and b directions

$D_n(t)$ deformation of nth "mode" SDF system due to $\ddot{u}_g(t)$

$D_{na}(t)$, $D_{nb}(t)$ $D_n(t)$ due to $\ddot{u}_{ga}(t)$ and $\ddot{u}_{gb}(t)$

D_n peak value of $D_n(t)$

D_{na}, D_{nb} peak values of $D_{na}(t)$ and $D_{nb}(t)$

D_{ny} see Eq. (3.23) and (3.24)

$\hat{D}_n$ inelastic median (or target) deformation

$\hat{D}_{na}$, $\hat{D}_{nb}$ inelastic median (or target) deformation in a and b directions

$\hat{D}_{no}$ elastic median deformation of the corresponding linear system

E_2 see Section 6.1.1, Step 12

f'_{jx}, f'_{jy} see Appendix A

$\mathbf{f}_s$ resisting force vector

$(\mathbf{f}_s)_i$ resisting force vector at time step i

$\mathbf{f}_{sx}$, $\mathbf{f}_{sy}$ x and y lateral resisting forces

$\mathbf{f}_{s\theta}$ resisting torque

$\mathbf{f}_{xn}$, $\mathbf{f}_{xn}$ see Eq. (3.17a and b)

$\mathbf{f}_{\theta n}$ see Eq. (3.17c)

F_{sn} see Eq. (3.15)

F_{sny} see Eqs. (3.23) and (3.24)

h see Section 5.4.1

i integer denoting time step, mode, or floor number

j integer denoting sub-step or floor number

$\mathbf{I}_O$ matrix of order N with $I_{O\,jj} = I_{O\,j}$, the moment of inertia of the jth floor diaphragm about a vertical axis trough the C.M.

$(\mathbf{k}_T)^{(j)}$ tangent stiffness matrix at $\mathbf{u}^{(j)}$

L_n, L_{na}, L_{nb} see Eq. (3.3)

L_{Rn} see Eq. (3.27)

$\mathbf{M}$ mass matrix

$\mathbf{m}$ matrix of order N with $m_{jj} = m_j$, the mass lumped at the jth floor level

M bending moment

M_n generalized mass for nth "mode"

M_n^* effective modal mass for nth "mode"

M_w moment magnitude of recorded earthquake

M_y yielding moment capacity

n integer denoting mode number

n_{EQ} number of ground motions

N number of floors

$\mathbf{p}_{eff}(t)$ effective earthquake force vector

$\mathbf{p}_{eff,na}(t)$ contribution of nth "mode" to $\mathbf{p}_{eff}(t)$ for the a-component of ground motion

$\mathbf{p}_{eff,nb}(t)$ contribution of nth "mode" to $\mathbf{p}_{eff}(t)$ for the a-component of ground motion

$\mathbf{p}_i$ excitation value at time i

$\hat{\mathbf{p}}_{i+1}$ see Eq. (2.10)

$q_n(t)$ nth modal coordinate

r combined peak modal response

$r(t)$ response quantity

$r_n(t)$ nth mode contribution to the response quantity $r(t)$

r_n peak modal response

r_{na}, r_{nb} peak modal responses due to $\ddot{u}_{ga}(t)$ and $\ddot{u}_{ga}(t)$

$r_{n+g,a}$, $r_{n+g,b}$ response values extracted from the pushover database at references displacements $u_{rn,a}$ and $u_{rn,b}$

r_T total responses (see Section 3.4, Step 10)

R_{JB} distance to the surface projection of fault rupture as defined by Joyner-Boore

R, R_{yn} yield strength reduction factor

R_{max} see Eq. (5.2)

SF scaling factor

SF_1, SF_2 see Section 6.2

SF_a, SF_b scaling factors for $\ddot{u}_{ga}(t)$ and $\ddot{u}_{ga}(t)$

$\mathbf{s}_a$, $\mathbf{s}_b$ spatial distribution of the effective earthquake forces in the a and b components of ground motion

$\mathbf{s}_{na}$, $\mathbf{s}_{nb}$ contribution of nth "mode" to $\mathbf{M}\boldsymbol{\iota}_a$ or $\mathbf{M}\boldsymbol{\iota}_b$

$\mathbf{s}_{xn,a}$, $\mathbf{s}_{xn,b}$ see Eq. (3.5)

$\mathbf{s}_{yn,a}$, $\mathbf{s}_{yn,b}$ see Eq. (3.5)

$\mathbf{s}_{\theta n,a}$ see Eq. (3.5)

$\mathbf{s}_n^*$, $\mathbf{s}_{na}^*$, $\mathbf{s}_{nb}^*$ see Eqs. (3.18) and (6.1)

t time

T_n nth natural period

T_c period that separates the acceleration-sensitive and the velocity-sensitive regions of the median response spectrum (Fig. 3.9)

$\mathbf{u}$, $\mathbf{u}(t)$ displacement vector

$\mathbf{u}_n(t)$ $\mathbf{u}(t)$ due to mode n

$\mathbf{u}_i$, $\dot{\mathbf{u}}_i$, $\ddot{\mathbf{u}}_i$ floor displacement, velocity and acceleration at time step i

$\mathbf{u}^{(j)}$ displacement vector at j th sub-step

u_{jx}, u_{jy} displacement of the C.M. of floor j along x and y axes

$u_{j\theta}$ rotation of floor j about C.M.

$\ddot{u}_{ga}(t)$, $\ddot{u}_{ga}(t)$ a and b components of ground acceleration

$\mathbf{u}_n(t)$ $\mathbf{u}(t)$ due to nth "mode"

u_{rn} displacement at the reference point, nth "mode"

$u_{rn,a}$, $u_{rn,b}$	displacement at the reference point for the nth "mode" due to a and b components of ground motion
u_{rxn}, u_{ryn}	reference displacement for the nth "mode" along x and y axes
$u_{r\theta n}$	reference rotation for the nth "mode"
u_{rg}	displacement at the reference point due to gravity loads
$\mathbf{u}_x$, $\mathbf{u}_y$	x and y-lateral floor displacements
$\mathbf{u}_\theta$	floor rotations
u_1, u_2, u_3	parameters of trilinear models (Fig. 4.16)
$\mathbf{u}'_x$, $\mathbf{u}'_y$	see Section 3.4 (Step 11) and Appendix A
u'_{jx}, u'_{jy}	see Section 3.4 (Step 11) and Appendix A
$\hat{u}$	median reference displacements
u_{rny}	see Section 3.3.2
u_{r1d}, u_{r1y}	see Section 5.4.1
V_{bn}	base shear, mode n
$V_{bn,a}$, $V_{bn,b}$	base shear due to the force distribution $\mathbf{s}^*_{n,a}$ and $\mathbf{s}^*_{n,b}$
w	effective seismic weight of the building
x, y	Cartesian coordinates
$\hat{x}$	geometric mean of a random variable x
x_i	ith value in a data set
$\mathbf{0}$	vector of zeros
$\mathbf{1}$	vector of ones

Greek symbols

α_e see Section 5.4.1

α_n post yield stiffness ratio

ε_{MPS} see Eq. (6.3) and Eq. (6.6)

$\varepsilon_{\text{ASCE}}$ see Section 6.2.1 (Step 6) and 6.2.2 (Step 8)

δ dispersion measure as defined in Eq. (6.1)

$\left(\Delta\mathbf{f}_s\right)^{(j)}$ see Eq. (2.11)

$\Delta\hat{\mathbf{p}}^{(j)}$, $\Delta\mathbf{u}^{(j)}$ see Eq. (2.11)

Δt time step size

Δ_{jx}^T, Δ_{jy}^T see Section 3.4 (Step 11) and Appendix A

Γ_n, Γ_{na}, Γ_{nb} see Eq. (3.3)

$\boldsymbol{\iota}_a$, $\boldsymbol{\iota}_b$ influence vectors associated with components $\ddot{u}_{ga}(t)$ and $\ddot{u}_{gb}(t)$ of the ground motion

λ_j jth event factor

ϕ_n nth natural vibration "mode"

ϕ_{xn}, ϕ_{yn}, $\phi_{\theta n}$ subvectors of ϕ_n

ϕ_{rn} component of ϕ_n at the reference point (or at the roof)

ζ_n damping ratio for nth "mode"

ω_n nth natural frequency (undamped) (rad/sec)